Design, Synthesis and Disposition Studies of New ISRIB Analogues, Targeting eIF2B, as Potential Candidates for enhancing protein synthesis rate

By Akeel Abdulkadhum Abo Alard

Thesis submitted to the University of Nottingham for the degree of Doctor of Philosophy

February 2021

Abstract

Neurodegenerative diseases represent a major cause of dementia, which is predominantly a disease of the elderly, and is characterised by a decline in cognitive functions and memory. All these diseases share a similar aetiology, *i.e.* the production and accumulation of misfolded proteins in the brain. This results in upregulation of the PERK/eIF2α-P pathway of the unfolded protein response (UPR), which in turn leads to reduction of protein synthesis. A recently discovered chemical inhibitor of the integrated stress response, ISRIB **1**, is reported to serve as a neuro-enhancer in healthy rodents and neuro-protectant in models of neurodegenerative and traumatic brain injury. *Trans*-ISRIB acts downstream of eIF2α-P, by destabilization of the ISR-specific eIF2B–eIF2(αP) complex. This occurs through direct engagement of eIF2Bδ by ISRIB, resulting in allosterically antagonizing the inhibitory effect of phosphorylated eIF2 on eIF2B, thus suppressing the integrated stress response (ISR) and allowing resumption of unstressed protein synthesis.

This project aims to design, synthesise and evaluate a library of ISRIB derivatives to scope out the overall SARs as best as possible. In addition, this project also aims to improving knowledge of the molecular target of the ISRIB through design, synthesise and evaluate a novel fluorescent ISRIB derivative in order to nail down the molecular target of this compound.

This study reports the design, synthesis and pharmacological results (carried out by Prof. David Ron laboratory) of a set of of ISRIB derivatives, based upon the parent ISRIB molecule. The pharmacological assay was designed to probe the

ability of these ligands to allosterically antagonising the inhibitory effect of phosphorylated eIF2 on eIF2B by measuring the fluorescence intensity of the CHOP::GFP reporter. A set of ISRIB analogues were designed and synthesised through modification of different motifs on the prototype ISRIB molecule. These include modifying the nature and position of substituents on the terminal phenyl moieties, investigation of replacing the central cyclohexane ring that joins the *O*-arylglycolamide side chains, and modification of the glycolamide linkage between the central cyclohexane and distal aryl rings (**Figure 1**).

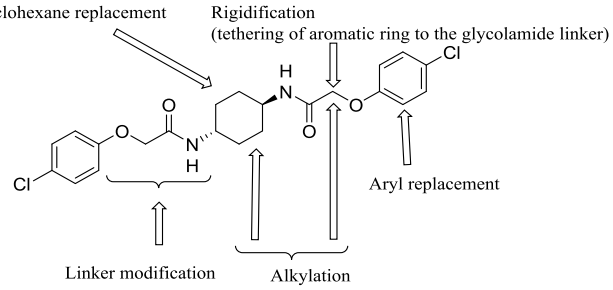


Figure 1: General overview of ISRIB **1** structural modifications investigated in this study.

The rationally designed ISRIB analogues afforded a comprehensive SAR study. Synthesis of ISRIB analogues with *para*-bromine substitution resulted in the identification of a bromo analogue with potency comparable to ISRIB. Our results also showed that modification of the cyclohexane core ring with a piperidinyl and piperazinyl core rings (heterocycloalkyl) resulted in novel analogues which displayed a potency with only two to three-fold lower than *trans*-ISRIB.

In this project, the *O*-arylglycolamide moiety was also explored and it was found that repositioning the carboxamide group on the central cyclohexane ring by inverting the amide group resulted in maintaining the activity. Interestingly, the pharmacological results showed that the inversion of carboxamide with tethering

the terminal ring to glycolamide linker through six-membered ring displayed a well tolerated result. Considering the SAR data, a set of rigidified analogues that possess chromane, benzodioxane and benzoxazine were designed and synthesised to interrogate ISRIB's interaction with eIF2B. These rigidified analogues allowed the generation of new structure-activity relationships and ultimately afforded a promising analogue, ISRIB analogue with benzoxazine moiety, to be used as s a suitable lead compound for design and synthesis of novel fluorescent ISRIB analogues. The N-H group of benzoxazine provided the anchor point to generate labelled ISRIB derivative **156e**, which contains a flexible linker terminated with 5/6-carboxyfluorescein moiety. This labelled ISRIB derivative was used as tracers for the development of direct competitive fluorescence polarisation (FP) binding assay (carried out by Prof. David Ron laboratory). This pharmacological tool was instrumental in demonstrating a direct interaction between ISRIB-type compounds and eIF2B.

Furthermore, this project also sought to develop new ISRIB analogues for enhancing the ADME properties, as the current ISRIB molecule has poor aqueous solubility and therefore is not orally bioavailable. ISRIB and other selected analogues (piperidine analogue **103**, piperazine analogue **108a** and benzoxazine analogue **145**) were selected for further *in vitro* ADME studies (aqueous solubility, Caco-2 permeability, and microsomal stability). These analogues were selected based on reported high potency at eIF2B receptors. The results showed a comparable ADME properties for ISRIB and other selected analogues.

Declaration

The work presented in this thesis is submitted to the University of Nottingham in support of my application for the degree of Doctor of Philosophy. Except where acknowledged in the text, I declare that this dissertation is my own work and is based on research that was undertaken by me in the School of Pharmacy/ Faculty of Science/ University of Nottingham.

Acknowledgments

I would like to express my grateful sincere to my supervisor Professor Peter Fischer for his continuous support throughout my PhD study. I am really grateful for his patience, enthusiasm, motivation and immense knowledge. His guidance helped me in all the time of research and writing of my thesis.

I would like to acknowledge the Higher Committee of Education Development of Iraq (HCED) and the Ministry of Higher Education and Scientific Research (Iraq) to give me this opportunity by sponsoring me during my PhD.

I would also like to thank my second supervisor Professor Barrie Kellam for his help and support. Special thanks go to Dr. Pavel Gershkovich, Dr. Jong Bong Lee and Dr. Catherine Ortori for giving me so many wonderful advices and help with disposition study.

I am really grateful to Professor David Ron and his team Dr. Ana Crespillo Cresado and Dr. Alisa Zyryanova at the Cambridge Institute for Medical Research (CIMR) for guidance, support and accomplished the biological study of this project.

I would also like to offer huge appreciation to Dr. Christophe Fromont and Dr. Divneet Kaur for their support, advice, friendship and sharing their expertise whenever I need. I would also like to thank my colleagues who made my project journey more enjoyable, in particular, Dr. Ali Hasson, Dr. Muhammed Al-Ameedee, Dr. Fadi Soukarieh, Dr. Xi Chen Lubna Hashmi and Foteini Damaskinaki for their help and friendship.

I am extremely grateful to my parents and my family in Iraq for almost unbelievable support and encouraging me throughout this experience. I am extremely thankful to my wife Masar Radhi and to my beloved daughters, who stood by my side in all times for letting me through all the difficulties. You are my little family who let me finish my PhD. My lovely angel, Fatima, you are buried in my heart, always lights my life up and won't forget you forever.

List of abbreviations

^{13}C NMR	Carbon nuclear magnetic resonance
^{1}H NMR	Proton nuclear magnetic resonance
2BAct	eIF2B activator
5'-UTR	5′ Untranslated region
AD	Alzheimer's diseases
ADME	Absorption, Distribution, Metabolism, and Excretion
ALS	Amyotrophic lateral sclerosis
ASK1	Apoptosis signalling-regulating kinase 1
ATF4	Activating transcription factor 4
ATF6	Activating transcription factor 6
ATP	Adenosine triphosphate
Aβ	Amyloid β
BACE1	Beta-site amyloid precursor protein cleaving enzyme 1
BiP	Binding immunoglobulin protein
BSA	Bovine serum albumin
bZIP	basic leucine zipper
CAA	Cerebral amyloid angiopathy
CaCo-2	Colorectal adenocarcinoma cells
CERAD	Consortium to Establish a Registry for Alzheimer's Disease
CHO-K1	Chinese hamster ovary
CHOP	Transcription factor C/EBP homologous protein
CIMR	Cambridge Institute for Medical Research
CK1	Casein kinase 1
CL	Clearance
CO	Carbon oxide
Conc.	Concentration
Cryo-EM	Cryo–electron microscopy
CSF	Cerebral spinal fluids
d	Doublet
DCM	Dichloromethane
DIPEA	Diisopropylethylamine
DMEM	Dulbecco's Modified Eagle Medium
DMF	Dimethylformamide
DMPK	Drug Metabolism and Pharmacokinetics
DMSO	Dimethyl sulfoxide
dsRBD	Double-stranded RNA binding domain
DYRK	Dual-specify tyrosine phosphorylated and regulated kinase
EC_{50}	Half maximal effective concentration
EDGs	Electronic donating group
eEF1A	Eukaryotic elongation factor 1A
eIF2B	Eukaryotic initiation factor 2B
eIF2α	Eukaryotic initiation factor 2 alpha
eIF2α-P	Eukaryotic initiation factor 2 alpha-Phosphorylation
eIF4E	Eukaryotic initiation factor 4E
eIF4F	Eukaryotic initiation factor 4F
eIF4H	Eukaryotic initiation factor 4H
ER	Endoplasmic reticulum
Et_3N	Triethylamine
EWGs	Electronic withdrawing group
FACS	Fluorescence-activated cell sorting
FBS	Fetal Bovine Serum

FP	Fluorescence polarisation
FTD	Frontotemporal dementia
GCN-2	General control non-derepressible-2
GDP	Guanosine diphosphate
GEF	guanine nucleotide exchange factor
GFP	Green fluorescent protein
GSK3	Glycogen synthase kinase 3
GTP	Guanosine triphosphate
HATU	Hexafluorophosphate Azabenzotriazole Tetramethyl Uronium
HBA	Hydrogen bond acceptor
HBD	Hydrogen bond donor
HBTU	Hexafluorophosphate Benzotriazole Tetramethyl Uronium
HD	Huntington diseases
His	Histidinol
HisRS	histidyl-tRNA synthetase
HPLC	High pressure liquid chromatography
HQC	high-quality control
HRI	Heme-regulated inhibitor kinase
HRMS	High resolution mass spectrometry
IC_{50}	Half maximal inhibitory concentration
IFNAR	Interferon receptors
ip	Intraperitoneal
IRE1α	Inositol-requiring enzyme 1α
IS	Internal standard
ISR	Integrated stress response
ISRIB	Integrated stress response inhibitor
J	Coupling constant
KI	Kinase insert
LLOQ	Lower limit of quantification
LQC	Low quality control
m	Multiplet
m/z	Mass to charge ratio
MAPK	Mitogen-activated protein kinase
MeOH	Methanol
Met	Methionyl
Mp	Melting point
MQC	Medium quality control
MRM	Multiple Reaction Monitoring
mRNAs	Messenger RNA
MS	Mass spectrometry
NDs	Neurodegenerative diseases
NFTs	Neurofibrillary tangles
NRF2	Nuclear erythroid 2 p45-related factor 2
nRot	Non-terminal freely rotatable bonds
PD	Parkinson’s diseases
PDB	Protein Data Bank
PERK	PKR-like ER kinase
PKA	Protein kinase A
PKC	Protein kinase C
PKR	Protein kinase RNA
ppm	Parts per million
PrP	Prion protein
q	Quartet
QC	Quality control
RE	Relative error

RSD	Relative standard deviation
s	Singlet
S1P	serine protease site-1
SARs	Structure activity relationships studies
SNP	single-nucleotide polymorphism
t	Triplet
TEER	Transepithelial electrical resistance
THF	Tetrahydrofuran
TLC	Thin layer chromatography
TMS	Tetramethylsilane
t_R	Retention time
tRNAs	Transfer RNA
uORFs	Upstream open reading frames
UPR	Unfolded protein response
VCI	Vascular cognitive impairment
VWMD	Vanishing White Matter Disease
XBP1	X-box binding protein
Zn	Zinc

List of contents

Abstract **I**
Declaration **IV**
Acknowledgments **V**
List of abbreviations **VII**
List of contents **X**
1. Introduction **1**
1.1. Translation of mRNAs 1
1.1.1. Regulation of eukaryotic translation initiation factors 2 (eIF2) 4
1.1.1.1. Phosphorylation of eIF2 5
1.1.1.2. Regulation of eIF2B 6
1.2. Structure of eIF2B 8
1.3. The eIF2 kinases: coping with stress 9
1.3.1. Endoplasmic reticulum 9
1.3.2. Unfolded protein response 10
1.3.3. Integrated stress response 13
1.3.4. eIF2-eIF2B complex in normal and UPR conditions 16
1.4. Neurodegenerative diseases 17
1.4.1. Molecular pathology of neurodegenerative diseases 19
1.4.2. Types of neurodegenerative disorders 21
1.4.2.1. Alzheimer's disease 21
1.4.2.2. Prion diseases 22
1.4.2.3. Parkinson's disease 25
1.5. Hopes and challenges for treatment of neurodegenerative disorders 25
1.5.1. Non-disease-specific approaches 25
1.5.2. Disease-specific and protein-specific approaches 25
1.5.3. Targeting dysregulation of the unfolded protein /integrated stress 26
1.5.3.1. Targeting eIF2, an eIF2 kinase inhibitors: 27
1.5.3.1.1. Drug-Receptor interaction 27
1.5.3.1.2. PERK inhibitors 29
1.5.3.1.3. HRI, PKR and GCN-2 inhibitors 30
1.5.3.2. Targeting eIF2B, an eIF2/eIF2B complex modulator 32
1.5.3.2.1. ISR inhibitor (ISRIB) 32
1.5.3.2.2. eIF2B Activator (2BAct) 35
1.6. Known structure-activity relationships (SAR) for ISRIB 37
1.7. Aims and objectives: 40
2. Design and synthesis of ISRIB analogues **42**
2.1. Introduction 42
2.2. Overview of rational drug design 43
2.3. Binding analysis of ISRIB with S. pombe eIF2B: Docking studies 44
2.4. Rational behind the design of ISRIB analogues 47
2.4.1. Truncated non-symmetrical ISRIB analogues 50
2.4.1.1. Synthetic strategy 51
2.4.1.2. Synthesis of truncated ISRIB analogues 52
2.4.2. Modification of the terminal aromatic rings 54
2.4.2.1. Synthetic strategy 56
2.4.2.2. Synthesis of of acid chloride and acid carboxylate fragments: *O*-arylglycolamide or *O*-heteroarylglycolamide side chains 57
2.4.2.3. Synthesis of non-symmetrical modified terminal aromatic ring analogues 59
2.4.2.4. Synthesis of symmetrical modified terminal aromatic ring analogues 62
2.4.3. Glycolamide linker modification 63

2.4.3.1. Synthetic strategy 66
2.4.3.2. Synthesis of non-symmetrical modified glycolamide linker analogues 67
2.4.3.3. Synthesis of reverse amide analogues 71
2.4.3.4. Synthesis of symmetrical modified glycolamide linker analogues 73
2.4.4. Modification of the central core-template that joins the O-arylglycolamide side chains 73
2.4.4.1. Synthetic strategy 77
2.4.4.2. Synthesis of aromatic, spiro, bicycle and acyclic central diamine core 78
2.4.4.3. Attempted synthesis of diamino-cyclohexanetetrol and but-2-ynediamide central core 80
2.4.4.4. Synthesis of 4-aminopiperidine and piperazine analogues 81
2.5. Conclusions 86
3. Pharmacological evaluation and structure-activity relationships of ISRIB analogues 89
3.1. Introduction 89
3.2. Biological assay to to measure the potency of ISRIB analogues 91
3.3. Pharmacology results and SAR of synthetic ISRIB analogues: 94
3.3.1. Pharmacology results: Truncated ISRIB analogues 94
3.3.2. Pharmacology results: Terminal aromatic ring-modified analogues 96
3.3.3. Structure-activity relationships of ISRIB analogues modified at the terminal aromatic moiety 99
3.3.4. Pharmacological results: Linker Modification 100
3.3.5. Structure-activity relationships of ISRIB analogues modified at the glycolamide linker 106
3.3.6. Pharmacological results: Central core ring modification 108
3.3.6.1. Aromatic, aliphatic, spiro and bicyclic analogues 108
3.3.6.2. Piperidine and piperazine analogues 112
3.3.6.3. Structure- activity relationships of ISRIB analogues modified at the central core ring 115
3.4. Conclusions 116
4. Fluorescent eIF2B ligand based on ISRIB modifications: Design, synthesis and evaluation 120
4.1. Introduction 120
4.2. Design of fluorescent ISRIB analogues 121
4.2.1. Identifying the appropriate site for fluorescent molecule attachment 122
4.2.1.1. Terminal aryl ring 123
4.2.1.2. Central cyclohexane core ring 124
4.2.1.3. Glycolamide linker: chromane, benzodioxane and benzoxazine analogues 126
4.2.2. Determining a suitable linker for Fluorescent ligation 128
4.3. Synthetic strategy 129
4.3.1. Synthesis of modified terminal ring analogue 130
4.3.2. Synthesis of modified core ring analogues 131
4.3.3. Synthesis of tethered glycolamide linkers (six-membered ring) 135
4.3.3.1. Synthesis of chromane and oxo-chromane fragments 135
4.3.3.2. Synthesis of benzodioxane and benzoxazine fragments 136
4.3.3.3. Synthesis of the chromane, benzodioxane and benzoxazine analogues 137
4.3.3.4. Synthesis of symmetrical analogues 138
4.3.4. Synthesis of fluorescent-ISRIB analogues 139
4.4. The biological evaluation of ISRIB-analogues 143
4.4.1. Pharmacology results and SAR of ISRIB analogues 144
4.4.1.1. Pharmacology of terminal rings and central core modifications 144
4.4.1.2. Pharmacology of glycolamide linker modifications: chromane, benzodioxane and benzoxazine analogues 146
4.4.1.3. Pharmacology of benzoxazine aniline-linker analogues 149

4.4.2. Fluorescence polarisation competition assay: general principle 152
4.4.2.1. Development of an eIF2B fluorescence polarisation assay 154
4.4.3. Mutagenesis cell analysis of the putative ISRIB-binding site 156
4.5. Conclusions 157
5. *In vitro* disposition studies of ISRIB and its analogues 159
5.1. Introduction 159
5.2. Solubility of ISRIB 161
5.3. Development and validation of simple and sensitive LC-MS/MS quantitative analytical method for detection of ISRIB analogues in in vitro studies 163
5.3.1. Validation criteria of LC-MS/MS developed method 164
5.3.1.1. Selectivity and sensitivity of LC-MS/MS method 164
5.3.1.2. Accuracy and precision of LC-MS/MS method 165
5.3.1.3. Linearity of LC-MS/MS method 165
5.4. Results and discussion 166
5.4.1. Optimization of the method 166
5.4.2. LC-MS/MS Method validation 167
5.4.2.1. Selectivity, Linearity and LLOQ 167
5.4.2.2. Accuracy and precision 170
5.4.3. Application of the developed method to in vitro ADME studies 171
5.4.3.1. Aqueous solubility assay 171
5.4.3.2. Microsomal stability assay 172
5.4.3.3. Caco-2 Permeability assay 174
5.5. ISRIB formulations 176
5.6. Conclusions 178
6. Conclusions and future work 180
6.1. General conclusions 180
6.1.1. Truncated and terminal ring-modified analogues 181
6.1.2. Glycolamide linker modification 182
6.1.3. Central core ring modification 184
6.1.4. Design and synthesis of a novel labelled ISRIB derivatives 187
6.1.5. *In vitro* ADME parameters assessment for ISRIB and other promising analogues 189
6.2. Future work 191
7. Experimental 197
7.1. Assays 197
7.1.1. CHOP::GFP assay 197
7.1.2. Aqueous solubility assay 198
7.1.2.1. Stock and working standard solutions preparation 198
7.1.2.2. Calibration curve and quality control (QC) samples preparation 198
7.1.2.3. LC-MS/MS method development and validation 198
7.1.2.4. Aqueous Solubility assay procedure 199
7.1.3. Permeability assay 200
7.1.3.1. Cell culture 200
7.1.3.2. Passage of cells 200
7.1.3.3. Seeding of cells 200
7.1.3.4. Caco-2 permeability assay 201
7.1.4. *In vitro* liver microsomal stability assay 201
7.1.5. Fluorescence polarization assay 203
7.2. ISRIB formulations 204
7.3. General Chemistry 205
Reference 310
Appendix 329

1. Introduction

Translation is the biological process by which messenger RNA is translated into proteins. Cells activate an intracellular signalling cascade to cope with the diverse array of stress stimuli. Members of this cascade regulate translation initiation factors in order to alleviate cellular injury.[1]

In the introduction, the mechanisms of translation initiation in eukaryotes will be explained. The focus will particularly be on the function, regulation, and structure of eIF2α and eIF2B. Moreover, the connection of these two factors with the unfolded protein response/integrated stress response (UPR/ISR) and the neurodegenerative disorders will also be reviewed. Furthermore, all the previous medicinal chemistry trials to target eIF2B in order to treat dementia will be shown in details.

1.1. Translation of mRNAs

mRNAs are translated in the 5´ to 3´ direction, and polypeptide chains are synthesized from the amino to the carboxy terminus.[2] Each amino acid is encoded by three bases in the mRNA called a codon, according to a nearly universal genetic code. Translation is performed on the ribosomes, tRNAs function as adaptors to facilitate the interconnection of the mRNA template and the amino acids being synthesised into protein.[3] mRNA translation consists of four basic stages: initiation, elongation, termination, and recycling.[4, 5] The initiation phase is known as the most principal step in protein synthesis. In

initiation, the ribosome is assembled at the initiation codon in the mRNA with a methionyl initiator tRNA bound in its peptidyl site (**Figure 1.1)**.[6]

The eIF2 has a principal role in the regulation of the rate-limiting step in translation process. During this step, eIF2 binds GTP and Met-tRNAi and facilitate the transferring of Met-tRNAi to the 40S ribosomal subunit. At the end of the initiation step, GTP bound to eIF2 is converted to GDP and subsequently the eIF2_GDP complex is released from the ribosome. This exchange is principally regulated by a second initiation factor, eIF2B.[7, 8]

Phosphorylation of eIF2 is thought to be the best understood mechanism to study the regulation of eukaryotic protein synthesis. Phosphorylation of the α- subunit results in conversion of eIF2 from a downstream target of eIF2B into a competitive inhibitor. As a result, phosphorylation of eIF2 on its α subunit leads to efficient inhibition of the formation of the eIF2_GTP_Met-tRNAi complex (known as ternary complex) and thus represses mRNA translation. A variety of abnormal medical and biological conditions leads to the phosphorylation of eIF2α such as viral infection, anaemia, apoptosis-associated disorders and certain stresses.[7, 9, 10]

The initiator tRNA must have a unique function distinguished from those of other tRNAs. It escapes binding to elongation factors; however, it binds directly to the ribosomal P site. This binding is efficiently carried out by the assistance of initiation factors. It also has an essential function in decoding the start codon, fine-tuning the frame for translation of the mRNA. Identity elements and modifications of the initiator tRNA are distinct from the elongator methionyl tRNA and aid it in carrying out its functions. These sequence elements set the

frame of the body of the initiator tRNA. Huge evidence indicates that the structure of the tRNA is crucial in transmitting the signal that the start codon has been established to the rest of the pre-initiation machinery.[11]

Despite the known fact that 43S complexes are substantially capable of 5'-end-dependent attachment to model mRNAs with entirely undefined 5'-UTRs, natural 5'-UTRs own fundamental secondary structure that loading of 43S complexes onto them demands the mutual action of eIF4F[12] and eIF4B or eIF4H. They play a key role in unwinding the cap in the 5'-UTR of mRNA and then preparing it for ribosomal binding.[13] eIF4F comprises the cap-binding protein eIF4E, the DEAD-box RNA helicase eIF4A and eIF4G, which functions as a "scaffold" that binds eIF4E, eIF4A, the poly(A)-binding protein (PABP) and eIF3.[14] The eukaryotic elongation factor eEF1A which is ortholog of the bacterial EF-Tu, attaches to the aminoacyl-tRNA in a GTP-dependent manner and subsequently immediate the tRNA to the A site of the ribosome complex.[15] When the tRNA recognizes the codon, it elicits GTP hydrolysis by eEF1A, releasing the factor and enhancing the aminoacyl-tRNA to be attached into the A site of the machinery.[16] mRNA translation termination happens when a stop codon enters the A site of the ribosomal machinery. It is mainly regulated by release factors eRF1 and eRF3 in eukaryotes. These factors produce a ternary eRF1/eRF3–guanosine triphosphate (GTP) complex. eRF1 functions to recognize the stop codon and then releases the newly formed protein. Simultaneously, it mediates GTP hydrolysis.[17]

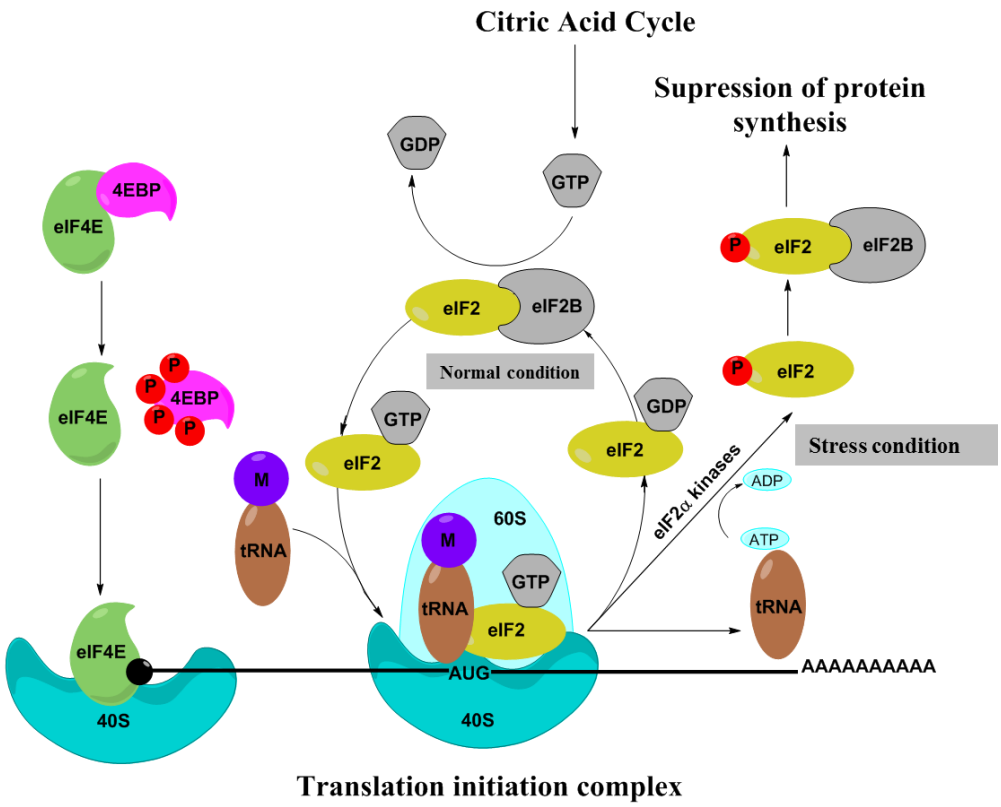


Figure 1.1: Eukaryotic translation initiation complex. The diagram shows the translation initiation machinery comprising methionyl tRNA, eIF2 and GTP assembles on the ribosomal subunits. It also shows the role of eIF2 in the regulation of this process. The Krebs cycle, which takes place in the mitochondria, produces ATP. ATP is produced by the enzyme ATP synthase, which converts ADP and phosphate to ATP. Hydrolysis of ATP to ADP and Pi is the source of phosphate in this reaction. ([13] with modification).

1.1.1. Regulation of eukaryotic translation initiation factors 2 (eIF2)

Recently, a considerable interest has grown in illustrating the regulatory mechanisms of mRNAs translation initiation and presenting their interconnection to neurodegenerative diseases.[18] The activity of numerous eukaryotic initiation factors is thought to be regulated through post-translational modifications for example phosphorylation, of specific binding proteins or both.[19] The most principal effectors of initiation step will be discussed in the following sections.

1.1.1.1. Phosphorylation of eIF2

Modification of eukaryotic translation initiation factors 2 activity is a major regulatory mechanism in global protein synthesis. eIF-2 is regulated through phosphorylation of single serine residue in the alpha subunit (known as Ser^{51}). In different cell types, four kinases control eIF2α phosphorylation in response to diverse stimuli.[20, 21] First, Protein kinase RNA (PKR), which is enhanced by double-stranded RNAs. Second, Haem-Regulated Inhibitor kinase (HRI), which is stimulated by deprivation of haem and also in osmotic or heat shock. Third, General Control Non-depressible GCN-2 which is triggered by conditions associated with amino acid starvation, and finally PKR-like endoplasmic reticulum kinase (PERK) which responds to ER stresses such as low levels of glucose and calcium, hypoxia as well as improper protein folding.

In addition, phosphorylation of multiple serine residues in the beta subunit of the global eukaryotic initiation factor 2 (known as $Ser^{2, 13, 67, 218}$) plays a role in its regulation too. The phosphorylation of β subunit is largely mediated by two protein kinases which are the Protein kinase C (PKC) and the cAMP-dependent protein kinase (PKA), that are indicated to modulate eIF2B activity at least *in vitro*.[22-24]

Basically, phosphorylation of the global eukaryotic initiation factor on its alpha subunit extremely impedes its binding to eIF2B leading to interception of the GDP.eIF2/GTP.eIF2 recycling, and eventually causing inhibition of cellular protein synthesis. On the other hand, the non-phosphorylated form of the global factor functions as a substrate to preserve eIF2B activity under normal physiological needs. Depending on the well-known fact that eIF2α shows higher

expression than eIF2B, one could conclude that a partial phosphorylation of the former is adequate for entire confinement of the latter.[25]

However, an exception to this role exists. It was found that the translation of transcripts harbouring upstream open reading frames (uORFs) is enhanced jointly with phosphorylation of eIF2α.[26] Activating transcription factor (ATF4) is a representative example of this regulatory mechanism. These transcripts contain a highly defined 5' methylated cap in their untranslated regions. Thus, they are normally weakly engaged in protein synthesis as the presence of the uORFs impairs the ribosomal machinery from attaching the target sequence in the RNA template. Sequestering eIF2B function leads to a reduction in the concentration of ternary complex, enabling the 40S ribosome complex to turn off the prohibiting ORF area and approach the coding region where it is replenished by a ternary complex and translates the target polypeptide chain.[27]

1.1.1.2. Regulation of eIF2B

The eukaryotic translation initiation factor 2 B (eIF2B) is a principal regulator of the general protein synthesis, serving as a guanine nucleotide exchange factor and controlling the recycling of the heterotrimeric G-protein, eIF2, which is a fundamental translation initiation factor as we mentioned earlier in this chapter.[28] Regulation of eIF2B occurs by multiple mechanisms. The eIF2B is considered to be a phosphoprotein and diverse phosphorylation sites have been indicated to be essential for its basal function as well as regulation of its activity. Besides the indirect impact of eIF2α phosphorylation on the regulation of eIF2B function, eIF2B activity is also regulated by direct phosphorylation by four kinases: CK1, CK2, Dual-specify Tyrosine Phosphorylated and Regulated Kinase (DYRK) and Glycogen Synthase Kinase 3 (GSK3). The GSK3 phosphorylates Ser^{535} in the ε

subunit of the human eIF2B in response to low insulin levels and thus negatively affects the function of the complex. This effect is mainly triggered by phosphorylation of Ser^{539} by the kinase DYRK.[29, 30] Moreover, phosphorylation of Ser^{525} occurs in response to conditions of amino acid deprivation and again results in repression of the complex activity. However, the kinases responsible for the latter modulation are still not well studied.[31]

Moreover, it has been shown that yeast eIF2B activity is impeded by the metabolic products of some amino acids such as butanol and 3-methylbutan-1-ol; however the underlying mechanism by which this happens is still not well understood.[32]

Various forms of eIF2B complex may exist in cells, the complete decamer complex and pentamer complex without eIF2Bα subunit.[33, 34] The expression of the individual subunits in the eIF2B complex is intrinsic to define the activity and also to determine its regulation by the main effectors of the integrated stress response (ISR). Interestingly, it has been found that incomplete eIF2B complexes is associated with a reduction in the GEF activity. The absence of the alpha subunit deems the eIF2B complex insensitive to the phosphorylated form of eIF2*α*. Accordingly, it has been concluded that the lack of eIF2Bα in cells leads to a decline in eIF2B activity. However, this makes the complexes insensitive to the inhibitory effect of eIF2 phosphorylation. Researcher have found that the interconnection of the alpha subunit with the other subunits of the complex is transient.[34, 35] Thus, regulation of eIF2B*α* expression levels sets the frame of the cellular response to ISR.

1.2. Structure of eIF2B

Eukaryotic translation initiation factor 2 B (eIF2B) is a multisubunit non identical decameric complex of two sets of each of the α-, β-, γ-, δ- and ε-subunits (**Figure 1.2**).[34, 36, 37] The α-, β- and δ-subunits form the regulatory subcomplex.[38] On the other hand, the γ- and ε-subunits constitute the catalytic subcomplex.[39] Researchers have demonstrated the crystal structure of eIF2B isolated from *Schizosaccharomyces pombe* as a native structure with a novel subunits arrangement.[40, 41] The two αβδ trimeric regulatory subcomplex binds two γε dimeric catalytic subcomplexes on its opposite sides. The interface for eIF2 was identified by performing surface-scanning photo-cross-linking analysis. The eIF2α-binding interface was found to be located far apart on the regulatory subcomplex, whereas the eIF2γ-binding interface is located on the catalytic subcomplex. The eIF2γ-binding interface is located in close proximity to the conserved NF motif and heat domain which are both in the ε subunit. The latter subunit is considered to be crucial for nucleotide exchange activity. Furthermore, a structural study was conducted showing the interconnection of the eIF2B complex with the phosphorylated form of eIF2α. The phosphorylated eIF2 generates a more robust connection than the unphosphorylated eIF2. Overall, these data showed that the phosphorylation of eIF2α produces non efficient eIF2–eIF2B complex[42], that abolishes nucleotide exchange on eIF2γ. Accordingly, it supports a structural basis for the eIF2B-mediated regulation of stress-induced translational regulation.[43]

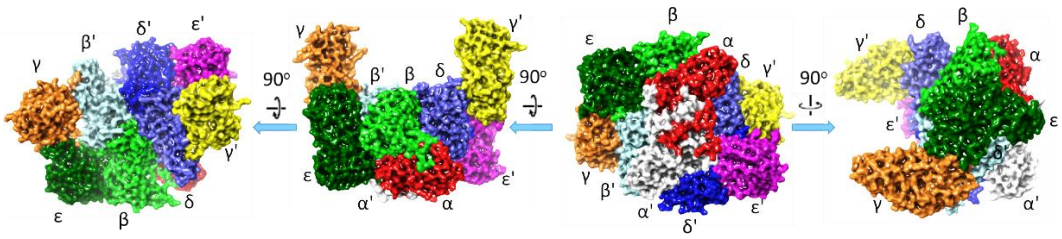


Figure 1.2: Overall structure of eIF2B according to *S. pombe* structure (PDB 5B04).[40] The α, β, γ, δ, and ε subunits showed in red, light green, brown, light blue and dark green, respectively. While, the α', β', γ', δ', and ε' subunits showed in grey, cyan, yellow, dark blue and purple, respectively; (generated using Schrödinger Maestro software).

Recently, in 2018 we determined the three-dimensional structure of the entire human eIF2B complex by cryo–electron microscopy (cryo-EM) at 4.1 Å.[44] In this study, human eIF2B bound to integrated stress response inhibitor (ISRIB) was purified from HeLa cell lysates and the structure of the complex was determined by cryo–electron microscopy.[44] Simultaneously, researchers have also found similar description of the eIF2B-ISRIB using cryo-EM as well.[45-47] The above studies are in parallel with the previous study published by Kashiwagi, [40] as they showed a high degree of similarity in the structure of human eIF2B and that of *Schizosaccharomyces pombe*.

1.3. The eIF2 kinases: coping with stress

In response to environmental stresses, a family of protein kinases phosphorylates eIF2 (eukaryotic initiation factor 2) to alleviate cellular injury or alternatively induce apoptosis.

1.3.1. Endoplasmic reticulum

The endoplasmic reticulum (ER) is a major site for folding and maturation of secretory, transmembrane, and ER resident proteins.[48] Disturbances that alter ER homeostasis result in accumulation of unfolded proteins (UPs), which is

considered as an impendence to all living cells.[49] As a protective feedback mechanism, cells activate an intracellular signalling cascade called the unfolded protein response (UPR) to cope with the cellular stress.[50] The UPR is an integrated intracellular signal transduction pathway functions to convey information about the protein folding status in the ER lumen to the cytoplasm and the nucleus.[51]

1.3.2. Unfolded protein response

In response to diverse ER stressors, eukaryotic cells activate a common signalling pathway, termed the unfolded protein response (UPR), to restore a conducive environment for proper protein folding.[52-54] Disruptions of the endoplasmic reticulum (ER) that perturb protein folding cause ER stress and elicit an unfolded protein response (UPR) that involves translational and transcriptional changes in gene expression aiming at expanding the ER processing capacity and alleviating cellular injury.[50, 55, 56] Three ER stress sensors implement the UPR: (1) the inositol-requiring transmembrane kinase/endoribonuclease 1 (IRE1), (2) the double-stranded RNA (PKR)–activated protein kinase-like eukaryotic initiation factor 2α kinase (PERK); and (3) the activating transcription factor-6 (ATF6) (**Figure 1.3**).[50, 57, 58]

IRE1 is considered the most conserved arm of the unfolded protein response. It presents in most species from yeast to humans. Mammalian IRE1 consists of two homologues, IRE1α and IRE1β.[59] The former is expressed in all cells and tissues, whereas the latter is specifically expressed in the intestinal epithelium.[60] IRE1α plays a key role in UPR, however the function of IRE1β in the UPR is still not fully understood. Activation of IRE1α results in cleavage of a 26-base fragment from the transcript encoding the X-box binding protein-1 (XBP1).[61] Spliced

Xbp1 transcript is translated into an active transcription factor, XBP1s, which controls transcriptional output of a wide variety of genes encoding proteins involved in the regulation of ER membrane biogenesis, ER protein folding and protein secretion from the cell.[62]

PERK is the second branch of the UPR signalling. It is structurally related to IRE1α, with an ER luminal dimerization domain and a cytosolic kinase domain. The principal effect of active PERK is the phosphorylation of the α subunit of eukaryotic translational initiation factor 2α (eIF2α) at Ser[51].[63, 64] This post-translational modification represses cellular protein synthesis to attenuate protein influx into the ER lumen.[65] Furthermore, it has been shown that phosphorylation of eIF2α alters the efficiency of initiation codon utilization (AUG) resulting in preferential translation of activating transcription factor-4 (ATF4).[66] ATF4 is a transcription factor that controls the transcriptional output of genes involved in ER function, ER stress– induced apoptosis, ER stress–mediated production of reactive oxygen species, as well as an inhibitory feedback mechanism through dephosphorylation of eIF2α to attenuate hyperactivation of the UPR signalling.[67] It has also been demonstrated that PERK can phosphorylate nuclear erythroid 2 p45-related factor 2 (NRF2) to induce the expression of antioxidant response genes such as heme oxygenase 1 and glutathione S-transferase.[68] Overall, the PERK–eIF2α branch of the UPR signalling regulates the redox balance during ER stress through activation of ATF4 and NRF2. PERK-mediated activation of ATF4 is upstream activator of transcription factor C/EBP homologous protein (CHOP), which is one of the ER stress pathways and is involved in apoptosis. Although CHOP is predominately activated by PERK signalling, IRE1 and ATF6 are involved in its upregulation as well.[69-71]

ATF6α is considered the third branch of the mammalian UPR signalling that is an ER-associated type 2 transmembrane basic leucine zipper (bZIP) transcription factor. ATF6β is a distant homologue of ATF6α. However, both of them are ubiquitously expressed in all tissues. After being released from BiP, ATF6α traffics to the Golgi apparatus for cleavage by serine protease site-1 (S1P) and metalloprotease site-2 (S2P). This allows the release of the transcription-activating form of ATF6, pATF6α(N).[72] The pATF6α(N) independently or synergistically acts with XBP1s in order to induce the expression of UPR target genes. The role of pATF6α(N) in mammalian development is not well-understood. Researchers found that mice lacking ATF6α do not show any fatal abnormalities. However, ATF6α-null mice have been found to be exquisitely sensitive to ER stress. Moreover, it has been demonstrated that embryonic lethal phenotype is associated with deletion of both ATF6α and ATF6β.[73, 74] Thus, the common function(s) of ATF6α and ATF6β is not fully understood and functional redundancy in early development is suggested.

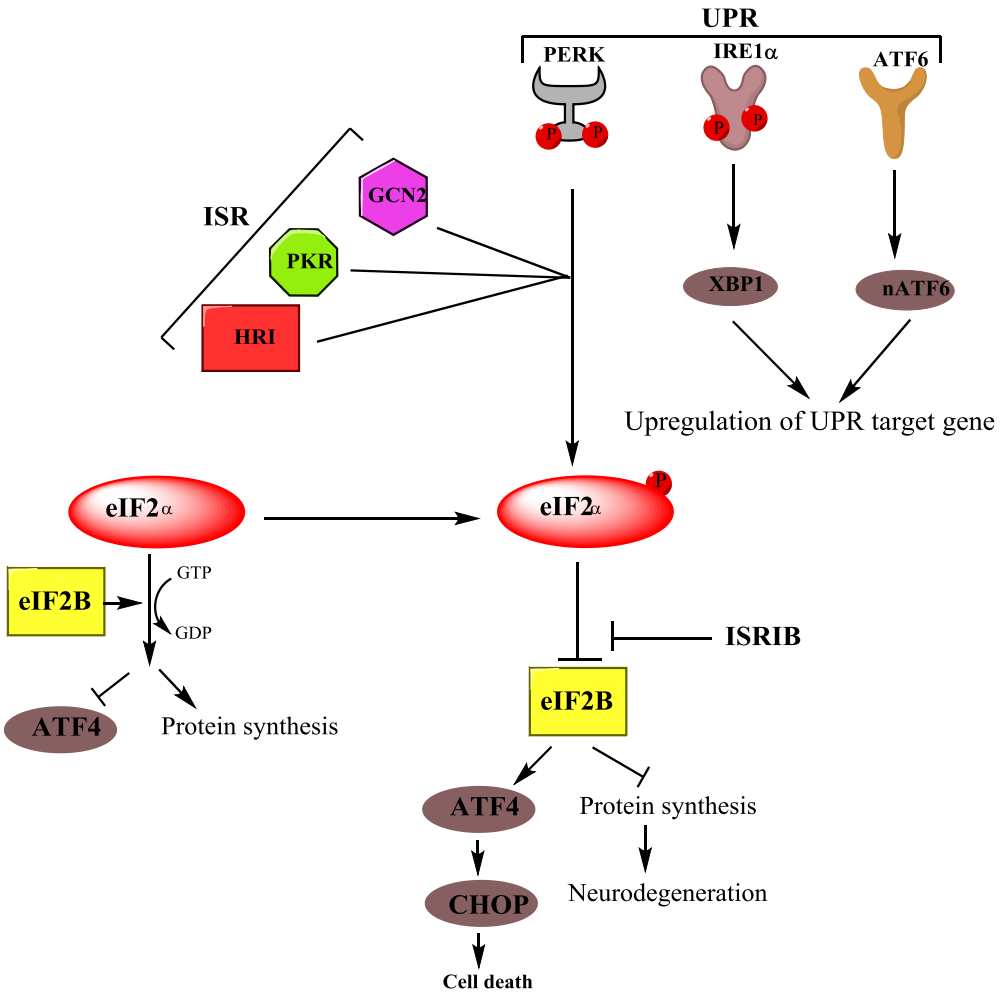


Figure 1.3: Scheme of the UPR/ISR signalling through eIF2α-P. Unfolded proteins can be detected by the components of the endoplasmic reticulum (ER) and that lead to unfolded protein response (UPR). This in part results in activating PERK which leads to phosphorylation of alpha subunit of eIF2α, which in turn results in reduced protein synthesis by preventing translation at the initiation level. eIF2α-P also leads to induced translation of specific transcription factor that induces the transcription of genes encoding for apoptotic proteins and enzymes for amino acid metabolism such as ATF4, which leads to activation of apoptosis pathway CHOP ([75] with modification).

1.3.3. Integrated stress response

In addition to the above-mentioned kinases in **1.2.2**, there are three other kinases that phosphorylate eIF2α in ISR pathway in response to diverse stress stimuli. These kinases are activated by various cellular stresses: general control nonderepressible-2 (GCN2) responds to amino acid starvation, the double-stranded RNA-activated protein kinase (PKR) activated during viral infection and the heme-regulated inhibitor kinase (HRI) activated in response to heme

deficiency. The cytoprotective signalling initiated upon phosphorylation of eIF2α through these kinases is known as the integrated stress response (ISR) (**Figure 1.3**).[76 77, 78]

Endoplasmic reticulum (ER) stress-induced activation of PKR-like ER kinase (PERK) and subsequent eukaryotic translation initiation factor 2α (eIF2α) phosphorylation lead to a repression of cyclin D1 protein expression, and thus cell cycle arrest in G1 phase. However, it is still not fully understood whether PERK is solely responsible for regulating cyclin D1 accumulation after activation of unfolded protein response pathway (UPR). It has been demonstrated that UPR dependent-cyclin D1 translational repression occurs independently of PERK. However, it remains dependent on phosphorylation of eIF2α. It has been found that phosphorylation of eIF2α in PERK-/- fibroblasts is attenuated, but not eliminated. This indicates that another eIF2α kinase functions in the absence of PERK. Researchers showed that PERK and GCN2 function to cooperatively regulate eIF2α phosphorylation and cyclin D1 translation after UPR activation.[69, 79]

GCN2 is a key sensor of amino acid availability and responsible for regulation of gene expression in response to amino acid deprivation and glucose deprivation in both yeast and mammalian cells.[80] However, the underlying mechanism is not well defined. Recent studies have shown that GCN2 is activated by other stimuli such as viral infection and UV irradiation.[81] GCN2 is structurally more complicated than other eIF2α kinases such as PERK and PKR. In addition to the typical eukaryotic kinase domain, it harbours a pseudo-kinase domain as well as a histidyl-tRNA synthetase (HisRS)-related domain. The latter has high binding affinity toward uncharged tRNAs than charged tRNAs. Activation of GCN2

occurs upon binding of uncharged transfer RNAs (tRNAs) to the HisRS domain of the protein. These accumulate in conditions with essential amino acids deprivation or when the synthesis of non-essential amino acid is attenuated. Like other eIF2α kinases, dimerization is thought to be central for activation.[82] Furthermore, autophosphorylation in the kinase activation loop at Thr^{882} and Thr^{887} is fundamental for optimal kinase activity. At present, the only identified downstream target of GCN2 is eIF2α.[83]

PKR was initially thought to be a kinase that phosphorylates eIF2α in response to viral infection, in order to block viral protein synthesis and induce apoptosis. Thereafter, it has been indicated that PKR has also a major role in cellular physiology. It can be activated in response to a variety of signals such as oxidative and ER stress, inflammatory signalling and growth factors. Furthermore, it plays a central role in the pathology of obesity as well as different kinds of tumours.[84] PKR is localized in the cytoplasmic and nuclear compartments and at its regulatory N-terminal region contains a double-stranded RNA binding domain (dsRBD) that composed of two ~70-amino-acid dsRNA binding motifs that are separated by an unstructured linker region. The C-terminal kinase domain constitutes the dimerization interface essential for PKR activation and performs the catalytic functions of the protein.[85] A pivotal characteristic that identifies PKR from the other eIF2α kinases is the variety of its downstream targets. In addition to the eIF2α, PKR can phosphorylate p53, facilitate activation of the STAT transcriptional activity as well as it can induce mitogen-activated protein kinase (MAPK) activity. Moreover, PKR induces nuclear factor-kappa B (NF-κB) activity, probably through activating the upstream inhibitor of κB kinase (IKK) complex.[86, 87]

The HRI kinase plays two major functions during development; it is implicated in coupling the synthesis of globin genes to the cellular level of heme.[88] Also it induces the survival of erythroid precursors when iron levels are deprived. It also functions in responses to stresses such as proteasome inhibition and arsenite exposure through not fully explained mechanisms.[89, 90]

The HRI protein has five domains. The unique domains which are the *N*-terminus and C-terminus. Also, the protein harbours two kinase regions flanking a central kinase insert (KI) domain. It has been found that heme molecules bind to both the *N*-terminus and KI regions. The *N*-terminus contains the stable heme binding site, required for hem's regulation of HRI. However, the KI harbours the reversible heme-binding site. The binding of heme molecule at both sites is regulated by flanking histidine residues.[91]

1.3.4. eIF2-eIF2B complex in normal and UPR conditions

The phosphorylated form of eIF2α fundamentally recognized by the central hexamer of the eIF2B (α2β2δ2). The central cavity, which is composed of one set of the α-, β-, and δ-subunits and located at each pole of the central hexamer, has a significant function in performing this role.[40, 41] It has been found that the interaction mode between eIF2 and eIF2B is dramatically changed by the phosphorylation status of eIF2. The unphosphorylated and phosphorylated forms of eIF2 localizes in distinct ways in the eIF2B central cavity. The eIF2-eIF2B complex has been identified at an overall resolution of 4.3 Å. The γ subunit of unphosphorylated eIF2 is sandwiched between the HEAT domain and the main body of eIF2Bε (**Figure 1.4**, **I**). This complex is considered as the "productive" form, in which eIF2B aids nucleotide exchange on eIF2. The *N*-terminal domain

(NTD) of eIF2α is identified by the β- and δ-subunits of the eIF2B central cavity.[47, 41]

On the other hand, eIF2(αP)-eIF2B complex, was recognized at an overall resolution of 4.6 Å. It has been shown that the binding mode of eIF2(αP) is different from that of the unphosphorylated eIF2. The NTD of the phosphorylated eIF2α extends between the α- and δ-subunits of the eIF2B, and eIF2γ docks onto eIF2Bγ (**Figure 1.4**, **II**). In this mode, eIF2γ does not interact with eIF2Bε, and the HEAT domain is not recognized at a fixed position. Accordingly, this complex is known as the non-productive structure as the nucleotide exchange function is deteriorated in response to stress conditions.[47]

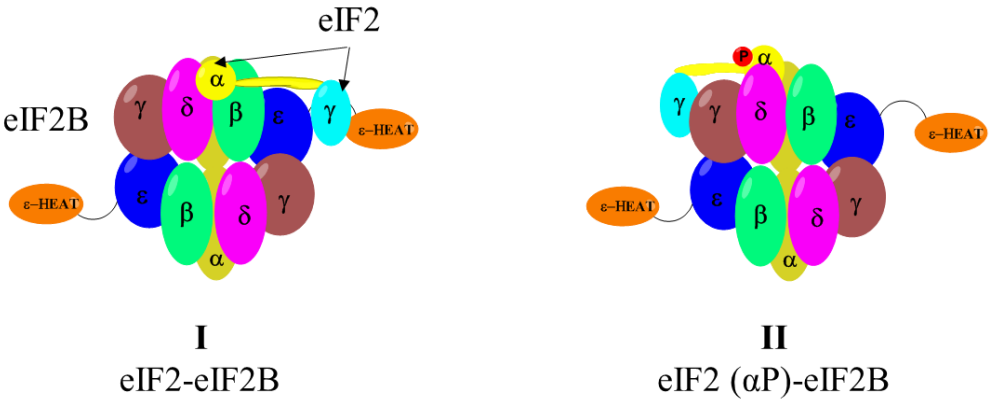


Figure 1.4: The structures of the eIF2-eIF2B and eIF2(αP)-eIF2B complexes. In model (I) the γ subunit of eIF2 is accommodated between the HEAT domain and the main body of eIF2Bε. Model (II) shows the docking of the γ-subunit of eIF2(αP) onto eIF2Bγ.

1.4. Neurodegenerative diseases

Neurodegenerative disorders are typically defined by progressive loss of selectively vulnerable populations of neurons, which contrasts with select static neuronal loss because of metabolic or toxic disorders. Neurodegenerative diseases can be broadly classified depending on their primary clinical features (e.g., dementia, Parkinsonism, or motor neuron disease). They can also be

classified according to the anatomic distribution of neurodegeneration (e.g., frontotemporal degenerations, extrapyramidal disorders, or spinocerebellar degenerations), or by their principal molecular abnormality.[92] The well-known neurodegenerative disorders are amyloidosis (Gerstmann –Stra¨ussler–Scheinker disease, familial British dementia and Alzheimer's disease), tauopathies (chronic traumatic encephalopathy, primary age-related tauopathy a-synucleinopathies, and Pick's disease) and TDP-43 proteinopathies (frontotemporal lobar degeneration and amyotrophic lateral sclerosis). The protein abnormalities present in these diseases show abnormal conformational properties.[93]

Dementia is a major and growing cause of morbidity and mortality worldwide, particularly in the elderly. Alzheimer's disease is the most common form of dementia worldwide and makes up 60%–80% of all dementia cases, affecting an estimated 24 million people globally. Although it can occur in younger persons, it is primarily a disease of the elderly. The prevalence of AD increases markedly with advancing age, with a greater than 15-fold increase reported between the ages of 65 and 85.[94]

With the advent of the basic machinery of the UPR signalling, it was found that all neurodegenerative diseases display characteristics of activated UPR or at least part of its signalling pathway. Importantly, UPR is considered as a crucial target to develop new modalities to prevent and treat neurodegenerative diseases by repressing the activity of specific effectors in this signalling pathway.[95] Later on in this chapter, we will review evidence for UPR/ISR activation in each neurodegenerative disorder individually and trials for targeting this signalling in a variety of models.

1.4.1. Molecular pathology of neurodegenerative diseases

Neurodegenerative disorders are defined by selective abnormality and progressive loss of synapses, neurons, glial cells and their networks. In addition, the diseases are characterized by pathological alteration in proteins that deposit primarily in the human brain and spinal cord.[96]

Researchers have proposed mechanisms to explain the pathological consequences of the neurodegenerative disorders which result in dementia and the resulting diversity of their disease phenotypes. They indicated five key explanations, specifically: 1) neurodegenerative disorders could be the direct consequence of neural ageing; 2) ageing may lead to differential breakdown of neuroanatomical pathways; 3) degeneration of anatomical pathways may cause the formation of 'reactive' proteins; 4) these proteins may behave as 'prion-like' proteins and spread along anatomical pathways; and 5) neurodegenerative disorders may be defined by diversity, heterogeneous phenotypes, and complicated pathology.[97, 98]

Persistent endoplasmic reticulum stress is considered to be a major characteristic of most neurodegenerative disorders including Parkinsonism, Alzheimer's disease and others.[75, 99] The ISR signalling has a key function in regulating intracellular homeostasis in diverse physiological conditions. Abnormal regulation of this signalling is found to be a significant etiologic factors in the pathogenesis of a many types of neurodegenerative diseases.[42] Dysregulation of ER signalling has been shown to be the main causative factor for neurodegenerative diseases, however chronic PERK signalling is an underlying factor leading to neuronal dysfunction-associated mortality.[100]

The UPR signalling is considered to be a key cellular response to dysregulated mRNA translation. Studies have demonstrated that chronic UPR upregulation could be measured by aberrant levels of the phosphorylated forms of both PERK and eIF2α.[101-103] Activation of UPR mediators leads to abnormal protein aggregation in the brain and subsequent development of neuropathological findings. The disclosure of ER stress mediators is used as a potential diagnostic tool for amyotrophic lateral sclerosis prognosis.[104] Upregulation of PERK has been revealed to be key underlying factor in the pathogenesis of progressive supranuclear palsy, as high levels of phosphorylated PERK and eIF2α-P were reported in the brain of *post-mortem* patients with neurodegenerative disorders.[101] In another conducted study, a high throughput genome analysis investigating for common variants implicating in the morbidity of progressive supranuclear palsy showed a single-nucleotide polymorphism (SNP) in intron 2 of the PERK gene, *EIF2AK3*.[105] Furthermore, overactivation of ER signalling was confirmed in animal models of neurodegenerative disorders. rTg4510 mice (express a repressible form of human tau) showed overexpression of the human tau mutation P301L implicated in frontotemporal dementia, whereas 5xFAD (express five mutations in amyloid beta) mice exhibit overexpression of several Alzheimer's disease-associated mutations.[106-108]

Aberrant regulation of eIF2B either by mutations or by post-translational modifications has been implicated in the development and progression of various neuronal dysfunctions such as developmental defects, intellectual impairments and neurodegeneration. Vanishing White Matter Disease (VWMD) is considered to be a profound interconnection between eIF2B dysregulation and neurodegeneration. It has been demonstrated that VWMD is principally caused

by distinct mutations in any of the five genes encoding the five subunits of the eIF2B complex. These mutations result in downregulation of eIF2B activity. The most common mutation is R113H, which is histidine to arginine mutation.[109] On the other hand, it is still not clear how eIF2B dysregulation causes hyper-sensitivity to chronic ER stress and contributes to the pathogenesis of VWMS.

1.4.2. Types of neurodegenerative disorders

1.4.2.1. Alzheimer's disease

Efficient cellular protein synthesis is mandatory to maintain synaptic plasticity and long-term memory. Growing evidence demonstrated that endoplasmic reticulum (ER) stress is intrinsically implicated in the development and progression of AD.[102, 110] Phosphorylated eIF2α has been found to dramatically repress global protein synthesis. Recently, researchers have shown that phosphorylated eIF2α is enhanced in the brain of post-mortem patient with Alzheimer's disease as well as AD animal models. Accordingly, they studied the influence of inhibiting kinases that directly phosphorylate eIF2 on the neurological manifestations such as synaptic plasticity and memory dysfunction in AD animal model. Importantly, it has been found that genetic inhibition of PERK (branch of eIF2α kinases) represses elevated eIF2α phosphorylation, restores alterations in protein synthesis and alleviates synaptic plasticity and spatial memory AD mice. Additionally, genetic deletion of the second branch of eIF2α kinases, GCN2, was associated with significant improvement in synaptic plasticity and long-term memory in AD animal model.[111]

Overall, the above findings revealed that altered phosphorylation of eIF2 is considered to be a novel molecular mechanism implicated in the pathogenesis of

AD-associated findings such as synaptic plasticity and memory deficit. More importantly, eIF2α kinases (PERK and GCN2) are suggested as potential target for the prevention and treatment of AD.

Overactivation of UPR in the brain of individuals with AD contributes to the alteration of protein aggregation and the occurrence of neuropathological features. The extracellular deposition of amyloid β protein (Aβ) fibrils and the intraneuronal accumulation of abnormally phosphorylated tau protein are considered the histopathologic hallmark of Alzheimer's disease (AD). Aβ and tau pathology in AD often follows a stereotypical pattern. This is represented as phases for Aβ deposition, based on the progressive involvement of isocortical areas, hippocampus and entorhinal cortex, basal ganglia and diencephalon, brainstem, and cerebellum. Aβ cerebral amyloid angiopathy (CAA) frequently but not necessarily associates with the parenchymal deposits and is distinguished as capillary (type 1) or non-capillary type (type 2), also showing three stages.[112, 113] The Consortium to Establish a Registry for Alzheimer's Disease (CERAD) criteria were based on the detection of argyrophilic neurotic plaques, which represent only a subset of Aβ immunomorphologies. Detecting Aβ deposits in the brain without tau pathology is not sufficient for the diagnosis of AD. Regarding tau pathology, the sequence of tau deposition starts in the transentorhinal cortex (stage I), followed by the entorhinal cortex (II), inferior (III) and middle temporal gyri (IV), followed by neocortical areas such as the occipital cortex (peristriate for stage V and striate cortex for stage VI).[114, 115]

1.4.2.2. Prion diseases

Prion diseases are fatal neurodegenerative diseases, their main pathogenic features are progressive loss of neurons, absence of inflammatory reaction, and

formation of vacuolation and also accumulation of aberrant deposits of prion protein (PrP). In diseased brain, PrP is considered the principal protein that accumulates extracellularly in the brain.[116] On the other hand, other proteins associated with other phenotypes of neurodegenerative disorders, such as hyper phosphorylated tau, amyloid-beta, and alpha-synuclein are accumulated as well. However, the mechanism of interactions of these proteins await clarification.[117]

The mechanisms which are responsible for neuropathologic features in prion disease is still not well studied. Prion disease is characterized by the accumulation of misfolded protein. Deposition of misfolded protein elicits the unfolded protein response which is considered to be a protective feedback mechanism. Overactivation of this signalling pathway leads to elevation of phosphorylated eIF2 and subsequently repression of global protein synthesis. It has been reported that deposition of prion protein in prion diseased-animal model results in persistent inhibition of cellular translation, this inhibition is mediated by phosphorylated eIF2α. Neuropathological features such as synaptic failure and neuronal loss were found to ensue from this inhibition. Studied have shown that genetic inhibition of eIF2α kinase(s) is associated with (1) a reduction in the level of the phosphorylated eIF2α, (2) a decline in the accumulation of prion protein in the hippocampus of prion-diseased mice and (3) alleviation of neurologic features including synaptic plasticity and neuronal impairment. On the other hand, using approaches to enhance eIF2α-P leads to increase morbidity and mortality in these animal models.[118] Thus, manipulation of this signalling pathway could open the gate to develop new therapies for prion disease and increasing the survival of patients.

1.4.2.3. Parkinson's disease

Parkinson's disease (PD) is a progressive neurodegenerative movement disease. It is primarily caused by the loss of dopaminergic neurons in the substantia nigra. The aetiology behind PD is not well understood. However, recently discovered clusters of genes are shown to be associated with a rare monogenic phenotype of the disorder. Furthermore, earlier research and new experimental animal studies have demonstrated important and novel insight into the molecular mechanisms involved in disease pathological progression.[119]

It has been reported that inefficient mitochondrial function, oxidative and nitrosative stress, the deposition of aberrant or misfolded proteins as well as ubiquitin-proteasome system dysfunction are shown to be the principal molecular pathways that commonly underlie the pathogenesis of PD.[120] Thus, in spite of the strong argument regarding the sole aetiology of Parkinsonism, it is very likely that oxidative stress, in addition to the mitochondrial dysfunction, are all intricately connected in a pathogenic feed-forward cycle responsible for the pathogenesis of PD.

At the molecular level, Parkinson's disease has similar underlying mechanism to the previously mentioned neurodegenerative diseases, namely the deposition of misfolded proteins in the brain. Persistent PERK overactivation has been reported in the brain of patients with PD. Recently, researchers have shown that oral administration of a PERK inhibitor (known as GSK2606414) is associated with a substantial neuroprotection through attenuation of dopaminergic neuronal loss in the substantia nigra in PD model. Similarly, downregulation of PERK signalling leads to enhancement of neuronal function in Parkinson's fly models (Pink1 and Parkin mutants).[121] Collectively, repressing PERK activity is

considered to be a major therapeutic target to inhibit the development and progression of PD.

1.5. Hopes and challenges for treatment of neurodegenerative disorders

More than 80,000 people in the UK have dementia: the majority of which is caused by Alzheimer's disease (AD), although vascular dementia and many of the related protein misfolding neurodegenerative disorders contribute to the clinical and social burden associated with dementia. Worldwide, this figure was 44.4 million in 2013, and is projected to increase to 77.6 million by 2030 and 135.5 million by 2050. Dementia is predominantly a disease of the elderly: as the population ages, the prevalence increases. Thus, paradoxically, as improvements in health and nutrition enhance longevity, the problem of aging-associated neurodegenerative disease increases, and currently no disease-modifying treatments exist.[94, 122]

1.5.1. Non disease-specific approaches

Non disease-specific approaches aim to reduce the progression of dementia. These modalities aim at increase blood flow to the brain microvasculature (using calcium channel antagonists, *e.g.* nivladipine)[123], or aim at harnessing neuroprotective effects of insulin signalling.[124] None of the above strategies have been shown to prevent neurodegeneration *in vivo*, although pre-clinical data have shown effects on amyloid load and cognition.

1.5.2. Disease-specific and protein-specific approaches

Notably, these strategies aim at reducing Aβ production or accumulation in AD. These include anti-Aβ antibodies[125], BACE inhibitors (targeting β-secretase to

reduce Aβ production from APP)[126], experimental treatments such as minocycline that reduce Aβ toxicity and alter the formation of tau species, and development of proteins and peptides aim at preventing Aβ aggregation.[127]

Researchers have investigated the amyloid cascade hypothesis in AD. They found that AD is a result of alterations in amyloid beta (Aβ) stability and accumulation. Arresting Aβ production by deactivating the first protease required for its production, β-secretase/BACE1, and leads to blocking AD progression. It has been found that small molecule (MK-8931) has a potential therapeutic effect. This drug reduces Aβ cerebral spinal fluids (CSF) production up to 92% and is well tolerated by patients. However, this great reduction in Aβ levels by BACE1 inhibition may result in severe adverse effects.[128]

In moderate AD patients, Aβ plaques have already been accumulated. BACE1 inhibitors prevent production of new Aβ plaques, and theoretically do not affect already existing Aβ deposits. Therefore, BACE1 inhibitors are potentially more useful at preventing AD progression rather than having therapeutic use.[129]

1.5.3. Targeting dysregulation of the unfolded protein /integrated stress response

Over the last decade, a growing evidence has been evolved regarding the underlying pathogenic mechanism in age-related neurodegenerative disorders.[130] Accordingly, recent studies have been conducted focusing on the dysregulation of unfolded protein/integrated stress response (UPR/ISR) as a potential therapeutic target to treat a neuropathological features associated with these diseases. It is based on *in vivo* demonstration of the neuroprotective effects of compounds identified by their ability to modulate the activity of the UPR/ISR.

These include (1) Inhibitors of eIF2 kinases such as PERK, HRI, PKR and GCN-2; and (2) modulators of the interactions between eIF2 and eIF2B, such as ISRIB and 2BAct. These compounds prevent neurodegeneration and restore cognition in various mouse models of neurodegeneration, through their effects on global protein synthesis rates in neurons. This approach is thus in contrast to the previous non disease-specific and disease-specific approaches.

1.5.3.1. Targeting eIF2, an eIF2 kinase inhibitors:

The eIF2α kinases are a family of four well-characterized serine-threonine kinases, PERK, PKR, GCN2 and HRI.[76] Altered eIF2 phosphorylation contribute to a wider range of pathological conditions. These include a range of neurodegenerative disorders, such as Alzheimer's disease[102], prion disease[116], and Parkinson's disease[119]. A multiple lines of evidence have emerged to suggest that inhibition of the eIF2 kinase are a potential therapeutic strategy for these diseases.

1.5.3.2. Drug-Receptor interaction

An insight into the drug-receptor interaction is noteworthy prior to exploring the mechanistic studies related to the known therapeutic modalities of neurodegenerative diseases. A receptor can be described as a molecule that recognizes specifically a second small molecule (for example a drug) whose binding mediates the regulation of a cellular process. Therefore, a receptor binds specifically a particular ligand. A ligand might result in activation or inactivation of a receptor.[131, 132] Drugs are categorized based on their intrinsic activity at a given receptor into the following types (**Figure 1.5**):

- Agonist binds to a protein receptor inducing its activation. Agonists are classifying into full, partial or inverse. A full agonist is characterized by high

efficacy and ability to elicit a full response upon occupying a relatively low proportion of receptors. A partial agonist produces lower activation than a full agonist, as it triggers sub-maximal efficacy even when coupling the total receptor population. Accordingly, they cannot elicit the maximal response, regardless of the concentration. An inverse agonist leads to an effect contradictory to that of an agonist, despite they interact with the same receptor binding-site.[131, 133]

- Antagonist binds to a protein receptor and mitigates the effect of an agonist. Antagonists can be classifying into competitive or non-competitive. Each class could produce either reversible or irreversible effects. A competitive antagonist interacts with the same binding site as the agonist, however it does not trigger its activation and therefore attenuates the agonist's effect. On the other hand, a non-competitive antagonist couples to an allosteric site on the receptor to inhibit activation of the receptor. A reversible antagonist interacts non-covalently with the receptor, however an irreversible antagonist covalently binds to the receptor and therefore cannot be displaced.[134]
- Allosteric modulators bind to the receptors at a site distinct from the active site. They induce a conformational alteration in the receptor, and therefore modify the affinity of the receptor for the endogenous ligand. Allosteric modulators are classified into positive or negative modulators. The former enhances the affinity, while the latter abrogates it through inducing a conformational change in the receptor.[135]

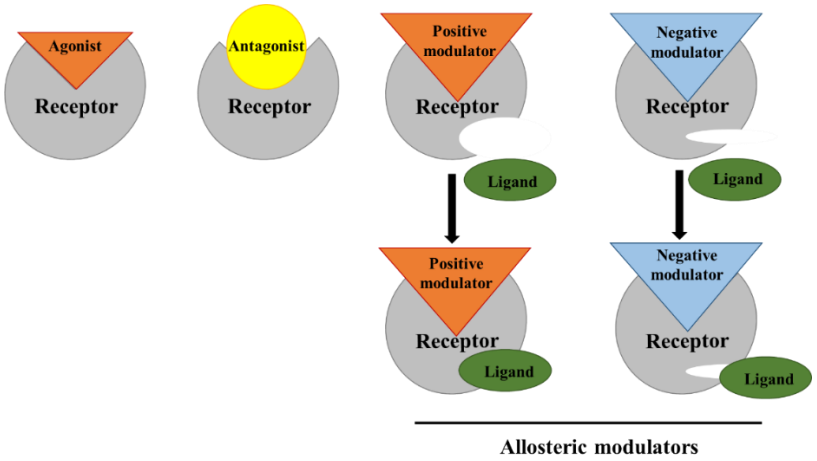


Figure 1.5: Drug-receptor interaction. This figure shows three types of drug-receptor interactions: agonist, antagonist and allosteric modulators (positive and negative).

1.5.3.2.1. PERK inhibitors

A potent PERK inhibitors, GSK2606414 **2** and GSK2656157 **3** (**Figure1.6**), have been identified for their ability to affect PERK function with an IC_{50} value of 0.4 nM and 0.9 nM, respectively.[136, 137] They are ATP-competitive inhibitors acting by downregulation the activity of PERK. Because of the excellent selectivity and potency, these compounds are considered a good tool to analyse the UPR and PERK in various therapeutic areas. These compounds were found to prevent PERK-P/eIF2α-P-mediated inhibition of protein synthesis which is responsible for the development and progression of neurodegenerative diseases.[138-140] They penetrate the blood brain barrier and reach the effective concentration after oral dosing. Crystal structure of GSK2606414 **2** in complex with PERK kinase showed a direct binding, the arylacetamide group and indoline ring both of them participate in better interaction between the inhibitor and PERK as measured in X-ray structure. In addition, the potency and bioavailability were improved by utilizing aromatic ring systems with electronic nature.[136, 141]

Since there are a variety of pathologic mechanisms responsible for the development of neurodegenerative diseases, it was thought that the inhibition of PERK with GSK2606414 **2** and GSK2656157 **3** is more desirable for neuroprotection than the focal inhibition at a later downstream level of the pathway. Although, this inhibition confers neuroprotection, it was associated with weight loss and hyperglycaemia due to insufficient insulin level which was attributed to pancreatic dysfunction.[137, 140]

It has been confirmed that PERK inhibition in PERK knockout mice is associated with abnormal pancreatic function and diabetes mellitus. PERK induces the degradation of interferon receptors (IFNAR). Consequently, the inhibition of PERK leads to an increase in the level of IFNAR and it will negatively affect the pancreatic tissues. The genetic deletion of IFNAR attenuates the pancreatic insufficiency and diabetes mellitus induced by PERK inhibition.[142]

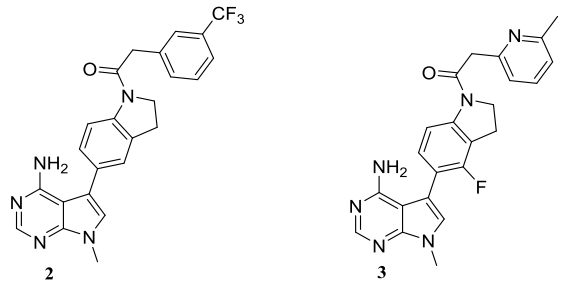


Figure 1.6: Chemical structures of PERK inhibitors: GSK2606414 **2** and GSK2656157 **3**.

1.5.3.2.2. HRI, PKR and GCN-2 inhibitors

Persistent activation of the ISR has been linked to the development of several neurological disorders, and modulation of the ISR promises new therapeutic strategies. The activity of HRI is potentially regulated by targeting two sites: the heme-binding site and the ATP-binding site. It has been found that heme is a natural repressor of HRI. When the level of heme is elevated, it targets the HRI dimer to inhibit its autophosphorylation resulting in repression of its activation.

Diffusible gases such as CO target the heme-binding domain to inhibit the activity of HRI.[143] Researchers have identified a high-throughput HRI kinase assay, to study the phosphorylation of HRI. They found that aminopyrazolindane compound **4** (**Figure 1.7**) show an ATP competitive inhibitory effect on the recombinant human HRI. The pIC_{50} for this compound is 7.5.[144] Unfortunately, this compound were characterized by low bioavailability and very rapid metabolism in rodent models. A subsequent trial was done using a group of indeno[1,2-c]pyrazoles compounds in an attempt to improve the pharmacokinetic profile. It has been found that these compounds have a more praising pharmacokinetic properties.[145]

PKR is a double stranded RNA dependent protein that has two copies of dsRNA-binding motif in its *N*-terminus. It also contains a kinase domain at the C-terminus. Thus, it has the ability to bind to numerous dsRNAs such as those that are considered as activators or inhibitors of PKR activity. It has been shown that 2-amino purine is a potential inhibitor of PKR activity by targeting its C-terminus.[146] On the other hand, 2-amino purine is considered as a non-selective PKR inhibitor as it inhibits the activity at millimolar concentration at which it also represses other kinases.[146] In another study carried out by Jammi *et al.*, ATP-binding site inhibitors were tested, they discovered a small molecule called compound #16 **5** with a PKR inhibitory effect (IC_{50} of 0.21 mM).[147]

In response to amino acids deprivation, GCN2 targets uncharged tRNAs to the HisRS resulting in translational control. Numerous GCN2 kinase inhibitors are known by their ability to inhibit eIF-2α phosphorylation such as strausporine, indirubin-30-monoxime and SP600124 **6**. Staurosporine is considered as a non-selective kinase inhibitor, thereby it is not further investigated. Various

indirubin-30-monoxime analogues were investigated. Spleen tyrosine kinase (SykI) inhibitor has been found to display more activity compared to other analogues. However, SP600124 **6** is known to possess the strongest potency as it has an IC_{50} of 2 mM.[148]

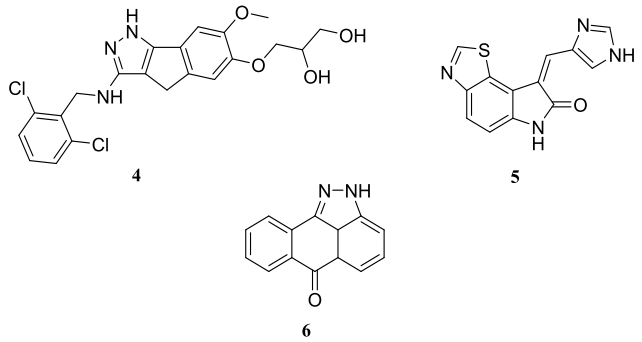


Figure 1.7: Chemical structure of HRI, PKR and GCN-2 inhibitors: aminopyrazolindane **4**, compound #16 **5** and SP600124 **6**, respectively.

1.5.3.3. Targeting eIF2B, an eIF2/eIF2B complex modulator

1.5.3.3.1. ISR Inhibitor (ISRIB)

Activation of the ISR in response to diverse stress stimuli leads to phosphorylation of the α-subunit of translation initiation factor eIF2. P-eIF2α acts on inhibiting eIF2B, and eventually causing repression of translation. Recently, a small-molecule ISR inhibitor (ISRIB) was identified as a potent inhibitor of the integrated stress response. It has been proposed that ISRIB may lower the sensitivity of eIF2B to eIF2α-P by making cells resistant to the effects of eIF2α phosphorylation, resulting in enhancement of protein synthesis.[149-151]

It has been initially suggested that ISRIB might reduce the sensitivity of eIF2B to eIF2α-P by making cells resistant to the effects of eIF2α phosphorylation, resulting in enhancement of protein synthesis.[149, 150] It has been found that ISRIB administration to mice results in enhancement of the cognitive memory.[149] Indeed in rodent models, this small molecule protects against neurodegeneration

caused by prion disease[152] and completely rescues cognitive deficits result from traumatic brain injuries.[153]

The understanding of how eIF2α-P modulates GEF activity is sketchy, but likely involves allostery, as mutations in GEF subunits (and others in eIF2) selectively impede regulation by eIF2α-P without affecting catalytic rate.[154] These features of ISR-impairing mutations are recapitulated by applying *trans*-ISRIB to cells. Strong evidence that ISRIB acting allosterically on the GEF is provided by recent biochemical observations and somatic cells pharmacogenetics: (1) ISRIB accelerates the GEF activity of purified eIF2B *in vitro,* compensating for the effects of eIF2α-P; and (2) mutations in the gene encoding the δ-subunit of eIF2B impart resistance to the effects of ISRIB *in vivo* and *in vitro*.[44, 45, 151, 155]

The molecular details of ISRIB's interaction with eIF2B remain to be learned. Since it was initially proposed that eIF2B is a symmetrical molecule composed of products of five subunits that come together as a dimer of pentamers[37], and as ISRIB is likewise symmetrical, it seems likely that ISRIB binds across the twofold symmetric dimer interface of eIF2B to regulate the GEF.[151] Recently, studies were conducted to identify eIF2B structure as a molecular target for ISRIB. As mention in section **1.2**, the structure of human eIF2B in complex with ISRIB was described using cryo–electron microscopy. The recent cry-electron microscopy shows that ISRIB binds into a pocket on the surface of eIF2B at the interface between the β and δ regulatory subunits (**Figure 1.8**). Mutagenesis of residues lining this pocket altered the hierarchical cellular response to ISRIB analogues in vivo and ISRIB binding in vitro. These findings point to a site in eIF2B that can be exploited by ISRIB to regulate translation.[44, 45]

Simultaneously, a study was conducted to further characterize the mechanism of action of ISRIB using sufficiently high resolution cryo-electron microscopy. Importantly, it was found that ISRIB stabilizes the most active decameric form of eIF2B and also it enhances GEF activity of a form lacking the alpha subunits. Despite the fact that ISRIB does not make a direct binding with the α subunit, it can elicit the incorporation of this subunit into the decamer complex. ISRIB enhances the stability of the symmetric interface of the β-δ core. Thus, eIF2B assembly plays a key role in regulating eIF2B activity, which in turn rescues mRNA translation during the ER stress and that can be further modulated by ISRIB.[45]

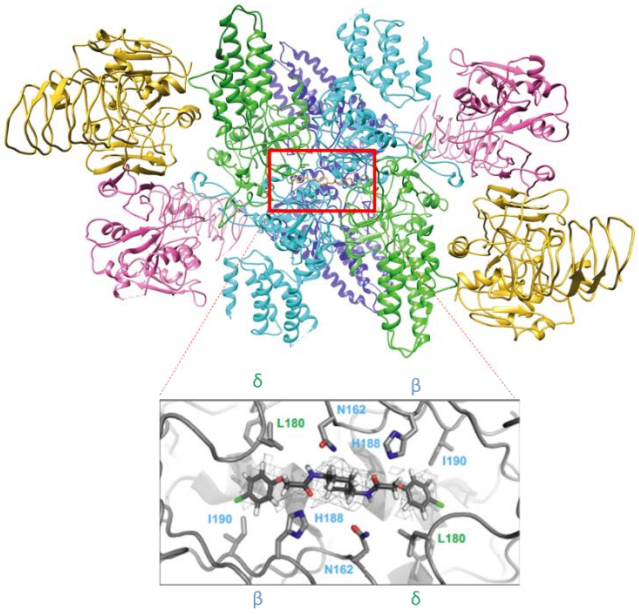


Figure 1.8: ISRIB-bound human eIF2B at the eIF2Bβδ dimer interface (central view) with close-up showing to the ISRIB-binding site; from cryo-EM analyses (PDB 6EZO).[44]

Most recently, biochemical, structural, and cell-based assays have been conducted to explain the mechanism of action of ISRIB. They have demonstrated that ISRIB functions as an allosteric antagonist against the inhibitory effect of phosphorylated eIF2 on guanine nucleotide exchange activity of eIF2B, eventually leads to inhibiting the ISR. This study revealed the antagonistic

relationship between the engagement of phosphorylated eIF2α and ISRIB as eIF2B ligands, at their corresponding binding sites. They have also addressed that engagement of ISRIB with eIF2B favours binding of unphosphorylated eIF2 as a substrate for nucleotide exchange. They have concluded a conceivable mechanism explaining the role of ISRIB in allosterically mediating the stabilization of the active decameric conformation of the eIF2B and thus reversing the ISR.[156]

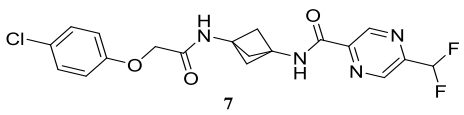
GEF activators, e.g. ISRIB, stand to burden the secretory pathway with more unfolded proteins and increase the level of ER stress. Severe dysregulation of GEF, as observed when eIF2α phosphorylation is completely uncoupled from ER stress (in humans with loss-of-function mutations in PERK or in mice treated with a potent PERK inhibitor), markedly compromises secretory tissues such as the exocrine pancreas and result in unacceptable toxicity. However, ISRIB, which is a partial allosteric activator of GEF and thus a partial inhibitor of the ISR, is well tolerated, with a good therapeutic window.[152, 157] ISRIB-like GEF activators with better bioavailability will make it easier to reproducibly titrate the beneficial and untoward effects of the compounds.

It has been demonstrated that systemic administration of ISRIB to wild-type rodents leads to cognition enhancement and also significant advancement in spatial and fear associated learning.[151] This effect is probably dependent on translation-mediated remodelling of neuronal synapses.[158, 159] Numerous studies have established that eIF2 phosphorylation is associated with a vast majority of neurodegenerative diseases and cancers, as well as normal aging.[160-163] Moreover, multiple mutations that impede eIF2B function result in a neurodegenerative disease of childhood known as vanishing white matter disease

(VWMD) that is mainly characterized by cerebellar ataxia, spasticity, hypersensitivity to head trauma and infection, coma and premature death.[155] ISRIB is characterized by good pharmacokinetic features, it rapidly crosses the blood-brain barrier and exhibits acceptable tolerability in mice. ISRIB rescues dysregulation in eIF2B activity resulted from numerous VWM mutations, by arresting aberrant ISR response.[164] Thus, ISRIB and related analogues serve as great candidates for treating VWMD and a variety of other devastating diseases requiring therapeutic options.[44, 151, 153, 164, 165]

1.5.3.3.2. eIF2B Activator (2BAct)

Recently, a small molecule knowing as 2BAct **7** (**Figure 1.9**), has been synthesised to overcome poor solubility and enhance pharmacokinetics properties associated with ISRIB.[166] The 2BAct **7** differs from ISRIB in both core ring portion, which has bicyclopentane instead of cyclohexane and *O*-arylglycolamide linker, which is replaced by 5-(difluoromethyl) pyrazine-2-carboxamide. This molecule displays similar activity to ISRIB molecule in a luciferase-reporter assay. 2BAct shows a significant normalizing impact on the transcriptomic and proteomic landscapes, myelin content, microglial activation, body weight and motor function of VWM mice. Preferably, it shows ability to penetrate blood brain barrier after oral dose (1 mg/kg or 30 mg/kg orally at a dosing volume of 10 mL/kg). However, the 2BAct molecule exhibits a remarkable anomaly in a dog cardiovascular model and this significantly makes it inappropriate for human dosing.[166]



7

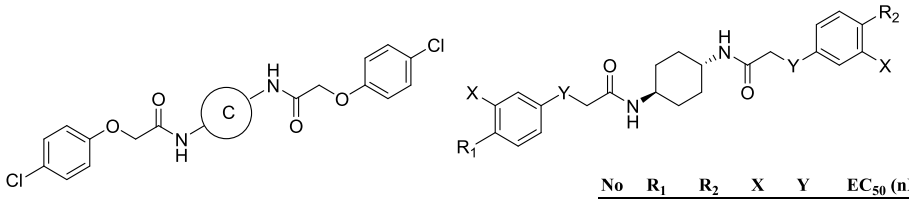
Figure 1.9: Chemical structure of 2BAct **7**.

1.6. Known structure-activity relationships (SAR) for ISRIB

As mention earlier, ISRIB **1** was recently identified as a novel molecule with a potent modulatory effect on the integrated stress response. ISRIB is a *meso* symmetric molecule as it is bisected into two identical parts by a mirror plane, so that it is achiral. The compound is characterised by two terminal aromatic rings linked to *trans*-cyclohexanediamine core ring by a glycolamide linker. ISRIB possessed a symmetric 1,4-cyclohexane ring in this position, thus depending on the stereochemistry at positions 1 and 4 of the cyclohexane ring, the ISRIB molecule can be synthesised as two diastereomers, *trans* **1** and *cis* **8** **(Figure 1.10)**. The published pharmacological data of two possible diastereomers showed that the *trans*-diastereomer **1** with an EC_{50} of 5 nM in cell-based luciferase reporter assay, have superior biological efficacy compared to the respective *cis* diastereomer.[149] This assay was established by Walter *et al.*[150] to identify the potency of ISRIB and its analogues through measuring luminescence following induction of ER stress with tunicamycin in the HEK293T cell line containing an ATF4 luciferase reporter. Induction of the ER stress acts on activating the PERK branch of the UPR signalling pathway and thus leads to eIF2α phosphorylation, de-repression of ATF4 translation and induction of the luciferase activity. The inhibition of the luciferase reporter activity was calculated and the compound concentration responsible for a half-maximal response in the luminescence signal was recorded as EC_{50} value.[149]

Generally, a limited set of SARs for conservative derivatives of ISRIB derivatives have been reported.[149-151, 167] In total, about 100 derivatives of ISRIB were synthesised and tested in a cell-based reporter assay, showing activity in the 0.6 nM > EC_{50} > 10 μM range.[149, 150] The distinguishing feature of all active

compounds is the fact that they are symmetrical. *Trans*-ISRIB itself is C2-symmetrical, and while not all active compounds have this two-fold rotational symmetry, they are nevertheless symmetrical in a pharmacophoric sense. The other important structural determinant of active compounds is the through-space distance between the symmetrical termini of the compounds. Although the exact required distance between these termini is difficult to assess from the known SARs due to the fact that all derivatives are flexible (8 or more non-terminal rotatable bonds, nRot), only compounds with a central 1,4-disubstituted 6-membered cyclic system (cyclohexyl or phenyl), which must be in the *trans*-geometry for cyclohexyl, are highly active. This suggests that the bioactive conformation is 'extended' rather than 'folded'. Replacing the central 6-membered cyclic system with 4-membered cyclic system as in compound **10** resulted in reduction in potency.



No	C	EC_{50} (nM)
1	*trans*-1,4-cyclohexyl	5
8	c*is*-1,4-cyclohexyl	600
9	1,4-phenyl	53
10	*trans*-1,3-cyclobutyl	142

No	R_1	R_2	X	Y	EC_{50} (nM)
11	Cl	Cl	F	O	0.6
12	Cl	Cl	CH_3	O	3.0
13	CN	CN	H	O	inactive
14	OMe	OMe	H	O	inactive
15	CF_3	CF_3	H	O	13
16	I	I	H	O	51
17	F	F	H	O	270
18	Cl	I	H	O	5
19	Cl	F	H	O	48
20	Cl	CF_3	H	O	10
21	Cl	CCH	H	O	inactive
22	Cl	Cl	H	NH	700
23	Cl	Cl	H	S	inactive
24	Cl	Cl	H	CH_2	inactive

Figure 1.10: Known structure activity relationships of ISRIB.

The substitution pattern of the terminal phenyl rings has been explored fairly extensively with the conclusion that small hydrophobic substituents *meta* or *para* give the most active compounds. *Trans*-ISRIB derivative with additional *meta*-fluoro substituents in the terminal phenyl groups as in compound **11**, resulted in

most active compound (EC_{50} = 0.6 nM). Hearn *et al*[167] showed that the replacement of both *para*-chloro substituents in ISRIB with other substituents which are relatively more hydrophilic than chlorine atoms such as cyano group **13** and methoxy group **14** were not tolerated. The size of *para*-substituents does not seem to be an issue, since, replacements with trifluoromethyl **15** or iodine **16**, were tolerated. However, *trans*-ISRIB derivatives with hydrophobic substituents at *para*-position in one of the terminal phenyl groups as in compounds **18**-**20** seems to be tolerated as well.

The distance (optimally 4 atoms) between the terminal phenyl and the central 6-membered rings also appears to be important, although this has not been assessed extensively. The linkers between the terminal and central rings appear to be amenable to structural modifications, with the exception of the ether O, which seems to be essential and could not be substituted, even with closely similar atoms such as S group as in compound **23**. This suggested that the electronic nature of the distal chlorophenyl ether moieties play an important role in interaction with the biological target. Overall, the reported SARs for conservative derivatives of ISRIB derivatives are summarised in the **Figure 1.11**.

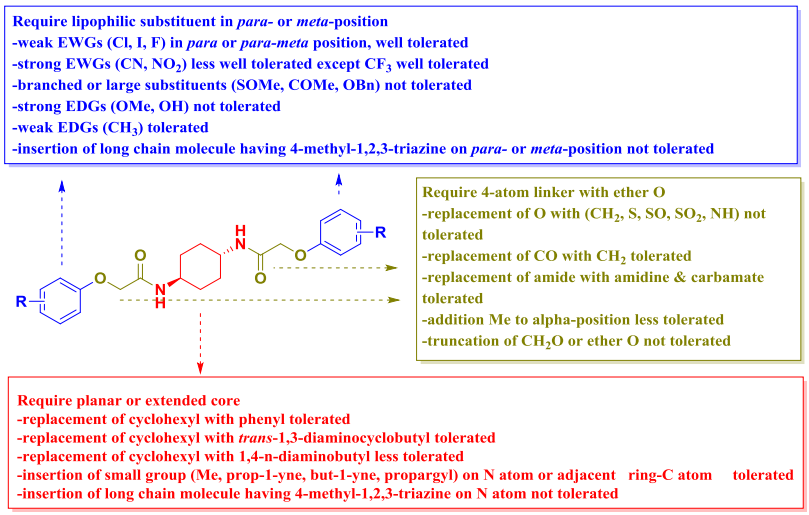


Figure 1.11: A breakdown of the Structure–activity relationships (SAR) data available for the key functional groups of ISRIB **1**.

1.7. Aims and objectives:

As highlighted earlier, neurodegenerative diseases pose an ever-increasing medical, social, and economic burden on society and health care systems worldwide, yet no efficient treatments exist. Modulation of protein synthesis *via* the eIF2/eIF2B signalling is a highly important target to prevent neurodegeneration and progression of dementia, yet there has been modest progress in developing a small molecule targeting this pathway. ISRIB exhibits enhancement in protein synthesis rate resulting in profound neuroprotection throughout the brain, recovery of memory, and preventing the progression of prion disease.[149, 151, 152, 168] In general, a limited set of SARs for ISRIB derivatives have been reported. [150, 167] Therefore, further efforts are required in order to build up a comprehensive structure activity relationships. In addition, the molecular details of ISRIB's interaction with eIF2B remained to be learned in order to understanding the molecular target of this compound. It is worth noting that cryo–electron microscopy structure for the human eIF2B in complex with ISRIB was conducted at the end of this PhD project.

Therefore, the project aims are divided into three parts:

- Design, synthesis and biological evaluation of a new ISRIB derivatives, with an aim to generate novel ISRIB analogues with high potency. The ISRIB analogues were intended to be optimized by set out extensive SAR studies approach using ISRIB itself as a lead compound.
- Design, synthesis and evaluation of a fluorescent ligand based on ISRIB itself, thereby making the ligand more visible for use as a molecular tool for biological assay such as fluorescence polarization (FP) assay. The main reason for creating a labelled ISRIB derivative and performing an FP assay was in order to nail down the molecular target of this compound.
- The other aim of the work in this thesis was to investigate the ADME parameters (aqueous solubility, Caco-2 permeability and microsomal stability) for ISRIB and other new promising ISRIB analogues. Then, the best candidate could be utilized in *in vivo* efficacy studies, using the mouse models for neurodegenerative diseases.

To achieve these major aims, the research project was undertaken with the following specific objectives:

- To design of new ISRIB derivatives, modifying different motifs on the structure of ISRIB and synthetic routes were adopted. A structure-activity relationship was then extracted to assist in understanding the key structural features that are responsible for activity.
- To identify suitable site for fluorescent ligation on ISRIB molecule, SAR studies and molecular modelling aided to select the appropriate lead compound.
- To achieve the outcome of the *in vitro* ADME studies, a quantitative analytical method was developed.

2. Design and synthesis of ISRIB analogues

2.1. Introduction

In this chapter, design and synthesis of new ISRIB analogues for the eIF2B receptor were described. This chapter aimed to look at SARs more generally, through synthesising some truncated non-symmetrical derivatives first, then modification of several key motifs on the prototype ISRIB molecule in order to establish a clear structure activity relationships.

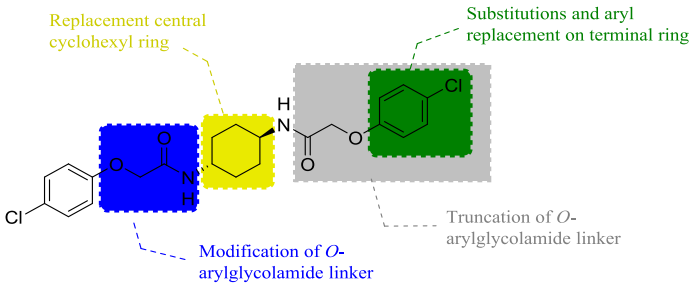


Figure 2.1: Area for investigation on ISRIB (**1**).

The modifications described in **Figure 2.1** was detailed in this chapter. These include modifying the position and nature of substituents on the terminal aromatic rings, investigation of replacement central ring that joins the *O*-arylglycolamide side chains, and modification of the glycolamide linkage between the central cyclohexane and distal aryl rings.

2.2. Overview of rational drug design

In its most basic sense, the concept of drug design includes the process of designing drug-like small molecules which are compatible in terms of size and charge with the receptor target molecule they interact with and bind to the appropriate binding site.[169] Traditionally, when there is little or no accurate structural information of the biological target, an analysis of a wide variety of quantitative structure activity relationships, biological and chemical properties of molecules which have shown good activity are often used. This aspect of the drug design strategy is known as ligand-based drug design. In the ligand-based drug design, the method relies on the knowledge of the ligand structure. The structure of ligand can come from NMR or X-ray crystallography studies.[170, 171] On the other hand, structure based drug design relies on knowledge of the three-dimensional structure of the biological target obtained through either an X-ray or NMR structure of the receptor-ligand complex.[171-173] Once knowing the ligand bound three-dimensional structure of the target, a large library of chemical compounds can be tested by virtual screening and that enables the discovery of potential new hits.[171]

Despite that, the broadest sense of rational drug design is about complementarity of ligands with the receptors, it is useful to think about flexibility, for both target and ligand. Both receptors and ligands are not in a fixed state under physiological conditions but behave dynamically and thus seem to have a clear effect on the whole process of drug discovery even when 3D-structure of the biological target molecule has been resolved.[172] Recently, a variety of methods have been applied based on combining information of these two categories of computer-aided drug design in order to enhance the results of these approaches.[173]

In relation to this project, published structure activity relationships of the ISRIB molecule[150, 151, 167] together with recently identified crystal structures of *Schizosaccharomyces pombe* eIF2B (PDB 5B04)[40, 41] will aid in designing new ISRIB analogues.

2.3. Binding analysis of ISRIB with *S. pombe* eIF2B: Docking studies

At the end of this PhD project, Alisa *et al*[44] and Jordan *et al*[45] have been published cryo–electron microscopy structure for the human eIF2B in complex with ISRIB- the first entire eIF2B crystal structure since that of *S. pombe* eIF2B in 2016.[40] Therefore, the availability of crystal structure for *S. pombe* (PDB 5B04) throughout the period of this project allowed its use in order to investigate the binding mode of the ISRIB and design analogues.

Examination of the *S. pombe* eIF2B X-ray crystal structure (PDB 5B04) immediately suggests a predicted binding site for ISRIB at the interface between the two β and δ subunit interfaces (**Figure 2.2, A**). Docking of ISRIB to this symmetrical site suggests a convincing binding pose (**Figure 2.2, B**). The *trans*-ISRIB molecule binds in an extended conformation across the two symmetrical pockets, which would clearly stabilise the eIF2B complex by immobilising the β-δ subunit interfaces. The terminal *para*-chlorobenzene rings reside in the hydrophobic pocket behind Asp^{255}. They form halogen bond and hydrogen aromatic interactions with residues of the two pockets that accommodate the aromatic end groups (Lys^{426} and Asp^{255}), respectively.

Furthermore, the magnitude of interactions of various polar components of ISRIB, *i.e.* the amide CO and NH groups, with residues of this pocket adds an

important contribution to the binding affinity. The residue V^{120} in *S. pombe* is defined as the narrowest point of entry into the ISRIB-binding site. In the modelled pose the NH amide groups are predicted to donate H-bonds to the backbone carbonyl *O* atoms of V^{120} (**Figure 2.2, C**). The V^{120} side chains lie above the ether CH_2 groups but do not make intimate contacts, as they point towards the exterior of the binding site. In addition, the central cyclohexane ring is located in a hydrophobic pocket close to the Val^{120} of both δ and δ' subunits, which forms the 'roof' of the central part of the binding pocket. Overall, the information obtained from this analysis of ISRIB binding site will be used to design further ISRIB derivatives and to rationalize the pharmacological data.

The above observations were further supported by *Kashiwagi et al.*[41] who showed that ISRIB molecule potentially interferes between the two δ subunits of eIF2B. Additional support for the ISRIB binding site has been achieved after describing the cryo–electron microscopy structure of human eIF2B with an ISRIB molecule bound within a deep cleft at the interface between the β and δ subunits of eIF2B.[44, 45]

Before the availability of the human eIF2B crystal structure, homology modelling was suggested as a potential approach. Therefore, a homology model of human eIF2B was built based upon the crystal structure of *S. pombe* (PDB 5B04) (**Figure 2.3**). The sequence alignments between human and *S. pombe* eIF2B (β and δ subunits) showed that human βeIF-2B and δeIF-2B share 37% and 35% sequence identity with *S. pombe* eIF2B, respectively (**Figure 2.4**).

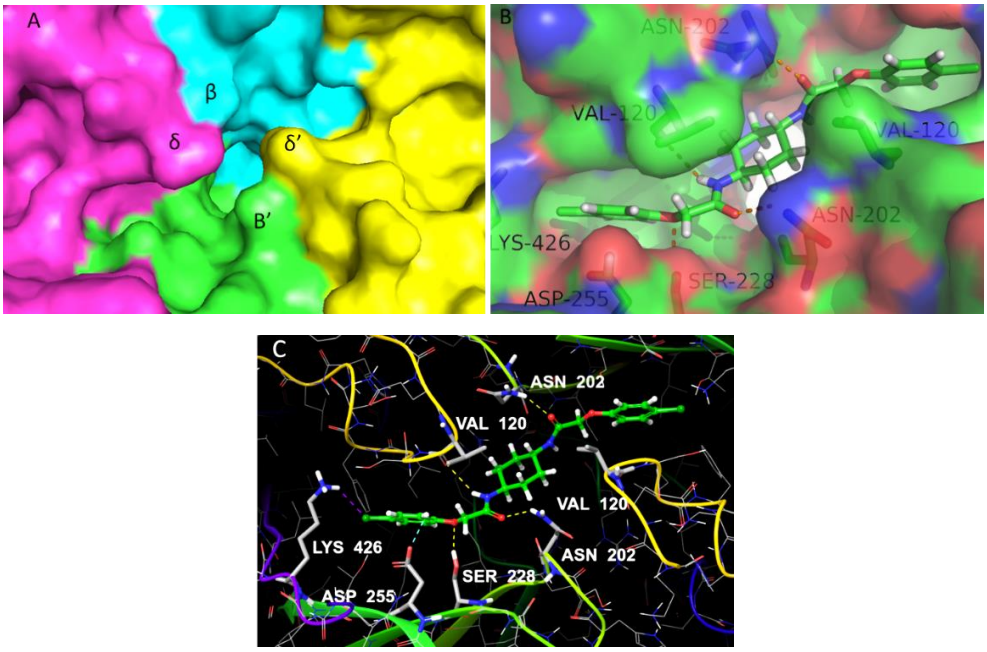


Figure 2.2: Predicted binding conformation of ISRIB with the eIF2B receptor: (A) eIF2B hydrophobic pocket located at the interface between the two β and δ subunit; (B) binding mode of ISRIB in the active site of eIF2B; (C) representation of residues involved in the interaction with ISRIB, numbering according to *S. pombe* structure (PDB 5B04); (The molecular docking studies were performed by using the Schrodinger Maestro software release 2016-1 and Pymol software, to explore the binding ability of ISRIB to the eIF2B (PDB: 5B04).

Docking ISRIB to this model results in similar binding poses but with somewhat less convincing ligand-receptor interactions, although the residues that appear to be in contact with ISRIB in the bound poses are comparatively well conserved. This means the modelling of eIF2B based on *S. pombe*, is not possible to provide an accurate prediction of the detailed ligand-receptor interaction. Therefore, the ISRIB binding site with *S. pombe* eIF2B (PDB 5B04) will be used in docking studies to design and rationalize the pharmacological results.

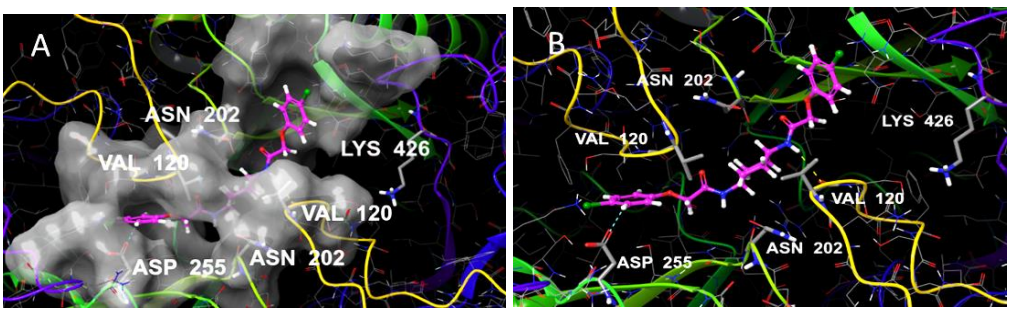


Figure 2.3: Predicted binding conformation of ISRIB with the homology model of human eIF2B receptor: (A) ISRIB binding mode and surface representation of homology model of eIF2B; (B) Representation of residues involved in the interaction with ISRIB in homology model of eIF2B. Homology model (created using Swiss-model tool).

Beta subunit



Delta subunit

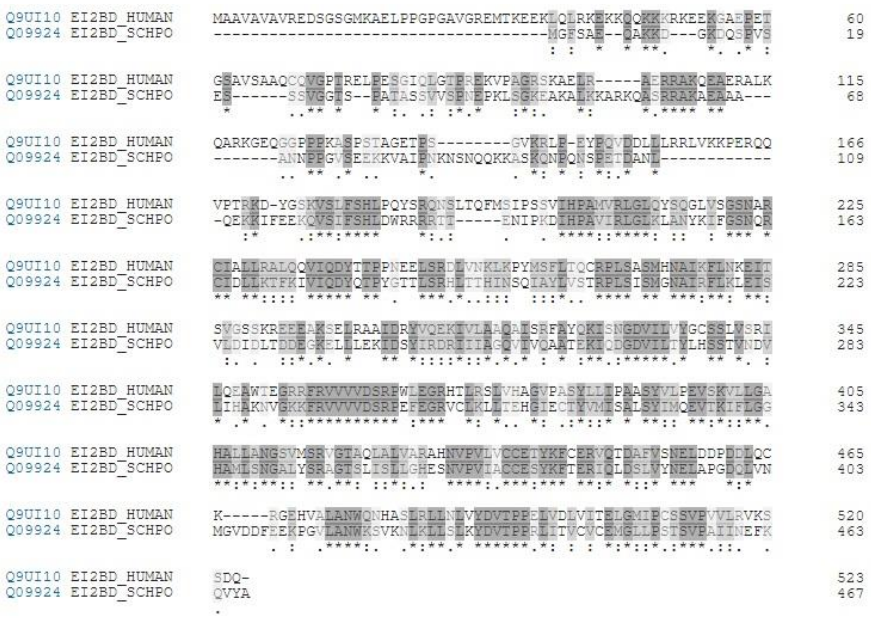


Figure 2.4: Sequence alignments between human and Schizosaccharomyces pombe eIF2B subunits beta and delta (created using UniPort alignment tool). ***** *indicates residue identity (highlighted dark grey): high residue similarity (highlighted light grey), and . low residue similarity.*

2.4. Rationale behind the design of ISRIB analogues

ISRIB is considered a useful tool to investigate the impact of modulates the interactions between eIF2 and eIF2B on protein synthesis rate in neuronal cells. There are limited studies published that investigate the SAR of ISRIB.[150, 151, 167] This in turn offers further possibilities for the development of new ISRIB derivatives. In addition, *trans*-ISRIB has a very low aqueous solubility and the

lack of oral bioavailability of this compound is likely due predominantly to this fact.[152] Low aqueous solubility arises probably from the molecular planarity and symmetry of ISRIB molecule which confer a tightly packed crystal structure. This could illustrate the high melting point of ISRIB molecule (271-274 °C) which suggests that the low solubility is probably due to thermodynamic stability in the solid state. Therefore, this study hypothesised that the disruption of molecular symmetry may help to lower the thermodynamic crystal stability, and thus improving its aqueous solubility.

Apart from lack of aqueous solubility, the other main drawback of ISRIB-like molecules is excessive flexibility. ISRIB has eight non-terminal freely rotatable bonds (nRot = 8, HBA = 4, HBD = 2 [calculated using the Chemicalize, ChemAxon (v14.8.4.0)]. Highly flexible molecules are known to be prone to target promiscuity, extensive metabolism, and limited permeability.[174] For this reason, conformationally restricted novel compounds will be sought.

Generally, integrating the known SAR into the design, will help with the aims of building up further SAR studies, improving knowledge regarding interactions at the active site, and enhancing ADMET properties. The formation of a different modified series of analogues was started. The new analogues were designed to be susceptible to a more parallel synthetic approach. Initially the idea was to prepare some obvious derivatives (non-symmetrical ones as well as replacement of individual components) to study SARs for potency and solubility optimisation, as well as to find out where we can attach handles for structural studies / identification. ISRIB derivatives will be sought by structural modifications of the prototype ISRIB's core cyclohexane ring, *O*-arylglycolamide side chain, and terminal aromatic rings. These analogues were

designed and synthesised in an attempt to provide novel molecules outside the scope of a relevant patent application (more details will be discussed in the following sections). Examples of target structures incorporating commercially available or readily synthesised starting materials for the proposed molecular cores, linkers, and terminal ring are summarised in the **Figure 2.5**.

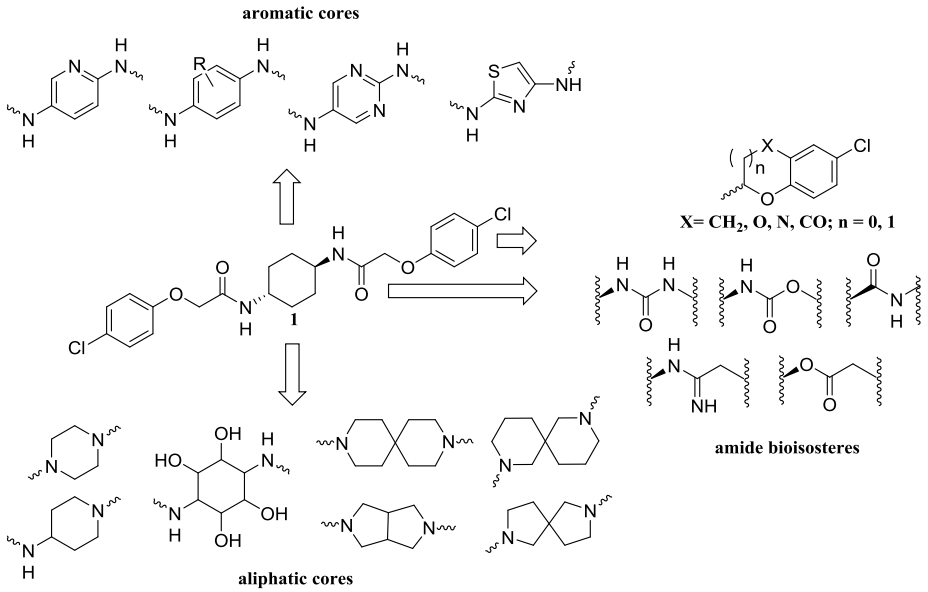


Figure 2.5: Overview of some ISRIB modifications intended to be generated in this study.

Depending on the stereochemistry at positions 1 and 4 of the cyclohexane ring, the ISRIB molecule can be synthesised as two diastereomers, *cis* and *trans*. The published pharmacological data of the two possible diastereomers showed that the *trans*-diastereomer (**1**), has a superior biological efficacy compared to the respective *cis*-diastereomer.[149] This finding suggests that the *trans*-conformation (chair-like) was more preferable for eIF2B binding than the *cis*-conformation (boat-like). For this reason, *trans*-configuration was retained in most of the analogues synthesised in this project.

2.4.1. Truncated non-symmetrical ISRIB analogues

The previous literatures demonstrate that the distinguishing feature of most active compounds is the fact that they are symmetrical (**Chapter 1**). However, it is important to point out that an absolute requirement for symmetry has not been originally explored by Walter *et al*[150], since compounds possessing at least one truncated *O*-arylglycolamide side chain have not been tested or reported. Initial medicinal chemistry will probe the structural requirements for enhancing protein synthesis rate by the mechanism elucidated for *trans*-ISRIB (**Chapter 1**), through systematically truncated and modified structure. Exploring the ISRIB structural requirements for efficient binding relationship with the target are important in aiding the development of appropriate modified analogues, as well as to determine which parts of the molecule can be altered to improve the physicochemical properties. Therefore, the purpose of this first set of compounds is to test the necessity of symmetry in the ISRIB molecule, to identify which parts of the molecule are required for pharmacological activity and which groups do not efficiently contribute to binding. Accordingly, the analogues that are truncated in one of the *O*-arylglycolamide side chain were synthesised. Initially, the analogues were designed by removing chlorine atom from one aryl distal ring, as shown in **Figure 2.6** (**a**). This process was continued until removing single one *O*-arylglycolamide side chain (**Figure 2.6, b-d**).

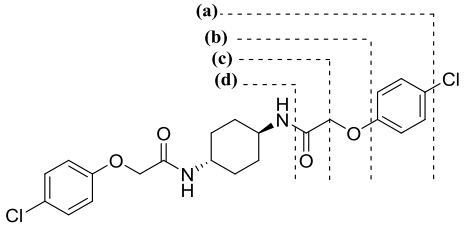


Figure 2.6. Overview of intended truncated structural modifications (a-d).

The truncated analogues also contribute in providing further SARs to understand the physicochemical properties. Generally, installation of halogen atoms and aromatic ring into a therapeutic small molecule candidate can affect a number of pharmacokinetic and physicochemical properties. Therefore, removal or replacement of one of the distal aryl halide ring might be helpful in solubility optimization via reduction of both molecular size and hydrophobicity.[175]

2.4.1.1. Synthetic strategy

In order to make various analogues of ISRIB, with truncated or with subtle changes in one of the linkers between the cyclohexane central ring and aromatic group, a strategy was needed to generate the effective analogues with the fewest synthetic steps.

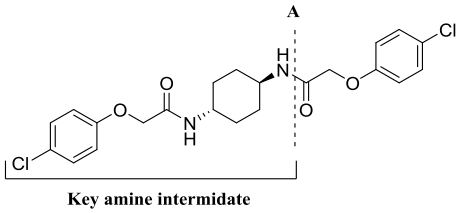


Figure 2.7: Disconnection (A) for the generation of truncated non-symmetrical ISRIB analogues.

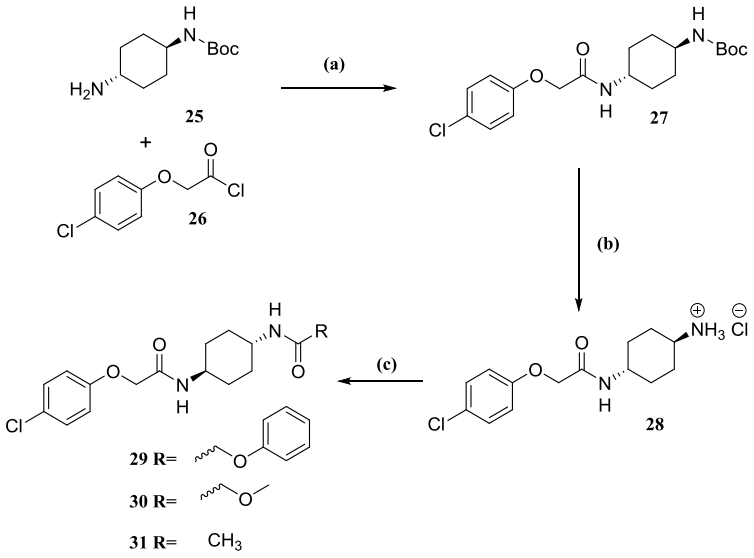
As shown in **Figure 2.7**, the disconnection (A) between the cyclohexane-1,4-diamine and one of the *O*-arylglycolamide side chain was deemed the best option to synthesise truncated ISRIB analogues. Synthesis of this key amine intermediate, (2-(4-chlorophenoxy)-*N*-[(1*R*,4*R*)-4-aminocyclohexyl]acetamide hydrochloride), was required to allows bulk production of the non-symmetrical analogues. A synthetic strategy to prepare key amine compound was reported previously by Sidrauski *et al*.[151]

2.4.1.2. Synthesis of truncated ISRIB analogues

A published procedure describing the synthesis of key amine intermediate **28** in 2-step process was employed.[151] Initially, the key starting material, mono Boc-protected *trans*-*N*-Boc-1,4-cyclohexanediamine **25**, is commercially available and was used to prepare non-symmetric ISRIB analogues, as illustrated in **Scheme 2.1**. In order to install a single *O*-arylglycolamide side chain on *trans*-*N*-Boc-1,4-cyclohexanediamine **25**, the commercially available 4-chlorophenoxy acetyl chloride **26** was used. A nucleophilic attack of the free amino group of *trans*-*N*-Boc-1,4-cyclohexanediamine **25** on the carbonyl group in the acid chloride leads to the formation of the *tert*-butyl *N*-[(1*R*,4*R*)-4-[2-(4-chlorophenoxy)acetamido]cyclohexyl]carbamate **27** with elimination of HCl. Additional base such as N,N-diisopropylethylamine (DIPEA) is usually required to avoid the conversion of the amine group into its unreactive HCl salt and to trap the formed HCl. The formation of this analogue proceeded with reaction times of 30 mins at 0 ^{o}C to 1 hour at room temperature and with high yields of up to 83%. The 2-(4-chlorophenoxy)-*N*-[(1*R*,4*R*)-4-aminocyclohexyl]acetamide hydrochloride **28**, was obtained in the hydrochloride salt form after removal of the Boc group by aid of acid, a concentrated HCl acid solution in dioxane was used for this purpose (**Scheme 2.1**).

Generation of truncated ISRIB analogues **29**-**31** was straightforward, via one step by coupling the **28** with the selected commercial available acid chlorides (phenoxyacetylchloride, methoxyacetylchloride and acetyl chloride) in the presence of N,N-diisopropylethylamine (DIPEA) (**Scheme 2.1**). Reaction with the carbonyl chloride reagents proceeded rapidly, in high yields. This method of coupling required dropwise addation of a solution of the reactive acyl chloride

to 2-(4-chlorophenoxy)-*N*-[(1*R*,4*R*)-4-aminocyclohexyl]acetamide **28** at 0 °C. The synthesis of the analogues continue with reaction times of 1 hour at room temperature and with yields between 87% and 96%. All of the analogues were purified by trituration with diethyl ether and characterised using LC-MS, ^{1}H NMR, and HRMS. HPLC (at 95% or above) was utilized to confirm the purity of the analogues.



Scheme 2.1: Synthetic of truncated ISRB analogues.
Reagents and conditions: (a) N,N-diisopropylethylamine (DIPEA), DCM, 0°C 30 mins to rt 1 h, 83%; (b) dioxane, MeOH, 4 N HCl/dioxane, rt, 96%; (c) phenoxyacetylchloride or methoxyacetylchloride or acetyl chloride, DIPEA, DCM, 0 °C 30 mins to rt 1 h, yields 87%-96%.

It was expected that analogue **27** may imply the existence of two rotamers (**Figure 2.8**, **27** and **27'**), probably due to the presence of a protecting group. Upon inspection of the ^{1}H NMR (DMSO-d_6) of the analogue **27**, only two peaks at 3.59 and 3.18 ppm corresponding to the two C-H of cyclohexane (^{C}Hx C*H*, blue and red) protons are observed **(Figure 2.8)**. The cyclohexane C-H (^{C}Hx C*H*) of analogue **27**, which is in close proximity to the carbamate of Boc-protecting group displayed a usual NMR spectrum, no rotamers are observed. Rotamers should have the same split pattern but different ppm, this could be noticed when

there is a restricted rotation around a chemical bond leading to two set of shift for some protons. In other words, identifying the same protons with different shifts, generally close to the moiety creating the hindrance, results from reducing rotation. Herein, it seems there is no steric hindrance effect as the *trans*-cyclohexane ring prevents the movement of the carbon. In addition, the two substituents on the *trans*-cyclohexane ring point to opposite faces, which mean less steric hindrance. It would be expected that rotamers might exist in *cis*-cyclohexane because the substituents would point to the same side, which means they are close to each other with high steric hindrance effect.

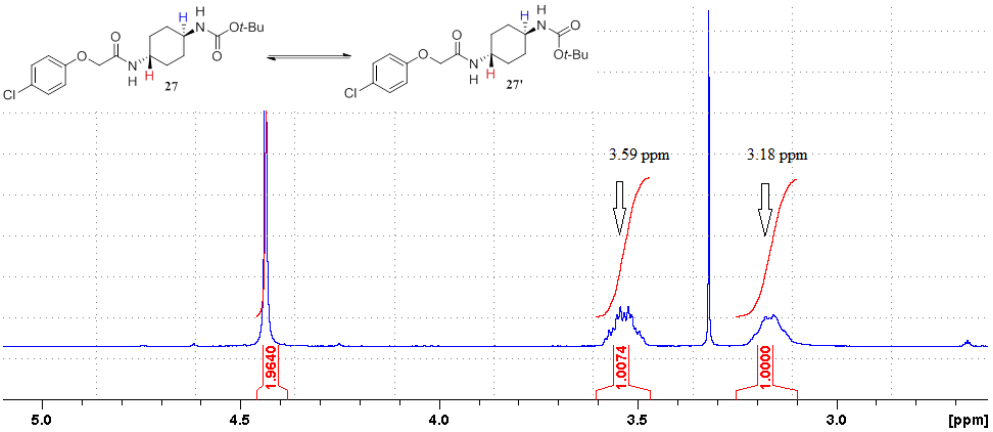


Figure 2.8: ^{1}H NMR spectrum of the analogue **27** (5.1−2.7 ppm region only). Upon inspection of the ^{1}H NMR (DMSO-d_6) of the analogue **27**, only two peaks at 3.59 and 3.18 ppm corresponding to the two C-H of cyclohexane (^{C}Hx C*H*, blue and red) protons are observed.

2.4.2. Modification of the terminal aromatic rings

The substitution pattern of the terminal phenyl rings has been explored fairly extensively with the conclusion that small hydrophobic *meta*/*para* substituents give the most active compounds (**Chapter 1**).[150, 151, 167] The modelled binding pose of ISRIB in eIF2B (**Figure 2.9**, **A**) showed a sufficient space around the two aromatic end groups for small substituents, which, depending on nature, can pick up a variety of interactions with residues of the two pockets. Modelling studies suggest that the halogen atom (*p*-Cl) in terminal aryl moiety interacts

with the binding site backbone fragment (NH) of Lys[426]. The chlorine substituent forms a short orthogonal multipolar aryl-Cl···H-N interactions with Lys[426] within the predicted pocket (**Figure 2.9**, **B**).

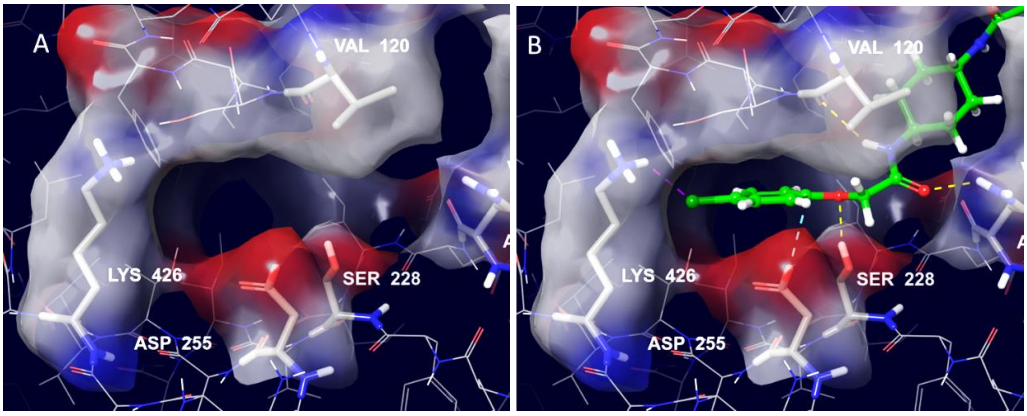


Figure 2.9: Predicted binding conformation of terminal aromatic ring of ISRIB with the eIF2B; (A) The hydrophobic pocket behind Asp[255] in the binding site; (B) Representation of residues involved in the interaction with terminal aromatic substituent; (generated using Schrödinger Maestro, from PDB entries: 5B04).

Therefore, in an attempt to further investigation the effects of substituents (in terms of steric, electronic and positional) on the terminal phenyl rings, non-symmetric and symmetric ISRIB analogues were considered to be of interest. The analogues comprised of *para*- bromo, trifluoromethyl and fluoro substituted phenol. A bromo substituent was selected as it is close in size and electronegativity to chlorine, which allows further investigation of steric and electronic effects of substitutions. Previously described aromatic ring substitutions such as trifluoromethyl and fluoro groups[167] were selected, in order to calibrate inter-assay variability.

Considering the comparatively high lipophilicity of ISRIB derivatives; it was considered prudent to investigate the replacement of the terminal phenyl rings with more polar heterocyclic systems or cyclic aliphatic ring. Lipophilicity significantly influences ADME properties.[176] The introduction of heteroaromatic rings such as pyridine or pyrimidine, which possess a basic

nitrogen atom on the molecule could potentially confer an higher aqueous solubility.[177] Pyridine or pyrimidine containing compounds exhibited intermediate solubility and low protein binding.[178] In addition, replacing the aryl ring with heterocyclic aromatic rings may improve the interaction with the binding site. The presence of heteroatoms, for example nitrogen in pyridine and pyrimidine, could be potentially involved in polar interactions with binding site residues. In particular, such replacement could still maintain π-stacking interactions. In this case, by introduction of a polar pyridinyl or pyrimidinyl rings, two novel analogues were designed, which were expected to possess improved physiochemical properties when compared to ISRIB. Accordingly, synthesis of non-symmetric and symmetric pyridine, pyrimidine and cyclohexane derivatives were attempted.

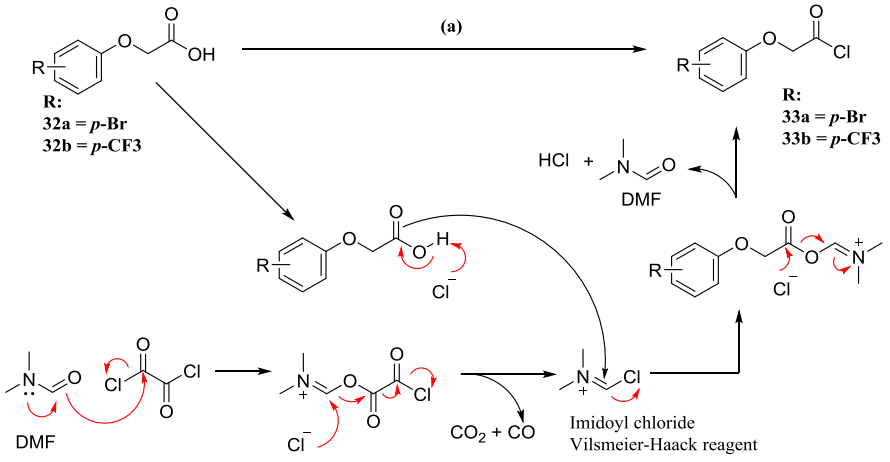
2.4.2.1. Synthetic strategy

In a similar way to the formation of the truncated analogues described in section **2.4.1.2**, the final non-symmetrical ISRIB analogues with modified terminal aromatic ring were obtained by amide coupling of 2-(4-chlorophenoxy)-*N*-[(1*R*,4*R*)-4-aminocyclohexyl]acetamide hydrochloride **28** with a series of acid chloride or carboxylic acid fragments. The strategy employed required separate synthesis of the acid chloride or carboxylic acid fragments (second *O*-arylglycolamide or *O*-heteroarylglycolamide side chain), before a final amide bond formation step. The synthesis of **28**, is detailed in section **2.4.1.2**. As in the classical route of the synthesis of the symmetric ISRIB analogues involves amide coupling of the *trans*-1,4-diaminocyclohexanen[151] in one step to synthesise the desired analogues. The new carboxylate fragments were reacted with the desired diamine to afford the required symmetric ISRIB analogues.

2.4.2.2. Synthesis of acid chloride and acid carboxylate fragments: *O*-arylglycolamide or *O*-heteroarylglycolamide side chains

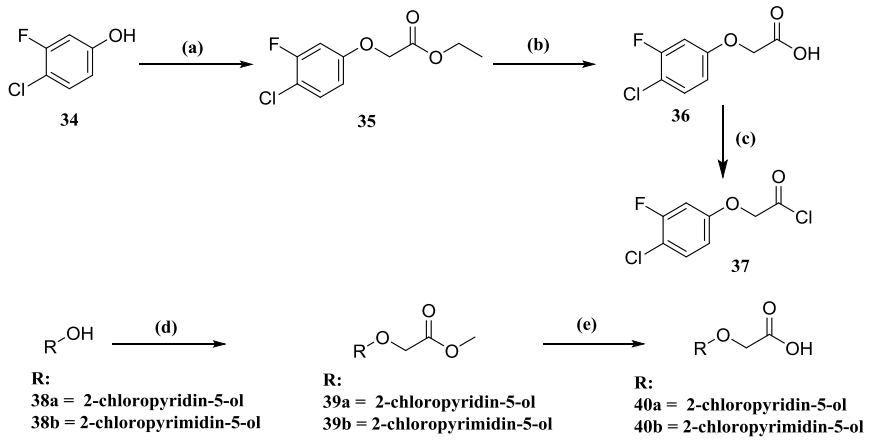
The *O*-arylglycolamide or *O*-heteroarylglycolamide side chains were constructed separately before using each in the amide coupling with analogue **28** or with diamine molecules. Initially, the commercially available 2-(4-bromophenoxy)acetic acid **32a** and 2-[4-(trifluoromethyl)phenoxy]acetic acid **32b** were converted to the acid chloride **33a** and **b** with the Villsmeier reagent (formed *in situ*) by mixing with oxalyl chloride in dichloromethane (**Scheme 2.2**) in presence of a few drops of dimethylformamide (DMF).[179, 180] The reaction proceeded in 2 hours at ambient temperature and the formed product was used in the next step without further purification. This allows fast reaction with amines to give the corresponding amide.[179]

The proposed reaction mechanism of acid chloride formation using oxalyl chloride was detailed in **Scheme 2.2**. This reaction involves conversion of DMF to the imidoyl chloride derivative (Vilsmeier–Haack reagent). The Vilsmeier–Haack reagent is the active chlorinating agent.



Scheme 2.2: Proposed reaction mechanism of 2-(4-bromophenoxy)acetyl chloride **33a** and 2-(4-(trifluoromethyl)phenoxy)acetyl chloride **33b**.
Reagents and conditions: (a) 2-(4-bromophenoxy)acetic acid **32a** or 2-[4-(trifluoromethyl)phenoxy]acetic acid **32b**, oxalylchloride, DCM, 2-drops of DMF, 0^{o} C to rt 2 h, 71% and 66%, respectively.

Since the majority of the *O*-arylglycolamide and *O*-heteroarylglycolamide side chains were not commercially feasible, their synthesis was required. The first step of the synthesis involved alkylation of the phenol, pyridinol and pyrimidinol (**34**, **38a** and **38b**, respectively), via Williamson ether synthesis[181] to generate ether compounds. The formation of the ether derivatives proceeded under reflux in the presence of potassium bicarbonate (K_2CO_3) with reaction times of 4 hours or overnight at room temperature. In the presence of a base, such as K_2CO_3, and heat, phenol, pyridinol and pyrimidinol react with an ethyl-2-bromoacetate or methyl bromoacetate to form an ether. First, the base deprotonates the hydroxyl group, creating an anion. This anion can then undergo a substitution reaction with an ethyl-2-bromoacetate or methyl bromoacetate to give desired ether derivatives **35**, **39a** and **39b** in yields from 80% to 90% after purification by column chromatography on silica (**Scheme 2.3)**. Using either ethyl-2-bromoacetate or methyl bromoacetate was based on their availability in the lab. The methyl and ethyl esters obtained were thereafter saponified to their corresponding carboxylic acids, using aqueous LiOH in a mixture of THF and water in yields from 81% to 90%. They were presumed to be pure enough, by ^{1}H and ^{13}C NMR, to be used directly in the next step, and were therefore used without further purification in the coupling step. 2-(4-chloro-3-fluorophenoxy)acetic acid **36** was converted to its corresponding acid chloride **37** by mixing with oxalyl chloride in DCM using a similar procedure previously employed in synthesising **33a** and **33b**.



Scheme 2.3: Synthesis of *O*-arylglycolamide or *O*-heteroarylglycolamide fragments. Reagents and conditions: (a) ethyl bromoacetate, MeCN, K2CO3, reflux, 4 hrs, 80%; (b) LiOH.H2O, THF/water (2:1), 4 hrs, 85%; (c) oxalylchloride, DCM, 2-drops of DMF, 0^{o} C to rt 2 h, 57%; (d) methyl bromoacetate, DMF or acetonitrile, K_2CO_3 or Cs_2CO_3, rt, overnight, 90% and 81%; (e) LiOH.H2O, THF/water (2:1), 4 hrs, 90%.

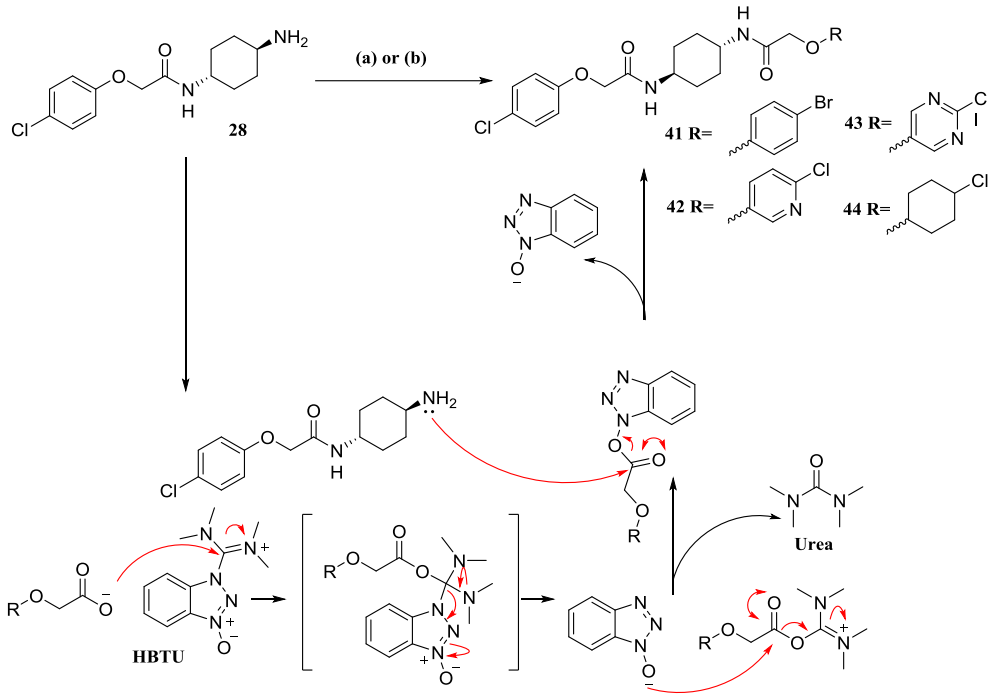
2.4.2.3. Synthesis of non-symmetrical modified terminal aromatic ring analogues

Two methods of amide coupling were performed in this project for the synthesis of non-symmetrical and symmetrical ISRIB analogues; (a) coupling reaction with acyl chloride (b) peptide coupling reagents. For the synthesis of non-symmetrical analogues, various reactions of 2-(4-chlorophenoxy)-*N*-[(1*R*,4*R*)-4-aminocyclohexyl]acetamide hydrochloride **28** were used to introduce the second *O*-arylglycolamide or *O*-heteroarylglycolamide side chain. For example, synthetic acid chloride 2-(4-bromophenoxy)acetyl chloride **33a** was reacted with compound **28** in the presence of DIPEA to afford the corresponding amide analogue **41** (**Scheme 2.4**). The formation of this analogue proceeded with reaction times of 30 mins at 0 ^{o}C to 2 hours at ambient temperature and with yield 66%.

The synthetic carboxylic acid derivatives **40a** and **40b** together with the commercially available 2-(cyclohexyloxy)acetic acid underwent carboxylate

activation with hexafluorophosphate benzotriazole tetramethyl uronium (HBTU), before the addition of the nucleophile. Coupling was achieved directly with amine compound **28** in the presence of triethylamine to give the required amide analogues **42-44**. The synthesis of these analogues continued with reaction times of 16 to overnight (analogues **42** to **44**), with yields between 76% and 86%. The analogues were purified by column chromatography using solvent mixtures of either dichloromethane / tetrahydrofuran or ethyl acetate / dichloromethane. Structural determination, of all prepared amides, was carried out using NMR, LC-MS and HRMS. HPLC (at 95% or above) was utilized to confirm the purity of the analogues.

The proposed reaction mechanism of HTBU-coupling reaction was detailed in **Scheme 2.4**. Triethylamine and carboxylic acid were mixed together and stirred for 10 minutes before adding HBTU. The deprotonated acid reacts with HBTU to produce active ester as an intermediate. This intermediate can then directly react with the amine to yield the corresponding amide.



Scheme 2.4: Synthesis of non-symmetrical modified terminal aromatic ring analogues and proposed reaction mechanism of HTBU-coupling reaction.
Reagents and conditions: (a) 4-bromophenoxy acetyl chloride **33a**, (DIPEA), DCM, 0ºC 30 mins to rt 2 h, 66%; (b) **40a**, **40b** and 2-(cyclohexyloxy)acetic acid, HBTU, DCM, Et3N, 16 h to overnight, yields 76% to 86%.

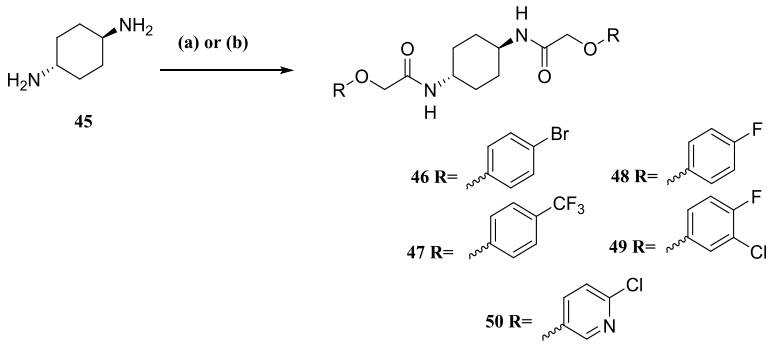
2.4.2.4. Synthesis of symmetrical modified terminal aromatic ring analogues

Symmetrical ISRIB analogues were prepared by direct reaction of synthetic *O*-arylglycolamide or *O*-heteroarylglycolamide side chains with the desired diamine to afford the required carboxamides **46**-**50** (**Scheme 2.5**). A synthetic route involves treatment of *trans*-1,4-cyclohexanediamine **45** with synthetic acyl chlorides **33a**, **33b** and **37** in dichloromethane in the presence of DIPEA to give the target amides **46**, **47** and **49**. The formation of these analogues was observed with reaction time of 30 mins at 0^{o} C to 2 hours at ambient temperature and with yields of 47%, 38% and 40%, respectively.

In comparison, analogue **47** was previously synthesised via peptide coupling reaction using a commercially available 2-[4-(trifluoromethyl)phenoxy]acetic

acid **32** and the resulted yield was 60%.[167] However, resynthesised of the same analogue **47** with different synthetic route by using synthetic acid chloride **33b** led to reducing the yield to 38%. In general, the formation of analogues **46**, **47** and **49** by using acid chlorides proceeded rapidly but with low yield, possibly due to the hydrolysis of acyl chloride. Acid chlorides are highly moisture sensitive, thus they would react with water and get converted back to corresponding acids which are not reactive towards amide reactions.

Analogues **46**, **47** and **49** were purified by trituration with diethyl ether, then separated by filtration and finally dried in vacuum. The structures of the final compounds were confirmed using NMR, LC-MS and HRMS. HPLC (at 95% or above) was utilized to confirm the purity of the analogues.



Scheme 2.5: Synthesis of symmetrical modified terminal aromatic ring.
Reagents and conditions: (a) **33a**, **33b,** and **37**, (DIPEA), DCM, 0^{o} C 30 mins to rt 2 h, 38% to 47%; (b) 4-fluorophenoxyacetic acid and **40a**, HBTU, DCM, Et3N, 15 h to overnight, yields 60 and 78%.

Subsequent analogues **48** and **50** were prepared by coupling the commercially available 4-fluorophenoxyacetic acid or synthetic carboxylic acid **40a** to *trans*-1,4-cyclohexanediamine **45**, using HBTU in the presence of triethylamine (**Scheme 2.5**). This afforded **48** and **50** in yields of 60% and 78% respectively, following purification using column chromatography utilizing solvent mixtures of either dichloromethane / tetrahydrofuran or ethyl acetate / dichloromethane.

The structures of the final compounds were confirmed using NMR, LC-MS and HRMS, while HPLC (at 95% or above) was utilized to confirm the purity of the analogues. Overall, good yields (60% and 78%) were once obtained for the coupling of carboxylic acids with amines and HBTU, but yield were poorer (40% - 47%) for the acid chlorides coupling derivatives. This is possibly due to the hydrolysis of acyl chlorides and/ or using the crude synthetic acyl chlorides directly in amide coupling without purification, contributing to the limited value in our coupling.

2.4.3. Modification of the glycolamide linker

The concept of bioisosterism is widely utilized in the rational modification of lead compounds. The definitions of classical bioisosters relate size, shape, polarity and electron distribution of the group with activity.[182]

The glycolamide linker, optimally 4 atoms, between the terminal phenyl and the central 6-membered core ring also appears to be important, although this has not been assessed extensively in the patent example.[150] There are limited studies cited in the literature that investigated the modification of the glycolamide linker. Among the modified linkers examined, amidine and carbamate were found to have activity, but still less potent than ISRIB.[150, 151, 167]

The glycolamide moiety could have an important role in imparting high eIF2B affinity. The polar feature of the linker, *O*-ether and amide moiety, allows it to serve as hydrogen bond donator and acceptor simultaneously (**Section 2.3**, **Figure 2.2**). On this basis, amide bioisosteres such as carbamate, urea, amidine, ester and inverted amide (**Figure 2.10**) were considered to be of interest. Installed different amide bioisosteres assist in ascertain the structural binding

pocket of the glycolamide linker in terms of its size, shape, electronic distribution, and lipophilicity. Amide isosteres have typically been of interest as a mean of modulating polarity, bioavailability and metabolism. These isosteric groups would also allow further SAR evaluation due to the diversity of substituents that could replace the amide moiety. Furthermore, to directly compare the replacement groups, the one side unsubstituted aryl ring was considered the optimal choice as a terminal group, although *p*-chloro substitution of this ring offers the best activity. In addition, unsubstituted rings as starting materials were found to be more highly feasible and economically more affordable.

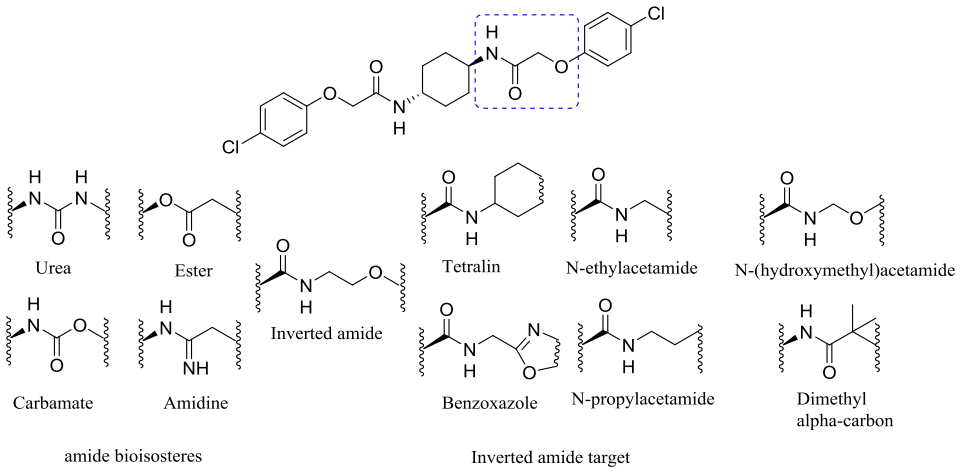


Figure 2.10: Intended target compounds obtained through modifications of the glycolamide moiety.

Inverted amide has very similar characterisctics to amide but reversed the orientation of both carbonyl and amine groups, which may function as a hydrogen bond acceptor and hydrogen bond donor, respectively.[183] The docking studies of reverse amide analogue **61c** (**Figure 2.11**) showed binding pose and receptor interactions similar to that of ISRIB at eIF2B. In addition, pharmacological results of analogue **61c** displayed EC_{50} value in the low-

nanomolar range (these results will be explained in details in **Chapter 3**). This indicates that the activity of eIF2B is retained by the presence of carboxamide inverted bioisosters.

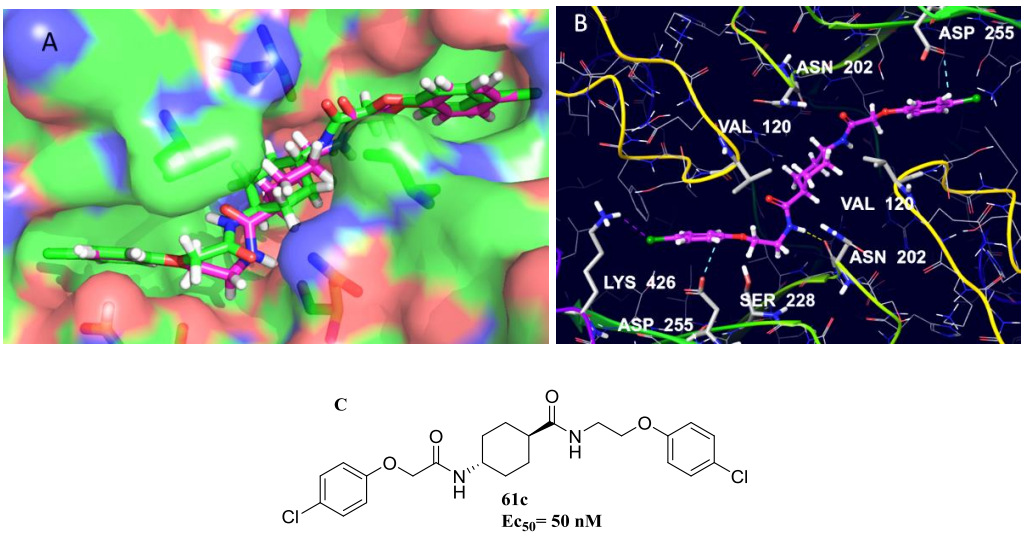


Figure 2.11: Predicted binding conformation of inverted amide analogue **61c** with the eIF2B; (A) Structural overlay of analogue **61c** (purple) and **ISRIB** (green) through hydrophobic pocket of eIF2B; (B) Representation of residues around analogue **61c** in the binding site; (generated using Schrödinger Maestro and Pymol software from PDB entries: 5B04); (C) chemical structure of analogue **61c**.

Based on these findings, it was deemed prudent to investigate more carboxamide inversion analogues (**Figure 2.10**). For example, analogues incorporating a restriction in rotational properties such as tetralin and benzoxazole were prepared. This optimisation would be helpful in disrupting the symmetry and can be useful as a platform for many different core rings modifications. Other investigated analogues demonstrate alteration in the nature and distance of the inverted carboxamide linkage through replacing one aryl ether bond with carbon linkage. Accordingly, synthesis of *N*-ethylacetamide and *N*-propylacetamide derivatives were attempted. However, difficulties were encountered to find the appropriate starting materials to synthesising inverted amide analogue with *N*-

(hydroxymethyl)acetamide linker (**Figure 2.10**), due to chemical instability of this moiety.

However, the literature investigated the α-carbon moiety of the glycolamide linker on one side by introducing a small bulky methyl group at this position. The results of this modification showed EC_{50} values in the low-nanomolar range, but still less potent than ISRIB.[167] Therefore, further steric effect at this position was investigated by designing analogues containing dimethyl group. Although it is not-considered as bioisosteres, this addition of dimethyl group was selected to ascertain if steric bulk at this position is tolerated which consequently assist in altering the crystal form/packing. In addition, further investigation of the α-carbon moiety may help in finding an appropriate site in the ISRIB molecule to insert a spacer with a tag molecule which can help in target identification.

In general, most analogues were modified at one *O*-arylglycolamide side chain, because it was clearly noticed from previously published SAR studies that the alteration of both sides resulted in loss of potency. However, some symmetrical analogues such as compounds containing amidine and mono/di-methyl α-carbon modifications were synthesised to further study the requirements of symmetry.

2.4.3.1. Synthetic strategy

Synthesis was implemented in a similar strategy to that described for the synthesis of non-symmetrical and symmetrical modified terminal aryl rings (**Section 2.4.2.1**). Once again, commercially available fragments of acid chloride and acid carboxylate were combined in a one step with 2-(4-chlorophenoxy)-*N*-[(1*R*,4*R*)-4-aminocyclohexyl]acetamide hydrochloride **28** or with *trans*-1,4-

diaminocyclohexane **45**, under basic condition to generate the desired symmetrical and non-symmetrical analogues.

A synthetic strategy to prepare amidine was reported previously in literature.[167] The classical route to synthesise amidine was carried out via Pinner reaction, which involves acid catalysed reaction of a nitrile with an alcohol to form an imidate salt.[184] The imidate was then converted into the amidine by treatment with amine in absolute ethanol.

Inverted amide analogues were prepared from commercially available *trans*-4-(Boc-amino)cyclohexanecarboxylic acid **51**. The synthetic strategy involved two steps. First, the instalment of appropriate inverted carboxamide side chains via coupling with *trans*-4-(Boc-amino)cyclohexanecarboxylic acid. Second, the removal of the Boc group to afford amine intermediate, which is then used to introduce the second *O*-arylglycolamide side chain by reaction with 4-chlorophenoxyacetyl chloride **26** (**Figure 2.12**). The selection of starting material with suitably protected amine, *trans*-4-(Boc-amino)cyclohexanecarboxylic acid **51**, rather than carboxylic protection group (such as ethyl esters) was to avoid the complication that could result from using ester group. In addition, compound **51** was found to be more available and cheaper.

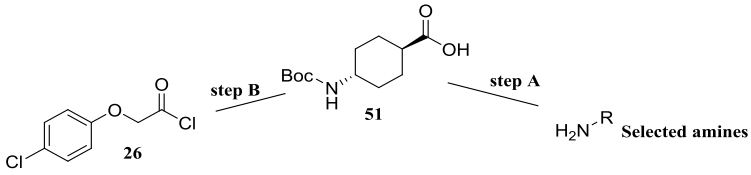
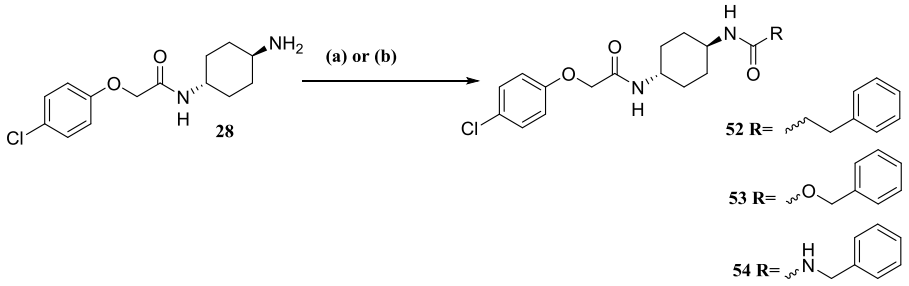


Figure 2.12: Strategy employed for synthesis reverse amide analogues.

2.4.3.2. Synthesis of non-symmetrical modified glycolamide linker analogues

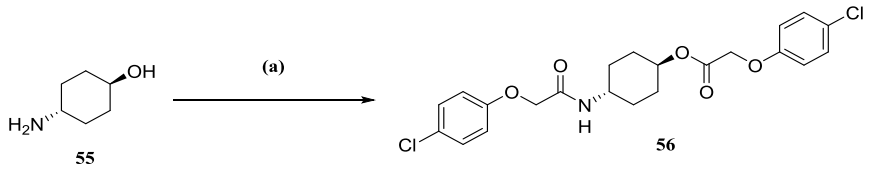
Synthesis of amide (**52**) and carbamate (**53**) analogues (**Scheme 2.6**) was taken place in a similar way to the previous coupling reaction with acyl chloride for the non-symmetrical terminal aromatic ring analogues. Selected commercially available hydrocinnamoyl chloride and benzyl chloroformate were condensed with synthetic key amine compound **28**, in the presence of DIPEA to afford the corresponding amide and carbamate derivatives respectively. The synthesis of the analogues continued with reaction times of 1 to 2 hours and with yields of 84% and 90%, respectively. Synthesis of derivative bearing urea group was also outlined in **Scheme 2.6**. The benzyl isocyanate underwent attack by a nucleophile amine group **28** in presence of DIPEA, to deliver the urea analogue **54** in yield 80%. Once again, all of the analogues were purified by trituration with diethyl ether and characterised using NMR, LC-MS and/or HRMS. HPLC (at 95% or above) was utilized to confirm the purity of the analogues.



Scheme 2.6: Synthesis of non-symmetrical modified glycolamide linker
Reagents and conditions: (a) hydrocinnamoyl chloride and benzyl chloroformate, (DIPEA), DCM, 0^{o} C 30 mins to rt 1-2 h, 84% and 90%; (b) benzyl isocyanate, DIPEA, DCM, 80%.

On the other hand, the use of *trans*-4-aminocyclohexanol **55** (**Scheme 2.7**) allowed simple conversion of the amine and alcohol termini to the desired amide and ester in one step. Treatment of *trans*-4-aminocyclohexanol **55** with excess

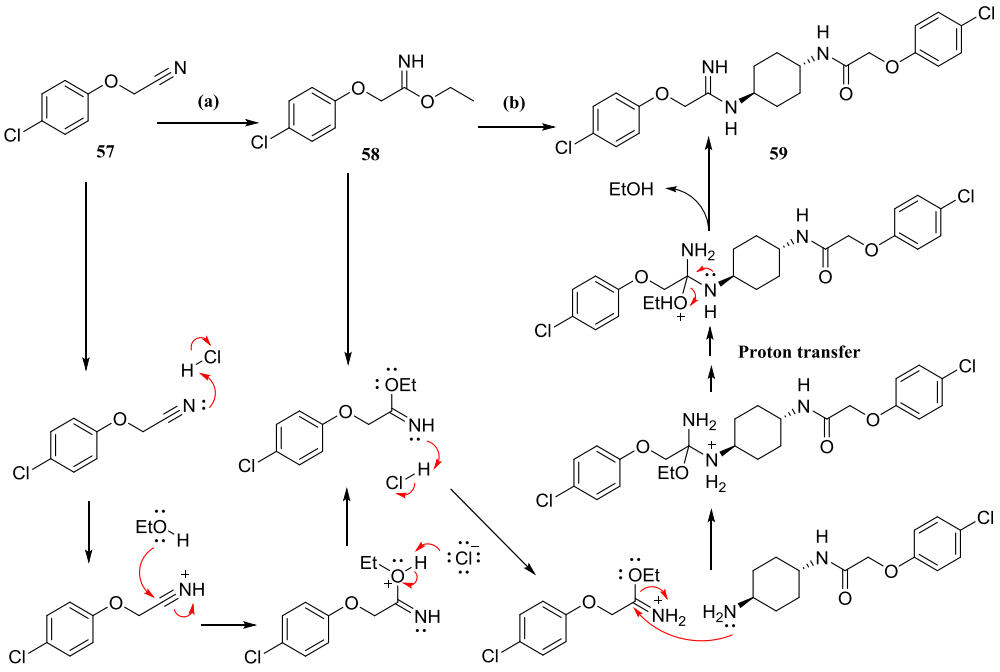
of 4-chloroacetylchloride in the presence of N,N-diisopropylethylamine afforded the corresponding ester-amide ISRIB analogue **56**. The formation of the compound **56** continued with reaction time of 7 hours and with a yield of 42%. The slow rate and low yield could be attributed to the poor nucleophilicity of the cyclic alcohol, and possibly the reaction may proceed more rapidly with more base addition to deprotonate the alcohol. In addition, the competition between the nucleophilic amine and alcohol to attack carbonyl of acid chloride is likely to be considered as well. Both amine and alcohol react with acid chloride with the same mechanism (nucleophilic addition elimination), but a nitrogen atom is more nucleophilic than an oxygen atom.



Scheme 2.7: Synthesis of analogue **56**, ester linker.
Reagents and conditions: (a) 4-chlorophenoxy acetyl chloride **26**, N,N-diisopropylethylamine (DIPEA), DCM, 0^{o} C 30 mins to rt 7 hs, 42%.

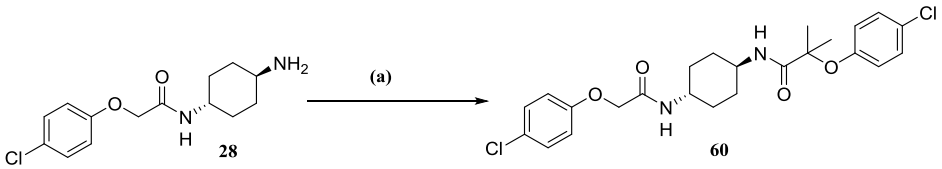
Synthesis of amidine analogue was carried out according to the literature procedure, via Pinner reaction.[167] This method involves the preparation of an imidate salt **58** by reaction of 4-chlorophenoxyacetonitrile **57** and ethanol in diethyl ether in the presence of hydrochloric acid solution (4M) in dioxane as catalyst **(Scheme 2.8)**. The reaction mixture proceeded with reaction times of around 18 hours to obtain crude ethyl 2-(4-chlorophenoxy)-ethanecarboximidate hydrochloride **58** as white solid that was used without further purification. The imidate salt was then converted into the amidine by treatment with amine compound **28** in ethanol in the presence of DIPEA. The formation of the amidine analogue **59** proceeded with reaction times of 18 hours and with a yield of 76%

after purification by column chromatography using a solvent mixture of 10% 1M ammonia methanolic solution and dichloromethane. The proposed reaction mechanism for the amidine formation is detailed in **Scheme 2.8**.



Scheme 2.8: Synthetic route to amidine analogue **59**.
Reagents and conditions; (a) diethyl ether, 4M solution of hydrochloric acid in dioxane, ethanol, overnight, rt; (b) **28**, ethanol, DIPEA, 18h, rt, 76%.

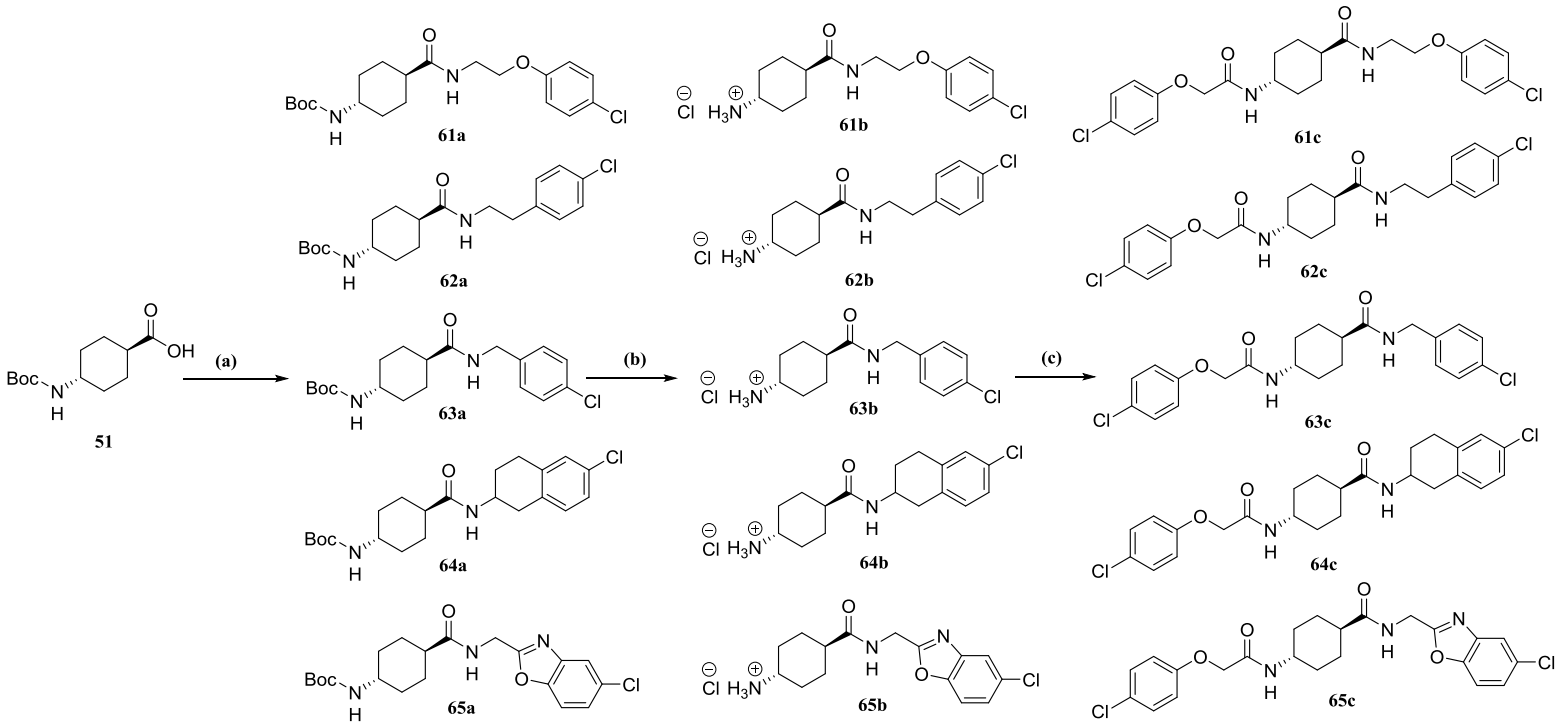
The synthesis of analogue with dimethyl group at the α-position of the glycolamide linker **60** is described in **Scheme 2.9**. The desired analogue obtained via union of commercially available 2-(4-chlorophenoxy)-2-methyl-propanoic acid with amine compound **28** aided by stoichiometric amounts of coupling reagent HBTU in the presence of triethylamine. The synthesis of the analogue continued with reaction times of 16 hours and with a yield of 94%.



Scheme 2.9: Synthesis of non-symmetrical analogue modified at α-position of the glycolamide linker **60**. Reagents and conditions: (a) **2**-(4-chlorophenoxy)-2-methylpropanoic acid, HBTU, DCM, Et_3N, 16 h, yield 94%.

2.4.3.3. Synthesis of reverse amide analogues

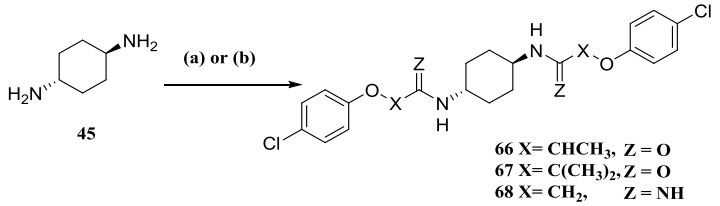
Inverted amide analogues **61c**-**65c** were synthesised from *trans*-4-(Boc-amino)cyclohexane carboxylic acid **51** as illustrated in **Scheme 2.10**. The latter was reacted with amines, 2-(4-chlorophenoxy)-ethylamine, 4-chlorobenzyl-amine, 2-(4-chlorophenyl)ethylamine, 2-amino-6-chloro-1,2,3,4-tetrahydro-naphthalene hydrochloride or 2-amino-5-chlorobenzoxazole using HBTU in the presence of triethylamine to produce Boc-protected inverted carboxamide side chain intermediates **61a**-**65a**. The synthesis of the intermediates continued with reaction times of 8h to 16h and with yields ranging from 72% to 92%. These amide intermediates then underwent standard amine Boc-deprotection in a mixture of methanol and 4N HCl/dioxane yielding the desired hydrochloride salts form of the analogues **61b**-**65b.** They were produced in high yield and purity, and then used in the next step without further purification. Finally, 4-chlorophenoxyacetylchloride **26** was used to install the second *O*-arylglycol-amide side chain, by reaction with free deprotected amino group of intermediates **61b**-**65b** to generate the final amide analogues **61c**-**65c**, in yields ranging from 69% to 91%. All of the analogues were purified by trituration with diethyl ether or by column chromatography, and characterised using NMR, LC-MS and/or HRMS. HPLC (at 95% or above) was utilized to confirm the purity of the analogues.



Scheme 2.10: Synthesis of invers amide analogues **61c**-**65c**.
Reagents and conditions: (a) 2-(4-chlorophenoxy)-ethylamine, 4-chlorobenzylamine, 2-(4-chlorophenyl)ethylamine, 2-amino-6-chloro-1,2,3,4-tetrahydronaphthalene HCl or 2-amino-5-chlorobenzoxazole, HBTU, DCM, Et_3N, 8 hr to overnight, yields 72% to 92%; (b) dioxane-MeOH (2:1), 4 N HCl/dioxane, rt; yields 90% to 95%; (c) 4-chlorophenoxy acetyl chloride, N,N-diisopropylethylamine, DCM, 0^{o}C 30 mins to rt 1-2 hr, yields 69% to 91%.

2.4.3.4. Synthesis of symmetrical modified glycolamide linker analogues

Further investigation to the symmetrical modification on both glycolamide linkers was carried out through synthesising the final desired analogues **66-68.** Synthesis of analogues **66** and **67** was implemented in a similar way to that described in **Section 2.4.2.4**. Once again, the *trans*-1,4-cyclohexanediamine **45** and commercially available 2-(4-chlorophenoxy)propanoic acid and 2-(4-chlorophenoxy)-2-methylpropanoic acid were coupled in one step using HBTU in the presence of triethylamine (**Scheme 2.11**). The formation of the analogues **66** and **67** required stirring for 18 hours with yields of 68% and 57%, respectively. The long reaction time is possibly due to steric hindrance of the methyl and dimethyl groups at the α-carbon position of the glycolamide linker. In addition, analogue **68** was obtained by Pinner reaction as described before in the synthesis of non-symmetrical amidine analogue **60**. Overnight stirring of *trans*-1,4-cyclohexanediamine **45**, in ethanol, with an excess of imidate salt **59** (ethyl 2-(4-chlorophenoxy)-ethanecarboximidate hydrochloride) resulted in generating the desired analogue **68** with 63% yield.



Scheme 2.11: Synthesis of symmetrical modified terminal aromatic ring.
Reagents and conditions: (a) 2-(4-chlorophenoxy)propanoic acid and 2-(4-chlorophenoxy)-2-methylpropanoic acid, HBTU, DCM, Et_3N, 18h, yields 68% and 57%; (b) **59**, ethanol, DIPEA, overnight, rt, 63%.

2.4.4. Modification of the central core-template that joins the *O*-arylglycolamide side chains

To gain further insight into the modification of the central cyclohexane ring, synthesis of series of analogues was initiated to give the opportunity to scope out

more SARs as fully as possible. Examples of target structures incorporating commercially available or readily synthesised materials for the proposed molecular cores are summarised in **Figure 2.13**.

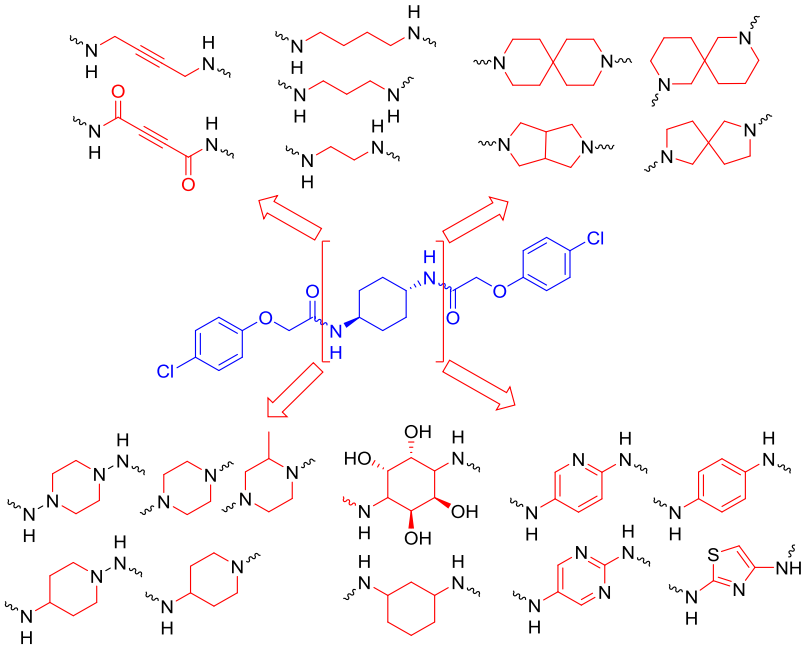


Figure 2.13: Overview of ISRIB restricted cores modification in this study.

In our continuing efforts toward the development of ISRIB-like molecules, focus was made on the development of novel spiro and bicyclic core ring analogues. The rationale for the use of the spiro and bicyclic motifs as alternatives for the central cyclohexane ring is derived from their generic spatial features. Introduction of spiro or bicyclic heterocyclic rings was used to rigidify and restrict the ligand conformation, which could potentially confer an even higher reduction in flexibility and thus target promiscuity upon binding.[185] Conformational restriction by introducing spiro or bicyclic rings can also potentially improve the bioavailability and reduce or redirect the metabolism.[186, 187] In addition, the greater three-dimensional structural features of these molecules will contribute in acquiring novel intellectual property novelty.[188] Accordingly, common spiro and bicycle scaffolds with five- or six-membered

ring such as diazaspiroundecane, diazaspirononane and diazabicycloctane were incorporated in replacing the cyclohexane cyclic ring (**Figure 2.13**).

Investigation into this region of ISRIB molecule has been extended with a variety of acyclic chain lengths. Modifications were made to allow comparison of replacing the cyclic central core over acyclic, and also to investigate the carbon spacing and orientation. These include alkyl molecular cores with two to four carbon such as ethyl, propyl and butyl derivatives as well as less flexible molecules such as alkynyl derivatives.

Moreover, the literature cited only one aromatic ring replacement to central cyclohexane, which is a simply aryl core and it turned out to be the best tolerated replacement.[151] Therefore, other aromatic rings equivalents to benzene with different electronic properties such as pyridine, pyrimidine and thiazol derivatives were selected for further investigation.

In order to explore the polarity of this portion (central core) of the ISRIB molecule, a comparison of a wide range of polar heterocyclic derivatives was a prerequisite. Accordingly, the non-polar hydrophobic cyclohexane ring was replaced by piperazine or piperidine derivatives to prepare novel analogues with heterocycloalkyl core rings. In addition, introducing core ring with nitrogen-containing heterocycles was expected to improve water solubility and binding efficiency to the target molecule, and therefore improve the pharmacokinetic profiles.[176, 189] Thus, a relatively simple way to make the ISRIB compound much more water-soluble would be to introduce the N atom into the cyclohexyl ring, therefore selection of piperazine or piperidine as a core ring could be helpful in achieving this purpose. Moreover, replacing cyclohexane ring with piperazine or

piperidine afford tertiary amide products, this could assist in exploring the relevance of the NH of amide group on receptor binding.

Generally, the rationale behind the selection of the piperidinyl or piperazinyl motifs as alternatives for the cyclohexane core ring is derived from their structural conformation similarity to the cyclohexane. Piperidine and piperazine prefer a chair conformation, similar to cyclohexane. This is further supported by docking studies which revealed that piperidinyl analogue **103** behaves similarly in binding pose as ISRIB at eIF2B binding site, mostly between the Val^{120} of the two δ subunit (**Figure 2.13**).

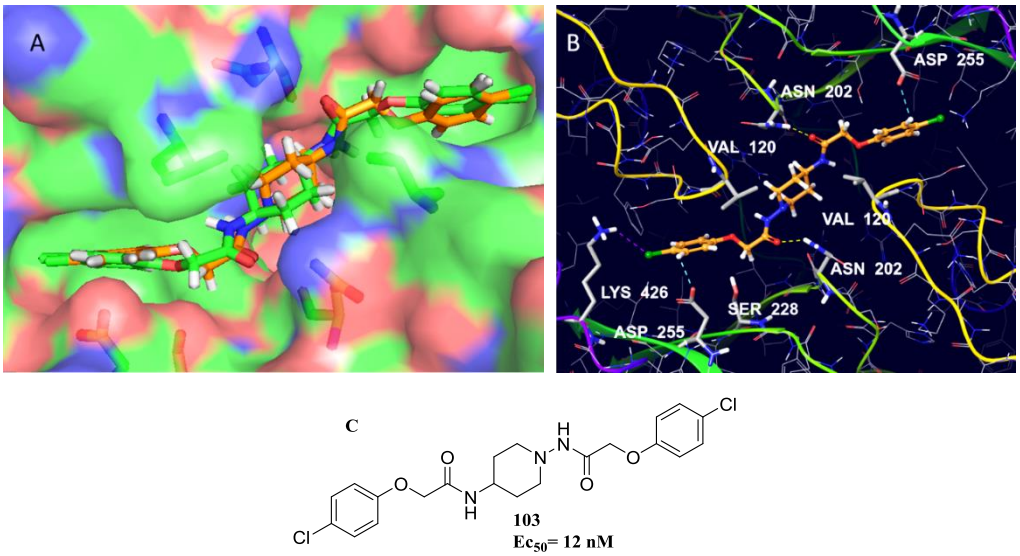


Figure 2.13: Predicted binding conformation of piperidinyl analogue **103** with the eIF2B; (A) Structural overlay of analogue **103** (brown) and ISRIB **1** (green) through hydrophobic pocket of eIF2B; (B) Representation of residues around analogue **103** in the binding site; (generated using Shrodinger Maestro and Pymol softwares from PDB entries: 5B04); (C) chemical structure of analogue **103**.

In addition, other modifications were made to the piperidinyl or piperazinyl motifs to investigate further structure activity relationships. These modifications involved exploring the effects of distance and nature of the glycolamide linker, which connects the nitrogen atom of cyclic piperidine with the terminal aromatic

rings. Accordingly, analogues having linker with three or four atoms, as well as linker with methylene group instead of carbonyl-amide moiety were synthesise.

Finally, the same principle of exploring the polarity of the central core was applied in selecting cyclohexanetetrol with four polar OH groups that could form further interactions due to the presence of numerous polar components. Furthermore, replacement of 1,4-diaminocyclohexane with 1,3-diaminocyclohexane was selected to further investigate the orientation effect. Hence, preparing these types of analogues to target eIF2B is warranted.

2.4.4.1. Synthetic strategy

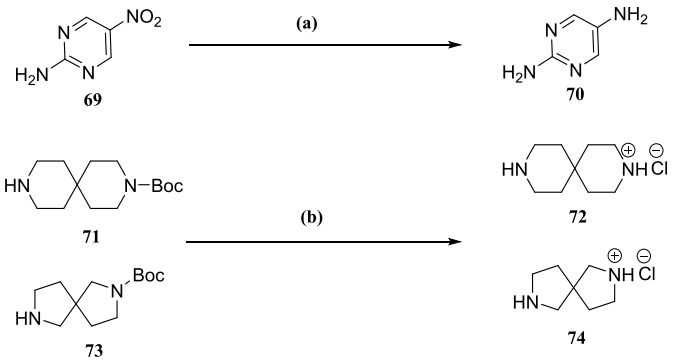
Chemically diverse library of ISRIB derivatives (spiro, bicyclo, acyclic, aromatic and heterocyclic) were synthesised to explore the effect that the central core change has on eIF2B activity in comparison with *trans*-cyclohexane. Once again, synthesis was adopted in a similar way to the formation of the symmetrical modified aryl ring analogues described in **Section 2.4.2.1**. The commercially available acid chloride, 4-chlorophenoxy acetyl chloride **26**, were reacted with the various diamine core ring in one step, under basic conditions to generate the desired analogues. Since they are commercially available at lower cost than corresponding free diamine molecule, some of the desired diamine core rings were prepared from the corresponding partially Boc-protected diamine after Boc-removing or from reduction of nitro group to amine.

Furthermore, the general synthetic strategy for the production of hydrazide derivatives from piperidinyl or piperazinyl were achieved via three steps. Initially, piperidine or piperazine underwent acid-catalysed reaction with sodium nitrite in acetic acid to form nitrosamines derivatives. Then, the nitrosamine group was reduced to the corresponding amine using zinc dust under acidic

conditions. Finally, acylation of amine group was formed with acyl chloride to afford hydrazide desired analogues.

2.4.4.2. Synthesis of aromatic, spiro, bicycle and acyclic central diamine core

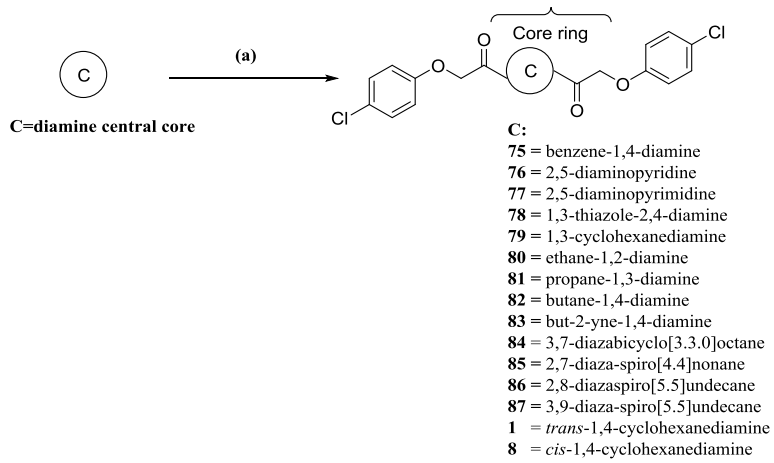
Since some of the molecules such as 2-amino-5-nitropyrimidine **69**, 2-Boc-2,7-diazaspiro[4.4]nonane **71** and 3-Boc-3,9-diazaspiro[5.5]undecane **73** were found to be more available and cheaper than the corresponding free diamine, therefore the first step involved conversion of these molecules to their corresponding free diamine core **70**, **72** and **74**, respectively (**Scheme 2.13**). Pyrimidine-2,5-diamine **70** was readily obtained through reduction of 2-amino-5-nitropyrimidine **69** by catalytic hydrogenation over Palladium on carbon in MeOH at room temperature, with a crude yield of 77%. Deprotection of the Boc-protected spiro compounds **71** and **73** was carried out by using a solution of 4N HCl/dioxane giving the corresponding hydrochloride salts **72** and **74** in yields of 87% and 96%, respectively, which were used in the next step without further purification.



Scheme 2.13: Synthesis of free diamine core ring molecules **70**, **72** and **74**.
Reagents and conditions: (a) Pd/C, H_2, MeOH, overnight, rt, 77%; (b) 4 N HCl/dioxane, rt, 87% and 96%.

The commercial availability of various central diamine core, allowed facile synthesis of a variety of modified central core analogues. 4-Chlorophenoxy acetyl chloride **26** was condensed with selected commercially available or

prepared diamines, in the presence of DIPEA to generate the corresponding amides **75**-**87**. The synthesis of the aromatic and acyclic analogues **75** to **83** continued with reaction times of 1 hour at room temperature and with yields between 76% and 91%. However, formation of the spiro and bicyclo analogues **84** to **87** proceeded with reaction times of 3 hours at room temperature and with yields between 22% and 66%. Introducing of the first *O*-arylglycolamide on the amine group of diamine core may be impedes another free amine from attacking 4-chlorophenoxy acetyl chloride to install the second *O*-arylglycolamide. This could be explained the poor yields obtained in the synthesis of spiro and bicyclo analogues. Therefore, it was observed that adding excess of 4-chlorophenoxy acetyl chloride was not useful to improve the yields. However, *trans* 1 and *cis* **8** ISRIB were achieved in similar way according to literature procedures.[167] All of the analogues were purified by trituration with diethyl ether or by column chromatography using solvent mixtures of dichloromethane and tetrahydrofuran. They were characterised using NMR, LC-MS and/or HRMS. HPLC (at 95% or above) was utilized to confirm the purity of the analogues.

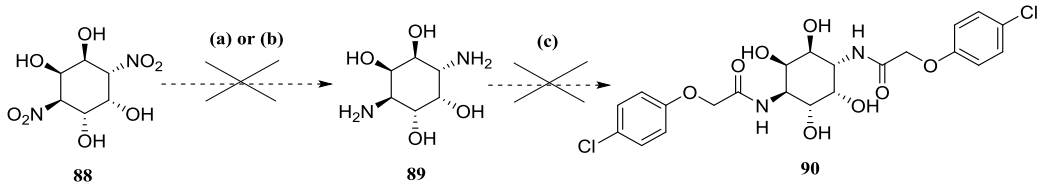


Scheme 2.14: Synthesis of analogues **75-87**, core ring analogues.
Reagents and conditions: (a) 4-chlorophenoxy acetyl chloride, N,N-diisopropylethylamine (DIPEA), DCM, 0^{o} C 30 mins to rt 3 hs, analogues **75-83** yields 76%-91%, analogues **84-87** yields 22% and 66%.

2.4.4.3. Attempted synthesis of diamino-cyclohexanetetrol and but-2-ynediamide central core

Two different attempts were made to reducing the nitro group on dinitro-cyclohexanetetrol **88** to the amine group to allow amide bond formation (**Scheme 2.5**). First, reducing of dinitro-cyclohexanetetrol **88** using zinc dust under acidic conditions was anticipated to generate the free diamine compound **89**. After removal of excess zinc dust via filtration through celite-pad and washing with aqueous 1N HCl solution, the resulting diamine salt produced **89** had turned into a waxy solid product. This product was not isolated, and directly involved in a reaction with 4-chlorophenoxy acetyl chloride **26** in the presence of DIPEA. Unfortunately, TLC and LC-MS analysis was not successful to demonstrate any product after 5 hours. It seems that the reduction of the nitro group to the amine group was not achieved by this method.

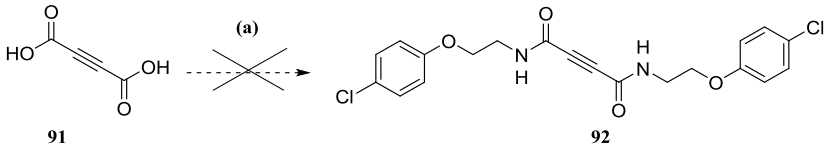
Second, reduction of nitro was attempted by using catalytic hydrogenation over Pd/C. Although the amine was expected to be formed (TLC analysis show a change in spot after overnight reaction indicating reduction of nitro to amine), formation of the desired amide analogue **90** was not evident by ^{1}H NMR and LC-MS analysis.



Scheme 2.15: Attempted synthesis of diamino-cyclohexanetetrol core ring **90**.
Reagents and conditions: (a) acetic acid, water, Zn dust, 3 h, rt; (b) Pd/C, H_2, MeOH, overnight, rt; (c) 4-chlorophenoxy acetyl chloride, N,N-diisopropylethylamine (DIPEA), DCM, 0^{o} C 30 mins to rt 3 hs.

Moreover, the reaction for the target compound **92** failed as well (**Scheme 2.16**). An attempt to purifying the crude material by column chromatography was

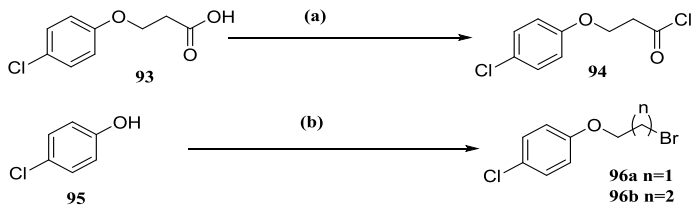
successful in isolating a major peak. Although the correct mass was displayed through LC-MS analysis, ^{1}H NMR chart indicated that the required final product had not formed.



Scheme 2.16: Attempted synthesis of but-2-ynediamide central core **92**.
Reagents and conditions: (a) 2-(4-chlorophenoxy)-ethylamine, HBTU, DMF, Et_3N, overnight.

2.4.4.4. Synthesis of 4-aminopiperidine and piperazine analogues

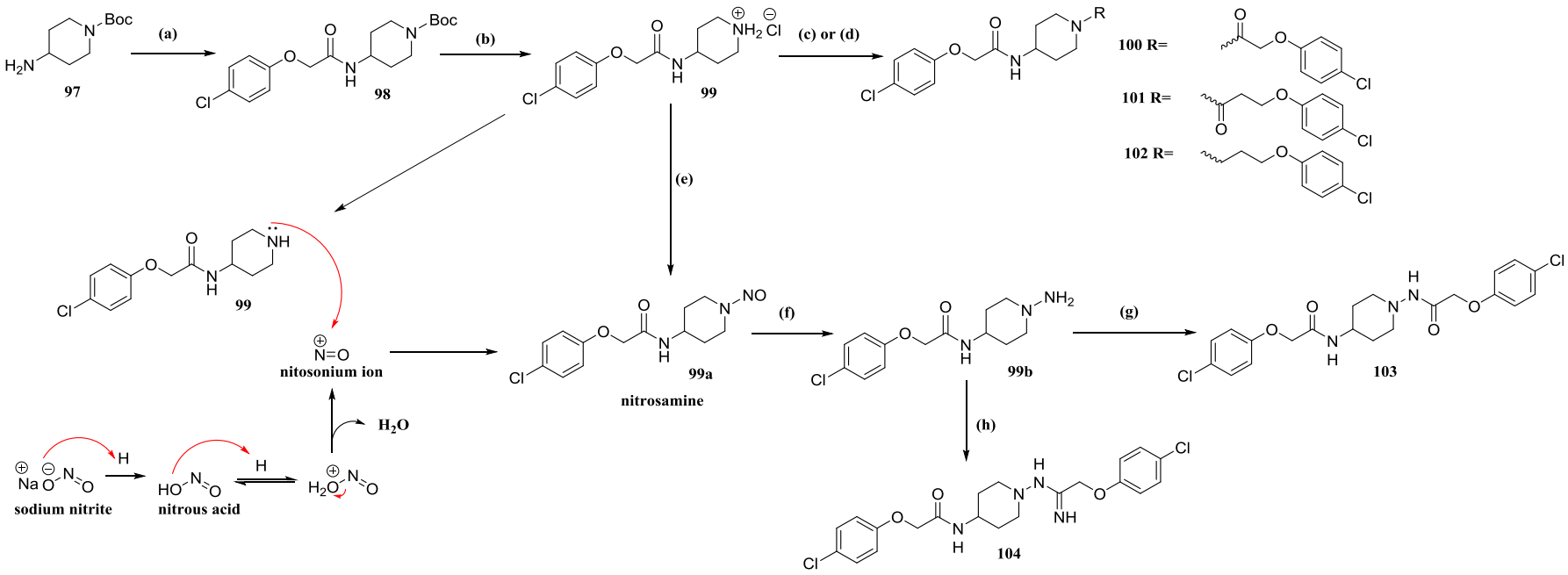
The commercially available 3-(*p*-chlorophenoxy)propionic acid **93** was converted to the corresponding acid chloride **94** by mixing with oxalyl chloride (**Scheme 2.17**) as described previously in section **2.4.2.2**. The reaction proceeded in 2 hours at ambient temperature with a yield of 81%. The acid chloride was used in the next step without further purification. Since the side chain fragments were commercially unavailable, their synthesis was required. Alkylation of *para*-chlorophenol **95** was conducted using potassium bicarbonate (K_2CO_3) as a base in DMF, and refluxing with an excess of ethylene dibromide or 1,3-dibrompropane to obtain 1-(2-bromoethoxy)-4-chlorobenzene **96a** and 1-(3-bromopropoxy)-4-chloro-benzene **96b**, respectively. These were used after purification by column chromatography using solvent mixtures of dichloromethane and petroleum ether.



Scheme 2.17: Synthesis of 3-(4-chlorophenoxy)propanoyl chloride **94**, 1-(2-bromoethoxy)-4-chlorobenzene **96a** and 1-(3-bromopropoxy)-4-chlorobenzene **96b**.
Reagents and conditions: (a) oxalylchloride, DCM, 2-drops of DMF, 0^{o} C to rt 2 h, 81%; (b) ethylene dibromide or 1,3-dibrompropane, K_2CO_3, DMF, reflux, 4 hrs, yield 51% and 58%.

The synthesis of piperidinyl analogues was carried out in the manner described in **Scheme 2.18**, which involved three to five steps. Initially, the commercially available 4-amino-1-Boc-piperidine **97** underwent acylation with 4-chlorophenoxyacetyl chloride **26** in the presence of DIPEA to obtain *tert*-butyl 4-[2-(4-chlorophenoxy)acetamido]piperidine-1-carboxylate **98** in high yield. Selection of 4-amino-1-Boc-piperidine **97** as a starting point to install first a single *O*-arylglycolamide side chain will help in monitoring the remaining steps of the synthesis by using LC-MS and TLC analysis. Deprotection of the Boc-protected amine group in compound **98** was carried out in acidic conditions using solution of 4N HCl/dioxane to give the corresponding hydrochloride salt **99** in yield 95% after recrystallization. The later hydrochloride salt **99** acts as a key intermediate in various reactions to prepare the piperidinyl analogues.

The piperidinyl analogues **100** and **101** were achieved in the same manner described in section **2.4.1.2**, via amide coupling of the intermediate **99** with 4-chlorophenoxyacetyl chloride **26** or 3-(4-chlorophenoxy)propanoyl chloride **94** in the presence of N,N-diisopropylethylamine (**Scheme 2.18**). High nucleophilicity of piperidine contributes to proceeding the reaction with the carbonyl chloride reagent rapidly and in high yields 72% and 92%. However, analogue **102** which has tertiary amine group was obtained through direct alkylation of piperidine amine group in intermediate **99** with 1-(3-bromopropoxy)-4-chlorobenzene **96b**, using K_2CO_3 as a base, and refluxing in methanol for 12 hours.



Scheme 2.18: Synthetic route to pipridinyl analogues and proposed reaction mechanism of nitrosamine.
Reagents and conditions: (a, c and g) 4-chlorophenoxy acetyl chloride **26** or 3-(4-chlorophenoxy)propanoyl chloride **94**, N,N-diisopropylethylamine, DCM, 0 ^{o}C 30 mins to rt 1-2 hr, yields 51% to 93%; (b) 4 N HCl/dioxane, rt, 95%; (d) 1-(3-bromopropoxy)-4-chlorobenzene **96b**, K_2CO_3, MeOH, reflux 60 ^{o}C, 12 hr, 53%; (e) sodium nitrite ($NaNO_2$), acetic acid, water, 10 hr, rt, 73%; (f) acetic acid, water, Zn dust, 10 hr, rt; (h) ethyl 2-(4-chlorophenoxy)ethanecarboximidate **59**, ethanol, DIPEA, overnight, rt, 45%.

However, generation of hydrazide **103** and imidamide **104** were obtained with moderate yields, via three steps from intermediate salt **99** (**Scheme 2.18**). Acid-catalysed reaction of intermediate **99** to nitrosamines derivative 2-(4-chloro-phenoxy)-*N*-(1-nitrosopiperidin-4-yl)acetamide **99a** was achieved via treatment with sodium nitrite in acetic acid and water. The proposed reaction mechanism of nitrosamines formation using sodium nitrite was detailed in **Scheme 2.18**. This reaction involves generation of nitrous acid by acidification of aqueous solution of sodium nitrite with acetic acid. The nitrosamine is usually produced by the reaction of nitrous acid (HNO_2) and secondary amine group of intermediate **99**. The nitrosamine **99a**, then underwent reduction to the amine derivative **99b** using zinc dust under acidic conditions. The reaction proceeded in 10 hours at ambient temperature with a yield of 66%. Finally, formal acylation of amine derivative **99b** with 4-chlorophenoxyacetyl chloride proceeded to afford the desired hydrazide analogue **103** after purification by flash column chromatography with a yield of 51%. It was observed that the hydrazide N-H proton of analogue **103** showed an uncommon NMR spectrum. It reveals a splitting of its peak between the usual downfield positions of 9.25ppm (50% split) and 8.78ppm (50% split) in DMSO (**Figure 2.14**).

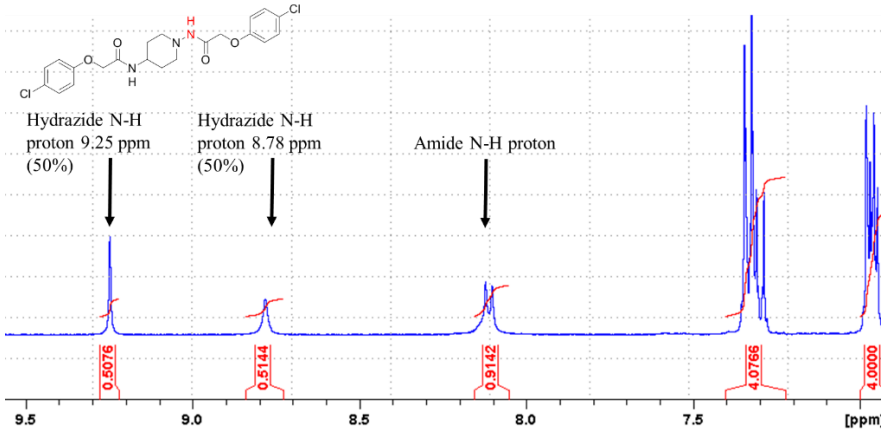
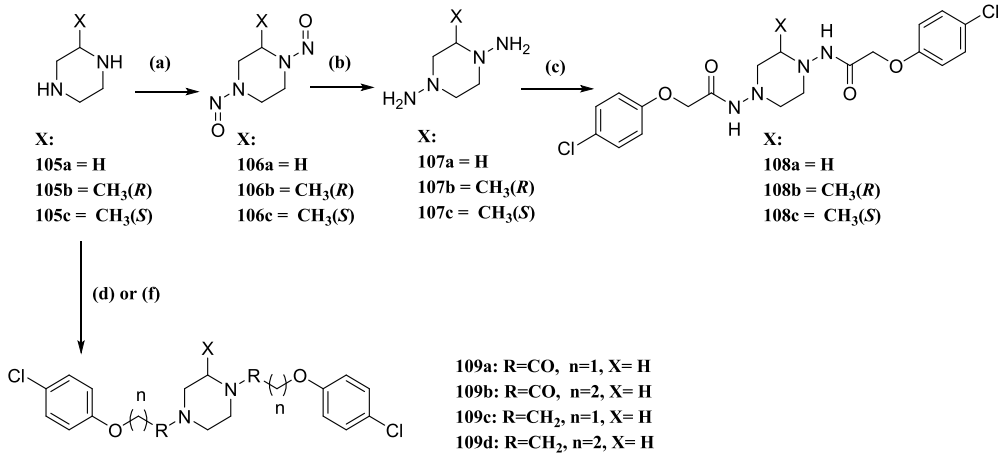


Figure 2.14: ^{1}H NMR spectrum of the analogue **103** (9.5−6.0 ppm region only), demonstrating the unccommon splitting of the hydrazide N-H proton.

Moreover, the synthesis of imidamide **104** was taken place in the same fashion described for the amidine derivative in section **2.4.3.2**. The amine derivative **99b** was reacted with imidate salt **59** in ethanol in the presence of DIPEA. The formation of the amidine analogue **104** continued overnight and with a yield of 45% after purification by column chromatography.

Furthermore, piperazinyl analogues **108a-108c (Scheme 2.19**), bearing di-hydrazide groups, were obtained in a similar manner to the previous piperidinyl analogue **115**. Piperazine **105a**, (*R*)2-methylpiperazine **105b** and (*S*)2-methylpiperazine **105c** were reacted with sodium nitrite in the presence of acetic acid to form nitrosamine derivatives **106a**-**106c**. In each case, under acidic conditions, zinc dust was used as reducing agent to generate the amine derivatives **107a-107c** from the nitrosamines groups. Finally, amide coupling of these amine derivatives with 4-chlorophenoxyacetyl chloride **26** in the presence of DIPEA gave the desired piperazinyl analogues **108a-108c** after purification by flash column chromatography with yields ranging from 36% to 70%.

Moreover, the synthesis of piperazinyl analogues **109a-109d** was carried out as described in **Scheme 2.19**. The commercially available piperazine **105a** was reacted with 4-chlorophenoxyacetyl chloride **26** or 3-(4-chlorophenoxy)propanoyl chloride **94** in the presence of DIPEA to obtain the piperazinyl analogues **109a** and **109b** in high yield of 95% and 75%, respectively. However, alkylation reaction with 1-(2-bromoethoxy)-4-chloro-benzene **96a** and 1-(3-bromopropoxy)-4-chlorobenzene **96b**, in the presence of potassium carbonate and MeOH under reflux at 60^{o} C afforded the desired analogues **109c** and **109d** in yields of 43% and 42%, respectively.



Scheme 2.19: Synthetic route of piperazinyl analogues **108a-108c** and **109a-109d**.
Reagents and conditions: (a) sodium nitrite ($NaNO_2$), acetic acid, water, 24 hr, rt; yields 68% to 89% (b) acetic acid, water, Zn dust, 10 hr, rt; yields 62 to 76% (c) 4-chlorophenoxy acetyl chloride **26**, DIPEA, DCM, 0 ^oC 30 mins to rt 1-2 hr, yields 36% to 70%; (d) 4-chlorophenoxy acetyl chloride **26** or 3-(4-chlorophenoxy)propanoyl chloride **94**, N,N-diisopropylethylamine, DCM, 0^oC 30 mins to rt 2 hr, yields 95% and 75%; (f) 1-(2-bromoethoxy)-4-chlorobenzene **96a** or 1-(3-bromopropoxy)-4-chlorobenzene **96b**, K_2CO_3, MeOH, reflux 60^o C, 10 hr, yields 43% and 42%.

2.5. Conclusions

Using ISRIB **1** as a starting lead compound, a huge library of ISRIB analogues were generated. Modifications of different moieties on ISRIB, allowed the formation of new analogues which were used for further SAR studies. The *S. pombe* eIF2B X-ray crystal structure was used in this project in order to provide an insight into how ISRIB binds to eIF2B. The docking study immediately suggested a binding site for ISRIB at the interface between the two β and δ subunit interfaces. Taking the conformation of ISRIB as a general templet for eIF2B binding, the structures of compounds synthesised in this project were designed and rationalized.

Several methods were adopted in this project to synthesize ISRIB analogues. They were mainly obtained through amide coupling, either by coupling reaction with acyl chloride or by peptide coupling reaction. The key amine intermediate

28 was obtained by following the literature procedure.[167] Various reactions of this key intermediate were then used to introduce a series of non-symmetrical ISRIB analogues. Four truncated analogues were synthesised by simple acylation reaction of acid chlorides with key amine intermediate **28** in order to explore the requirements for symmetry.

The terminal aromatic ring is the initial modified moiety in the ISRIB structure. This skeleton was designed with the aim of further exploring the steric, electronic and positional effects of substituents on the terminal phenyl rings. The terminal moiety was also manipulated by the addition of several polar heteroaromatic ring such as pyridine or pyrimidine, with the aim to enhance the hydrophilicity and potency. A total of ten compounds were synthesised bearing modifications at the terminal rings of the ISRIB structure.

Moreover, a total of fourteen compounds were synthesised bearing modifications at the glycolamide linker of the ISRIB structure. Five amide bioisosteres groups (carbamate, urea, amidine, ester and inverted amide) were appended at the glycolamide moiety in order to mimic the similar interactions and improve the target binding. The α-position (carbon atom) of the glycolamide linker was also manipulated by the addition of dimethyl group with the aim to ascertain if steric bulk in that position is tolerated.

A series of analogues modified at the central core ring were successfully synthesised. This modification aimed to further explore the effect of replacing cyclohexane core ring on potency. A total of thirteen compounds were synthesised bearing spiro, bicyclo, acyclic, aromatic and heterocyclic central core. In addition, new piperidine and piperazine derived scaffolds were

synthesised based on their structural conformation similarity to cyclohexane ring. This skeleton was designed with the aim of minimising the lipophilicity of ISRIB in order to overcome the observed lack of aqueous solubility. The next step set out to evaluate these analogues by using a cell-based assay, which will be discussed thoroughly in the next chapter.

3. Pharmacological evaluation and structure-activity relationships of ISRIB analogues

3.1. Introduction

As outlined in **Chapter 2**, modified ISRIB analogues were designed and synthesised to serve as a neuro-protectant through enhancing the protein synthesis rate. These analogues were mainly classified based on the modified structural part such as the core ring, linkers and terminal aryl ring of the original ISRIB structure. Furthermore, resynthesising of the previously published compounds were included in each round in order to calibrate inter-assay variability.

This chapter describes the pharmacology of a series of ISRIB analogues, in order to further understanding the SAR. To evaluate the pharmacological properties of synthetic ISRIB analogues, they all had to undergo a biological assay (cell-based assay, section **3.2**). In addition, eIF2B crystal structure (PDB 5B04)[40] represents a valuable resource for docking studies, so it was used to model the binding mode of the rationally designed ligands.

As mentioned earlier in **Chapter 1**, eIF2 is required for the initiation of most forms of eukaryotic translation. It is a complex consisting of α, β, and γ subunits, which binds GTP and the initiator Met-tRNA to form a ternary eIF2A–GTP–Met-tRNAi complex that in turn binds the 40S ribosomal subunit in order to

select the initiating AUG codon for the translation of a given gene. On base-pairing of the AUG codon with the Met-tRNA, GTP is hydrolysed to GDP, leaving the binary and inactive eIF2–GDP complex. This in turn is reactivated to eIF2–GTP by the eIF2 GEF eIF2B.[7]

ISR signals converge on Ser^{51} of eIF2α via the kinases PERK (responds to accumulation of unfolded proteins in the ER), GCN2 (responds to amino acid starvation and UV light), PKR (responds to viral infection), and HRI (responds to haeme deficiency). Upon phosphorylation of its α subunit, eIF2 becomes a competitive inhibitor of its GEF eIF2B. The tight binding of phosphorylated eIF2 to eIF2B prevents loading of the eIF2 complex with GTP, therefore blocking ternary complex formation and translation initiation. Since eIF2B is less abundant than eIF2, phosphorylation of a small fraction of total cellular eIF2 has a dramatic effect on overall eIF2B activity.[21]

Under conditions of reduced protein synthesis as experienced by activation of the ISR, a small group of mRNAs with upstream ORFs in their 5'UTR are transcriptionally upregulated. These include ATF4 (a CREB transcription factor) and CHOP (a pro-apoptotic transcription factor). Phosphorylation of eIF2α therefore leads to preferential translation of key regulator molecules under the control of the ATF4 and CHOP transcription factors, although general protein synthesis is suppressed. These regulators orchestrate all aspects of the ISR.[66, 69]

ISRIB and its active analogues have been found to suppress the ISR not by preventing eIF2α phosphorylation, but by allosterically antagonising the inhibitory effect of phosphorylated eIF2 on eIF2B. ISRIB derivatives bind the decameric eIF2B complex, which results in destabilization of the ISR-specific

eIF2B–eIF2(αP) complex, and recruitment of eIF2–GDP as a substrate to the active eIF2B–ISRIB complex, thus suppressing the ISR and allowing resumption of unstressed protein synthesis.[156]

3.2. Biological assay to measure the potency of ISRIB analogues

To assess the action of the synthesised ISRIB analogues in cultured cells, CHOP::GFP reporter assay was employed.[168] The basis for the bioassay used to quantitate the cellular activity of ISRIB analogues takes advantage of one of the ISR-upregulated transcription factors: CHOP. For this purpose a CHO-K1 cell line was employed, which contains a stably integrated plasmid that combines the promoter of the mouse Ddit3/CHOP gene fused to green fluorescent protein (CHOP::GFP). In order to activate the ISR in CHO-K1 cells, these were first treated with histidinol, which indirectly activates the GCN2 branch of the ISR (**Figure 3.1**). Cells were then treated with ISRIB derivatives and concentration–response curves were established following quantitation of the CHOP::GFP reporter by FACS (**Figure 3.2**). An active ISRIB analogue displays a concentration-dependent suppression of the reporter as the ISR is switched off, whereas an inactive analogue has no influence on histidinol-induced ISR and hence sustained reporter expression is observed.

Research collaborators have been previously reported that deregulated expression of a phosphatase that de-phosphorylates eIF2α (thus tuning down the ISR) inhibits reporter activity.[190] More recently, they have also showed that the reporter is unresponsive to stress induced by histidinol in cells compromised in their ability to mount an ISR by a mutation in eIF2α that renders it non-phosphorylatable. These findings clearly indicate that the increase in fluorescent signal in stressed cells specifically reflects activity of the ISR.

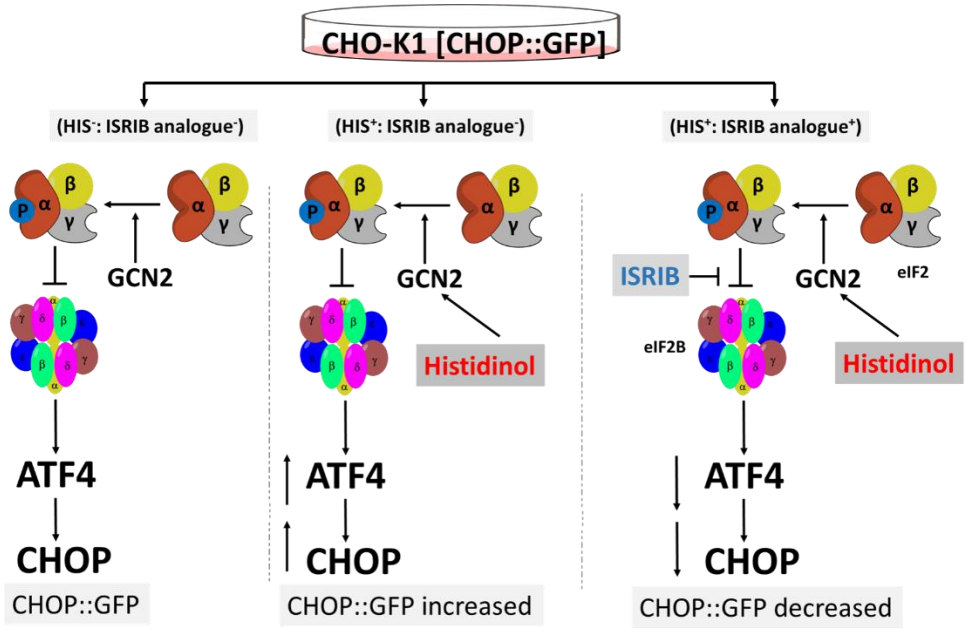


Figure 3.1: Schematic diagram of the CHOP::GFP fluorescent reporter assay:
Exposure to histidinol (His) promotes CHOP::GFP expression which is measured by fluorescent activated cell sorting (FACS); CHO-K1 cells have an ISR transcriptional reporter CHOP::GFR; (HIS^-: ISRIB $analogue^-$) untreated CHO-K1 cells; (HIS^+: ISRIB $analogue^-$) histidinol treated CHO-K1 cells; (HIS^+: ISRIB $analogue^+$) histidinol and ISRIB analogues treated CHO-K1 cells.

The concentration range used to characterise the compounds was from 1 nM to 10000 nM, compounds were tested in a single 12-point titration series. The dynamic range of the assay is defined by the difference in GFP signal between the His+ (treated) and His- (untreated) cells. Inclusion of ISRIB analogues diminishes the response of CHOP::GFP to histidinol. The detection of ISR inhibition (% CHOP::GFP signal expression) is thus defined according to the following equation:

% ISR inhibition = 100 x [Signal (His+) - Signal (His+ with ISRIB analogue)]÷ [Signal (His+) - Signal (His-)].

The half-maximal EC_{50} values reported herein reflect the compound concentration that produces a half-maximal response in the CHOP::GFP signal following induction of ISR. The EC_{50}values of all tested analogues refer to the

sigmoidal part of the concentration-response curves, regardless of whether 100% CHOP::GFP signal reached at the top concentration. Therefore, compounds that reach near 100% CHOP::GFP signal at the top concentration are considered full ISR inhibitor, as in ISRIB. *Trans*-ISRIB showed significant potency at all tested concentrations (**Figure 3.2**), it has EC_{50} of 5.3 nM with a percentage of ISR inhibition equaling 91%. *Trans*-ISRIB exhibited a peak effect at lower concentrations, compared with *cis*-ISRIB which showed peak effect at high concentration with an EC_{50} of 188 nM. On the other hand, analogue **75** is considered to be a partial ISR inhibitor, the maximum CHOP::GFP signal reached was 71% and the half-maximal value between background and 50% CHOP::GFP signal was 67 nM.

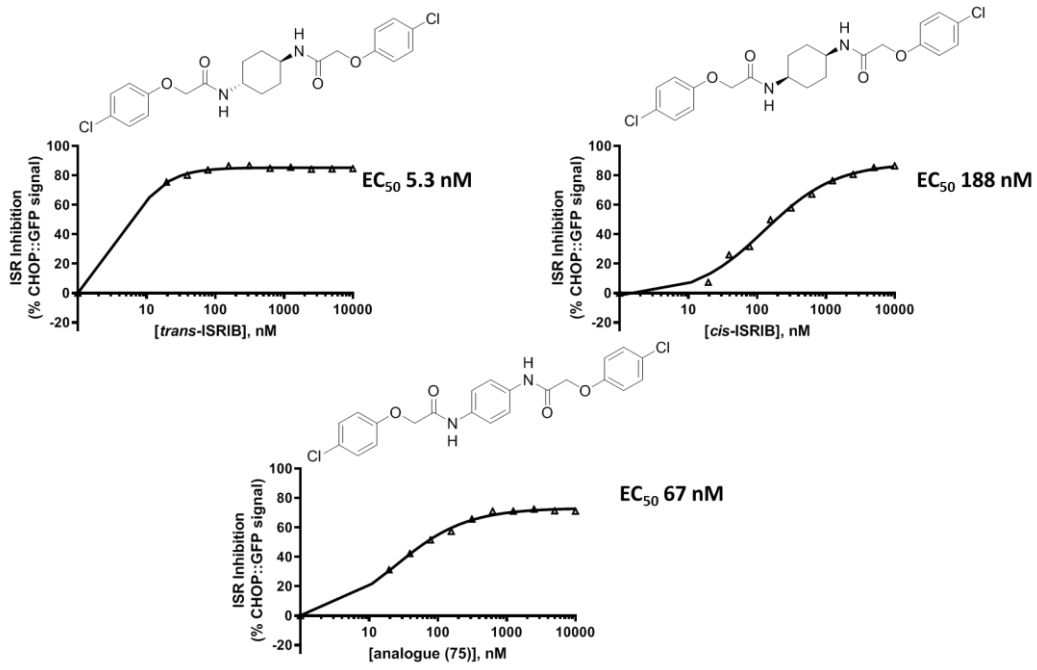


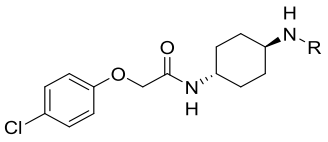
Figure 3.2: *trans*-ISRIB, *cis*-ISRIB and analogue **75** inhibit the ISR in CHO-K1 cells. Inhibition of ISR activated CHOP::GFP signal, stimulated upon treating the cells with histidinol (HIS) (0.5 mM), in the presence of escalating concentrations of *trans*, cis-ISRIB and analogue **75**. Shown is a representative from three independent experiments conducted for *trans*-ISRIB and of a single 12-point titration experiment conducted for ISRIB analogues. Concentration of ISRIB and its analogues is represented on a log10 scale. Curve fitting and EC_{50} was generated using agonist vs. response function on GraphPad Prism.[44]

3.3. Pharmacological results and SAR of synthetic ISRIB analogues

It should be clearly noted from the beginning of this section that all SAR studies were guided by measuring the CHOP::GFP expression by FACS as described above in section **3.2**. The pharmacology work was accomplished at the Cambridge Institute for Medical Research (CIMR) by the team of Professor David Ron.

3.3.1. Pharmacology results: Truncated ISRIB analogues

The EC_{50} values of the successfully synthesised truncated analogues **28-31**, are compared to the relevant ISRIB in **Table 3.1**. The ISR inhibition (% CHOP::GFP signal) at 10 μM are calculated according to the equation in section **3.2**.



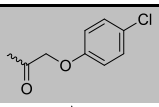
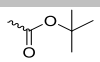
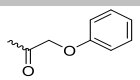
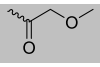
Ligand	R	ISR inhibition % CHOP::GFP signal at 10 μM	EC_{50}
1		91	5.3 nM
27		-	Inactive
28	H	-	Inactive
29		85	128 nM
30		20	Inactive
31		-	Inactive

Table 3.1: EC_{50} and ISR inhibition (% CHOP::GFP signal at 10 μM) of truncated ISRIB analogues **27**-**31**, *trans*-ISRIB prepared as positive controls for biological studies. Shown is a representative from three independent experiments conducted for *trans*-ISRIB and of a single 12-point titration experiment conducted for ISRIB analogues.

Truncated ISRIB analogues were prepared to assess the requirements for symmetry through examining the importance of the *O*-arylglycolamide moiety for activity. Apart from analogue **29**, the remaining truncated ISRIB analogues showed a complete loss of effect in the reporter assay (**Table 3.1**). The lack of

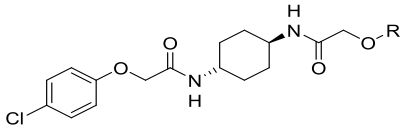
activity for these analogues could be related to the loss of the *O*-arylglycolamide components which are important to interact with residues in the ligand binding domain. Remarkably, the analogue **29** retained measurable activity, 26-fold less potent than ISRIB. This finding suggested that the steric and electronic nature of the distal aryl moieties is a prerequisite for the binding of ISRIB analogues to their target. Thus, it seems that the 4-chlorophenyl ether is ideal for activity.

In general, the pharmacology results in **Table 3.1** indicate that truncation was not tolerated, perhaps less expected is the fact that subtle modifications such as removing chlorine atom (analogue **29**) also had a dramatic impact on activity. Indeed, these results reflect contribution of electronic and steric effect of this substitution (chlorine atom), which may cause preferential interactions in the eIF2B receptors. Meanwhile, absence of activity due to removing of aryl group in analogue **30**, indicates that eIF2B receptor has bulk-preferring pockets, in particular at this part of the binding site for the compound.

Docking studies, shown in **Chapter 2**, illustrate that ISRIB binds in an extended conformation across the two symmetrical pockets of eIF2B. Thus, truncation of the overall length of ISRIB is very poorly tolerated. It appears that the presence of the both *O*-arylglycolamide side chains (symmetrical) promotes the potency. Furthermore, it seems that lipophilicity also plays a vital role in the pharmacological activity and permeability of the compounds across the cell membranes. Removal of both lipophilic groups (chloro substituent and phenyl ring) decreased the lipophilicity of analogue **30** [($logD_{7.4}$ =1.26, calculated using the ChemAxon chemoinformatics platform (v14.8.4.0)], thereby making it less cell permeable and hence reducing its potency.

3.3.2. Pharmacology results: Terminal aromatic ring-modified analogues

The pharmacology results, and subsequent SAR of the newly synthesised non-symmetrical analogues, are presented in **Table 3.2.**



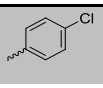
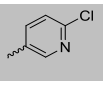
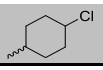
Ligand	R	ISR inhibition % CHOP::GFP signal at 10 μM	EC_{50}
1		91	5.3 nM
41		89	0.6 nM
42		86	126 nM
43		51	1.6 μM
44		-	Inactive

Table 3.2: EC_{50} and ISR inhibition (% CHOP::GFP signal at 10 μM) of ISRIB analogues modified at the terminal aromatic ring moiety **41**-**44**. Shown is a representative from three independent experiments conducted for *trans*-ISRIB and of a single 12-point titration experiment conducted for ISRIB analogues.

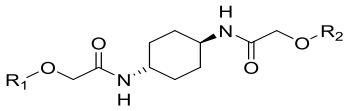
Examining the data in **Table 3.2** suggests that the modification pattern on the phenyl ring is important for optimum binding. As can be seen, the pseudo-symmetric ISRIB analogue **41** showed a replacement of the *para*-chloro group of one terminal aromatic ring by *para*-bromo group. The *para*-Br **41** is of a particular interest, as it shows higher potency than ISRIB molecule. The bromine substituent is very close to chlorine in terms of steric and electronic characteristics. The approximate resemblance in atomic radius (Van der Waals radius) between chlorine (1.80Å) and bromine (1.95Å) atoms[191] may mean that the *para*-Br substituent produces a similar steric presence to chlorine. There also appears to be contributing the lipophilicity factor, the bromine substituent is a little more lipophilic than chlorine. Therefore, bromine atom might increase the lipophilicity of *para*-Br **41** and this plays an important role in enhancing the

membrane permeation.[192] Overall, the high activity of the *para*-Br analogue can be attributed to either the sterically and electronically effect, the lipophilic effect or a combination of both.

When comparing the pyridine **42** and pyrimidine **43** derivatives in relation to ISRIB, it appears that the replacement of the terminal phenyl ring with a polar heterocyclic aromatic rings resulted in reduced the potency. This could indicate that the electronic nature of benzene ring may be important for binding with the eIF2B receptor. Pyridine and pyrimidine are less electronic than benzene, the nitrogen atom present in pyridine and pyrimidine is more electronegative than the carbon and acts like an electron withdrawing group and thus reduces the electron density in the ring. This effect can be clearly observed on comparing the pyrimidine **43** with pyridine **42** analogues. The pyrimidine **43** displayed more obvious reduction in potency (EC_{50} in micromolar range) than pyridine **42** (EC_{50} in nanomolar range), due to lower electron density in the aromatic pyrimidine ring. In addition, the partially retained potency imparted by pyridine analogue and the deleterious effect of pyrimidine analogue may indicate that more polar components of heterocyclic system in the terminal position might interact in a unfavorable way with residues in the binding site.

Moreover, replacement of terminal aromatic ring with cyclic aliphatic ring (cyclohexane) as in analogue **44** displayed a loss in potency. The reduction in potency appears to arise from the change in conformation which may cause non-preferential interactions with the eIF2B receptors. Cyclohexane ring is not a flat ring like benzene and the free rotation around carbon-carbon single bonds, allows cyclohexane ring to exist in a variety of conformations.

The variability in pharmacologic results across the eIF2B receptor with these simple modifications, indicates the necessity for more modifications to both parts of the terminal aromatic rings (**Table 3.3**). The design of symmetric ISRIB analogues focused on *p*-Br and pyridine groups, which exhibited well tolerated results in the non-symmetrical pattern. In addition, some of the symmetric ISRIB analogues have been resynthesised in order to calibrate inter-assay variability.



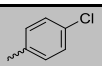
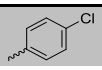
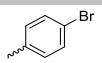
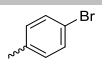
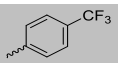
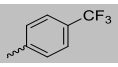
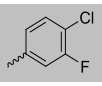
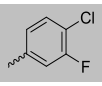
Ligand	R_1	R_2	ISR inhibition % CHOP::GFP signal at 10 μM	EC_{50}
1			91	5.3 nM
46			77	0.7 nM
47			83	8 nM
48			80	134 nM
49			92	0.5 nM
50			-	Inactive

Table 3.3: EC_{50} and ISR inhibition (% CHOP::GFP signal at 10 μM) of symmetrical ISRIB analogues modified at both terminal aromatic ring moieties **46**-**50**. Shown is a representative from three independent experiments conducted for trans-ISRIB and of a single 12-point titration experiment conducted for ISRIB analogues.

The symmetrical *p*-Br **46** derivative displayed a comparable activity to the corresponding non-symmetrical *p*-Br **41** analogue, which were both higher than the parent ISRIB molecule. However, the replacement of the chlorine substituent by a trifluoro substituent at the *para*-position of the phenyl ring as in **47** displayed a slight reduction in activity than ISRIB. This is possibly due to the strong electronic withdrawing effect of the CF_3, which reduces the electron density at the π system of the aryl ring and perhaps affects the binding at eIF2B. Furthermore, the replacement of chlorine with a more electronegative fluorine substituent **48**, which has a less lipophilic effect than chlorine, reduced

the potency by more than 27-fold. It is suggested that the electron withdrawing properties of the halogen substituents might drive the activity of the ligands. In addition, there also appears to be contributing steric factors in binding interaction at eIF2B. However, the resynthesis of di-substituted *p*-Cl/*m*-F **49** analogue have higher potency than ISRIB, thus both substitution patterns can be accommodated at the receptor.

Moreover, the replacement of aryl ring with pyridine on both sides as in analogue **50** resulted in a complete loss of potency in the cell-based assay. Again, the introduction of pyridine on both sides might lead to further reducing the electron density in both terminal rings, as well as the presence of nitrogen in the ring has a negative influence on the target binding.

Overall, when the symmetrical analogues *p*-Br **46** and pyridine **50** are compared to their non-symmetrical analogues **41** and **42**, it is evident that the above observations regarding the electronic nature and steric effect of the substituents on the phenyl ring are important for optimum binding. Moreover, some terminal ring analogues such as *p*-CF_3 **47**, *p*-F **48** and *p*-Cl/*m*-F **49** have been resynthesised in order to calibrate inter-assay variability, and clearly noted that the results were comparable with the literature.[167]

3.3.3. Structure-activity relationships of ISRIB analogues modified at the terminal aromatic moiety

Modifications of the terminal phenyl rings in ISRIB, allow various structure-activity relationships to be implied. SAR analysis demonstrated that the presence of *p*-bromo substituent in one or both terminal rings displays a slightly higher or comparable potency to ISRIB. This suggests a preference for electronic and size

characteristics closely similar to chlorine atom on the aromatic ring, as other known halogens substituents do not display comparable results to ISRIB.[167]

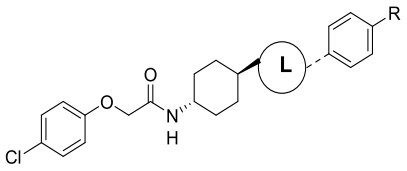
In terms of replacing aromatic ring with polar heterocyclic aromatic systems, it is evident that these strategies cause a reduction in activity of 26-fold in pyridine analogue, relative to aryl ring. The reduction in potency imparted by this modification can be more deleterious if the aryl ring is replaced by pyrimidine ring or if both terminal aromatic rings were replaced by pyridine rings. This indicates that the presence of terminal aryl rings is critical for compounds activity. Overall, the high sensitivity of the terminal aryl ring to modifications reflects the crucial role of this group in mediating the interaction with the biological target, which is important for binding affinity.

3.3.4. Pharmacology results: Linker-modified analogues

A comparison of parent ISRIB **1** or analogue **29** and that of the non-symmetric linker-modified analogues is made on a pharmacological basis in **Table 3.4**. If the unsubstituted derivative **29** is taken as a benchmark, it is obvious that the replacement of the glycolamide linker from one side with propanamide linker **52** (where the ether linkage replaced with methylene moiety) resulted in a significant reduction in activity. In comparison to the oxygen group of ether, the methylene (CH_2) moiety has no hydrogen bond acceptor activity. This demonstrates that an electronegative group (probably a hydrogen bond acceptor), at this position, is crucial for activity.

Bioisosteric replacement of the amide group with a carbamate **53** caused a significant decrease in potency, while urea **54** gave rise to a complete obliteration. This illustrates the importance of the α-carbon atom (CH_2 group which links amide and *O*-aryl ether) in promoting eIF2B binding. The presence

of polar and electronegative oxygen or N-H groups present on the carbamate **53** and urea **54** respectively, appears to be particularly detrimental in comparison to amide **29** (where the corresponding group is CH_2). The marked rise in activity of amide **29**, with respect to the carbamate and urea, reveals that the presence of a relatively less electronegative CH_2 group is preferable for binding with receptor.



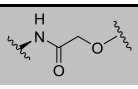
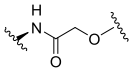
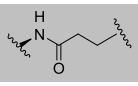
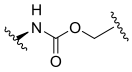
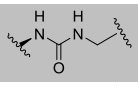
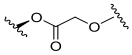
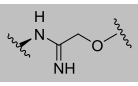
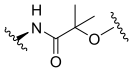
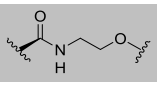
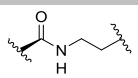
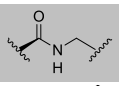
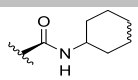
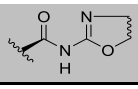
Ligand	L	R	ISR inhibition % CHOP::GFP signal at 10 μM	EC_{50}
1		Cl	91	5.3 nM
29		H	85	128 nM
52		H	55	7.3 μM
53		H	52	5.4 μM
54		H	-	Inactive
56		Cl	-	Inactive
59		Cl	62	1.5 μM
60		Cl	50	7.4 μM
61c		Cl	75	50 nM
62c		Cl	73	55 nM
63c		Cl	75	80 nM
64c		Cl	70	56 nM
65c		Cl	73	364 nM

Table 3.4: EC_{50} and ISR inhibition (% CHOP::GFP signal at 10 μM) of ISRIB analogues modified at the glycolamide linker **52**-**65c**. Shown is a representative from three independent experiments conducted for *trans*-ISRIB and of a single 12-point titration experiment conducted for ISRIB analogues.

Replacement of the amide bond with an ester **56** caused a complete loss in potency. This is possibly attributed to multiple factors including (1) the high vulnerability of ester for rapid *in vivo* hydrolysis,[193] or (2) the difference of hydrogen bond formation in comparison with amide, as ester has weak hydrogen bond acceptors with no hydrogen bond donor functionality.

Amidine analogue **59** displayed a 300-fold reduction in potency over the amide of ISRIB. It could be suggested that the amide and amidine would show similar features, on the basis of the above knowledge regarding the N-H group. The difference noticed may be attributed to the differing nature of the amide and amidine groups. There is a variation in the polarity across the C=O bond in amide and the C=NH in amidine, the O is more electronegative than N. The amide carbonyl C=O has the ability to serve as an efficient hydrogen bond acceptor, whereas the C=NH acts as a hydrogen bond donor. Overall, this confirms that the amide bond oxygen is affordable for modification.

However, investigation of the steric effect at the α-carbon atom was also attempted. Addition of small hydrophobic dimethyl group in this position as in analogue **60** exhibited a reduction in potency in relation to ISRIB. This indicates that a large group is not tolerated at the α-carbon position. However, introducing a dimethyl group on the α-carbon disrupts the molecular planarity and symmetry, and might accordingly improve the solubility.[194, 195] This effect was evident by measuring the melting point of analogue **55** (207-210 °C), which was significantly lower than ISRIB **(**271-274 °C).

The remaining compounds from **Table 3.4** possess reverse amide at one side of the central cyclohexane ring. Remarkably, repositioning the carboxamide moiety

to a simple reverse amide linkage retains reasonable activity. Interestingly, all these inverted amide motifs **61c**-**61c** had promising results and gave the best among all the linker modifications explored. This indicates that reversing the orientation of the carbonyl and amine groups in inverted amide analogues, retains the hydrogen bonding properties of an amide.

The inverted amide analogue **61c** displayed a slight reduction in potency compared to the ISRIB (only 10-fold less than ISRIB), even with the enlargement of *O*-arylglycolamide side chain to five atom spacer linking between terminal phenyl ring and central cyclohexane ring. Analysis of the predicted binding mode of reverse amide **61c** suggested that the orientation of the inverted amide moiety occupies the same pocket in eIF2B as the amide moiety of ISRIB (**Figure 3.3**). Additionally, the modelling study confirmed that **61c** showed similar binding affinity pattern as ISRIB through the formation of strong hydrogen bond, as in the amide nitrogen of the inverted amide. This could be attributed to the reduced distance between the amino acid hydrogen bond acceptor (carbonyl oxygen of Asn^{202}) and the inverted amide nitrogen donor.

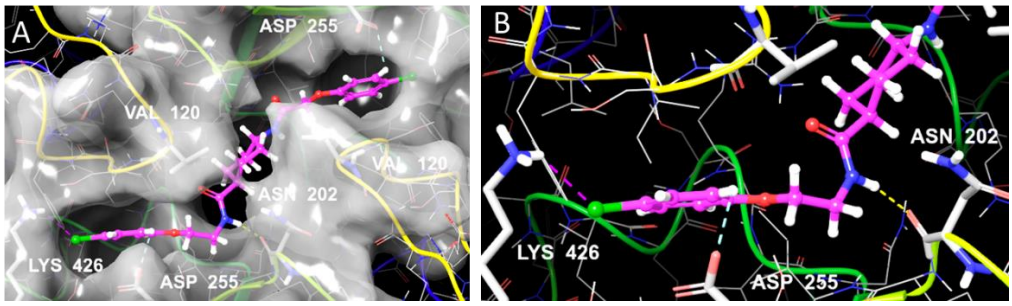


Figure 3.3: Predicted binding conformation of inverted amide analogue **61c** with the eIF2B; (A) Surface representation of analogue **61c**; (B) Representation of residues of eIF2B involved in the interaction with analogue **61c**; (generated using Shrodinger Maestro and Pymol softwares from PDB entries: 5B04).

The two inverted amide analogues **62c** and **63c** displayed, to some extent, striking differences in their activity profile. *N*-propyl acetamide analogue **62c**

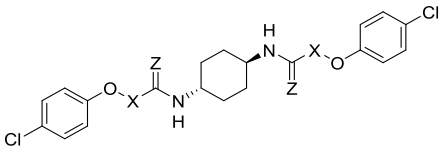
showed a slight decrease in potency relative to ISRIB **1**, while *N*-ethyl acetamide **63c** has a much lower activity than ISRIB. It appears that four atom spacer between terminal phenyl ring and central cyclohexane ring is optimum for activity rather than three atom spacer. The difference observed in the results may be attributed to perturbing the orientation of the terminal aromatic ring. In addition, the steric hindrance effect of the phenyl moiety must be considered, as the phenyl of the *N*-ethyl acetamide **63c** could hinder the interaction of amino acid residues with the nitrogen group of inverted amide moiety.

However, the pharmacological result of *N*-propyl acetamide analogue **62c** is very interesting, as it challenges some observations made previously by Hearn *et al*[167] and this project for propanamide analogue **52**. Inverted amide analogue **62c** retained acceptable potency relative to ISRIB in contrast to propanamide analogue **52** which showed significant reduction in activity, although they both hold same replacement of ether linkage with methylene (CH_2) group. The difficulties encountered with the synthesis of *N*-(hydroxymethyl)acetamide linker, point out the limitations to draw further conclusion regarding the effect of the electronegative oxygen atom with a possibility of hydrogen bond acceptor at this position.

Finally, *N*-cyclohexylacetamide **64c** and *N*-(4,5-dihydrooxazol-2-yl) acetamide **65c** exhibited considerable results with 11 to 72-fold reduction in potency relative to ISRIB **1**. The tethering of terminal aromatic ring with the inverted amide linker by five- or six-membered ring resulted in restricted rotation and reduced flexibility. Both analogues have two less rotatable bonds than ISRIB [nRot = 6, calculated using the Chemicalize, ChemAxon (v14.8.4.0)]. The number of rotatable bonds influences, in particular, bioavailability and binding

potency, as the molecule has to adopt a fixed conformation to bind, and to pass through a membrane. *N*-cyclohexylacetamide **64c** retains better activity than *N*-(4,5-dihydrooxazol-2-yl) acetamide **65c**. It appears that the tethering with six-membered ring preserves the orientation of the *para*-chlorobenzene moiety. However, connecting with a five-membered ring has an effect on the overall conformational preferences, resulting in uncomfortable accommodation of *para*-chlorobenzene group at the receptor.

On the other hand, three symmetric ISRIB analogues bearing modifications on both glycolamide linker were synthesised and evaluated in **Table 3.5**.



Ligand	X	Z	ISR inhibition % CHOP::GFP signal at 10 μM	EC_{50}
1	CH_2	O	91	5.3 nM
66	$CHCH_3$	O	-	Inactive
67	$C(CH_3)_2$	O	-	Inactive
68	CH_2	NH	-	Inactive

Table 3.5: EC_{50} and ISR inhibition (% CHOP::GFP signal at 10 μM) of symmetrical ISRIB analogues modified at both glycolamide linker **66**-**68**. Shown is a representative from three independent experiments conducted for *trans*-ISRIB and of a single 12-point titration experiment conducted for ISRIB analogues.

The strategy of adding mono- or di-methyl groups (**66** and **67**) at the α-carbon atom of both *O*-arylglycolamide side chains led to a complete drop in activity. The loss of potency associated with this modification suggests the possibility of space restriction around the α-position of the glycolamide linker. Addition of mono- or di-methyl groups is either considered too bulky or might affect the overall conformational preference of the molecule.

However, it was still unclear if the oxygen atom of amide carbonyl was important on both sides, so symmetrical amidine analogue **68** was sought. Results showed that changing the oxygen atom of amide carbonyl in both sides to an N-H resulted in a total loss of activity, thus confirming the necessity of amide oxygen for potency. Also, the replacement of amide with amidine in both sides could lead to synthesis of high polar compound which could affect the cellular penetration process.

3.3.5. Structure-activity relationships of ISRIB analogues modified at the glycolamide linker

Several structure-activity relationships were achieved from modifications of the glycolamide moiety. The best potency was retained by the parent glycolamide ISRIB **1**. Bioisosteric analogues with both hydrogen bond donor and acceptor functionalities (carbamate, urea and ester) led to a uniformly inactive compounds. The presence of a relatively less electronegative atom (α-carbon, CH_2) is considered to be essential, this could be reflected with the significant reduction in potency upon replacing this group with higher electronegative O and N-H in carbamate and urea, respectively.

Among all the functional groups explored as direct isosteres, or other modifications (i.e. addition of mono- or di-methyl groups at the α-carbon), only the inverted amide analogues maintained some potency in relation to ISRIB. Reversing the orientation of the hydrogen bond donor and acceptor in amide moiety was shown to be tolerated, nonetheless, inverted amides were slightly less potent than the corresponding amides. As such, the amide group and unsubstituted α-carbon atom are essential for receptor binding. On the other hand, the initial observations suggested the oxygen group (i.e. ether) adjacent to

the terminal aryl ring seems to be essential as a hydrogen bond acceptor and could not be substituted with a carbon atom. Subsequently, replacement of this group with carbon atom within the inverted amide analogue was tolerated. Full analysis cannot be conducted due to difficulties in the synthesis of *N*-(hydroxymethyl)acetamide linker, which could have help draw further conclusion regarding the effect of electronegative oxygen atom at this position.

The SAR analysis of inverted amide with diverse side chain lengths indicated that *N*-(2-methoxyethyl)acetamide **61c**, *N*-propyl acetamide **62c** or *N*-ethyl acetamide **63c** were well tolerated, however the length of the spacer affected the potency of the compounds. For example, the inverse amide with three atom spacer produced a slight reduction in potency (16-fold less than ISRIB). On the other hand, both four and five atoms spacer retained potency with 10 to 11-fold lower than ISRIB, respectively. Further investigations would be needed to detect the optimal length of the linker. In addition to the electronic nature and length of linker, tethering terminal ring to the *O*-arylglycolamide linker through six-membered ring is considered a well-tolerated modification at eIF2B. Finally, in the case of symmetrical analogues, the modification of both glycolamide linkers were not tolerated.

To conclude, the ability to adjust the glycolamide linker without greatly detrimental effect on overall activity indicates this part of ISRIB appears to be amenable to more comprehensive structural modifications. This in turn could offer a more enhanced activity profile or could facilitate finding appropriate site in the ISRIB for connecting a ‘tag’ molecule.

3.3.6. Pharmacology results: Central core ring modification

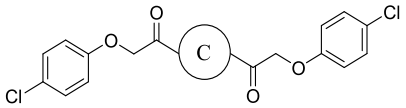
The central cyclohexane ring that joins the *O*-arylglycolamide side chains has been explored through synthesising different core ring modification analogues. The EC_{50} values of successfully synthesised central core ring modification analogues, are compared to the parent cyclohexane core ring compound (ISRIB) in **Tables 3.6**-**3.8**.

3.3.6.1. Aromatic, aliphatic, spiro and bicyclic analogues

Table 3.6 shows the pharmacological results of replacing the parent cyclohexane core ring with different aromatic, aliphatic, bicyclic and spiro core moieties. Examination of the results demonstrates that the replacement of the *trans*-1,4-cyclohexane ring with aromatic aryl core **75** seems to be the best tolerated replacement for cyclohexyl moiety among all other replacements, but still 14-fold less potent than ISRIB. This result is comparable to a previous pharmacological result quoted in the literature.[167]

Replacement of *trans*-1,4-cyclohexane ring with highly polar aromatic rings, such as pyridine **76** and pyrimidine **77**, resulted in a significant reduction in potency. It could be expected that the pyridine or pyrimidine and aryl would show similar features, regarding the planarity. The difference observed may be attributed to the diverse electronic nature of the aryl and pyridine or pyrimidine rings. There is a difference in the electron density across the aromatic rings in aryl, pyridine and pyrimidine. Both pyridine and pyrimidine have lower charge density due to the electron withdrawing effect of the nitrogen atoms. The lower potency associated with the polar pyridine and pyrimidine could also be explained by losing the aromatic hydrogen bonding which might participate in binding interaction between ligand and receptor. Additionally, the polar aromatic

rings could impede the penetration over cell wall in a cell-based assay. Overall, the marked drop in potency of the pyridine and pyrimidine, with respect to both *trans*-1,4-cyclohexane and aryl, reveals that the presence of nonpolar core is important for binding affinity.



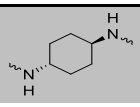
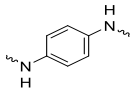
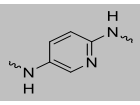
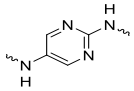
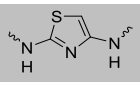
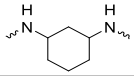
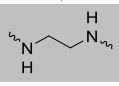
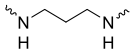
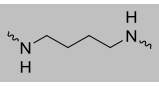
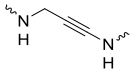
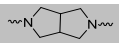
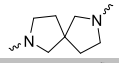
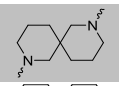
Ligand	A	ISR inhibition % CHOP::GFP signal at 10 μM	EC_{50}
1		91	5.3 nM
75		71	67 nM
76		60	1.2 μM
77		-	Inactive
78		-	Inactive
79		-	Inactive
80		85	834 nM
81		56	8.4 μM
82		84	535 nM
83		-	Inactive
84		58	7.3 μM
85		60	4.1 μM
86		58	6.7 μM
87		60	1.8 μM

Table 3.6: EC_{50} and ISR inhibition (% CHOP::GFP signal at 10 μM) of ISRIB analogues modified at the central core moiety **75**-**87**. Shown is a representative from three independent experiments conducted for *trans*-ISRIB and of a single 12-point titration experiment conducted for ISRIB analogues.

The remaining aromatic analogues tested, thiazole **78**, showed a complete drop in potency relative to ISRIB. Moreover, replacement of *trans*-1,4-cyclohexane

ring with 1,3-diaminocyclohexane **79** resulted in a dramatic loss of activity as well.

All of the acyclic linear cores consisting of two **80**, three **81** or four **82** carbons were significantly less potent than ISRIB, but the new SAR revealed a preference for four carbon over two and three carbon spacing. This suggests that the central spacer distance plays an essential role in properly orienting the two *O*-arylglycolamide side chains in space. The calculated end-to-end distance of the 1,4- diamino-butane derivative **82** equals 22.18 Å, this is comparable to the distance in parent ISRIB 21.71 Å, as shown in **Figure 3.4**. Additionally, the high flexibility of 1,4- diamino-butane **82** (nRot = 11) may contribute to reducing the potency by making the molecule more subjected to target promiscuity. Consistent with this, reducing flexibility by forcing the alkane core spacer further apart with an alkynyl spacer as in 1,4-diamino-but-2-yne **83** led to a complete loss of measurable potency. This is possibly due to a potential shortening in the end-to-end distance 16.77 Å of analogue **83** which could disturb the binding with eIF2B.

However, replacement of *trans*-1,4-diaminocyclohexane ring with bicyclic-pyrrolidine **84** and spiro-pyrrolidine analogue **85** resulted in a significant drop in potency. Moreover, the two spiro compounds with six-membered ring **86** and **87**, resulted in even greater reduction of activity. In comparison to ISRIB which exhibits secondary amides, all bicyclic and spiro analogues afforded tertiary amide products i.e. no hydrogen bond donor possibility at the amide group. This indicates that the presence of hydrogen bond donor feature (as in ISRIB amide N-H) contributes to a greater interaction with the receptor. Additionally, the presence of bicyclic and spiro core may result in imposing a drastic

conformational change in the molecule leading to a reduction in potency. Overall, analysis of SAR indicated a preference for an extended binding conformation in which both side chains project equatorially cross the two symmetrical pockets, from the plane of the central ring. Additionally, it implied that the distance separating the *O*-arylglycolamide side chains is strongly correlated with the activity of ISRIB analogues.

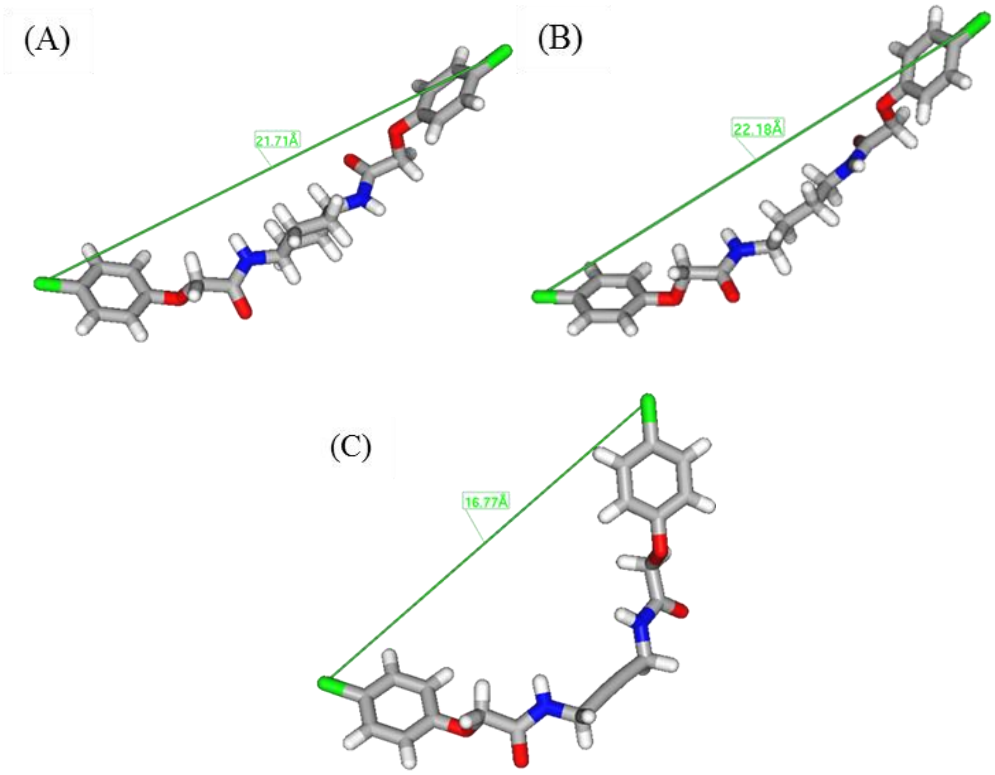
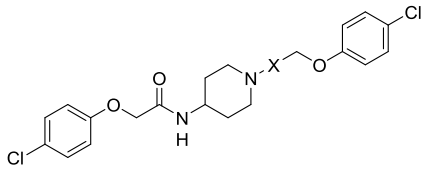


Figure 3.4: End-to-end distance of *trans*-ISRIB, **82** and **83**.
The structures have been energetically minimized, (A) *trans*-ISRIB; (B) analogue **82**; (C) analogue **83**, (generated using Marvin Space software).

Due to difficulties in synthesising the diamino-cyclohexanetetrol **90** and but-2-ynediamide **92** derivatives, a further SAR could not be performed, particularly with regard to determining the effect of the hydrogen bond donors (Hydroxyl groups) on the cyclohexane core ring.

3.3.6.2. Piperidine and piperazine analogues

To gain further insight into the effect of modification of the central core ring, cyclohexyl moiety was replaced by heterocycloalkyl piperidinyl and piperazinyl rings. Pharmacology data for the replacement of *trans*-1,4-cyclohexane ring with 4-amino piperidine is particularly interesting (**Table 3.7**). All analogues exhibited a variable extents of potency, which is clearly attributed to the type of functional group (X in table/scheme **3.7**). These results indicated a preference for the piperidine conformation, which is similar to the chair conformation of cyclohexane.



Ligand	X	ISR inhibition % CHOP::GFP signal at 10 μM	EC_{50}
100	(C=O)	82	1.5 μM
101	$(C=O)CH_2$	87	367 nM
102	CH_2-CH_2	83	154 nM
103	NH(C=O)	87	12 nM
104	NH(C=NH)	90	8 nM

Table 3.7: EC_{50} and ISR inhibition (% CHOP::GFP signal at 10 μM) of ISRIB analogues with piperidinyl core ring **100**-**104**. Shown is a representative from three independent experiments conducted for *trans*-ISRIB and of a single 12-point titration experiment conducted for ISRIB analogues.

The two piperidine analogues **100** and **101** display obvious differences in their activity profile. In general, *O*-arylacetamide and *O*-arylpropanamide were coupled directly to the *N*-piperidine to affording tertiary amide products. *N*-piperidine with *O*-arylacetamide **100** retains low potency relative to ISRIB. Conversely, *N*-piperidine with *O*-arylpropanamide **101** has a higher potency than analogue **100**. Again, these results suggested that the distance of around 4 atoms between the central core and the terminal aromatic rings was optimal for activity, also a slight move in carbonyl group toward the central core ring was tolerated.

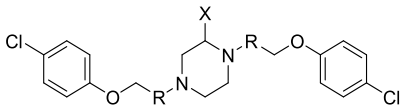
Interestingly, removal of the amide carbonyl moiety from analogue **101** through replacement with methylene group as in tertiary *N*-piperidine **102**, resulted in an improved potency in comparison with **101**. This could be the result of the preferable conformational change in the molecule which leads to an enhancement in potency.

Thus, our efforts were focused on core modifications close in structure to 1,4-diaminocyclohexane central core. Replacement of *trans*-1,4-diaminocyclohexane ring with piperidine-1,4-diamine afforded hydrazide analogue **103**. This analogue displayed the best profile compared to other analogues containing the piperidine core ring, it was only three-fold less active than ISRIB **1**. This indicates that the presence of a hydrogen bond donor activity (N-H group of the amide) adjacent to the central ring, is perhaps crucial for binding to the eIF2B receptor, and it appears to be necessary for high activity. In addition, the presence of a piperidine-1,4-diamine moiety promotes occupying a similar pose in the binding site in comparison to *trans*-1,4-diaminocyclohexane. This probably contributes to orienting the two *O*-arylacetamide side chains in a similar way as in ISRIB (**Chapter 2**, **Figure 2.13**).

Remarkably, replacement of the amide moiety in **103** with amidine **104** retains activity in relation to ISRIB. It appears that amide and amidine, which are sterically similar, show a striking similarity in hydrogen-bond pattern. However, this result challenges some observation made previously by this project for amidine analogue **59** (where the central core is *trans*-1,4-diaminocyclohexane (**Table 3.4**). Amidine analogue **104** with piperidine-1,4-diamine core ring retains an acceptable potency relative to ISRIB, whereas amidine analogue **59** with

trans-1,4-diaminocyclohexane core ring has a significant reduction in activity in comparison to ISRIB.

In parallel with the above modifications, piperazine ring underwent similar modifications as 4-aminopiperidine ring. The pharmacological results for the piperazine analogues are illustrated in **Table 3.8**.



Ligand	X	R	ISR inhibition % CHOP::GFP signal at 10 μM	EC_{50}
108a	H	NH(C=O)	90	12 nM
108b	CH_3 (*S*)	NH(C=O)	80	245 nM
108c	CH_3 (*R*)	NH(C=O)	81	165 nM
109a	H	(C=O)	-	Inactive
109b	H	$(C=O)CH_2$	-	Inactive
109c	H	CH_2	-	Inactive
109d	H	CH_2-CH_2	-	Inactive

Table 3.8: EC_{50} and ISR inhibition (% CHOP::GFP signal at 10 μM) of ISRIB analogues with piperazinyl core ring (**108a**-**109d**). Shown is a representative from three independent experiments conducted for *trans*-ISRIB and of a single 12-point titration experiment conducted for ISRIB analogues.

The piperazine-1,4-diamine analogues **108a-c** showed a similar profile to the piperidine-1,4-diamine analogues. The piperazine-1,4-diamine analogue **108a** revealed a significant potency with only a three-fold drop in activity compared to ISRIB **1**. This result added a weight to the previous results that piperidine-1,4-diamine analogue **103** exhibits a greater potency when compared to the other analogues containing piperidine core ring. However, insertion of a small methyl group at piperazine-1,4-diamine ring as in analogues **108b-c** led to a gradual loss of activity for both *S* and *R* configurations. The *R*-enantiomer **108c** is more active than the *S*-enantiomer **108b**. It therefore appears that the increasing bulk at central core leads to a reduction in potency, with the potential that insertion of a

small methyl group could impede the accommodation of central core moiety at eIF2B binding site.

Finally, the remaining piperazine analogues **109a-d** possess tertiary amide or tertiary amine at both sides of the piperazine core ring. Remarkably, these changes to the nature of core ring confer quite large changes to the potency of each analogue. This effect is possibly due to the absence of the amide N-H groups in both sides, which appears to offering an acceptable activity. In addition, formation of tertiary amide or tertiary amine results in extensive conformational change in the entire molecule, thus leading to deteriorating the proper fit for binding and consequent reduction in potency. This could also result in making these analogues too basic to engage in the essential hydrogen bonding. Overall, the lower potency of these analogues may further point towards the importance of preserving at least one N-H group of the amide adjacent to the central ring (*O*-arylglycolamide linker) in this area.

3.3.6.3. Structure-activity relationships of ISRIB analogues modified at the central core ring

The modifications to the central core ring in ISRIB **1**, allow several structural-activity relationships to be concluded. Analysis of SAR indicated that the best tolerated aromatic core ring was retained by the simple aryl core **75**. The presence of highly polar aromatic rings such as pyridine **76** and pyrimidine **77** greatly reduced the potency in relation to ISRIB. This happens in a seemingly electronic-sensitive mode, as is obvious in the loss of potency of the pyrimidine **77**. This referred that the cyclohexyl group is important for the overall binding geometry, some modifications (*e.g.* phenyl) are tolerated but binding affinity is slightly reduced.

In the case of ISRIB analogues bearing acyclic linkers of two, three and four carbons, SAR studies revealed a preference for a cyclic (cyclohexane) central core over acyclic, and also for four carbon atoms over two and three carbon spacing. This indicates that the central spacer has a key role in properly orienting the two *O*-arylglycolamide side chains in space.

In terms of spiro and bicyclic core ring replacement, it is evident that these cause a reduction in potency, relative to *trans*-1,4-diaminocyclohexane ring. The reduction in potency is more drastic for the bicyclic than the spiro analogues.

Exchange of the 1,4-diaminocyclohexane ring with heterocyclic ring systems such as piperidine-1,4-diamine or piperazine-1,4-diamine, resulted in compounds with relatively similar potency to the parent ISRIB. The presence of secondary amide group on both sides of the piperidine or piperazine core is essential for activity since it may participate in an H-bond interaction with eIF2B. It appears that if this particular H-bond is lost as in tertiary amide group of the piperidine or piperazine core, ligand potency decreases.

To conclude, the ability to modify the cyclohexane ring without great deleterious influence on potency reveals that this part of the molecule is susceptible to more modifications that could offer an enhanced aqueous solubility profile.

3.4. Conclusions

A series of compounds derived from modification at different ISRIB moieties have been synthesised and their pharmacological activities have been evaluated. These modifications led to the establishment of new SAR and afforded several compounds having a high potency. Efforts were initially focused on the truncated ISRIB analogues to assess the requirement for symmetry. Remarkably, truncated

ISRIB analogues are very poorly tolerated. Of the truncated analogues prepared, only the analogue **29** (where the one chlorine atom removed from distal aromatic ring) retained a measurable activity, but still less potent than the parent ISRIB molecule.

Of the analogues with substitutions of the terminal aromatic ring, the *para*-bromo analogues of non-symmetrical **41** and symmetrical **46** were found to have the highest potency of the series. However, to further investigate the importance of phenyl ring for binding, two additional ligands were synthesized in which the phenyl ring was replaced by a pyridine **42** and a pyrimidine **43** heterocyclic rings. Replacement of aromatic ring with polar heterocyclic aromatic system displays a significant reduction in potency. This indicates the presence of terminal aryl ring is critical for compounds activity.

Efforts were then turned to the glycolamide linker. The results confirmed that the bioisosters of the amide moiety such as carbamate, urea and ester lead to loss of potency, whereas repositioning the carboxamide moiety to a simple reverse amide isoster results in a tolerated level of potency. This indicates that reversing the orientation of the carbonyl and amine groups in the inverted amide analogues, retains the hydrogen bonding properties of secondary amide.

The inverse amide linker with four and three atom spacer **62c** and **63c** displayed good potency profiles. However, it appears that four atoms spacer, between terminal phenyl ring and central cyclohexane ring, is optimal for activity rather than three atoms spacer. Furthermore, binding of terminal aromatic ring with the inverted amide linker such as *N*-cyclohexylacetamide **64c** and *N*-(4,5-dihydrooxazol-2-yl) acetamide **65c** demonstrated well tolerated results. The *N*-

cyclohexylacetamide **64c** was slightly more active than *N*-(4,5-dihydrooxazol-2-yl) acetamide **65c**. It appears that the tethering with six-membered ring was more favourable for the orientation of *para*-chlorobenzene moiety than the five-membered ring.

However, the insertion of a methyl group at the α-carbon atom which links amide and *O*-aryl ether led to loss of activity most likely due to a conformational change in the ligands binding mode. The results confirmed that increasing steric bulk at this position decreased eIF2B receptor affinity. Therefore, it was concluded that the α-carbon atom which links amide and *O*-aryl ether was crucial for potency.

Finally, the importance of the central core ring was investigated by synthesising and testing different modified core ring analogues. Of the central aromatic ring derivatives, aryl core **75** showed the best tolerated replacement for cyclohexyl core moiety, but still 14-fold less potent than ISRIB **1**. The remaining analogues, with highly polar aromatic rings such as pyridine **76** and pyrimidine **77**, showed a significant reduction in potency. The acyclic analogues with linear alkyl core of two **80**, three **81** or four **82** carbons show a reduction in potency relevant to the parent ISRIB. However, new SAR studies revealed a preference for four carbons over two and three carbons spacing. Forcing the alkane core spacer further apart with an alkynyl spacer **83** caused a drastic decrease in potency. The bicyclic and spiro analogues **84**-**87** resulted in a bigger drop in potency. The reduction in the activity of the bicyclic and spiro core can be attributed to either a conformational changes effect, tertiary amide products of bicyclic and spiro analogues or a combination of both.

The piperidine and piperazine analogues have a high level of potency among all the core ring replacements explored. Exchange of the 1,4-diaminocyclohexane

ring with heterocyclic ring systems such as piperidine-1,4-diamine **103** and **104** or piperazine-1,4-diamine piperazine **108a**, resulted in compounds with a relatively similar potency to the parent ISRIB **1**. However, insertion of small methyl group at piperazine-1,4-diamine ring **108a** led to a slight decrease in potency for *R*-enantiomer **108c** rather than *S*-enantiomer **108b**. The importance of the amide NH was also investigated through synthesising and testing tertiary amide piperidine and piperazine analogues **100**, **101** and **109a-b**. These analogues showed that the NH of the amide is essential for activity, as these analogues have less activity in comparison to secondary amide piperidine and piperazine analogues **103** and **108a**.

Overall, the rationally designed ISRIB analogues afforded a comprehensive SAR study. Importantly, three analogues with a comparable potency to ISRIB were achieved: bromo **41**, piperidine-1,4-diamine **103** and piperazine-1,4-diamine piperazine **108a**. **Figure 3.5** summarizes the types of modifications which have been carried out.

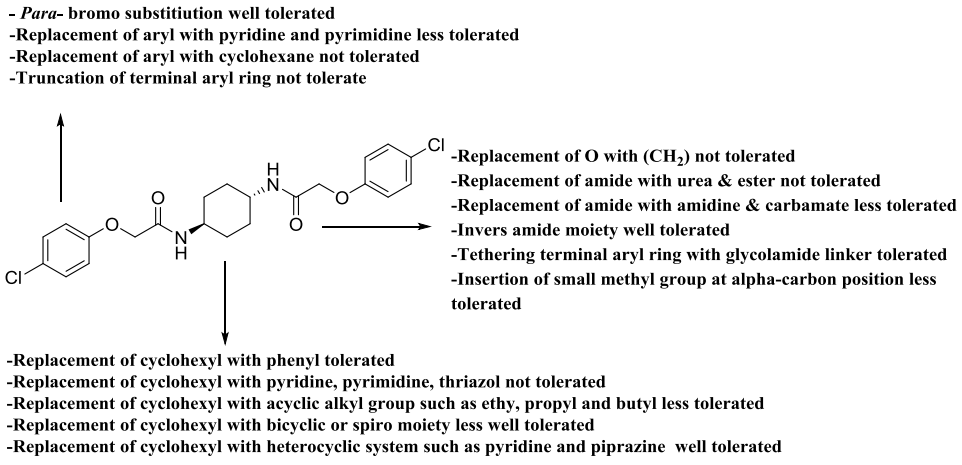


Figure 3.5: Summary of SAR of ISRIB derivative

4. Fluorescent eIF2B ligand based on ISRIB modifications: Design, synthesis and evaluation

4.1. Introduction

As outlined in **Chapter 1**, *trans*-ISRIB acts downstream of eIF2α-P by modulating the activity of the eIF2B through binding of eIF2Bβ and eIF2Bδ, thus restoring eIF2B activity and subsequently enhancing protein synthesis.[151, 167] One of the project's aims is to probe this scenario by designing and synthesising novel labelled ISRIB derivatives that would assist in established a fluorescence polarization assay in order to nail down the molecular target of this compound.

Noteworthy that the data pointing the direct binding of eIF2B by ISRIB through cryo–electron microscopy structure for the human eIF2B in complex with ISRIB was came late in this PhD period. Therefore, during the PhD, creating a labelled ISRIB derivative was considered a valuable molecular tool for biological assay in order to further investigation the molecular target of this compound. There has previously been no published work investigating fluorescent molecule ligated to ISRIB. Thus, a further investigation of ISRIB was needed in order to meet the essential requirements to successfully creating a fluorescent molecule ligand. This chapter therefore, describes the design and synthesis of fluorescent ISRIB analogues targeting the eIF2B receptor. The main aim of this chapter is

continuing the investigation of various ISRIB modifications to determine the suitable sites for fluorescent molecule attachment. In addition, this chapter explains the inventive process of finding the appropriate linker lengths and types of attaching a 'tag' molecule to that linker. Of note though, in this chapter we utilise the SAR detailed in **Chapter 3** to continue the investigation of central core and glycolamide linker of ISRIB to help identifying the possible sites for fluorescent molecule ligation.

Overall, the ultimate aim of this chapter is creating a labelled ISRIB derivative, primarily for use to further our knowledge of the molecular target of ISRIB, eIF2B, and to establish a fluorescence polarisation-based assay. Thus, the synthesis of fluorescein-labelled ISRIB derivatives assisted the project's collaborators in analysing the signal response in fluorescence polarisation (FP) assay to be utilized for further support the binding studies *in vitro*. It is worth noting here that this work came late in this PhD period and the full data is therefore incomplete.

4.2. Design of fluorescent ISRIB analogues

Generally, designing probes in the absence of detailed information about the potential target or binding site is very challenging task. In such cases, SAR information can be very helpful in designing the appropriate probes to assist in structural studies.[196] The strategy to obtain appropriate fluorescein-labelled ISRIB derivatives is related to the efforts aiming at attaching 'handles' to the molecules that may eventually be exploited for attachment of groups that would facilitate labelling.

Two main factors need to be considered when designing fluorescent compounds. Firstly, where on the ISRIB molecule should modification take place to identify the appropriate site for fluorescent molecule attachment? Secondly, what is the appropriate linker (in terms of length and type) required for conjugation, to reach the purpose of removing the fluorescent molecule far enough away from the ISRIB molecule to reduce the impact of interference on its eIF2B receptor binding? These factors will be studied individually and the rationale behind the choices are discussed.

4.2.1. Identifying the appropriate site for fluorescent molecule attachment

Currently, there is a lack of comprehensive studies into suitable sites for fluorescent molecule ligation to ISRIB molecule, with simple attempts to creat a fluorescent ligand based on ISRIB itself.[150] Thus, an investigation into appropriate site for fluorescent molecule attachment is required before the work and expense of synthesising fluorescent compounds. One of the important criteria for the development of fluorescent molecule is determination of an suitable site within the chosen ideal eIF2B ligand, ISRIB, to be modified for fluorescent molecule ligation. ISRIB has three practical sites that could be investigated for fluorescent molecule ligation: the terminal aryl ring, the glycolamide side chain and the central cyclohexane core ring (**Figure 4.1**). These also represent the areas where most SAR studies in this project have been carried out. Therefore, extensive SAR studies have been applied in the current project, to identify the appropriate site in the ligand molecule that can be used to link a spacer and then attach to a fluorescent-labelled molecule. Of note though, is that replacement of the cyclohexane core ring by phenyl ring is tolerated as well and may provide alternative possibilities for fluorescent molecule ligation.

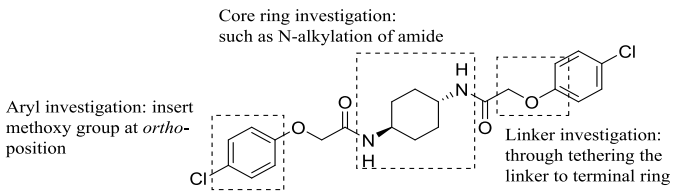


Figure 4.1: Overview of the investigated sites on ISRIB molecule in this study to identify the appropriate site to link a spacer attached to a fluorescent labelled molecule.

4.2.1.1.Terminal aryl ring

The first candidate for fluorescent molecule conjugation is the terminal aromatic ring, and this is especially the case because of the extensive studies already performed on the impact of different substitutions. Previous work by Walter *et al*[150], investigated the *para* or *meta* position of ISRIB as a potential site where a fluorescent group could be attached via a triazole linker (**Figure 4.2**).

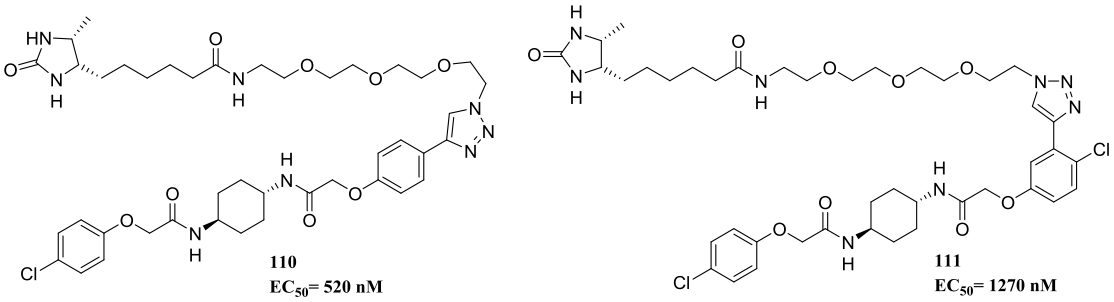


Figure 4.2: Modifications at *para* or *meta* positions of the terminal aryl ring by attaching a triazole linker.[150]

The results have been shown that the linker attachment at the *para* (**110**) or *meta* (**111**) positions leads to a substantial reduction of activity. Even though, the relatively *para*-substitution analogue retained a degree of potency.[150] This suggested that if there was no enough space in the active site for triazole linker with long alkyl chain at the *para* or *meta*-position, one as relatively bulky as a fluorescent group could abrogate binding affinity. The original ISRIB molecule, which is properly accommodated into the active site, does not have a triazole linker with long alkyl chain. This linker had to be incorporated to avoid

quenching of the fluorescent group by the terminal aryl ring, and this could eventually contribute to increasing the substitution size beyond what the eIF2B receptor can easily accommodate. It could also that the *para* or *meta*-positions are not able to allow orientation of the attached linker far away from interfering with the binding site, however an *ortho*-position might. Therefore, the *ortho*-position could prove a promising position for investigation, especially as no other published research has been carried out studying a substitution at this position. Accordingly, synthesis of *ortho*-methoxy phenyl derivative was attempted. A methoxy substituent was selected to evaluate how a bulky, electron rich substituent at *ortho*-position affects eIF2B receptor binding. If increasing the steric bulk at *ortho*-position was tolerated, it is likely to be that further extension of the *ortho*-substitution might do the same.

4.2.1.2.Central cyclohexane core ring

The central cyclohexane ring was considered essential for eIF2B activity. A review of the literature promptly determined that the interest in finding a suitable site for linker attachment has mainly stayed focused on modifications NH-amide or carbon atom of cyclohexylamide group.[150] In a similar fashion to the terminal ring modification in section **4.2.1.1**, the reported ligands have a triazole linker with long alkyl chain attached to the NH-amide **112** or carbon atom of cyclohexylamide moiety and displayed no detectable activity on the eIF2B receptor. [150] In addition, Walter *et al*[150] attempted other simple modifications of cyclohexane ring, through generating *N*-alkyl amide derivatives by inserting but-1-yne **113** on NH-amide or inserting prop-1-yne **114** group on carbon atom of cyclohexylamide group (**Figure 4.3**).

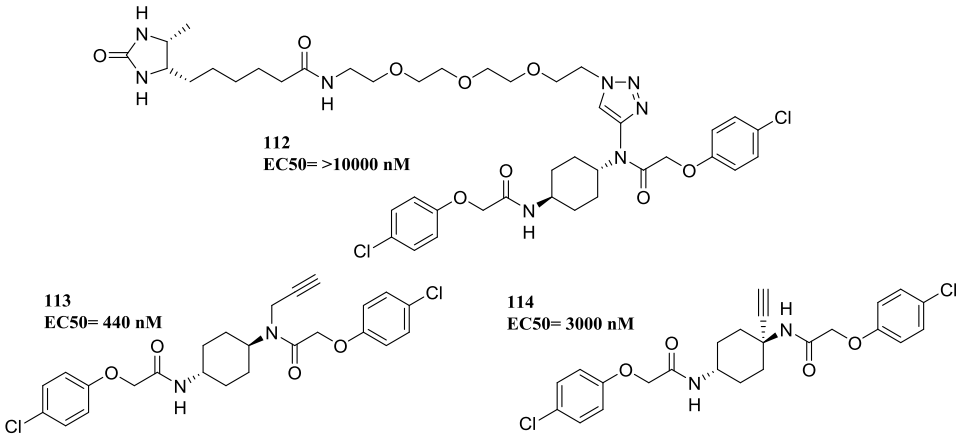


Figure 4.3: Modification at NH-amide or carbon atom of cyclohexylamide group of core ring system.[150]

Previous results have been shown that insertion of prop-1-yne on the carbon atom resulted in a small reduction in potency. Insertion of but-1-yne on NH-amide resulted in retaining a degree of activity albeit with a 60-fold drop compare to ISRIB. The NH-amide and carbon atom of cyclohexane core ring could tolerate both prop-1-yne and but-1-yne substitutions.[150] The fact that the cyclohexane core ring substitution results in a moderate reduction of activity compared to ISRIB was very encouraging, and demonstrates that there was at the least some room for cyclohexane core ring modifications. This suggested that fluorescent molecule ligation at the NH-amide could be appropriate, and it may be a useful target in developing further SAR. However, there is lack of evidence on whether a large hydrophobic molecule would be suitable for insertion at the NH-amide of cyclohexane ring. Therefore, analogue was synthesised by inserting benzyl molecule on NH-amide moiety, to explore the possibility of tolerating a hydrophobic aromatic group at this position to be then used for linker attachment. Also, a small hydrophobic alkyl group such as methyl was inserted on NH-amide of cyclohexyl amide moiety, but unfortunately their synthesis

failed. Even so, this hydrophobic group was investigated with NH-amide of phenyl core ring.

As mentioned before in **Chapter 3**, the replacement of cyclohexane core ring by phenyl ring is tolerated and may present alternative opportunities for fluorescent molecule attachment. Therefore, benzene-1,4-diamine core ring was used as a starting point to design other analogues possessing methyl group inserted on NH-amide or methoxy group connected directly to aryl core ring.

4.2.1.3. Glycolamide linker: chromane, benzodioxane and benzoxazine analogues

The SAR data of the inverted amide analogues (**Chapter 3**), confirms that tethering of terminal aromatic ring with the glycolamide linker by five or six-membered ring is a suitable prospect for investigation. Considering the tolerated result for the analogue **64c** (where tethering performed with six-membered ring) suggested that such modification can be accommodated by the binding site. Therefore, another strategy was followed in this project to focus on designing analogues by modifying the aryl ether moiety via tethering to glycolamide linker with a six-membered system. Accordingly, tethering of the neighbouring aromatic ring to the α-carbon atom in the form of a chromane group was performed first. The selection of chromane system was based on the following considerations. First, the possibility of tolerated conservative modifications of the glycolamide moiety, especially after the promising results of terminally tethered analogue **64c**. Second, substitution on the terminal phenyl ring which suggests that an area, around the aromatic end group can tolerate a reasonable degree of steric bulk (**Chapter 3**). Finally, the docking studies of ISRIB (**Figure 4.4: A**) demonstrated that one of the aromatic end groups is coplanar with the *O*-

CH_2 linker. This suggests there is some room for rigidification around the aryl ether moiety by means of cyclisation.

The chromane system was the first logical choice and was further examined to guide our decision on where to locate the fluorescent dye upon the ISRIB molecule. Docking studies of chromane analogues clearly suggested that the benzylic carbon atom of the chromane system would face the solvent-accessible entry into the putative ISRIB-binding site of eIF2B (**Figure 4.4: B**). They also showed that the benzylic carbon was in an ideal position within the molecule to elaborate a linker for fluorescent molecule attachment. Therefore, other analogues were designed to explore whether the replacement of chromane system with the oxo-chromane, dihydro benzodioxane, dihydro benzoxazine and oxo-benzoxazine systems (**Figure 4.4: C**) would result in maintaining or enhancing the activity. Overall, the cyclisation of aryl ether moiety is a promising modification for fluorescent attachment, both with the potential to permit attachment of a linker and also the ability to accommodate different functional groups.

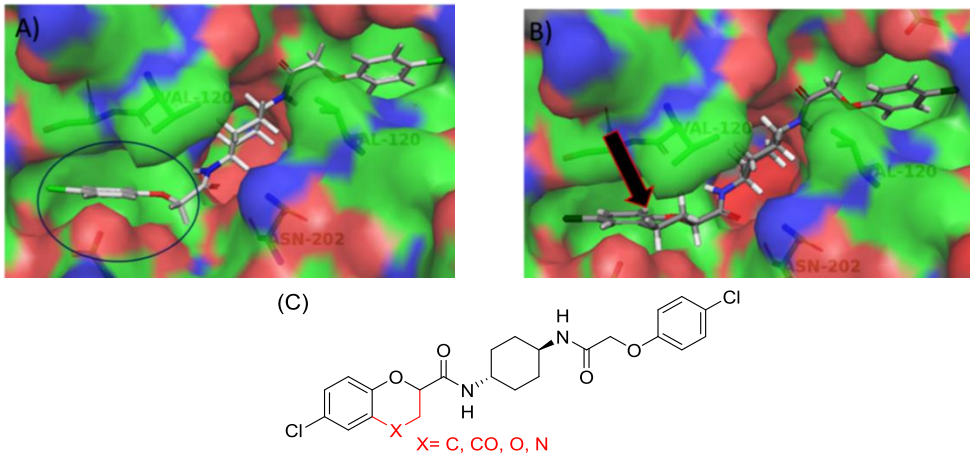


Figure 4.4: Predicted binding conformation of chromane analogue **142** with the eIF2B; (A) Shows the binding mode of ISRIB in the active site of eIF2B. The circle shown in indigo explain the co-planarity of the aromatic ring with O-CH2 moiety; (B) Surface representation of chromane analogue. The black arrow refers to benzylic C of the chromane system which is clearly shown to lie at the face of solvent-accessible entry of the receptor; (C) Overview of the modified aryl ether portion of ISRIB molecule in this study, X= C (chromane) X= CO (oxo-chromane), X= O (benzodioxane), and X= N (benzoxazine).

4.2.2. Determining a suitable linker for Fluorescent ligation

The considered strategy regarding the determination of a suitable linker involves synthesising a number of analogues with differing alkyl chain lengths, and evaluating the pharmacology of all of these analogues. The binding mode illustrated above (**Figure 4.4: B**) suggests that the **X** atom will be exposed to the solvent side of the ISRIB-binding site (under the V^{120} side chain). If this turns out to be the case, we can introduce an alkyl chain **R** (**Figure 4.5**) that might help with the anchoring of a linker and fluorescent molecules. A small investigation was conducted regarding the length of the linker involved. Therefore, derivatives were designed through preparing compounds, where **R (≠ H)** group was attached to **X**. Initially, small groups such as methyl and acetyl were installed on **X**. Rationale behind this strategy was to ascertain if steric bulk in that position was tolerated. If this was the case, these small groups were then elaborated with bulkier groups such as methoxypropane or methyl propionate which could be connected with short or long alkyl linker and help to couple a fluorescent dye. Accordingly, benzoxazine and oxo-chromane analogues were selected as starting materials for the basic design of fluorescent-ISRIB analogues. Precursor molecules having short or long linker terminating in a primary amine were designed and synthesised to generate the fluorescent labelled compounds. As a result, the fluorescently labelled derivatives were synthesised by incorporating a flexible linker terminating in a 5/6-carboxyfluorescein moiety, FAM-NHS, which aided in demonstrating ISRIB's interaction with eIF2B.

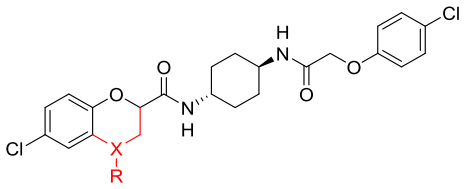


Figure 4.5: Overview of synthesis of fluorescent-ISRIB derivative in this study, R= methyl or acetyl etc.

4.3. Synthetic strategy:

Synthetic strategies for the topics discussed in sections **4.2.1** to **4.2.3** resemble to some extent the strategies applied in **Chapter 2**. To generate the required efficient analogue, a synthetic strategy involving fewest reaction steps as well as the possibility to explore any promising intermediates' SAR was implemented. In order to prepare various analogues of ISRIB, with terminal ring or central core modification, the synthesis followed a similar strategy to that described for synthesising non-symmetrical and symmetrical modified terminal aryl rings (Section **2.4.2.1**). Synthetic fragments of acid carboxylate were combined in a one step with 2-(4-chlorophenoxy)-*N*-[(1*R*,4*R*)-4-aminocyclohexyl]acetamide hydrochloride **28** or with commercially available diamine core ring, under basic conditions to generate the desired analogues. Furthermore, the strategy applied to methylate one core amine group to study the corresponding *N*-Methyl amide was reductive amination reaction rather than direct treatment with an alkylating agent, in order to avoid the formation of the undesired tertiary amine.

The synthetic route for the production of chromane, benzodioxane and benzoxazine analogues involves reactions of the corresponding carboxylic acids with 2-(4-chlorophenoxy)-*N*-[(1*R*,4*R*)-4-aminocyclohexyl]acetamide hydrochloride **28** in one step, under basic condition to generate the desired analogues. On this basis, the strategy considered required separate synthesis of the carboxylic acid fragments, before the final amide coupling step.

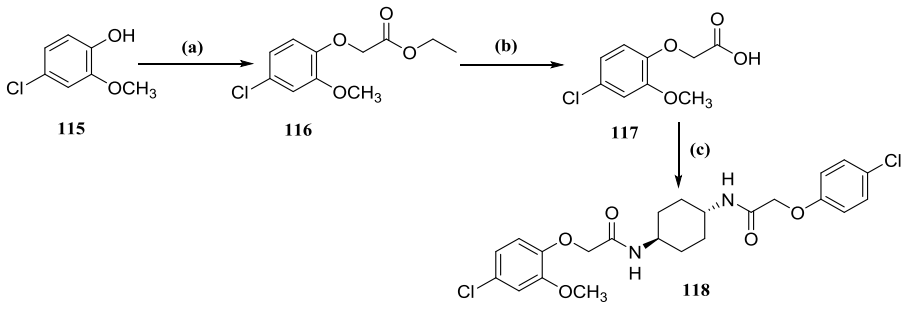
Furthermore, the general synthetic strategy for the production of fluorescent derivatives from benzodioxane was achieved via installing the linker only without the fluorescent molecule. The synthesis of a number of benzodioxane analogues with diverse linker lengths and evaluating their activity, enhance our knowledge of structure activity relationships on the effect of substitution at the aniline position of benzodioxane. Linker ligation to the benzodioxane ring before coupling to any fluorescent molecule assists in preserving the potentially expensive fluorescent FAM-NHS. In addition, this acts on protecting fluorescent analogues from any chemical or light degradation resulted from being inserted during the early stages of synthesis.

4.3.1. Synthesis of modified terminal ring analogue

The synthesis of (4-chloro-2-methoxyphenoxy)acetic acid **117** fragment was similar to the route described in section **2.4.2.2** (**Chapter 2**). This involved alkylation of the 4-chloro-2-methoxyphenol **115**, via Williamson ether synthesis to generate ether **116**. The formation of the ether derivative proceeded under the reflux in the presence of potassium bicarbonate (K_2CO_3) and ethyl-2-bromoacetate with a reaction time of 4 hours. The substitution reaction with ethyl-2-bromoacetate gave the desired ether derivative **116** in yields of 80%, after purification by column chromatography **(Scheme 4.1)**. The ethyl ester obtained was consequently saponified to the corresponding carboxylic acid, using aqueous LiOH in a mixture of THF and water in 81% yield. The acid was deemed to be pure enough, by ^{1}H and ^{13}C NMR, to be used directly in the next coupling step without further purification.

For synthesising analogue **118**, the synthetic carboxylic acid **117** underwent carboxylate activation with (HBTU), before the addition of nucleophile.

Coupling was achieved directly with 2-(4-chlorophenoxy)-*N*-[(1*R*,4*R*)-4-aminocyclohexyl]acetamide hydrochloride **28** in the presence of triethylamine to give the desired amide analogue **118**. The formation of the analogue continued with reaction times of 19 hours at room temperature and 76% yield. The desired analogue was purified by column chromatography using solvent mixtures of dichloromethane and ethyl acetate and the structural determination was carried out using ^{1}H NMR, ^{13}C NMR, LC-MS and/or HRMS.



Scheme 4.1: Synthesis of of modified terminal ring analogue.
Reagents and conditions: (a) ethyl bromoacetate, MeCN, K_2CO_3, reflux, 4 hrs, 80%; (b) $LiOH.H_2O$, THF/water (2:1), 4 hrs, 81%; (c) **28**, HBTU, DCM, Et_3N, 19 h, 76%.

4.3.2. Synthesis of modified core ring analogues

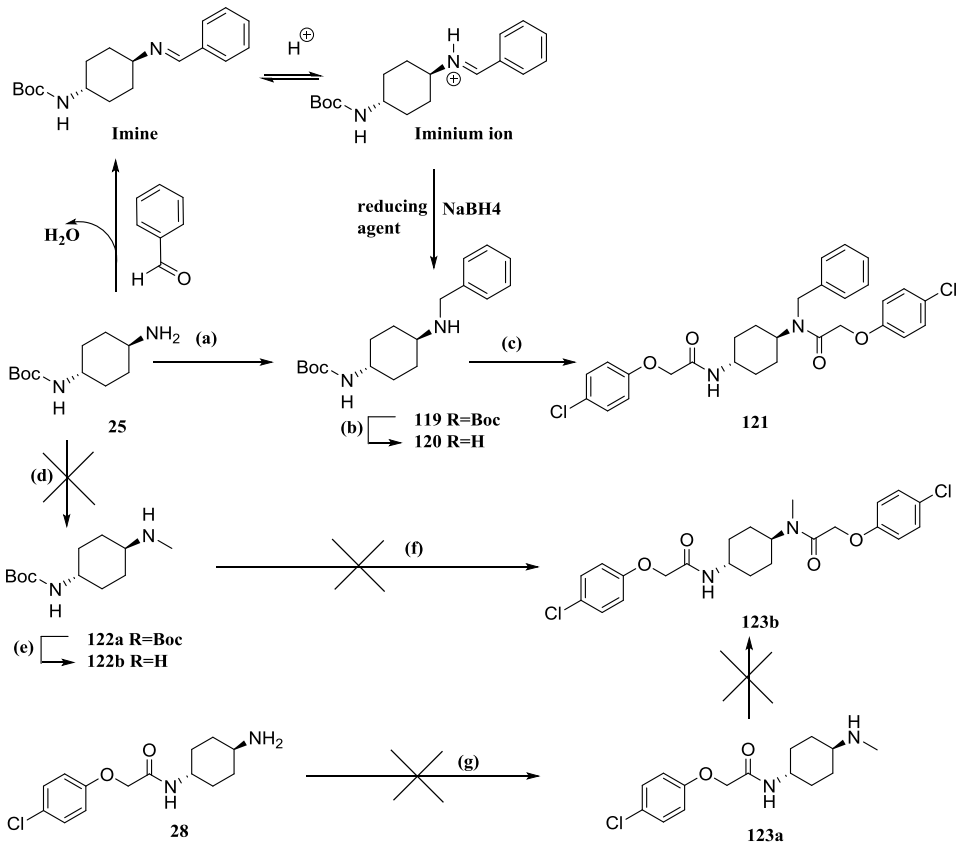
To identify the suitable site in ISRIB which can be used to attach spacer holding a labelled molecule, modified core ring analogues were synthesised. Reductive amination reaction was carried out to synthesise amide-*N*-benzyl analogue **121** (**Scheme 4.2**). This reaction involves one- or two-step procedure in which *N*-Boc-*trans*-1,4-cyclohexanediamine and benzaldehyde were condensed in ethanol for 3 hours to afford an imine or iminium ion. This step happened prior to the addition of $NaBH_4$ to allow sufficient time for the imine formation. Thereafter, reducing agent ($NaBH_4$) reacted selectively with iminium ions to form a secondary amine compound **119** in 33% yield. The lower yield might be due to reducing the rest of the benzaldehyde to an alcohol before it has the chance

to form the iminium. The later was subjected to acid-mediated removal of the Boc group by treatment with a concentrated HCl acid solution in dioxane to release the amine group as hydrochloride salt **120**. This can then directly react with 4-chlorophenoxy acetyl chloride **26** to afford the corresponding tertiary benzylamide analogue **121** with a low yield of 37%. The desired analogue was purified by column chromatography using solvent mixtures of dichloromethane and ethyl acetate and the structural determination was carried out using ^{1}H NMR, ^{13}C NMR LC-MS and/or HRMS.

Although this reaction was successful for the synthesis of tertiary amide compound **121** using benzyldehyde, the reductive amination using formaldehyde failed to give the expected tertiary amide analogue **123b**. Multiple attempts using excess of formaldehyde to react with *N*-Boc-*trans*-1,4-cyclohexanediamine in ethanol for 3-6 hours were attempted to produce the required compound **122a**. A After extraction with ether, the organic phase was washed with brine and concentrated under the vacuum, a crude solid product **122a** was not isolated but immediately subjected to Boc-deprotection and directly reacted with 4-chlorophenoxy acetyl chloride **26**. Unfortunately, the desired final tertiary amide analogue **123b** was not detected in any of the attempted reactions. The white solid obtained from this reaction was analysed by LC-MS and ^{1}H NMR. The LC-MS analysis showed multiple peaks and ^{1}H NMR spectra demonstrated a series of wide peaks uncharacteristic of analogue **123b**, and relative peak integrations did not correlate with the desired structure of analogue **123b**.

Other attempt to obtain the target compound **123b** through the reaction between key amine compound **28** and formaldehyde failed too (**Scheme 4.2**). The key amine compound **28** and formaldehyde were condensed in ethanol in the

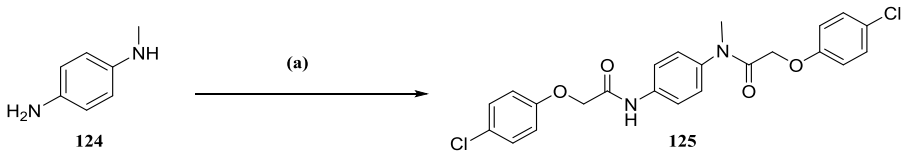
presence of reducing agent ($NaBH_4$) to form a secondary amine compound **123a**. The white solid obtained from this reaction was analysed by LC-MS but the collected peaks did not display the correct mass, indicated the desired product had not formed.



Scheme 4.2: Synthesis of modified cyclohexane core ring analogue **121** and **123b** and proposed reaction mechanism of reductive amination.
Reagents and conditions: (a) benzaldehyde, ethanol, $NaBH_4$, 2M NaOH, rt, 3hrs, 51%; (b and e) dioxane, MeOH, 4 N HCl/dioxane, rt, 96%; (c and f) 4-chlorophenoxy acetyl chloride, DIPEA, DCM, 0^oC 30 mins to rt 3 h, 37%; (d and g) formaldehyde, ethanol, $NaBH_4$, 2M NaOH , rt, 3-6 hrs.

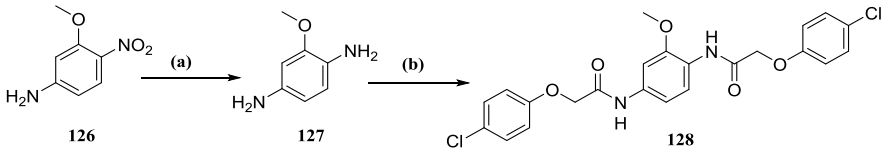
Since the insertion of methyl on NH-group of cyclohexanediamine **25** was not successful, synthesis of the remaining modified core ring analogues was attempted from the *p*-phenylenediamine core ring. The commercial availability of the 1-*N*-methylbenzene-4-diamine increased the feasibility of the reaction to produce the desired outcome. As shown in **Scheme 4.3**, synthetic route involves treatment of 1-*N*-methylbenzene-4-diamine **124** with 4-chlorophenoxy acetyl

chloride **26** in dichloromethane in the presence of DIPEA to produce the target amide analogue **125**. The formation of the analogue continued with reaction times of 30 mins at 0° C to 1 hour at ambient temperature and with a yield of 71%.



Scheme 4.3: Synthetic route for amide analogue **125**.
Reagents and conditions: (a) 4-chlorophenoxy acetyl chloride **26**, DIPEA, DCM, 0°C 30 mins to rt 1 h, 71%.

2-Methoxybenzene-1,4-diamine **127** was obtained from the reduction of 3-methoxy-4-nitroaniline **126** to corresponding free diamine over Palladium on carbon in MeOH and hydrogen, with a conversion yield of 73% (**Scheme 4.4)**. Similarly to analogue **125**, treatment of 2-methoxybenzene-1,4-diamine **127** with 4-chlorophenoxy acetyl chloride **26** in dichloromethane in the presence of DIPEA produced the target analogue **128**. The reaction time proceeded for 30 mins at 0° C then 1 hour at room temperature and with a yield of 82%.



Scheme 4.4: Synthetic route for analogue **128**.
Reagents and conditions: (a) Pd/C, H_2, MeOH, overnight, rt, 95%; (b) 4-chlorophenoxy acetyl chloride **26**, DIPEA, DCM, 0° C 30 mins to rt 1 h, 82%.

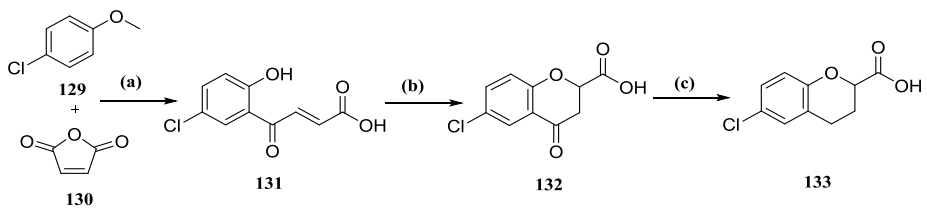
4.3.3. Synthesis of tethered glycolamide linkers (six-membered ring)

The synthetic route of chromane, oxo-chromine, benzodioxane and benzoxazine analogues involves amide coupling reaction of the corresponding carboxylic acid fragments with the key amine molecule **28**. On this base, the strategy required

separate synthesis of the chromane, oxo-chromine, benzodioxane and benzoxazine fragments, before using each in the amide coupling step.

4.3.3.1.Synthesis of chromane and oxo-chromane fragments

Generation of oxo-chromane **132** and chromane **133** fragments were relatively straightforward, and high yielding, in two-three steps starting from commercially available materials (**Scheme 4.5)**. A previously published procedure was followed in order to obtain the desired targets.[197]



Scheme 4.5: Synthetic route of oxo-chromane **132** and chromine **133** fragments.
Reagents and conditions: (a) $AlCl_3$, DCE, reflux, 71%; (b) water, 1N NaOH, 100 ^oC, 85%; (c) TFA, triethylsilane, reflux, 3 days, 1N NaOH, 6N HCl, 93%.

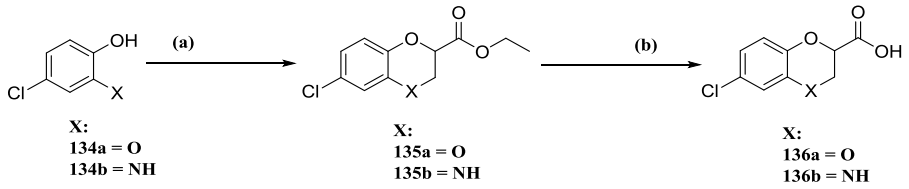
Friedel-Craft reaction of *p*-chloroanisole **129** with maleic anhydride **130** afforded the 3-(4-chlorobenzoyl)acrylic acid **131**. In this reaction, the methoxy group was readily cleaved and only the phenol was isolated. In addition, the electron-withdrawing effect of the ketone makes the product less reactive than the original *p*-chloroanisole, therefore, multiple acylation did not occur. The synthesis of compound **131** continued with reaction times of 1 hour and 71% yield.

The second step to the synthesis to the chromane fragment **133** involves intramolecular cyclization of 3-(4-chlorobenzoyl)acrylic acid **131** in water and 1N NaOH, followed by acidification to afford the oxo-chromane-carboxylic acid **132**. The cyclization results from nucleophilic attack of the α-phenolate at the β-position of α,β-unsaturated carbonyl compound **131**. The formation of the

compound **132** proceeded under reflux in 3 hours and 85% yield. Finally, the ketone moiety of oxo-chromane **132** was reduced to chromane **133**. This was achieved in strong acidic conditions with a good yield (93%) by employing the method involving trifluoracetic acid and trietylsilane according to the published procedure.[198]

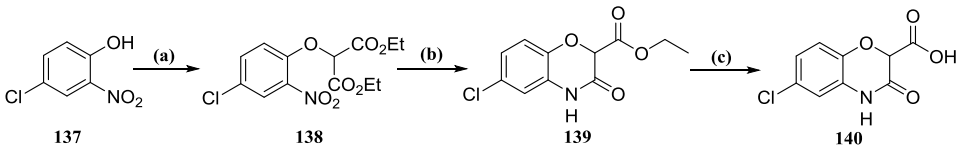
4.3.3.2.Synthesis of benzodioxane and benzoxazine fragments

The synthetic routes for benzodioxane and benzoxazine fragments was achieved via following the literature procedures.[199] The regioisomeric mixture of benzodioxane and benzoxazine esters **135a,b**, were obtained in yields of 74% and 55%, respectively by condensation of 4-chlorocatechol **134a** or 2-amino-4-chlorophenol **134b** with ethyl 2,3-dibromopropionate in the presence of potassium carbonate (**Scheme 4.6**). The desired analogues were purified by column chromatography using solvent mixtures of petroleum ether and ethyl acetate and the structural determination was carried out using NMR and LC-MS. Saponification of benzodioxane and benzoxazine esters **135a,b** produced the corresponding carboxylic acids **136a** and **136b**, respectively. In both instances, a high yield was achieved (93% and 88%), by using concentrated lithium hydroxide solution. They were deemed to be pure enough, by LC-MS, to be used directly in the next step without further purification.



Scheme 4.6: Synthetic route of benzodioxane **136a** and benzoxazine **136b** fragments. Reagents and conditions: (a) 4-chlorocatechol or 2-amino-4-chlorophenol, ethyl-2,3-dibromopropionate, K_2CO_3, acetone, reflux, 20 hrs, 74% and 55% yields respectively; (b) $LiOH.H_2O$, THF/water (2:1), 3-4 hrs, 93% and 88% yields respectively.

The initial step to prepare the benzoxazine fragment **140** was synthesised from the nitro-phenoxy-malonic acid diethyl ester **138**. This intermediate was achieved via ether synthesis by treatment of 4-chloro-2-nitrophenol **137** with diethyl-2-bromomalonate in the presence of K_2CO_3. The formation of the ether derivative proceeded at room temperature and 18 hours reaction time, in yield of 45% after purification by column chromatography (**Scheme 4.7)**. The later compound was reduced using sodium dithionite ($Na_2S_2O_4$) to afford benzoxazine-ester **139** with yield of 85%. The final step was saponification of the benzoxazine ethyl carboxylate **139** to produce the corresponding 6-chloro-3-oxo-3,4-dihydro-2H-1,4-benzoxazine-2-carboxylic acid **140**, using aqueous LiOH in a mixture of THF and water in 85% yield.

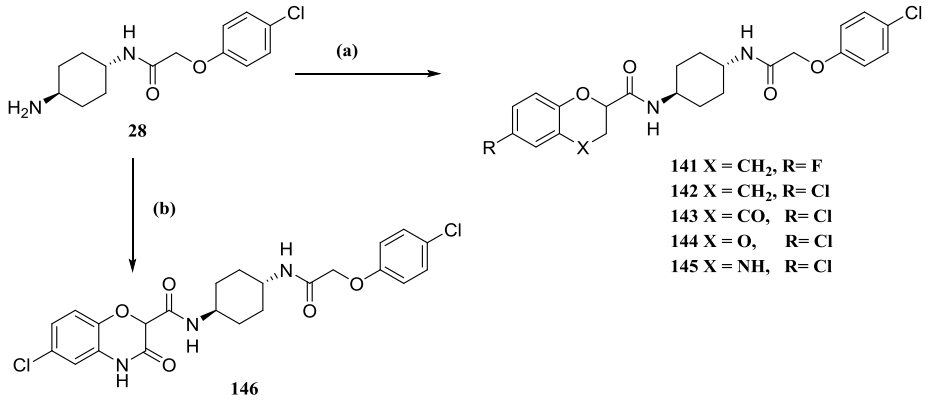


Scheme 4.7: Synthetic route of benzoxazine-one **140** fragment.
Reagents and conditions: (a) diethyl-2-bromomalonate, K_2CO_3, DMF, rt, 45%; (b) $Na_2S_2O_4$, EtOH:H_2O (4:5), reflux, 5h, 85%; (c) LiOH.H2O, THF/water (2:1), 3 hr, 85%.

4.3.3.3.Synthesis of the chromane, benzodioxane and benzoxazine analogues

The general synthetic approach for the chromane, benzodioxane and benzoxazine analogues is summarized in **Scheme 4.8**. The commercially available 6-fluorochromane-carboxylic acid and synthetic chromane, oxo-chromane benzodioxane and benzoxazine fragments underwent carboxylate activation with HBTU, before the addition of nucleophile. Amide coupling was achieved directly with key amine intermediate **28** in the presence of triethylamine to produce the required analogues **141-146**. The synthesis of the analogues continue with reaction times of 15 hr and with yields between 61%

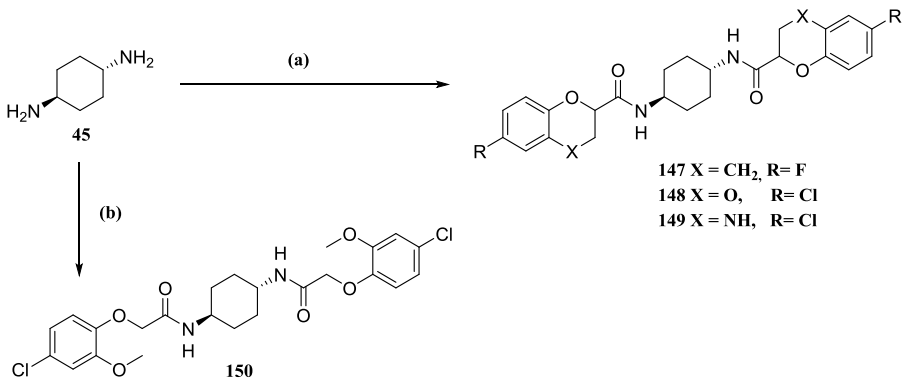
and 86%. The analogues were purified by column chromatography using solvent mixtures of dichloromethane and tetrahydrofuran. Structural determination, of all amide analogues, was carried out using NMR, LC-MS and HRMS. HPLC (at 95% or above) was utilized to confirm the purity of the analogues.



Scheme 4.8: Synthesis of the chromane, benzodioxane and benzoxazine analogues.
Reagents and conditions: (a) 6-fluorochromane-carboxylic acid, **133**, **132**, **136a** and **136b**, HBTU, DCM, Et_3N, 15 hr, yields 65% to 86%; (b) **140**, HBTU, DCM, Et_3N, overnight, yield 61%.

4.3.3.4.Synthesis of symmetrical analogues

In order to further SAR studies, interesting symmetrical analogues were synthesised for more investigation of the requirement of symmetry. In a similar way to the formation of the symmetrical terminal ring modified analogues described in **Chapter 2**, the desired symmetrical analogues were obtained by amide coupling of *trans*-1,4-cyclohexanediamine **45** with a series of selected fragments (**Scheme 4.9**). The synthetic carboxylic acid fragments were combined in a one step with *trans*-1,4-cyclohexanediamine **45**, using HBTU as coupling agent to generate the desired symmetrical analogues **147-150**, with yields between 50% to 91%.

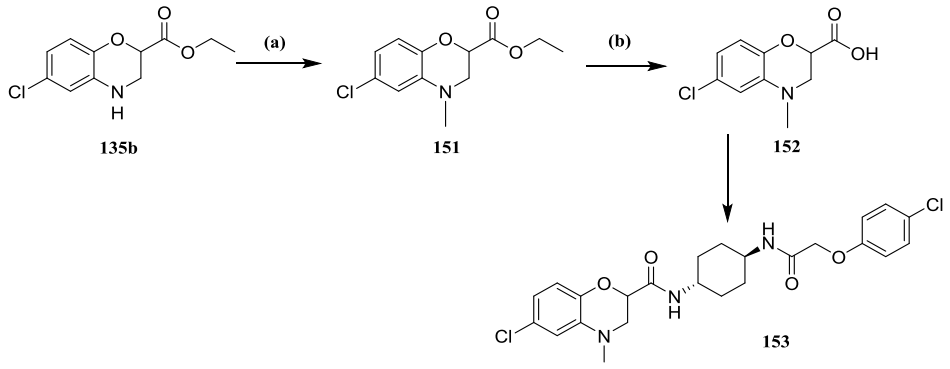


Scheme 4.9: Synthesis of the symmetrical analogues **147**to **150**.
Reagents and conditions: (a) 6-fluorochromane-carboxylic acid, **136a** and **136b**, HBTU, DCM, Et_3N, 15 h, yields 50% to 91%; (b) **117**, HBTU, DCM, Et_3N, overnight, yield 79%.

4.3.4. Synthesis of fluorescent-ISRIB analogues

As mention before, nitrogen atom of the benzoxazine fragment can be considered as a suitable site for conjugation with a fluorescent molecule. Therefore, a series of analogues with different linkers on the aniline nitrogen were synthesised. The method employed in **Scheme 4.10** to synthesise **153** required the initial synthesis of the 6-chloro-4-methyl-3,4-dihydro-2H-1,4-benzoxazine-2-carboxylic acid fragment **152**. This method utilised methodology that produced intermediate benzoxazine carboxylate **135b** (Section **4.3.3.2**). **135b** was selected as a starting material to alkylate the aniline, perhaps preventing potential undesired side product formation if the reaction started directly with benzoxazine analogue **145**. Benzoxazine carboxylate **135b** reacted with methyl iodide in the presence of K_2CO_3 in DMF to generate ethyl 6-chloro-4-methyl-3,4-dihydro-2H-1,4-benzoxazine-2-carboxylate **151**. The reaction proceeded in 3 hours with 57% yield after purification by column chromatography. The later coumpound was subjected to ester hydrolysis to produce the corresponding carboxylic acid fragment **152**, using aqueous LiOH in a mixture of THF and water in 95% yield. The synthetic carboxylic acid **152** underwent carboxylate activation with HBTU, before coupling with 2-(4-chlorophenoxy)-*N*-[(1*R*,4*R*)-4-

aminocyclohexyl]acetamide hydrochloride **28** in the presence of triethylamine to give the desired amide analogue **153**. The formation of the analogue proceeded overnight with a good yield after purification by column chromatography.



Scheme 4.10: Synthetic route of analogue **153**.
Reagents and conditions: (a) methyl iodide, K_2CO_3, DMF, 40 ^oC, 3 hr, 57%; (b) $LiOH.H_2O$, THF/water (2:1), 3 hr, 95%; (c) **28**, HBTU, DCM, Et_3N, overnight, yields 84%.

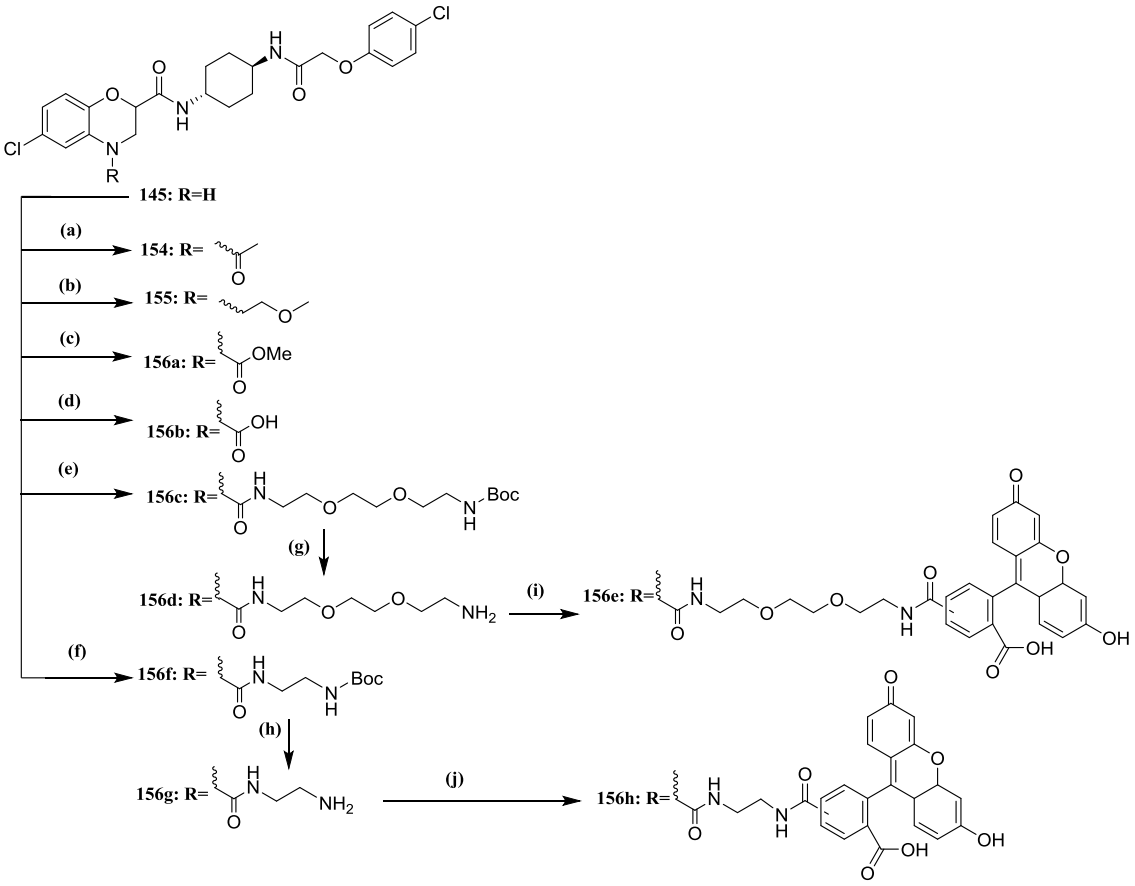
As shown in **Scheme 4.11**, the majority of other analogues were obtained from the benzoxazine **145**. This analogue underwent nucleophilic substitution reactions with a variety of alkylating agents to provide the desired analogues **154-156a**. Initially, direct reaction of benzoxazine **145** with acetyl chloride was attempted to generate analogue **154**. This acylation method of aniline group needed dropwise addition of a solution of the reactive acetyl chloride to the benzoxazine at 0^o C. The reaction then proceeded for 3 hours at room temperature with yield of 45% after purification by column chromatography.

In contrast to the synthesis of methyl benzoxazine analogue **153**, the synthesis of analogues **155** was done in one step through alkylation the full molecule of benzoxazine **145** rather than the benzoxazine carboxylate **135b** as did for the synthesis of methyl benzoxazine analogue **153**. Although further efforts was employed for purified the final mixture, but the synthesis route was successful in reducing the time to obtain the desired compound. Benzoxazine analogue **145**

was reacted with 2-bromoethyl methyl ether under standard conditions to alkylate aniline group in the presence of K_2CO_3 and NaI in DMF. The reaction proceeded overnight at 125°C with a yield of 35% after purification by column chromatography to produce analogue **155**.

The same methodology was followed for the synthesis of the fluorescent ligands **156e** and **156h**, using analogue **156a** as a starting point. The later was achieved in a similar manner to the synthesis of analogue **155**. Benzoxazine nitrogen aniline **145** was alkylated with methyl bromoacetate in the presence of K_2CO_3 and NaI in DMF to generate analogue **156a** (**Scheme 4.5**) with moderate yield. The ester **156a** underwent saponification to produce the corresponding carboxylic acid analogue **156b**, using aqueous LiOH in a mixture of THF and water in 84% yield. To avoid exposing the fragile/sensitive fluorescent dye to forcing chemical conditions, the linker was built first without the fluorescent molecule by using mono-Boc protected diaminoalkyl linkers. The carboxylic acid **156b** was coupled directly to the linkers using HBTU as coupling agent, to produce short and long chain analogues **156c** and **156f**. The formation of these analogues proceeded in 6 to 9 hours with yields of 63% and 80% after being purified by column chromatography. Deprotection of the Boc group resulted in exposed the primary amine which was conjugated to the NHS-Fluorescein derivative (**Scheme 4.11**). By using the commercially available NHS-Fluorescein, which is an amine-reactive derivative of the fluorescein dye, it is possible to label the primary amine of the linkers in the presence of triethylamine at 31° C to generate the fluorescent tagged ISRIB analogues **156e** and **156h**. The fluorescent analogues were purified by semi-preparative HPLC with yields of

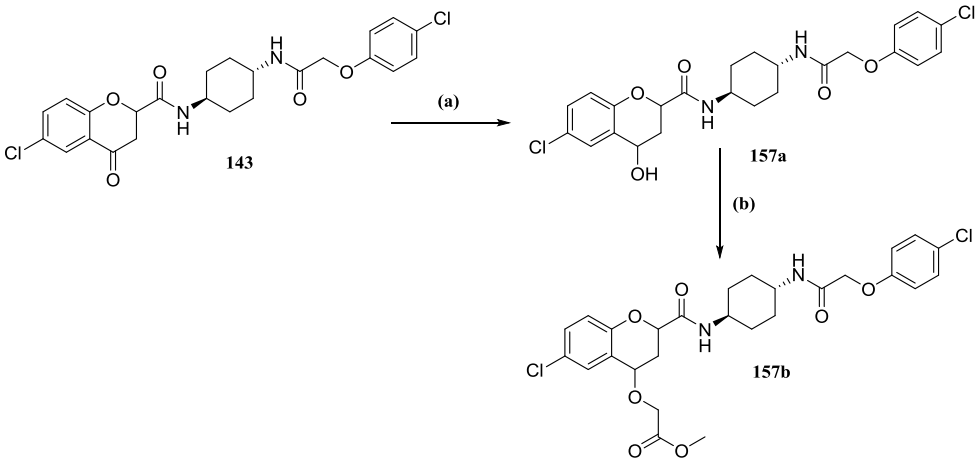
75% and 80% respectively. Structural confirmation of the fluorescent analogues, was verified by using ^{1}H NMR and HRMS.



Scheme 4.11: Synthetic route of fluorescent-ISRIB analogues **154-156a-h**.
Reagents and conditions: (a) acetyl chloride, DIPEA, DCM, 30 min 0 ^{o}C to 3 hr at rt, 45%; (b and c) 2-bromoethyl methyl ether or methyl bromoacetate, NaI, K_2CO_3, DMF,125 ^{o}C overnight, 35% and 67%; (d) LiOH.H_2O, THF/water (2:1), 3 hr, 84%; (e and f) *tert*-butyl (2-(2-(2-aminoethoxy)ethoxy)ethyl)carbamate or *tert*-Butyl *N*-(2-aminoethyl) carbamate, HBTU, Et_3N, DCM; 6-9 h, yields 80% and 63%; (g and h) dioxane, MeOH, 4 N HCl/dioxane, rt, 98% and 95%; (i and j) 5/6-carboxyfluorescein succinimidyl ester, Et_3N, DMF, 31 ^{o}C, overnight, 75% and 80%.

Oxo-chromane analogue **143** was also selected as a potential candidate to introduce a linker. This ketone analogue was subjected to a reduction process in the presence of sodium borohydride ($NaBH_4$) to produce chromanol analogue **157a** (**Scheme 4.12**). Conversion of ketone to alcohol depends on the strength of the reducing agent, therefore the relatively weak reducing agent such as sodium borohydride is typically used for this purpose. The chromanol analogue

157a, was then subjected to etherification using chemistry of Williamson ether synthesis.[180] The hydroxy deprotonation of chromanol **157a** with NaH, followed by treatment with methyl bromoacetate produced the desired acetate analogue **157b** in 86% yield.



Scheme 4.12: Synthetic route of analogues **157a,b**.
Reagents and conditions: (a) $NaBH_4$, DCE, 2h, 95%; (g) Sodium hydride 60% dispersion in mineral oil, methyl bromoacetate, DMF, 3h, 86%.

4.4. The biological evaluation of ISRIB-analogues

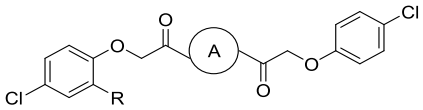
The above analogues which were designed to be used in structural studies elucidation for eIF2B underwent different biological assays. First, the GFP reporter gene assay, described previously in **Chapter 3**, was used to guide SAR studies in this project. Second, competitive binding assay such as Fluorescence Polarisation (FP) assay[44] which was designed to probe the ability of the fluorescent ligand to bind to the isolated eIF2B protein *in vitro*. Finally, the mutagenesis cell analysis[44] to assist in identifying the cellular target of ISRIB molecule. Once again, this work was accomplished at the Cambridge Institute for Medical Research (CIMR) by the team of Professor David Ron.

4.4.1. Pharmacology results and SAR of ISRIB analogues

All synthesised ISRIB-analogues were assessed for their potency by employing the cell-based GFP reporter assay described previously in **Chapter 3**.

4.4.1.1.Pharmacology of terminal rings and central core modifications

The EC_{50} values of the successfully synthesised terminal and core modified ring analogues, are compared to the relevant ISRIB in **Table 4.1**.



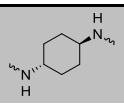
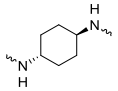
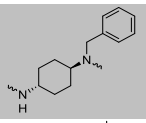
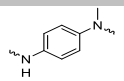
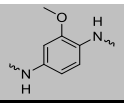
Ligand	A	R	ISR inhibition % CHOP::GFP signal at 10 μM	EC_{50}
1		H	91	5.3 nM
118		OCH_3	87	644 nM
121		H	-	inactive
125		H	85	1.5 μM
128		H	-	inactive

Table 4.1: EC_{50} and ISR inhibition (% CHOP::GFP signal at 10 μM) of ISRIB analogues modified at the terminal and central core moiety **118**-**128**. Shown is a representative from three independent experiments conducted for *trans*-ISRIB and of a single 12-point titration experiment conducted for ISRIB analogues.

The *ortho*-methoxy analogue **118** was synthesised to investigate whether the bulky substitutions on *ortho*-position could tolerate a linker attachment. The results demonstrate that increasing the steric bulk at this position leads to 130 folds reduction in potency in relation to ISRIB. The reduction in potency suggests that there may be a limit to the *ortho*-substitution size that can be accommodated, and that even small substitutions such as a methoxy hinders

binding. Additionally, there may be steric effects on the ether group adjacent to the terminal ring, due to the proximity of the *ortho*-substituent.

The substitutions on *ortho*-position can also be used to compare with the known *meta*/*para* substitutions pattern (**Chapter 1**). In comparison, the *ortho*/*para* substitution analogue **118** showed less activity than all the previously known *meta/para* substitution analogues.[151] The presence of methoxy group in *ortho*-position of the terminal aromatic ring would result in disrupting the conformation of the terminal aromatic ring, thus the substitution patterns can resist the accommodation at the receptor. Indeed, the lower potency suggests that favourable interaction of *para*-chloro substituent alone is diminished by the neighbouring *ortho* bulky methoxy group. More compounds, with different electron donating and withdrawing functional groups of various sizes at *ortho*-position, would need to be generated to illustrate whether the position, size or electronic nature of a substituent produces the greater impact.

On the other hand, the NH-amide of ISRIB was modified by incorporating large benzyl group into NH-amide of *trans*-1,4-cyclohexanediamine core ring **121**. This modification resulted in a loss of activity. This loss of activity is in line with results of other modified core ring ISRIB-analogues developed by Walter *et al*[150], showing a gradual reduction of potency with the incorporation of small group (but-1-yne) and insertion of long chain molecule (Section **4.2.1.2**). Thus, this finding revealed that there are no evident ways of incorporating large group into NH-amide of core ring that would facilitate the visibility of ligand in target identification assay. However, insertion of the small hydrophobic methyl group at the NH-amide of benzene-1,4-diamine core ring **125** led to a significant drop in potency, which cannot be illustrated on the basis of its size, and is possibly

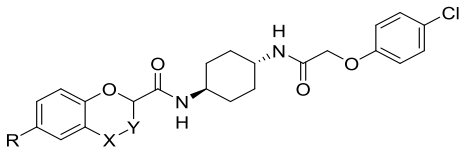
attributed to the intolerance of this region of the active site to the hydrophobic groups. This also support previous research that showed incorporation of small group (but-1-yne) into NH-amide of core ring causes a significant reduction in potency.[150] Lastly, the introduction of methoxy group at carbon atom of benzene-1,4-diamine core ring as in analogue **128** resulted in a complete loss of activity. This result suggests that insertion of such bulky group at this position might perturb the accommodation of ligand at binding site.

Overall, the terminal aromatic ring and central core ring are unlikely to be suitable sites for fluorescent attachment, although it would have seemed obvious choice for attachment. This might be due to the fact that both aromatic terminal ring and central ring orientation as being essential for the efficacy of ISRIB, as it is thought to be responsible for activating the eIF2B receptors. Therefore, any modification at these positions lead to great loss in potency.

4.4.1.2.Pharmacology of glycolamide linker modifications: chromane, benzodioxane and benzoxazine analogues

All glycolamide linker modifications (chromane, benzodioxane and benzoxazine analogues), were assessed for their potency and the results of the assay are shown in **Table 4-2**. As mentioned previously in section **4.2.1.3**, the approach of tethering terminal aromatic moiety to the α-carbon atom of glycolamide linker by six-membered ring, could be considered a good alternative to modifying the ISRIB without dramatic loss of bioactivity, by rigidifying the molecule without disturbing its binding conformation. Indeed, apart from **146**, it was pleasant to find that very good potency of the analogues studied was retained in comparison to ISRIB itself. The chromane **141** and **142**, oxo-chromane **143**, benzodioxane **144** and benzoxazine **145** derivatives all had a high level of activity, at a

concentration of 10 μM, indicating that such conformational restriction doesn't disrupt eIF2B receptor binding significantly. The simple Chromane analogues **141** and **142** still showed good activity, with only a 7-10 fold reduction in activity compared to ISRIB. This result emphasises the importance of the chemical structure of the chromane part of the ISRIB analogues. Chromane group acts on restricting the bond rotation and thus in turn may enhance bioavailability.



Ligand	R	X	Y	ISR inhibition % CHOP::GFP signal at 10 μM	EC_{50}
141	F	CH_2	CH_2	95	51 nM
142	Cl	CH_2	CH_2	94	34 nM
143	Cl	CO	CH_2	81	60 nM
144	Cl	O	CH_2	95	55 nM
145	Cl	NH	CH_2	98	8 nM
146	Cl	NH	CO	60	715 nM

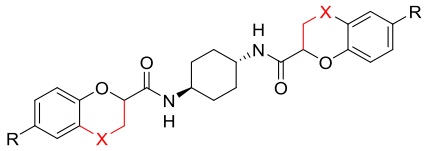
Table 4.2: EC_{50} and ISR inhibition (% CHOP::GFP signal at 10 μM) of ISRIB analogues modified at the glycolamide linker **141**-**146**. Shown is a representative from three independent experiments conducted for *trans*-ISRIB and of a single 12-point titration experiment conducted for ISRIB analogues.

Simple modification to the benzylic carbon of chromane **142** suggests there is room for extension around the benzylic carbon. One possibility is by introducing a carbonyl group as oxo-chromane **143**, the carbonyl introduction was neutral in terms of activity. However, placing the benzylic carbon group with an oxygen **144** (benzodioxane) or nitrogen **145** (benzoxazine) led to enhancing the activity. Changing the hydrophobic nature of the of benzylic carbon to a hydrophilic oxygen **144** had the same activity of chromane **142**, while changing to amine **145** led to higher potency and only 2-fold less potent than ISRIB molecule. This suggested that electronics nature or a hydrogen bond features at this position might plays an important role for enhancing the interaction with the receptor. A

comparison between the chromane **142,** oxo-chromane **143,** benzodioxane **144** and benzoxazine **145** analogues shows that there is a slightly greater affinity for the hydrogen bond donor (as in NH-aniline group of benzoxazine **145**) rather than the hydrogen bond acceptor of other analogues (oxygen and carbonyl group). This could indicate that a hydrogen bond donor at this position could offer a further interaction with the receptor.

However, when comparing the oxo-benzoxazine **146** and benzoxazine **145** analogues, it appears that a carbonyl group reduced the activity by 150-fold in comparison to ISRIB. These results suggest that there may be a size limit that can be accommodated at this position.

On the other hand, the characteristic feature of all above analogues is the alteration of only one glycolamide linker with keeping the other linker side chain without any modification. In this study, further investigation for the requirement of symmetry was employed through modifying glycolamide linker at both sides of the ISRIB molecule (**Table 4.3**). With regard to the di-chromane **147** and di-benzodioxane **148** analogues, the general effect of this modification is a substantial drop in potency when compared with chromane **142** and benzodioxane **144**. Apart from **147** and **148**, the di-benzoxazine analogue **149** maintained the activity in comparison with benzoxazine **145**. These results support the above suggestion, which indicates that a hydrogen bond donor (NH group of di-benzocaine **149)** at this position might play an important role for enhancing the interaction with the receptor.



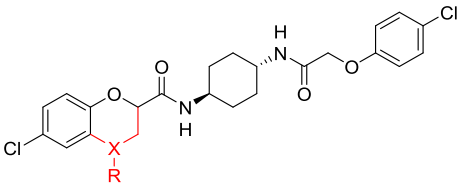
Ligand	X	R	ISR inhibition % CHOP::GFP signal at 10 µM	EC_{50}
147	CH_2	F	20	inactive
148	O	Cl	61	3.2 µM
149	NH	Cl	93	15 nM

Table 4.3: EC_{50} and ISR inhibition (% CHOP::GFP signal at 10 µM) of symmetrical ISRIB analogues modified at the glycolamide linker **147**-**149**. Shown is a representative from three independent experiments conducted for *trans*-ISRIB and of a single 12-point titration experiment conducted for ISRIB analogues.

Overall, unlike the terminal ring and central core ring, there is no accumulating evidence suggesting that fluorescent attachment at the NH-aniline group of benzoxazine **145** would be inappropriate. Therefore, the modified glycolamide linker analogues particularly benzoxazine **145**, which showed considerable activity in a cell-based assay, was selected to act as a precursor for further optimization to the synthesis of fluorescent derivatives. Furthermore, the non-symmetrical derivatives are more active than their symmetrical counterparts, suggesting that the tethering of the aromatic ring to *O*-CH_2 linker is better tolerated if only present on one side of the molecule.

4.4.1.3.Pharmacology of benzoxazine aniline-linker analogues

All synthesised benzoxazine and chromanol linker analogues, were assessed for their potency (**Table 4.4**). The findings from Walter *et al*[150] and our SAR studies revealed that there are no obvious ways of incorporating specific atoms or groups into ISRIB that would make the ligand more visible in target identification assays. Our SAR results (Section **4.4.1.1**) suggested that such modification cannot be easily achieved from the central portion or terminal aromatic ring of ISRIB.



Ligand	X	R	ISR inhibition % CHOP::GFP signal at 10 μM	EC_{50}
153	N	CH_3	89	67 nM
154	N	$COCH_3$	83	1 μM
155	N	$CH_2CH_2OCH_3$	82	93 nM
156a	N	CH_2COOCH_3	84	120 nM
157a	CH	OH	91	289 nM
157b	CH	OCH_2COOCH_3	94	1.1 μM

Table 4.4: EC_{50} and ISR inhibition (% CHOP::GFP signal at 10 μM) of ISRIB analogues with benzoxazine or oxo-chromane linker **153**-**157b**. Shown is a representative from three independent experiments conducted for *trans*-ISRIB and of a single 12-point titration experiment conducted for ISRIB analogues.

However, benzoxazine analogue which retained high activity (Section **4.4.1.2**) through tethering the aryl ether portion represents a promising modification for the purpose of synthesising fluorescent derivatives. It was concluded that this analogue possessed the essential parameters (retaining good activity and possessing suitable site that can accept molecular extension with bulky substituents) which were needed for favourable ligation with a fluorescent molecule. Thus, the first candidate for fluorescent molecule attachment is the aniline group in benzoxazine. As illustrated in **Table 4.4**, several analogues were prepared and examined to find the most appropriate spacer (**R**). Introducing a small hydrophobic methyl group at this position as shown in *N*-methyl benzoxazine **153** analogue, resulted in maintaining the activity, with an 14-fold reduction in comparison to the benzoxazine analogue **145**. This result suggested that such small steric effect in this position is tolerated and accommodated in the receptor binding site. However, increasing the bulk of the **R** substituent from *N*-methyl to *N*-acetyl as shown in *N*-acetyl benzoxazine **154** analogue resulted in a significant reduction of potency. The *N*-acetyl benzoxazine **154** led to a high drop in potency, which suggests that there may be a limit to the **R** substituent

size that can be accommodated, and that hydrophilic carbonyl group might greatly hinder the binding. Although the *N*-acetyl benzoxazine analogue **154** was found to be a poor eIF2B receptor ligand, replacing the *N*-acetyl with *N*-methoxyethane **155** resulted in a significant regain in activity. This finding cannot be illustrated by the effect of size, and is poosibly suggested that bulky substitution at the *N*-position of benzoxazine, could be accepted with differing degrees, with at least one CH_2 group close to amine group of benzoxazine is preferred for the activity.

The later results encouraged us to continue this work toward further understanding of the SAR of *N*-benzoxazine substitutions. Introduction of methyl propionate group as shown in *N*-methyl propionate benzoxazine **156a** analogue, also resulted in retaining activity which is equipotent with *N*-methyl benzoxazine analogue **153**. These results support the previous finding that analogues with one CH_2 close to amine group of benzoxazine have greater effect on eIF2B receptor binding affinity. The finding that increasing linker length is not associated with a concomitant reduction in potency, e.g the *N*-methoxyethane benzoxazine **155** and *N*-methyl propionate benzoxazine **156a** having similar activity to the *N*-methyl benzoxazine **154**, suggests that the *N*-benzoxazine position is not deep-seated within the active site. It is therefore highly expected that the long spacer could be oriented outside the solvent-accessible entry of the binding site, without hindering the putative ISRIB-binding site of eIF2B. As a consequence of this results, *N*-methyl propionate benzoxazine **156a** was used as a platform to synthesise several analogues with short or long spacer terminated with fluorescent moiety **156b-h** (**Scheme 4.11**). The synthesised fluorescently labelled ISRIB analogues **156e** and **156h** were not tested due to time constraints,

and this unfortunately leaves the results table lacking important information. However, the fluorescent analogue **156e** was used to establish a fluorescent polarisation-based assay (details in section **4.4.2.1**)

On the other hand, oxo-chromane analogue was also investigated for their possibility to conjugate the fluorescent dye. The results of **Table 4.4** demonstrate that the carbonyl position was also suitable for ligation. Optimizing the carbonyl group of oxo-chromane derivative through modifying it to the alcohol, chromanol **157a**, resulted in retaining the activity. However, the *O*-methyl propionate **157b** demonstrated a significant reduction in potency compared with the same substitution in the *N*-methyl propionate **156a**. Nevertheless, this finding still presents a promising result. This further signifies the results of the *N*-benzoxazine linker series above, which proposed that modification at the aniline position is not embedded within the active site. Therefore, benzoxazine analogue **145** was chosen as a preferred analogue to be attached to a fluorescent molecule.

4.2.2. Fluorescence polarisation competition assay: general principle

The homogenous fluorescent technique such as fluorescence polarisation (FP) assays is an attractive high throughput application, widely used to measure the binding interaction between two molecules and to examine protein-ligand binding affinity in the process of drug discovery. It has priority among other assays because it offers a respected effectiveness, quick analysis, low cost and high precision.[200] In the FP technique (**Figure 4.5**), the non-polarised light spread in different directions from the excitation beam. The filter polarisers are arranged to let light waves passing the excitation light only in one direction plane.[200] The polarised light acts on exciting the fluorescent molecule to emit polarised light as well. When the fluorescent ligand binds to a large molecule, it

will tend to decrease the rate of tumbling and lead to increase the fluorescent polarisation of the emitted light. However, when this small fluorescent ligand is freely moving (rapid rotation due to non-binding to other large molecules) in the solution, it will tend to decrease the initial polarisation due to reflecting the light by radiating at different directions and this resulting in low fluorescent polarisation. Thus, the emission effect of polarised light is decreased with freely moving fluorophores in the solution, whereas it is increased with reducing the rate of freely tumbling fluorophores (**Figure 4.5**).

This basic idea of FP assay is widely applied in numerous research fields to study the ligand-protein interaction. In FP assays, monitoring competitive binding is possible to determine the affinity of unlabelled ligand that competes with ligand labelled with fluorescent molecule for binding with the same binding site in the target receptor. The stable complex moves slower when a fluorescently labelled ligand binds to the target protein, thus resulting in expected high polarisation signal. However, when the fluorescent labelled molecule is displaced from the binding site by an unlabelled competitive ligand, a consequent decrease in fluorescent polarisation is observed.[200-202]

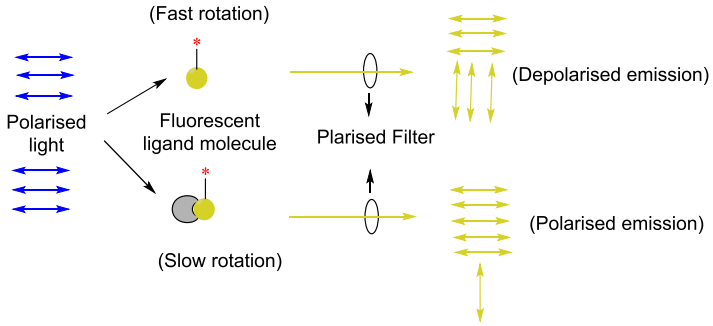


Figure 4.5: Principle of fluorescence polarisation. (Reproduced from Hall *et al*[202]).

4.2.2.1.Development of an eIF2B fluorescence polarisation assay

The synthesis of fluorescently labelled ISRIB analogues facilitates the employment of FP technique in probing ligand binding to eIF2B. Fluorescein-labelled ISRIB analogue **FL-156e** represents a valuable instrument in demonstrating a direct interaction between ISRIB-type compounds and eIF2B. The assay has been developed at the Cambridge Institute for Medical Research by Prof. David Ron team. The eIF2B is a GEF biologically stabilised by ISRIB binding.[151] To better understand this binding process, an FP competition assay was developed by collaborators to report the binding of a synthetic fluorescent-labelled ISRIB analogue with eIF2B.[44] The assay was conducted by measuring the FP signal of the labelled probe **FL-156e** at various concentrations using 2000 nM of the probe as a standard. The FP signal was stable across all dilutions above 100 nM, lower dilutions were fluctuating. Therefore, 100 nM of **FL-156e** was chosen to be used as as optimum in all the further binding assays (**Figure 4.6, A**).

Furthermore, Ron *et al*[44] set out to investigate its binding specificity. A concentration of 100 nM of **FL-156e** was tested for unspecific binding using various dilutions of bovine serum albumin (BSA) (**Figure 4.6, B**). The shift in FP was observed at concentrations of BSA above 40 ug (i.e. above 2000 nM).

After checking the binding specificity, **FL-156e (**100 nM) was challenged with various concentrations of human eIF2B (hu_eIF2B) (**Figure 4.6, C**). The FP shift was observed at concentrations of hu_eIF2B as low as 60 nM. Since the amount of the purified protein was quite limited, a concentration of 250 nM of hu_eIF2B was used in combination with 100 nM **FL-156e** for further analysis of competitive binding of the unlabelled *trans*-ISRIB to hu_eIF2B.

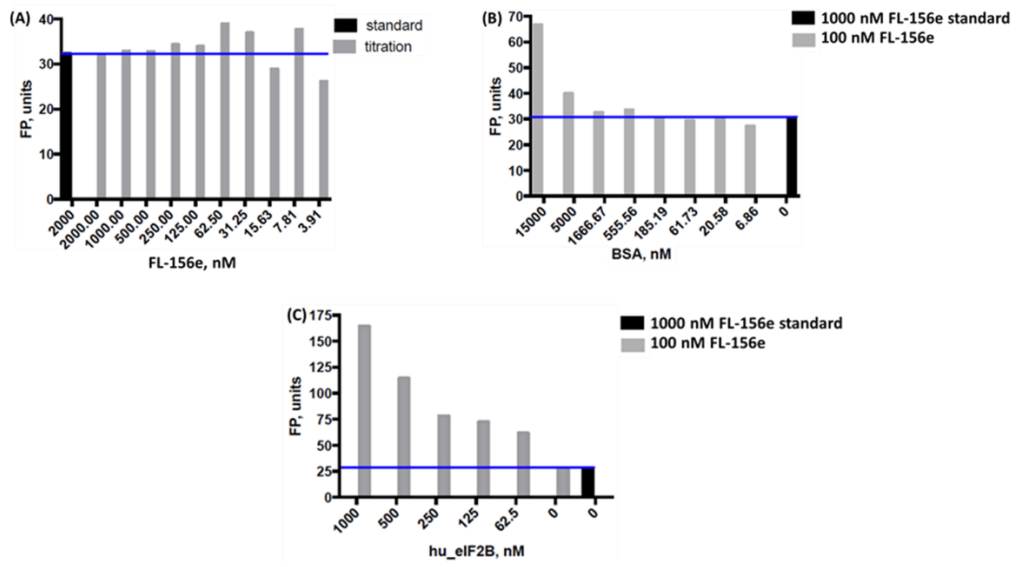


Figure 4.6: A) Titration of **FL-156e**; B) Binding of **FL-156e** to BSA; C) Binding of **FL-156e** to hu_eIF2B.

Obviously, the increased fluorescence polarization (FP) signal was observed from the direct binding of fluorescent ISRIB analogue **156e** and purified eIF2B, FP was increased with increasing concentrations of eIF2B (**Figure 4.7: A**). Therefore, FP competition assay was performed, in which the unlabelled ISRIB molecule effectively competes for eIF2B in samples containing fixed concentrations of purified human eIF2B (30 nM) and fluorescent probe (2.5 nM). Polarisation of samples were recorded in the presence of increasing concentrations of unlabelled *trans*-ISRIB with an EC_{50} in the nanomolar range, as observed for ISRIB action in cells (**Figure 4.7: B**). Thus, the FP assay likely reported the engagement of the labelled ISRIB analogue in targeting the same site on eIF2B that is relevant to ISRIB action.

Binding of the fluorescent probe to eIF2B in the competition experiments was expressed as a fraction of relative polarization signal (%P) over the dynamic range of the assay. Relative polarization was calculated by subtracting background FP (P_{bg}) from experimental FP (P_{ex}) ($P = P_{ex} - P_{bg}$). The minimal FP

(P_{min}) observed when no eIF2B was added and the maximal FP (P_{max}) with eIF2B alone (in the presence of probe and in absence of non-fluorescent competitor compounds) define the dynamic range of the assay. Values of relative polarization for any assay point ($\%P_n$) were calculated using the formula $\%P_n=(P_n-P_{min})/P_{max}-P_{min})*100$).

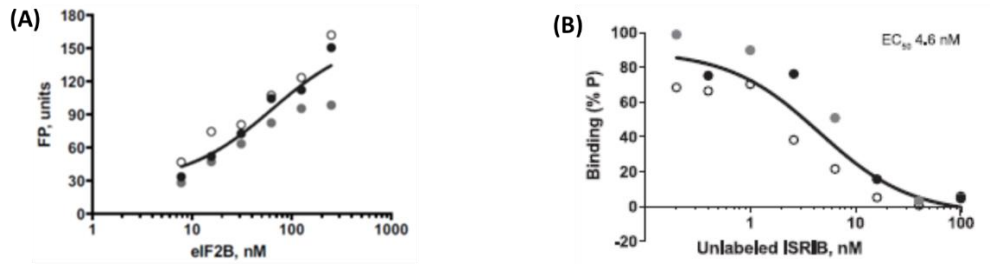


Figure 4.7: Fluorescence polarization (FP) assays showing binding of ISRIB to human eIF2B. (A) A plot of the FP signal arising from fluorescein-labelled ISRIB analogue **FL-156e** (2.5 nM) as a function of the concentration of eIF2B in the sample. (B) A plot of the relative FP signal arising from samples with fluorescein labelled **FL-156e** (2.5 nM) bound to purified human eIF2B (30 nM) in the presence of the indicated concentration of unlabelled *trans*-ISRIB introduced as a competitor. Concentrations of eIF2B and ISRIB on respective plots are represented on a log10 scale. Curve fitting and EC_{50} was generated using agonist versus response function on GraphPad Prism; Shown are values of three independently acquired measurements.[44]

4.2.3. Mutagenesis cell analysis of the putative ISRIB-binding site

To test ISRIB binding features, CRISPR-Cas9 was used to select random mutations of residues lining the ISRIB-binding pocket.[40, 44, 151, 167] Mutagenesis of residues lining the ISRIB-binding pocket altered the hierarchical cellular response to ISRIB derivatives *in vivo* and ISRIB binding *in vitro*. Therefore, if these mutations are residues that line the ISRIB binding pockets, they might selectively alter the sensitivity to one ISRIB derivative over another. Thus, the hierarchy of EC_{50} of various ISRIB derivatives would be different depending on the type of ISRIB resistant mutation and might differ from the hierarchy of EC_{50} of the different derivatives established in wildtype cells. Such findings could be a powerful argument that the residues affected by the mutations determine the nature of the ligand binding pocket and are thus likely proximal to it. The

overview of the previous SAR studies helped to select a small number of ISRIB derivatives that are structurally diverse and cover a relevant range of a sensitive EC_{50} for study in the mutant cell lines. Therefore, chromane **142** and benzoxazine **145** were chosen with ISRIB **1** to perform the mutation assay and study possible ISRIB resistance in mutant cell lines.[44]

4.3. Conclusions

The present study has successfully generated and assessed a series of new ISRIB analogues to investigate a suitable site for fluorescent ligation. In addition, a series of *N*-benzoxazine linker analogues and *N*-benzoxazine fluorescently labelled ISRIB analogues was successfully synthesised, with varying linker length, coupled to NHS-fluorescein molecule.

To identify an appropriate site within the ISRIB molecule to be modified for fluorescent molecule conjugation, three practical sites were investigated (terminal aryl ring, central cyclohexane core ring and glycolamide linker). Pharmacological analysis of series of ISRIB analogues with *ortho*-substitution at terminal ring or with NH-amide alkylation at central core ring showed a general reduction of potency. Although, *ortho*-substitution analogue **118** did not lead to complete loss of potency, suggesting that an area around the *ortho*-position of terminal ring when bound to the eIF2B receptor, can tolerate a reasonable degree of steric bulk. However, both of these positions (NH-amide and *ortho*-substitution) proved unlikely to be an appropriate site for fluorescent attachment.

However, the modified aryl glycol amide tether analogues such as chromane, oxo-chromane, benzodioxane and benzoxazine led to molecules with significant

residual activity, indicating that there is sufficient space around the receptor active site to accommodate such modification. The success of the modified aryl ether portion analogues greatly contributed to designing a fluorescently labelled eIF2B receptor ligand. Among these analogues, benzoxazine **145** showed the best results with only a 4-fold drop in potency.

The amine group in benzoxazine analogue **145** was ideal to explore the possibility of using this site for molecular extension with linker conjugation to assist in synthesis of a labelled molecule. Various linker lengths and types were selected to assist in this endeavour. The aim was to produce a steric substitution ranging from small to large in size for investigation. Analysing the results of series of *N*-benzoxazine linker analogues showed a general tolerability of linker sizes when the nitrogen was alkylated with CH_2 group. This suggests that an area around the *N*-benzoxazine position of ISRIB, when bound to the eIF2B receptor, can permit an acceptable extent of steric bulk. Finally, this series showed promising results with the *N*-methyl propionate benzoxazine **156a** linker analogues, which was coupled directly to long and short linkers conjugated to the NHS-Fluorescein to synthesise the fluorescent ISRIB analogues **156e** and **156h**, respectively. It is unfortunate that none of the fluorescently labelled ISRIB analogues were tested for detection the EC_{50} values due to time constraints, however the fluorescent ISRIB analogue **156e** was successfully used in demonstrating the direct interaction between ISRIB-type compounds and eIF2B, by using it in the FP binding assay and were successfully used in support the results of cryo-microscopy to definitively proven the binding mode of ISRIB and elF2B.

5. *In vitro* disposition studies of ISRIB and its analogues

5.2. Introduction

Disposition studies (ADME: absorption, distribution, metabolism and excretion) are general terms that include the processes that determine the concentration of candidate compounds within cells or in plasma. The disposition study together with pharmacokinetics studies, play an important role in the discovery and development of new drug candidate compounds.[203] Development of an oral CNS agent can often be limited by the undesirable pharmacokinetic features such as low aqueous solubility, poor permeability and rapid clearance, which are the most critical considerations that control the oral bioavailability of drugs.[204, 205] Therefore, *in vitro* biopharmaceutical screening of drug candidates is implemented from early stages of drug discovery and development processes, as understanding of solubility and permeability is essential to achieve acceptable oral bioavailability.[204, 205] Determination of theses parameters represent an important considerations in determining the right drug candidate to progress further to preclinical animal testing. Insufficient information about these parameters would result in many complications regarding the time and the cost during preclinical *in vivo* pharmacokinetic evaluations. Moreover, assessment of theses parameters *in vitro* could be utilised prior to *in vivo* experimentations in order to aid the development of experiments. Many studies only considered one or two in *vitro* biopharmaceutical assessment parameters before conducting the *in vivo* pharmacokinetic evaluations, however this can mislead the process of discovery.[206, 207] The oral absorption is a result of assessment of several factors

such as permeability, solubility and metabolic stability.[205, 208] Therefore, a comprehensive *in vitro* biopharmaceutical parameters evaluation is necessary to select the most promising candidates which could be further tested for *in vivo* pharmacokinetic study.

This chapter describes *in vitro* ADME parameters assessment (aqueous solubility, Caco-2 permeability and microsomal stability) of ISRIB and other promising analogues. In this study, *trans*-ISRIB, piperidine analogue **103**, piperazine analogue **108a** and benzoxazine analogue **145** were selected for further *in vitro* ADME studies, as they have the highest eIF2B receptors activity (**Figure 5.1**). The main aim of this chapter is to investigate the biopharmaceutical properties of ISRIB and its selected analogues. In order to do this, LC-MS/MS quantitative analytical method was developed, this method was used to achieve the outcome of the *in vitro* ADME parameters. Furthermore, this project was also concerned with the development of appropriate formulation systems for oral administration of ISRIB and other promising compounds to be delivered for preclinical studies which aimed at defining the therapeutic margin of lead compounds.

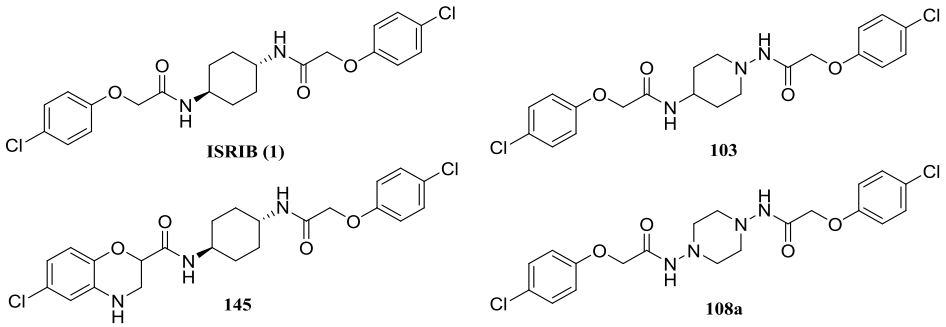


Figure 5.1: Structures of ISRIB **1** and other promising analogues **103**, **108a** and **145** selected for *in vitro* ADME studies.

5.3. Solubility of ISRIB

Aqueous solubility is one of the most important biopharmaceutical properties in drug discovery and development. Solubility is related to the ADMET properties as the drug must be soluble to be absorbed across the cell membrane and then reaches the target.[204, 209] ISRIB has very low aqueous solubility (predicted solubility is 0.00051 mg/ml, logS= -5.9, **Table 5.1**) and the lack of oral bioavailability of this compound is likely due predominantly to this fact. The lipophilicity of ISRIB is moderate (predicted $logD_{7.4}$ =3.56), so it would not have been expected to have such a low aqueous solubility based on its polarity-lipophilicity balance. The preclinical *in vivo* pharmacokinetic profile of ISRIB confirmed this issue and recommended the administration of ISRIB by intraperitoneal (ip) injection.[152] ISRIB penetrates the blood–brain barrier and displayed acceptable mouse brain: plasma ratio at various doses in wild-type mice, it showed 8 hr half-life in plasma with approximately 60 nM brain concentration, after 24 hr of a single intraperitoneal (ip) injection (dose, 2.5 mg/kg).[149, 152] Acceptable mouse brain–plasma ratio, exposure following i.p. dosing, and predicted lipophilicity (logP/D = 3.56) suggest acceptable permeability and metabolic stability, however no measurable blood or brain levels detected after the oral administration.[152]

The main challenge in terms of medicinal chemistry was to find mechanistic equivalents of ISRIB that possess ADMET properties suitable for the development of an oral CNS agent in terms of solubility, lipophilicity, permeability, brain-to-blood distribution, metabolism, and safety. Generally, lipophilicity represents the main factor responsible for low solubility.[175] Lipophilicity significantly influences ADMET properties and can be valued by

partition or distribution coefficient (logP or logD). Compounds with moderate lipophilicity ($logD_{7.4}$ 0-3, optimal $logD_{7.4}$ ~2) generally possess good balance between solubility and permeability, and are optimal for drug development.[209] Therefore, the standard approach that medicinal chemists follow to overcome poor solubility involves adjustment of the optimal molecular lipophilicity. The simple way to obtain molecular adjustment is through structural modification by replacing hydrophobic carbon atoms with more polar heteroatoms, the most common selected atoms are oxygen or nitrogen.[175, 188] Given the lipophilic nature of ISRIB (predicted $logD_{7.4}$ =3.56), its structure was further modified to achieve less lipophilicity values and facilitate oral administration. A polar ring form, piperidine and piperazine (**Table 5.1),** was then developed by introducing a core ring with nitrogen-atom instead of cyclohexane ring. Introduction of a polar moiety into ISRIB reduced the predicted lipophilicity of candidate's analogues **103** (predicted $logD_{7.4}$ =2.11) and **108a** (predicted $logD_{7.4}$ =1.58). However, failing to improve aqueous solubility and low predicted solubility of both piperidine **103** (predicted solubility 0.00055 mg/ml) and piperazine **108a** (predicted solubility 0.00136 mg/ml) were observed (**Table 5.1**). Based on these results, it was considered interesting to *in vitro* examine whether there is any improvement in aqueous solubility in comparable to the predicted results, especially since the predicted $logD_{7.4}$ for these derivatives are significantly lower than ISRIB.

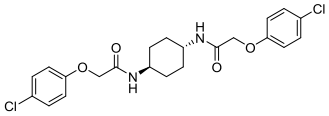
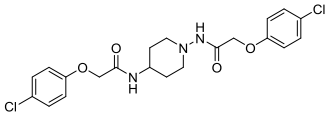
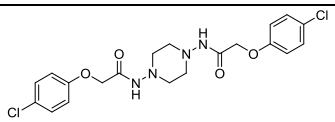
Compound	Structure	Solubility (mg/ml)	logS	$logD_{7.4}$	HBA/HBD
ISRIB **1**		0.000519	-5.9	3.56	4/2
103		0.000551	-5.9	2.11	5/2
108a		0.00136	-5.5	1.58	6/2

Table 5.1: Predicted physicochemical properties of ISRIB **1**, **103** and **108a** (calculated using Chemicalize, ChemAxon chemoinformatics platform (v14.8.4.0)).

5.4. Development and validation of simple and sensitive LC-MS/MS quantitative analytical method for detection of ISRIB analogues in *in vitro* studies

Since ISRIB has very low aqueous solubility, a sensitive method should be considered to measure its aqueous solubility, this method was supposed to achieve very low concentration nearly (10 nM). Initially, an UV-LC analytical method was employed for quantification of ISRIB in water. However, this method was limited because it requires a high concentration to achieve a measurable peak representative chromatogram. This could be consider as a major limitation for assess aqueous solubility and ADME studies as sample concentration is usually substantially very low in these studies. In a previously published study, ISRIB quantitative analysis was performed by LC-MS/MS analytical method to detect the ISRIB concentration in brain and plasma of animal models.[152] This method achieved good sensitivity with low plasma concentration of 10 ng/mL (22 nM) and had been applied in preclinical pharmacokinetic studies. However, this study was focused on measuring the concentration of ISRIB in blood and brain tissue. Therefore, it did not report

specific details on the analytical procedure such as lower limit of quantification (LLOQ), quantification range, use of an internal standard and validation.

Therefore, this study aimed to develop a sensitive LC-MS/MS quantitative analytical method for measuring the concentration of selected compounds in *in vitro* assays (solubility assay, Caco-2 permeability and microsomal stability). The assay was developed using LC-MS/MS and full validation of the method was performed to meet the regulations of the FDA. The developed and validated method was applied to *in vitro* pharmacokinetic study for mouse and human plasma.

5.4.2. **Validation criteria of the LC-MS/MS method**

A full validation of the LC-MS/MS quantitative bioanalytical method was performed in accordance with the guideline established by the FDA.[210]

5.4.2.1.Selectivity and sensitivity of the LC-MS/MS method

The selectivity of the analytical LC-MS/MS method was evaluated by comparing the Multiple Reaction Monitoring (MRM) chromatograms of the aqueous, rat and human plasma blank samples with the MRM chromatograms of blank samples spiked with ISRIB, **103**, **108a** and internal slandered (**IS**). The goal of this comparison is to examine the presence of any interference with the assay at the LLOQ obtained from the *in vitro* pharmacokinetic experiment. Whereas, the sensitivity of this method was validated by determining the LLOQ of the selected compounds. The validated LLOQ was the lowest tested concentration of ISRIB and other promising analogues in spiked aqueous, rat and human plasma samples that have sufficient accuracy and precision of relative error (RE) within ±20% and relative standard deviation (RSD) ≤20%, respectively, from both intra-and inter-day analyses.[210] RE and RSD will be discussed in the following section.

5.4.2.2.Accuracy and precision of LC-MS/MS method

Accuracy and precision were revealed as relative error (RE) and relative standard deviation (RSD), respectively. Generally, accuracy was determined as the percentage of the mean calculated concentration versus nominal concentration, while the precision was revealed as the coefficient of variation at each concentration.[211, 212] Accuracy and precision of the method were validated by analysing five replicates of quality control (QC) samples [LLOQ, low QC (LQC), medium QC (MQC) and high QC (HQC)] on the same day for intra-day assay and five consecutive days for inter-day assay. The acceptable criteria for accuracy and precision were RE within ±15% and RSD ≤15%, respectively, for both intra- and inter-day runs, with the except at the LLOQ where it should not deviate by more than 20 %.[211]

5.4.2.3.Linearity of LC-MS/MS method

Calibration curves for all tested compounds were established at the same range (10 – 10000 nM) with 10 nM as LLOQ. Each calibration curve included a blank sample (diluent with IS solution only) and a tested sample (working solution spiked with diluent and IS solution). The linearity of the assay was obtained by plotting the peak area ratios of tested compounds to the IS against nominal concentration to achieve calibration curves. In general, calibration curves with correlation coefficient value of 0.99 or greater were considered to be acceptable.

5.5. Results and discussion

5.5.2. Optimization of the LC-MS/MS method

This study was carried out to develop a specific and sensitive LC-MS/MS method for the simultaneous studying of ISRIB and its analogues **103**, **108a** and **145** in term of aqueous solubility, Caco-2 permeability and microsomal stability assays. The organic component of the mobile phase aws acetonitrile, which was chosen because it showed improved assay sensitivity over other solvents including methanol. Subsequently, a binary gradient elution consisting of acetonitrile and distilled water was chosen as a mobile phase. For chromatographic separations, conventional C_{18} Gemini column (3 μm, Phenomenex, USA) was evaluated in this study and was given an appropriate separation efficiency, retention time, peak shape and acceptable sensitivity. **Figure 5.2** demonstrates the product ion mass spectra achieved for ISRIB, **103**, **108a**, **145** and **IS** with the expected structures of their most considerable product ions. In the full scan Q1 mass spectrum, the protonated molecular ions $[M + H]^+$ of ISRIB, **103**, **108a**, **145** and **IS** were found at m/z = 451.0, 452.0, 453.0, 478.2 and 417.0, respectively. The mass transitions of the precursor to the product ion were monitored at m/z 451.0→266.2 for ISRIB, 452.0→267.2 for **103**, 453.0→85.2 for **108a**, 478.2 →266.0 for **145** and 417.0→266.0 for **IS**.

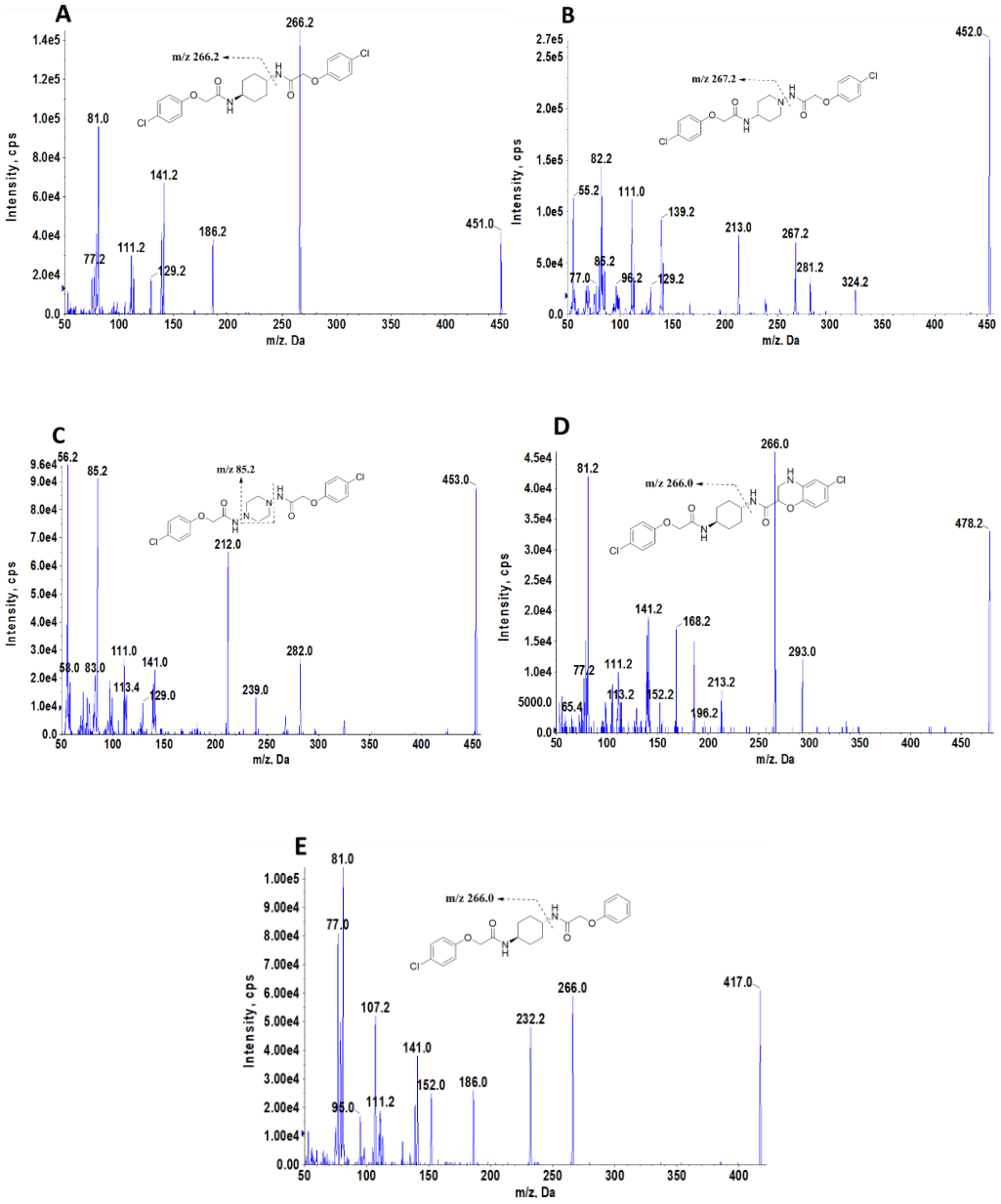


Figure 5.2: Product ion mass spectra of protonated compounds: (A); ISRIB **1** (m/z= 451.0→266.2), (B); **103** (m/z= 452.0→267.2), (C); **108a** (m/z= 453.0→85.2), (D); **145** (m/z= 478.2 →266.0), and (E); **IS** (m/z= 417.0→266.0).

5.5.3. **LC-MS/MS Method validation**

5.5.3.1.Selectivity, Linearity and LLOQ

The selectivity of the LC-MS/MS method was elucidated as interference peaks from blank samples that were efficiently isolated from the peak of all tested compounds, no endogenous or extraneous peaks interferences were noticed in the chromatograms of various tested compounds. **Figure 5.3** demonstrates the

representative MRM chromatograms of ISRIB, **103**, **108a** and **IS** in aqueous solution, human and rat plasma obtained at LLOQ. Under the optimal chromatographic condition described above ISRIB, **103**, **108a** and **IS** were eluted at 2.26, 2.18, 2.13 and 2.22 min, respectively, and the total chromatographic run time for all tested compounds was maintained at 3.5 min. This figure showed that endogenous peaks that originate from blank samples, which were used in *in vitro* ADME experiments, did not showing any interfere with the peaks of interest. Therefore, the current data indicate appropriate assay selectivity for the simultaneous analysis of ISRIB, **103**, **108a** and **IS**. Overall, ISRIB, **103**, **108a**, **145** and **IS** in all assay's samples were well separated from endogenous interferences under the same chromatographic conditions. For the analysis of ISRIB, **103**, **108a** and **145,** the calibration curves were linear over the concentration range from 10 to 10000 nM for water solubility, microsomal stability and Caco-2 permeability assays, with correlation coefficients of 0.99 or greater. The achieved value of LLOQ was 10 nM of all tested compounds for aqueous, human and rat plasma. The signal-to-noise ratios determined at LLOQ in various matrices were >20.

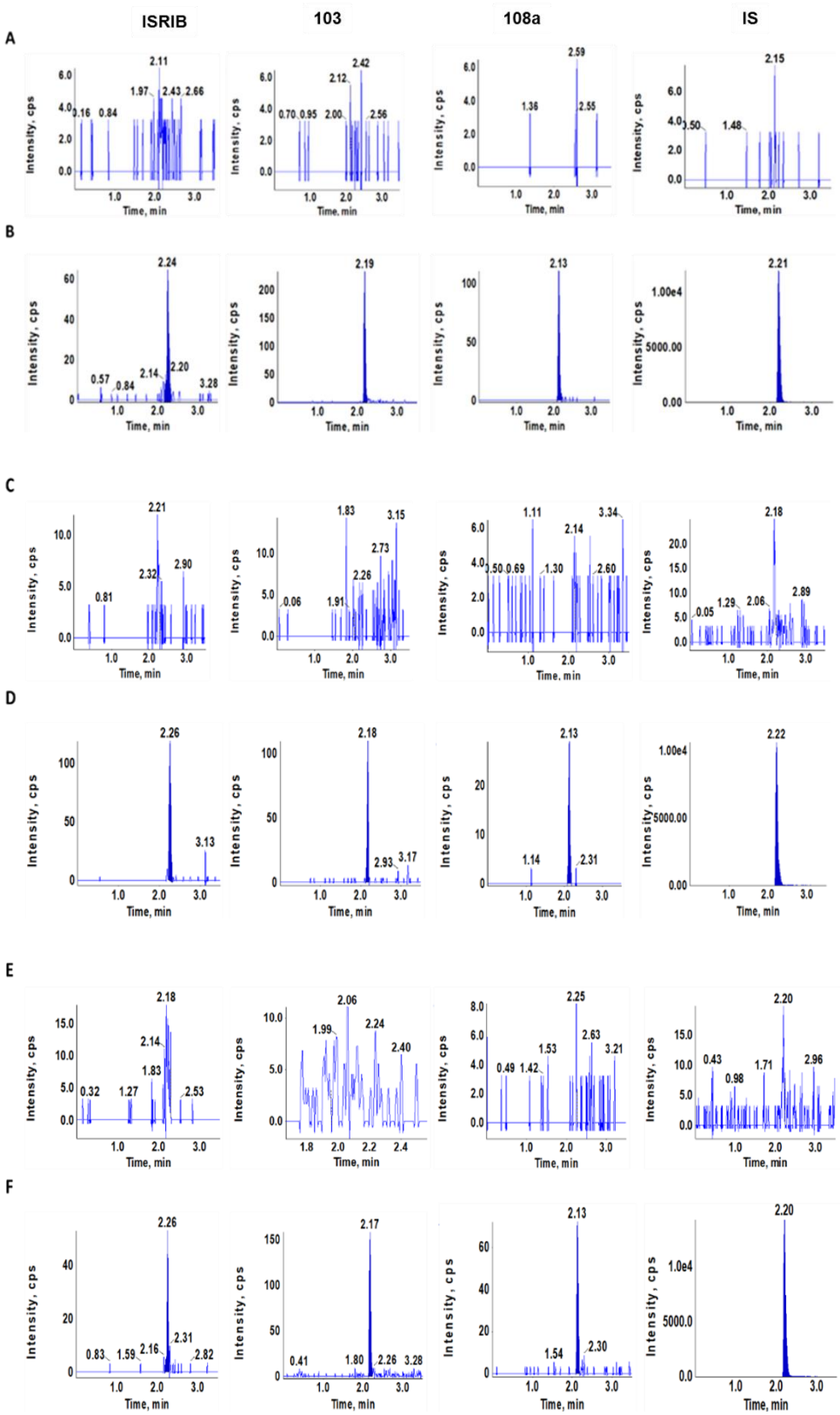


Figure 5.3: Representative MRM chromatograms of ISRIB **1**, **103**, **108a** and **IS** obtained for (**A**) blank aqueous solution, (**B**) aqueous solution at LLOQ (10 nM for ISRIB **1**, **103**, **108a** and 1000 nM for **IS**), (**C**) blank human plasma, (**D**) human plasma obtained at LLOQ (10 nM for ISRIB **1**, **103**, **108a** and 1000 nM for **IS**), (**E**) blank rat plasma, (**F**) rat plasma obtained at LLOQ (10 nM for ISRIB **1**, **103**, **108a** and 1000 nM for **IS**).

5.5.3.2.Accuracy and precision

Accuracy and precision, showed as RE and RSD, for intra- and inter-day validations are shown in **Table 5.2**. This table shows intra-and inter-day accuracy and precision obtained by assaying LLOQ, low, medium, and high QC samples of ISRIB, **103** and **108a** on five consecutive days with 5 replicates each day. The values for all QC samples (LLOQ, LQC, MQC and HQC) were within the acceptable range (RE within ±15% and RSD <15% for all QC samples and RE within ±20% and RSD <20% for LLOQ). The intra- and inter-day accuracy was from 100.1 to 107.7%, 88.3 to 109%, and 95.7 to 105.8% for ISRIB, **103** and **108a**, respectively, and the intra- and inter-day precision was ≤9.24%, ≤8.6%, and ≤12.2% for ISRIB, **103** and **108a**, respectively, for all concentrations. These intra- and inter-day accuracy and precision data were all within the acceptable range. These results indicate that the developed method was able to determine the ISRIB and other selected analogues with appropriate accuracy and precision.[211]

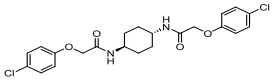
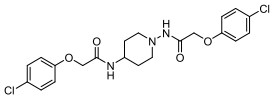
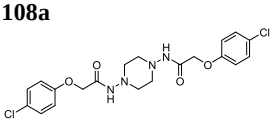
Compound	**Levels**	**Intra-day**		**Inter-day**	
		Accuracy RE%	**Precision RSD%**	**Accuracy RE%**	**Precision RSD%**
ISRIB **1** 	**LLOQ** (10nM)	107.1	9.24	102.3	6.98
	LQC (15nM)	100.3	9.14	107.0	7.11
	MQC (200nM)	107.7	6.13	101	4.32
	HQC (8000nM)	106.7	7.13	100.1	7.24
103 	**LLOQ** (10nM)	109.0	4.69	97.1	6.32
	LQC (15nM)	94.5	4.35	102.1	6.44
	MQC (200nM)	88.3	1.34	93.0	8.60
	HQC (8000nM)	103.5	1.73	103.2	8.11
108a 	**LLOQ** (10nM)	95.7	4.5	99.7	12.2
	LQC (15nM)	98.6	7.3	105.8	6.8
	MQC (200nM)	100.8	3.8	100.1	6.2
	HQC (8000nM)	100.5	4.7	98.2	5.9

Table 5.2: Accuracy and precision data of the detection ISRIB**, 103** and **108a** in diluent (intra- and inter-day n=5 each), RSD; relative standard error, RE; relative error, LLOQ; lower limit of quantification, LQC, MQC and HQC; lower, medium and high-quality controls samples, respectively.

5.4.3. Applications of the developed method to *in vitro* ADME studies

The developed method was successfully applied to the aqueous solubility, permeability and microsomal stability studies. The assay sensitivity was adequate to quantify ISRIB, **103**, **108a** and **145** levels over a sufficient sampling time period. In this study, aqueous solubility, Caco-2 permeability and microsomal stability assays were involved to evaluate the biopharmaceutical properties and to facilitate the development of the most promising candidates.

5.4.3.1.Aqueous solubility assay

The validated LC-MS/MS method was applied to assess the solubility of ISRIB, **103** and **108a** in distilled water to provide information on solubilisation behaviour of tested compounds in water. The concentration of selected compounds was detected in distilled water samples by measuring the area response with LC-MS/MS analysis and the results were then calculated by applying them on calibrated curve of the selected compounds individually. **Table 5.3** summarizes the concentration of ISRIB, **103** and **108a** detected in the distilled water samples. Clearly, all the tested compounds showed very low solubility in distilled water (practically insoluble). ISRIB demonstrate lowest concentration (0.00027 mg/mL), these results could give an explanation of the previous finding obtained regarding loss of oral bioavailability of ISRIB after oral administration.[152] Piperidine analogue **103** and piperazine analogue **108a** analogues exhibited unnoticeable enhancement in solubility, although their predicated solubility showed a slight improvement particularly to piperazine analogue **108a**. This was unexpected as a nitrogen group should increase the polarity of a compound and one could expect improved aqueous solubility from this substitution. Therefore, it is suggested that there could be high probability

of thermodynamic stability effect similar to ISRIB. This effect overcomes the introduction of a polar amine group into the central cyclohexane ring. This claim was clearly noticed by measuring the melting points of piperidine analogue **103 (**257-260 °C) and piperazine analogue **108a** (271-275 °C), which were approximately similar to ISRIB **(**271-274 °C).

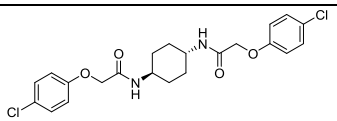
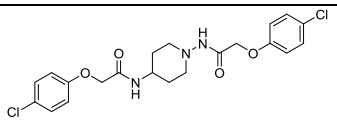
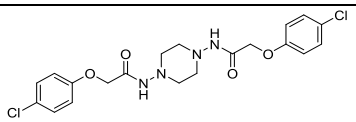
Compound	**Structure**	**Aqueous Solubility (nM)**	**Aqueous solubility (mg/ml)**	**Predicted solubility (mg/ml)**
ISRIB **1**		599.6 ± 10.5	0.000271	0.000519
103		703.3 ± 17.2	0.000317	0.000551
108a		740.6 ± 8.0	0.000355	0.00136

Table 5.3: Solubility of ISRIB **1**, **103** and **108a** in distilled water; predicted concentration (mg/mL) of ISRIB**, 103** and **108a** (calculated using Chemicalize, ChemAxon chemoinformatics platform (v14.8.4.0)).

5.4.3.2.Microsomal stability assay

Metabolic stability results of the ISRIB and other selected analogues obtained by means of human and rat liver microsomes are shown in **Tables 5.4** and **5.5**. In this study, verapamil (the first calcium channel blocker introduced into therapy[213]) was used as a reference standard compound to evaluate the metabolic stability. The literatures demonstrate that the verapamil is susceptible to extensive oxidative metabolism controled by cytochrome P450 enzymes with less than 5% of an oral dose being excreted unchanged in urine.[214,215] In this project, verapamil revealed a high intrinsic clearance (Cl_{int}) values of 124.9 ml/min/kg (**Table 5.4**), these results are in agreement with previously reported results (122 ml/min/kg) in prediction of human clearance assay.[215] In general, all

compounds showed slow metabolism and therefore low CL_{int} values in both tested species. The results showed that the piperidine analogue **103** was predicted to be the least affected by the hepatic first-pass metabolism as this compound had the highest F_h (The fraction of the compound that enters the liver and passes through it unchanged) value from both species tested. Substitution of the cyclohexyl ring of ISRIB with piperidine group **103** resulted in approximately equivalent metabolic stability. While, substitution of the cyclohexyl ring of ISRIB with piperazine group **108a** resulted in a slight decrease in metabolic stability. In addition, tethering the terminal aromatic ring of ISRIB to glycolamide linker by formation of benzoxazine **145** also resulted in decreased metabolic stability but to less extent. Concerning the differences between the two species, CL_{int} was consistently higher in the rat but overall the F_h values were comparable.

Overall, considering the general concept of metabolic stability assay, which states that the compounds with $Fh \leq 30\%$ are highly vulnerable for extensive hepatic first-pass metabolism.[216, 217] Therefore, ISRIB and other promising analogues were predicted to be less influenced by the hepatic first-pass metabolism during the oral absorption process.

Human				
Compounds	**$t_{1/2}$, (min)**	**CL_{int} (mL/min/kg)**	**Well-stirred model**	
			CL_h (mL/min/kg)	**F_h (%)**
Verapamil	13.94 ± 0.54	124.9 ± 4.7	17.75 ± 0.10	14.2 ± 0.5
ISRIB **1**	102.78 ± 30.36	25.70 ± 7.9	17.30 ± 3.63	68.7 ± 6.6
103	112.75 ± 6.69	22.10 ± 1.4	15.76 ± 0.68	71.4 ± 1.2
108a	62.42 ± 14.74	29.00 ± 4.7	11.96 ± 1.23	42.2 ± 6.0
145	74.36 ± 13.57	34.20 ± 6.6	21.00 ± 2.46	62.0 ± 4.5

Table 5.4: Metabolic stability of ISRIB **1**, **103**, **108a**, **145** and verapamil in human liver microsomes (mean ± SD)
Well-stirred model[215]: $CL_h = Q \cdot CLint / (Q + CLint)$; CL_h= hepatic clearance, Q= represents hepatic blood flow rate.

Rat				
Compounds	**$t_{1/2}$, (min)**	**CL_{int} (mL/min/kg)**	**Well-stirred model**	
			CL_h (mL/min/kg)	**F_h (%)**
ISRIB **1**	45.03 ± 4.09	38.8 ± 3.7	13.48 ± 0.43	34.9 ± 2.1
103	61.57 ± 11.69	28.9 ± 4.9	11.99 ± 2.9	42.1 ± 4.4
108a	54.79 ± 5.82	45.5 ± 5.1	24.9 ± 1.5	54.9 ± 2.7
145	37.29 ± 3.81	47.0 ± 5.0	14.34 ± 0.46	30.7 ± 2.2

Table 5.5: Metabolic stability of ISRIB **1**, **103, 108a, 145** and verapamil in rat liver microsomes (mean ± SD)
Well-stirred model[215]: $CL_h = Q \cdot CLint / (Q + CLint)$; CL_h= hepatic clearance, Q= represents hepatic blood flow rate.

5.4.3.3.Caco-2 permeability assay

The use of *in vitro* Caco-2 permeability assay to study the absorption of substances is widely accepted and popular.[214] Caco-2 is a heterogeneous human epithelial colorectal adenocarcinoma cells that have P-glycoprotein efflux transporters, various enzymes, microvilli, and tight cellular junctions mimicking the intestine.[214] *In vitro* permeability studies, has commonly used to screening compounds for both intestinal permeability and efflux liability.[214, 218] In this cell-based assay, the permeability of the candidates compounds can be assessed in both directions (**Figure 5.4**), from the apical to the basolateral side (A–B) and from basolateral to apical side (B–A). Thus, it can assist in determining the involvement of carrier-mediated transport or carrier-mediated efflux mechanisms.[219, 220]

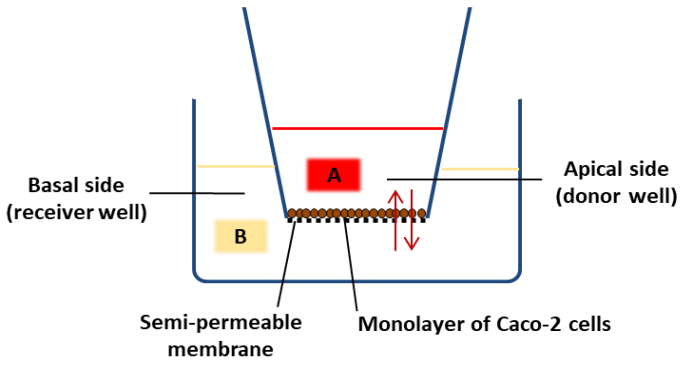


Figure 5.4: Diagram of a Caco-2 permeability assay (Reproduced from Ina *et al.*[220]).

In the current project, permeation experiments across monolayers of Caco-2 cell were applied for assessment of the permeability for ISRIB and other promising analogues. Accordingly, ISRIB and the selected analogues were subjected to the permeability assay, in addition verapamil was also used as a reference standard to evaluate the permeability experiment. Caco-2 cell monolayers grown on flask were incubated with ISRIB, **103, 108a, 145** and verapamil, samples were taken after 30, 60, 90 and 120 min and subsequently analysed by previously reported developed LC-MS/MS method. No chromatograms peaks were detected in all samples including ISRIB and its promising analogues at both (A–B) and (B–A) directions through full time period of experiments. However, a detectable peak was observed for the positive control (verapamil), which indicates suitability of the assay for the analysis of ISRIB and its analogues. These results mean that ISRIB and selected analogues could not be qualified as permeable according to the data obtained from Caco-2 cells permeability experiments. This indicates that they could be a substrates for the efflux transporters, such as p-glycoprotein, especially as the positive control (verapamil) gave acceptable results during the experiment, and it is known to be a potent inhibitor of P-glycoprotein function.[221] [222, 223] The lack of permeability could be potentially important, as the ISRIB and its analogues are intended for CNS treatment, where substrates for such efflux transporters can be limited by the abundant of p-glycoprotein transporters identified at the BBB, which is considered greatest obstacle to effective CNS drug delivery.[224, 225] Lack of permeability measurements usually indicates that the absorptive potential of the tested compounds is not optimal. Thus, poor permeability due to efflux transporters, could give an additional explanation for the lack of oral bioavailability of ISRIB molecule after oral administration.[152]

5.5. ISRIB formulations

Another phase of this project was concerned mainly with preparing an appropriate preclinical formulation for oral administration of ISRIB and other promising compounds. Accordingly, a pre-formulation analysis was performed in order to design an appropriate formulation.

As mention earlier, *trans*-ISRIB has very low aqueous solubility and lacks oral bioavailability. Therefore, most previously published *in vivo* studies of ISRIB utilized intra peritoneal (ip) route. Formulations were prepared at concentrations equivalent to 2.5 mg/mL of ISRIB for intra peritoneal administration. A mixture of DMSO diluted in PEG 400 (1:1) was used as a dosing vehicle for intra peritoneal administration.[149, 152]

Generally, low aqueous solubility of new drug candidates is the major hurdle encountered with development and supply of preclinical formulations. The favored process for preliminary preclinical evaluation of drug candidate involve preparing a simple aqueous solution formulation. The aqueous solution permit for ease of administration, similarity of content, and facilitate of preparation. Aqueous solution normally contains the desired substances dissolved in a suitable solvent. However, in case of poor aqueous solubility of candidates, a monophasic aqueous mixture of ISRIB in water is not efficient. Inthis case, the use of alternative strategies that involves formulating cosolvent-based systems. This path is widely used to formulate poorly soluble compounds through combination of different solvents to enhance compounds solubility. Accordingly, various cosolvent-based systems were attempted (**Table 5.6**). Usually, the major concern associated with cosolvent-based approach is the re-precipitation of tested compounds during dilution with aqueous solutions.

Therefore, when preparing cosolvents solution, it was important to ensure that a low-solubility compound is not re-precipitated for at least through the period from the time of preparing to the time of experiment. Different of excipients uses in preclinical formulation are listed in **Table 5.6**. For ISRIB preclinical formulation **A** to **C**, various cosolvents with different percentages were performed to overcome the re-precipitation of ISRIB. Among these formulations, **B** and **C** cosolvents showed a clear solution with the aid of heat and sonication even after leaving the solution at ambient temperature overnight, indicating its suitability for preclinical studies.

Formulation	Excipient	Percent of excipients used (v/v)
A	Polyethylene glycol 400 Ethanol Distilled water	60% 10% 30%
B	Polyethylene glycol 400 Ethanol Distilled water	70% 10% 20%
C	Polyethylene glycol 400 Distilled water	80% 20%
D	Propylene glycol 400 Trioctanoate	50% 50%
E	Propylene glycol 400 Gelucire 44/14	50% 50%
F	Propylene glycol 400 Tween-80	50% 50%
G	Propylene glycol 400 Peceol	50% 50%
H	Propylene glycol 400 Labrasol	50% 50%
I	Propylene glycol 400 Labrafac	50% 50%

Table 5.6: Types and percentages of ingredients used in preclinical formulations.

However, this PhD project was also attempted to explore whether there is possible direction toward lipid-based formulations which could potentially be used in pre-clinical/clinical studies. Lipid-based formulations showed an essential role in the formulation of molecules with poor solubility and permeability, thus solubilizing of ISRIB in a suitable oily vehicle was attempted.

Various lipid-based excipients were investigated, **D** to **I** (**Table 5.6**). Starting with the less complex lipid-based excipient as in trioctanoate (**D**), a suspension was obtained after mixing ISRIB with trioctanoate and PEG. Trioctanoate is a medium-chain triglyceride characterised by good digestion efficiency and low cost. The formation of suspension indicated that ISRIB was not soluble, thus showing the inappropriateness of this type of lipid-formulation. Thereafter, more complex lipid-based excipients were used such as Gelucire 44/14, Peceol, Tween-80, Labrafac and Labrasol. Among all these lipid-based excipients, Labrasol (**H**) showed a clear solution indicating that ISRIB has dissolved and hence it is possible to be used as a lipid-formulation for preclinical studies. Labrasol is known to have a hydrophilic–lipophilic balance (HLB) of 14.[226] This value reflects its amphiphilic features making it good solubilizing agent for lipophilic drug candidates, also it is widely used in formulations in an attempt to enhance oral absorption.

5.6. Conclusions

In this chapter, a traditional *in vitro* biopharmaceutical experiments were employed in order to assess the ADME parameters of ISRIB and other promising candidate prior to *in vivo* experimentation. For the simultaneous determination of ISRIB and other promising analogues using *in vitro* ADME studies, a development and validation of novel and sensitive bioanalytical method (LC–MS/MS) were established. The bioanalytical method was an important part of this project as all determinations of concentrations in any samples was accomplished by means of LC–MS/MS. The LLOQ achieved by this method was 10 nM, which was sufficient to describe the biopharmaceutical parameters of ISRIB and its analogues. The developed method was successfully applied to

the *in vitro* ADME parameters assessment (aqueous solubility, Caco-2 permeability and microsomal stability). From these assessments, accurate aqueous solubility results were obtained for ISRIB, piperidine analogue **103** and piperazine analogue **108a**, for which the solubility was relatively very low at 0.000271, 0.000317 and 0.000355 mg/mL, respectively. It has been demonstrated in this study that chemical modification for solubility optimisation resulted in slight improvement of the aqueous solubility. In addition, it was found that ISRIB and its analogues would have slow metabolism and therefore were predicted to be less influenced by the hepatic first-pass metabolism during the oral absorption process. Also, it was concluded from the Caco-2 cells permeability experiments that ISRIB and selected analogues could not be qualified as permeable compounds, as they could be P-glycoprotein substrates.

Overall structure-property relationship analysis of the ISRIB and its analogues showed that the replacement of the cyclohexane ring of ISRIB with a heterocyclic ring (piperidine or piperazine) or modified glycolamide linker as in benzoxazine resulted in comparable aqueous solubility and metabolic stability, and no permeability across Caco-2 cell monolayers.

Moreover, a pre-formulation analysis was performed in order to find appropriate formulations for oral administration which could potentially be used in pre-clinical/clinical studies. It was found that a cosolvents system of PEG-400/ethanol/water (7:1:2) and PEG-400/water (8:2) as well as a lipid-based excipient, Labrasol, were succeeded to achieve this purpose.

6. Conclusions and future work

6.1. General conclusions

The ISR plays an important role in stress resistance and in mammals is implicated in metabolism, immunity and memory. Activation of the ISR pathway and subsequent high levels of eIF2α-P lead to inhibition of protein synthesis at the level of initiation.[118] A recently discovered chemical inhibitor of ISR, ISRIB, modulates the interactions between eIF2 and eIF2B and is reported to serve as neuroenhancer in healthy rodents and neuroprotector in models of neurodegeneration and traumatic brain injury.[118, 167, 227] ISRIB has been recently published with a limited set of SAR.[150, 151] Furthermore, the molecular details of ISRIB's interaction with eIF2B remained to be explored.

In this project ISRIB **1** was used as an initial lead compound to generate a huge library of ISRIB analogues. These synthesised analogues underwent *in vitro* testing for their action as ISR inhibitors through targeting eIF2B receptors (carried out by Prof. David Ron). Gratifyingly, the EC_{50} of *trans*-ISRIB (5.3 nM) was found to be nearly identical to the literature value (5 nM).[150, 151]

Modification of various moieties on the parent ISRIB molecule, allowed the production of new SAR and ultimately afforded analogues with potency comparable to ISRIB such as bromo analogue **41**, piperidine analogue **103**, piperazine analogue **108a** and benzoxazine analogue **145**. The latter was selected for the synthesis of fluorescein-labelled ISRIB derivatives to assist in demonstrating the direct interaction between ISRIB-type compounds and eIF2B,

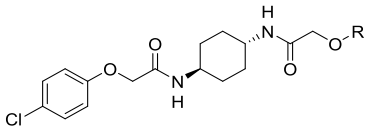
by using it in the FP binding assay. In general, a summary of the SAR observed with ISRIB derivatives is given below.

6.1.1. Truncated and terminal ring-modified analogues

The truncated analogues synthesised were a broad structural exploration to determine ISRIB structural requirements for efficient binding relationship with the target. Overall, the pharmacological results of truncated ISRIB analogues revealed that even subtle modifications as in removal of chlorine atom in analogue **29** (**Table 6.1**) have an obvious impact on activity. The 2-(4-chlorophenoxy) acetamide chain seems to be essential for the binding at eIF2B receptors.

The terminal aromatic ring of the ISRIB is sensitive to substituent changes. The *p*-Br substitution results in a significant increase in potency, relative to the ISRIB. This *para*-substitution offers an increase in potency in both symmetrical and non-symmetrical analogues (EC_{50}=0.6 nM). The other *p*-F, *p*-CF_3 and *o*-OCH_3 analogues generally caused a slight reduction in activity than ISRIB. Overall, it is likely that the steric and electronic features of the substituent is important in determining the best binding with eIF2B receptor.

On the other hand, simple aromatic analogues bearing either polar heterocyclic or alicyclic rings revealed a decrease in potency. The pyridine analogue **42** showed activity albeit with a 26-fold reduction of activity, whilst pyrimidine analogue **43** have EC_{50} values of 1.6 μM. The electronic nature of phenyl ring is likely to be responsible for the best binding with the eIF2B receptor.



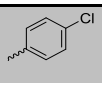
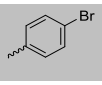
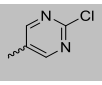
Ligand	R	ISR inhibition % CHOP::GFP signal at 10 μM	EC_{50}
1		91	5.3 nM
29		85	128 nM
41		89	0.6 nM
42		86	127 nM
43		51	1.6 μM

Table 6.1: EC_{50} and ISR inhibition (% CHOP::GFP signal at 10 μM) of ISRIB analogues modified at terminal aromatic moiety. Shown is a representative from three independent experiments conducted for trans-ISRIB and of a single 12-point titration experiment conducted for ISRIB analogues.

6.1.2. Glycolamide linker Modification

The next series of ISRIB analogues were designed to explore the modification of the *O*-arylglycolamide linker. Accordingly, a set of non-symmetric and symmetric ISRIB analogues bearing modified glycolamide linker were prepared and evaluated. Isosteres of the amide moiety were investigated, including carbamate, urea, ester, amidine and inverted amide (**Table 6.2**). Additionally, the steric effect at the α-carbon atom (which link between amide group and *O*-aryl ether) was also explored. Some of these analogues did not offer a promising result in comparison to ISRIB, even though they administered some structure activity relationship data.

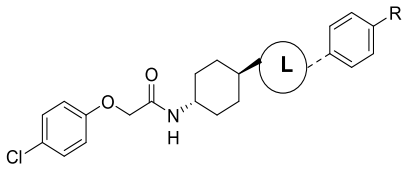
Overall, the parent amide moiety of ISRIB retained the best activity amongst all the isosteric replacements. Generally, bioisosteric replacement of the amide group with a carbamate **53** and urea **54** resulted in a lower potency than ISRIB. This may indicate that the CH_2 group (which links amide and *O*-aryl ether) have

very specific role affecting receptor binding. The ester **56** displays complete reduction in potency, which may indicate the important role of hydrogen-bond donor motif (amide NH), ester has weak hydrogen bond acceptors with no hydrogen bond donor functionality. The amidine analogue **59** is found to be less well tolerated than amide group in this area.

Furthermore, introducing di-methyl group on the α-carbon of *O*-arylglycolamide linker resulted in a complete loss of activity, which may suggest a space restriction around the α-position of the glycolamide linker which may be affected by addition of methyl groups.

The inverted carboxamide analogues **61c**-**65c** displays a promising results. This indicates that reversing the orientation of the carbonyl and amine groups in inverted amide analogues, retains the hydrogen bonding properties of an amide. Interestingly, it seems that the "oxygen" of ether group can be omitted as in analogues **62c** and **63c**. Furthermore, linking of the terminal aromatic ring with the inverted amide linker by six-membered ring leads to considerable results with 70-fold slight reduction in potency relative to ISRIB. This indicates that restricted rotation and thus reduced flexibility have an important role in receptor binding.

A complete investigation of analogue bearing glycolamide linker with inverted amide moiety, *N*-(hydroxymethyl)acetamide linker could not be achieved due to a limitation of its synthesis. Thus, the effect of inverted amide group at this position could not be further concluded.



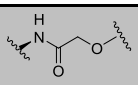
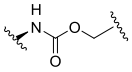
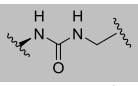
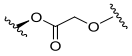
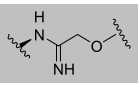
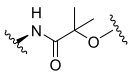
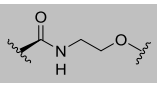
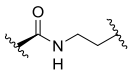
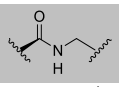
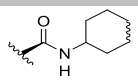
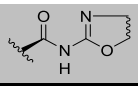
Ligand	L	R	ISR inhibition % CHOP::GFP signal at 10 μM	EC_{50}
1		H	91	5.3 nM
53		H	52	5.4 μM
54		H	-	Inactive
56		Cl	-	Inactive
59		Cl	62	1.5 μM
60		Cl	50	7.4 μM
61c		Cl	75	50 nM
62c		Cl	73	55 nM
63c		Cl	75	81 nM
64c		Cl	70	56 nM
65c		Cl	73	364 nM

Table 6.2: EC_{50} and ISR inhibition (% CHOP::GFP signal at 10 μM) of ISRIB analogues modified at the glycolamide linker. Shown is a representative from three independent experiments conducted for *trans*-ISRIB and of a single 12-point titration experiment conducted for ISRIB analogues.

6.1.3. Central core ring modification

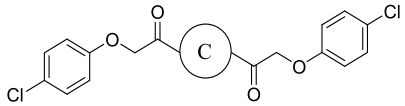
The central cyclohexane ring was investigated, including a variety of aromatic rings, acyclic linear cores, spiro, bicycle and heterocyclic rings (**Table 6.3**). The obtained results together with previously published studies[150, 167] demonstrate that the replacement of the cyclohexane ring with a flat phenyl moiety **75** was tolerated with only 14-fold drop in potency. However, replacement of phenyl moiety with more polar aromatic rings such as pyridine **76** and pyrimidine **77**,

resulted in lower potency compared to the parent ISRIB. This reveals that the electronic properties of the central aromatic group is a key in determining the binding profile of these compounds. Also, this could be either explained by the loss of aromatic hydrogen bonding which might participate in binding interaction between ligand and receptor.

The acyclic linear cores analogues **80**-**82** resulted in a lower potency than the parent ISRIB. The results showed a preference for four carbon over two and three carbon spacing, which suggest that the central spacer distance plays an essential role in properly orienting the two *O*-arylglycolamide side chains in space.

Novel central core modification was investigated, whereby the cyclohexane core ring was replaced with bicyclic and spiro groups **84**-**87**. These analogues exhibited a lower level of potency compared to ISRIB. The presence of bicyclic and spiro core is likely to be responsible for the inappropriate orientation of the central core moiety in binding site, thus leading to a reduction in potency. In addition, the absence of N-H groups in bicyclic and spiro analogues (which afforded tertiary amide products) resulted in lack of ability to act as hydrogen bond donor. This indicates that the two N-H groups of secondary amides present on both sides of ISRIB have very specific role in receptor binding.

To establish whether this was indeed the case, further work still needs to be done in order to confirm these finding. For example, production of different bicyclic and spiro analogues bearing hydrazide moiety which afford secondary amide products. Thus, the important role of the N-H groups could be further investigated to provide more structure activity relationship data.



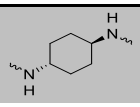
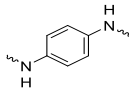
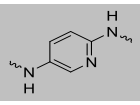
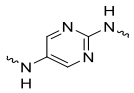
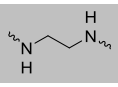
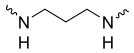
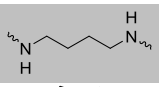
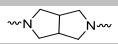
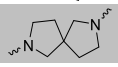
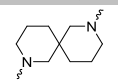
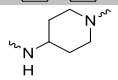
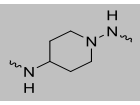
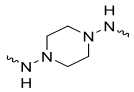
Ligand	A	ISR inhibition % CHOP::GFP signal at 10 μM	EC_{50}
1		91	5.3 nM
75		71	67 nM
76		60	1.2 μM
77		-	Inactive
80		85	834 nM
81		56	8.4 μM
82		84	535 nM
84		58	7.3 μM
85		60	4.1 μM
86		58	7.6 μM
87		60	1.8 μM
101		87	367 nM
103		87	12 nM
108a		90	12 nM

Table 6.3: EC_{50} and ISR inhibition (% CHOP::GFP signal at 10 μM) of ISRIB analogues modified at the central core moiety. Shown is a representative from three independent experiments conducted for *trans*-ISRIB and of a single 12-point titration experiment conducted for ISRIB analogues.

Moreover, central core basing on piperazine and 4-aminopiperidine were synthesised as a more direct replacement for cyclohexane ring. The piperidinyl analogue **101** with tertiary amide group, exhibited a lower level of potency with 74-fold less than ISRIB. However, piperidine-1,4-diamine analogue **103** (which afforded secondary amide group) regained activity with EC_{50} equals to 12 nM. Similar promising results were achieved from piperazine-1,4-diamine analogue

108a with 3-fold less than ISRIB. Thus piperidine-1,4-diamine **103** and piperazine-1,4-diamine **108a** compounds were found to have higher potency than all modified core ring analogues. This indicates that preserving of amide N-H group adjacent to the central ring is important for high activity.

6.1.4. Design and synthesis of a novel labelled ISRIB derivatives

The other effort in this project was focused on design, synthesis and evaluation a series of ISRIB analogues, with an overall focus on generating novel labelled ISRIB derivatives for use as a tool in the molecular assays. The literatures were examined for any related SAR studies that could assist in the determination of appropriate site on the ISRIB where fluorescent molecule ligation is well tolerated. The terminal ring, central core ring and glycolamide linker moieties of ISRIB were preferentially selected to identify the impact of diverse modifications on eIF2B receptor binding affinity.

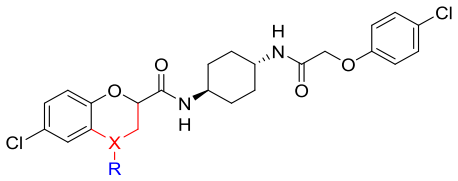
Therefore, an extensive SAR studies have been applied in the current project, for the identification of an appropriate site in the ligand molecule that can be used to link a spacer attached to a marker molecule. The results confirmed that the modifications at terminal ring and central core ring decreased the potency, thus both of these moieties do not considered to be a good sites for fluorescent attachment.

The efforts then focused on the glycolamide moiety, various groups were considered to be able to serve as platform for the synthesis of a fluorescent labelled molecule (**Table 6.4**). This was achievable through a scaffold based on tethering the neighbouring aromatic ring to the α-carbon atom in the form of a chromane group as in analogue **142**. The result observed from cell-binding assay revealed that this modification is well tolerated with a 7-fold less potent

compared to the parent ISRIB. Docking studies of chromane analogue **142** (**Chapter 4**) suggested that the benzylic carbon of the chromane system would face the solvent-accessible space. This orientation was crucial for the next step of the plan, which involved synthesising analogues to investigate that if the replacement of chromane with benzodioxane **144** or benzoxazine **145** would have similar promising results. Thus, modifications showed that the replacement of benzylic carbon with oxygen as in benzodioxane analogue **144** retained similar activity to chromane analogue **142**. However, replacement with nitrogen to generate benzoxazine analogue **145**, provided the most potent analogue among these modified derivatives, which was only 2-fold less potent than ISRIB. The N-H group of benzoxazine analogue **145** provided the anchoring point for further modifications in the creation of a labelled molecule. Therefore, the N-H position of benzoxazine analogue **145** was selected to identify the effect of a range of substitutions at this position on receptor activity. The results showed that increasing steric bulk at this position as in analogues **153**, **155**, **156a** maintain the potency with approximately 14-24 fold drop in activity compared with the corresponding benzoxazine analogue **145**. These results indicates that bulky substitution at the N-H position of benzoxazine **145**, could be tolerated. Rationale behind this strategy was to synthesise derivatives with short or long linker that would facilitate labelling.

The success of the N-H substituted benzoxazine **145** series, support the designing of a labelled ISRIB analogues. The N-H position was selected as a potential site for ligation. Two different linker lengths were chosen to aid in this development, aiming to generate a flexible short and long linker terminated with a 5/6-carboxyfluorescein moiety (FAM-NHS) for investigation. Two novel

fluorescent analogues **156e** and **156h** were synthesised. The FAM- analogue **156e** was successfully used as a tool in the FP binding assay to demonstrate a direct interaction between ISRIB-type compounds and eIF2B.[44] This work came late in this PhD period and therefore fluorescently labelled ISRIB analogues **156e** and **156h** were not tested in cell-based assays. However, further work still needs to be done in order to gain further knowledge, for example production of an array of different linker lengths and types, as well as different fluorescent molecules for investigation.



Ligand	X	R	ISR inhibition % CHOP::GFP signal at 10 μM	EC_{50}
142	CH_2	-	94	34 nM
144	O	-	95	55 nM
145	N	H	98	8 nM
153	N	CH_3	89	67 nM
155	N	$CH_2CH_2OCH_3$	82	93 nM
156a	N	CH_2COOCH_3	84	120 nM

Table 6.4: EC_{50} and ISR inhibition (% CHOP::GFP signal at 10 μM) of ISRIB analogues modified at the glycolamide moiety to synthesis labelled ISRIB derivatives. Shown is a representative from three independent experiments conducted for *trans*-ISRIB and of a single 12-point titration experiment conducted for ISRIB analogues.

6.1.5. *In vitro* ADME parameters assessment for ISRIB and other promising analogues

Another approach of this PhD project was *in vitro* ADMET parameters assessment of ISRIB and other selected candidates in order to including these compounds with *in vivo* experimentation. ISRIB and other three analogues (piperidine **103**, piperazine **108a**, and benzoxazine **145**) were selected for this

study based on their potency at eIF2B receptor. *In vitro* ADMET parameters were evaluated in terms of aqueous solubility, permeability, metabolic stability and the results were determined using a development and validation of novel and sensitive bioanalytical method (LC–MS/MS).

Although it was expected that the move the N into the cyclohexyl ring as in piperidine **103**, piperazine **108a**, would make the ISRIB compounds much more water-soluble, but the aqueous solubility experiment exhibit a comparable aqueous solubility results. In general, a very low aqueous solubility was recorded for ISRIB and other analogues (piperidine **103**, piperazine **108a**). This suggested a high probability of thermodynamic effect in the crystal packing, which overcomes the effect of addition polar N group that could make the compound more soluble in polar solvents such as water.

Moreover, the bioanalytical method was applied in permeability and metabolic stability studies. ISRIB and selected analogues demonstrated a slow metabolism and therefore were predicted to be less vulnerable for extensive hepatic first-pass metabolism. Additionally, ISRIB and selected analogues did not show a significant permeability feature from Caco-2 cells permeability experiments.

However, in this PhD project a pre-formulation optimisation was sought in order to preparing appropriate formulations for oral administration which could potentially be used in pre-clinical/clinical studies. The results obtained showed the cosolvents system of PEG-400/ethanol/water (7:1:2) and PEG-400/water (8:2) as well as a lipid-based excipient, Labrasol, were considered a promising formulation to be used for in vivo studies.

6.2. Future work

The possibility of developing ISRIB analogues that possess physicochemical and ADMET properties suitable for the development of an oral once-daily CNS agent in terms of solubility, lipophilicity, permeability, blood-to-brain distribution, metabolism, and safety pharmacology is still of therapeutic interest. In this project, a series of ISRIB analogues have been developed to function as neuro enhancer and protector. These ligands were derived from the ISRIB structure and were modified at the core ring, glycolamide linkers and terminal aryl ring. Considering the data acquired from the pharmacological studies, the series of *para*-bromo aryl substitution, inverted carboxamide, phenyl, piperidinyl and piperazinyl core rings, explained in **Chapter 3**, represent the most promising potential compounds to be used as leads for future work. Previous work has provide diverse avenues for subsequent investigations, these are detailed below.

- The SAR studies (**Chapter 3**) showed that *para*-bromo aryl substitution and inverted carboxamide analogues led to enhance or maintain the potency compared to ISRIB. These scaffolds could provide a principle for the development of novel eIF2B ligands. Different molecular cores (**Figure 6.1**), whilst retaining *para*-bromo and inverted carboxamide motifs could potentially result in analogues with promising results. This work may prove useful to break the symmetry in order to provide a diversity of modifications as well as enhance physicochemical parameters.
- The spiro core modified analogues displayed lower, but acceptable, potency than ISRIB. These analogues share similar feature which is

tertiary amide structure. A more detailed study into the position and characteristics of the amide groups linking between the spiro core ring and *O*-aryl ether motifs could be of use. It is known that the tertiary amide linkage point is far less flexible as they become three dimensional rather than two dimensional (flat) with the NH. Therefore, a shift on the position of NH-amide could potentially permit fine-tuning of their activity. Since a few examples of spiro and bicyclic have been elucidated so far, a broader range could afford this possibility. Thus, a larger library of analogues (**Figure 6.1**) with different molecular cores could be generated to clarify whether it is positional or conformational effects that are important for the lower activity of spiro and bicyclic analogues. Some of these analogues could be extended to provide secondary diamide or hydrazide derivative. Amending the spiro and bicyclic scaffold by altering tertiary amide to hydrazide derivative can also probe the hypothesis that was presented earlier, to interpret the regained activity in hydrazide analogues (piperidinyl **103** and piperazinyl **108a**).

- The novel heterocycloalkyl piperidinyl **103** and piperazinyl **108a** analogues, acts as platform sis for more extensive modification. Therefore, piperidinyl and piperazinyl could be substituted for more heterocyclic rings of differing size such as diazocane and diazabicyclononane (**Figure 6.1**). This could assess the ability of the target to tolerate bulkier structures compared with the cyclohexane group. Furthermore, replacement of piperidinyl and piperazinyl with other heterocyclic such as diketopiperazines and azabicyclo-diamine could prove useful attempt to improve solubility.

- Replacement of cyclohexane core moiety with phenyl ring displayed a well-tolerated result. Therefore, there is much scope for investigation of the phenyl ring. Extension of the phenyl moiety or replacement of the phenyl ring with the saturated bioisosteres could potentially result in compounds with higher potency than ISRIB. In addition, benzene analogues have poor water solubility due to a π-stacking in the crystal lattice,[228, 229] therefore replacing the benzene ring with saturated bioisosteres would result in improvement of the physicochemical properties by disrupting the π-stacking.[230-232]
- Thereafter, depending on the new findings other ADMET assays of new key compounds could be established (quantitative thermodynamic and kinetic solubility, Caco-2 permeability, microsomal stability, plasma and brain protein binding). Then, if a lead candidate emerges, it could be progressed to *in vivo* efficacy studies, using the mouse models for neurodegenerative disease. The mouse models could be prion-infected mice and tauopathic mice[227], but also other relevant models may be investigated as well. The main criteria for success at the above point will be progress towards novel compounds with improved lipophilic ligand efficiency and aqueous solubility, while retaining potency and efficacy comparable to *trans*-ISRIB. Moreover, success in establishing a hit target profile for a set of compounds in terms of cellular ISRIB-like activity with interpretable SARs allows to create further derivatives of ISRIB. These derivatives might be tagged to further understand the mechanism of action and explore more refined structural determination. Success might enable to develop other direct measurements of eIF2B-ISRIB

affinity and potentially enable to add a bulky moiety to the derivative to generate a difference in the CryoEM density map. Thereby it could be added to other assay cascade for the support of the structural studies of eIF2B to further confirm that ISRIB indeed binds where we think it does.

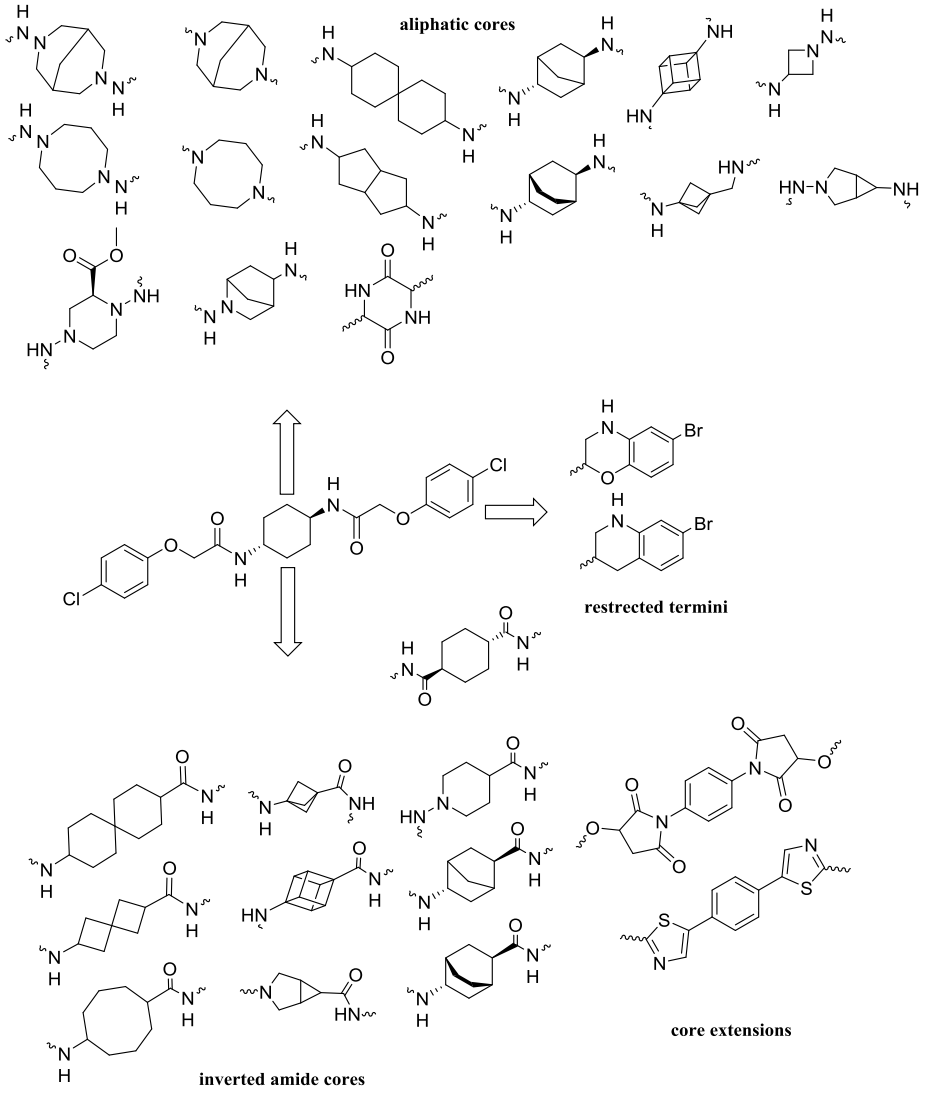


Figure 6.1: Overview for the future work proposed molecular cores, linkers and extensions to amend ISRIB molecule based on para-bromo aryl, inverted carboxamide, and piperidinyl analogues.

As mention before, at the end of this PhD project, Alisa *et al*[44] and Jordan *et al*[45] have been published cryo–electron microscopy structure for the human eIF2B in complex with ISRIB. Considering the conformation of ISRIB as a general templet for binding at the human eIF2B, the structures of the analogues

synthesised in this project could be subjected to modelling experiments and subsequent comparison with the *S. pombe* eIF2B, might show essential favourable or disfavourable interactions important for the higher potency of analogues including **103**, **108a** and **145**. Determination of these essential amino acids, or even those close to the binding site which could possibly be evaluated, would develop the platform of structural modifications designed to approach them.

The other avenue that needs further investigation is the labelled ISRIB derivatives. The limitation of time in this PhD project resulted in incomplete data of the already synthesised fluorescent analogues **156e** and **156h**. Therefore, pharmacological evaluation of the synthesised fluorescent analogues **156e** and **156h** were required. In addition, further validation of the ability of the analogues **156e** and **156h** as a fluorescent probe was required to assist in the development of an FP assay. Furthermore, chromanol analogue **157a** which has previously been found to tolerate a particular substitution like the N-position of benzoxazine **145**, is also a candidate for fluorescent ligation. Therefore, effort may continue to investigation of alcohol position in chromanol **157a** in order to create a diverse series of chromanol **157a** derivatives.

The development of fluorescent ISRIB derivatives is considered an important biological tool for the whole field of research interest. Therefore, further work can be performed in order to gain further knowledge regards the creating labelled ISRIB derivatives, for example production of various linker lengths and types, as well as different fluorescent molecules for investigation. Thereafter, the most promising labelled ISRIB derivatives could be evaluated on the basis of *in vitro* assays. The derivatives with only a linker attached first could be evaluated to

select the suitable linker length and type. Thereafter, different types of fluorescent molecules linked to the suitable linker could also be assessed to select the most promising compound.

On the other hand, additional Caco-2 cell-based permeability assay with P-glycoprotein inhibitor are still required. This would contribute to further understanding the limiting factor for cellular uptake and the poor permeability of the ISRIB and other selected candidates achieved through the Caco-2 permeability monolayer of Caco-2 cells (**Chapter 5**). Thereafter, the results achieved of the *in vitro* biopharmaceutical assays could be incorporated into *in silico* simulation (using GastroPlusTM) to predict the pharmacokinetics in humans and rats following oral administration. GastroPlusTM software was used as a tool that compiles the factors which could affect oral bioavailability and provide reasonable pharmacokinetic prediction.[233] Additionally, *in vivo* pharmacokinetic experiments could also performed in order to efficiently identify orally bioavailable drug candidates.

Furthermore, due to time constraints this project did not get around to doing *in vivo* work. Therefore, the developed formulation from **Chapter 5** could be potentially included in further future studies. It still to be interesting to investigate if the developed lipid formulation (Labrasol) and cosolvents system of PEG-400/ethanol/water (7:1:2) and PEG-400/water (8:2) will increase the bioavailability *in vivo* studies.

7. Experimental

7.1. Assays

7.1.1. CHOP::GFP

This assay was carried out by Professor David Ron's laboratory team in Cambridge Institute for Medical Research (CIMR). All SARs studies were guided by measuring the CHOP::GFP expression by FACS. The compounds were solubilised in DMSO at 10 mM and applied to CHO-K1 cells at the specified concentrations. 40 x 10_3 CHO-K1 cells carrying a stable CHOP::GFP reporter transgene were plated in 6 well plates. Two days later the culture medium was replaced with 2 mL of fresh medium and compounds added. Immediately before analysis, the cells were washed with PBS and collected in PBS containing 4 mM EDTA. Single cell fluorescent signals (10,000/sample) measured by FACS Calibur (Beckton Dickinson). FlowJosoftware was used to analyze the data. The CHO-K1 cells were treated with 0.5 mM Histidinol for 16-20h in presence or absence of the different derivatives. Then compounds have been checked their ability to counteract ISR activation (measured by increased in fluorescence of CHOP::GFP reporter) by Histidinol. The concentration range used to characterise the compounds was from 10 uM to 1 nM. Single cell fluorescent signals measured by FACS Calibur (Beckton Dickinson). FlowJo software was used to analyse the data.

The dynamic range of the assay is defined by the difference in GFP signal between the His+ (treated) and His- (untreated) cells. Inclusion of ISR inhibitors (ISRIB analogues) diminishes the response of CHOP::GFP to Histidinol. The % response is thus defined as:

% ISR inhibition = 100 x [Signal (His+) - Signal (His+ with ISRIB analogue)]÷ [Signal (His+) - Signal (His-)].

EC_{50} was generated using agonist vs. response function on GraphPad Prism.

7.1.2. Aqueous solubility assay

7.1.2.1. Stock and working standard solutions preparation

The Stock standard solutions of tested compounds were individually prepared at concentration (500 uM) by dissolving 1.12 mg, 1.13 mg and 1.13 mg of ISRIB **1**, **103** and **108a**, respectively in 5 mL MeOH. Working standard solutions of 250 uM and 10 uM, were prepared for tested compounds by further dilution of stock solution in MeOH to make up to a total volume 5 mL. The working standard solutions were diluted in MeOH (1 mL total sample volume) immediately before preparation of calibration curves to provide working solution concentrations at 0.2, 0.4, 1, 2, 5, 10, 20, 50, 100 and 200 uM. The working IS standard solution was prepared by further dilution with MeOH to provide the IS concentration of 1uM.

7.1.2.2. Calibration curve and quality control (QC) samples preparation

Tested compounds calibration curves were prepared at concentrations of 10, 20, 50, 100, 250, 500, 1000, 2500, 5000, and 10,000 nM by spiking 50 µL of the appropriate working solution of compounds into a 950 µL of diluent to make up to a total sample volume of 1000 µL. The diluent prepared from mixing 500 µL water, 400 µL MeOH and 50 µL IS.

7.1.2.3. LC-MS/MS method development and validation

The tested compounds (2 uM) were prepared from 100 uM stock solution for each compound, then used in setup and optimization Ms-Ms method for

solubility measurement. The assay linearity was established by plotting the peak area ratios of ISRIB **1**, **103** and **108a** to the IS versus theoretical concentrations. Correlation coefficients of 0.99 or greater was acceptable. Analysing five replicates of the lowest standard on the calibration curve was used to measure the LLOQ. The LLOQ could be described as the lowest concentration of ISRIB **1**, **103** and **108a** that resulted in signal-to-noise (S/N) ratio >10, with acceptable accuracy and precision (<20 %). Accuracy and precision were assessed by analysing five replicates of different concentrations of each ISRIB and selected analogues at LLOQ, low, medium, and high QC concentrations on the same day (intra-day) and four consecutive days (inter-day). The accuracy was defined as the percentage of the mean calculated versus nominal concentrations, while the precision means the coefficient of variation at each concentration. The criteria for accuracy and precision were considered to be acceptable if they are within ±15 % relative error from the theoretical values and within ±15 % relative standard deviation.

7.1.2.4. Aqueous Solubility assay procedure

Three replicates of tested compounds samples were prepared at concentration of 500 uM by mixing the desired weighted of compounds (ISRIB= 1.127 mg, **103**= 1.130 mg and **108a**= 1.132 mg) in 5 mL water. These mixtures stirred overnight at ambient temperature, filtered over filter syringe and then the area response was measured with LC-Ms/Ms analysis. The preliminary result calculated by applied on compounds calibration curve individually.

7.1.3. Permeability assay

7.1.3.1. Cell culture

The cells used throughout this study were Caco-2 cells and maintained in Dulbecco's Modified Eagle Medium (DMEM), which was supplemented with 10% Fetal Bovine Serum (FBS) and 1% penicillin streptomycin. Caco-2 cells were cultured at 37° C, 5 % CO2 and 95% relative humidity.

7.1.3.2. Passage of cells

Caco-2 cells were passaged twice every 7 days. Cells were passaged in 75 cm^2 cell culture flasks (Corning Inc, Corning, NY) at 1×104 cells/cm^2 at least twice before seeding. Firstly, the DMEM was aspirated and the cells were then washed twice with pre-warmed DPBS at 37° C. Trypsin-EDTA (4 mL) was added and the cells were incubated at 37 °C for 5 minutes. Then, the effect of trypsin-EDTA was stopped through added DMEM (10 mL) and the cell suspension was transfer into 15 mL Falcon tubes and centrifuged at 1200 rpm for 3 minutes. Discard supernatant and resuscitate cells with 10 mL DMEM, count resuscitated cells and then transfer 0.3 mL of the resuscitate cells into new 75 cm2 cell culture flasks with 10 mL DMEM.

7.1.3.3. Seeding of cells

The Caco-2 cells seed into 24-well Multiwell system (Transwell® plates, Cat 351181 Corning Inc, Corning, NY). Seeding density will be 3.75×104 cells/cm^2. Resuscitate cells to give 2.8125 x 10^4 cells/mL and seed 400 µL into each well, and then added 35 mL of DMEM medium into reservoir of Transwell® plates. The DMEM medium was then replaced every other day thereafter for 21 days before permeability assay.

7.1.3.4. Caco-2 permeability assay

The Caco-2 monolayers were washed twice with transport buffer (HBSS buffer supplemented with 5 mL of 1 M HEPES and pH adjusted to 7.4 using HCl or NaOH on one day before assay). The cells were then allowed to equilibrate for 30 min at 37 °C with the transport buffer. The integrity of the cell monolayer was verified by measuring the transepithelial electrical resistance (TEER) with EVOM-2 instrument (World Precision Instruments, Sarasota, FL). The Caco-2 monolayers with TEER values between 260-450 Ωcm^2 were used in the permeability assay.[219] Decant transport buffer and prepare 24-well plate with receiver solution. Then, prepared donor solutions (5940 µL of transport buffer + 60 µL of 50 µM tested compounds). Added donor solution (300 µL) to the apical side for assessment of apical to basolateral and 1 mL to the basolateral side for assessment basolateral to apical, and then begin permeability assay (use shaking incubator at 100 rpm, 37° C). Then, withdraw 350 µL of samples from receiver well for basolateral side at 30, 60, 90 and 120 min and replace with transport buffer of equal volume to the samples was replaced each time. At 120 min, withdraw 125 µL of sample from the apical side and replace with transport buffer. At the end of the assay, TEER was measured again to assess if there any unknown effect of tested compounds on the monolayers. The concentration of samples was measured by LC-Ms/Ms method. All experiments were performed in triplicates.

7.1.4. *In vitro* liver microsomal stability assay

Metabolic stability assays are typically performed using Human or rat liver microsomes[214, 233] The test compounds (ISRIB **103**, **108a** and **145**) was dissolved in DMSO and diluted to the desired concentration with DMSO and water. The

reaction mixture was composed of the following: 65 mM of potassium phosphate buffer (pH 7.4), 11 mM of MgCl2, 0.5 mg/mL of microsomes and 1.1 μM of tested compounds. The reaction was initiated with addition of 1 mM NADPH. The reaction mixture was incubated with cofactors at 37° C. Samples (100 μL) were withdrawn from the reaction mixture at 4 sampling time points over 30 min (0, 10, 20 and 30 min). At each time point, the reaction was terminated with Methanol (300 μL). The experiment was performed in triplicate, the samples are centrifuged and the relative parent compound depletion or loss was determined by LC-MS/MS.

The concentration-time profiles from microsomal stability results were plotted in semi-log plot. Half-life of the tested compounds was calculated using the following equation:

$t_{1/2} = 0.693/k$

(k) Represent the slope of the linear regression from the plot of log percentage of test compound remaining versus time.

The intrinsic clearance (CLint) was calculated by the following equation:

$$\text{CLint} = \frac{0693}{t1/2} * \frac{\text{mL incubation}}{\text{mg microsomes}} * \frac{\text{mg microsomes}}{\text{g liver}} * \frac{\text{g liver}}{\text{kg body weight}}$$

The mg microsomes/g liver and g liver/kg body weight values equal 48.8 and 25.7 for humans and 44.8 and 40.0 for rats, respectively.

The CLint values in each species were then used to predict the hepatic clearance (CL_h) by using the well-stirred model.

Well-stirred model: $CL_h = Q \cdot CLint / (Q + CLint)$

The CL_h values were then used to calculate the hepatic extraction ratio (E_h) using the following equation:

$E_h = CL_h / Q$

Q represents hepatic blood flow rate, which was 20.7 and 55.2 mL/min/kg for humans and rats, respectively.

The E_h values were then used to calculate the fraction of the compound that enters the liver and passes through it unchanged (Fh) by using the following equation:

$Fh = 1 – Eh$

7.1.5. Fluorescence polarization assay

This assay was carried out by Professor David Ron's laboratory team in Cambridge Institute for Medical Research (CIMR). For the measurements of fluorescent polarization (FP) CLARIO star machine (BMG Labtech) with polarized 482 nm (excitation) and 530 nm (emission) filters have been used. All measurements were done at room temperature in 384-well round bottom polystyrene plates (3677, Corning) with a reaction volume of 20 µL equilibrated in the assay buffer [50 mM Tris (pH7.4), 150 mM NaCl, 2 mM MgCl2, 0.01% Triton, 1 mM DTT] for 10 minutes and either read directly or read 25 minutes after addition of unlabelled competitor. The fluorescein-labelled analogue (**156e)** was used in the range of 1-100 nM with corresponding amounts of purified eIF2B of 30-250 nM. Each measurement point was either an average of six readings every 30 seconds (for eIF2B dose-response) or five readings every 60 seconds (for unlabelled competitor assay). Binding of the fluorescent probe to eIF2B in the competition experiments was expressed as a fraction of relative

polarization signal (%P) over the dynamic range of the assay. Relative polarization was calculated by subtracting background FP (P_{bg}) from experimental FP (P_{ex}) ($P = P_{ex} - P_{bg}$). The minimal FP (P_{min}) observed when no eIF2B was added and the maximal FP (P_{max}) with eIF2B alone (in the presence of probe and in absence of non-fluorescent competitor compounds) define the dynamic range of the assay. Values of relative polarization for any assay point ($\%P_n$) were calculated using the formula $\%P_n=(P_n-P_{min})/P_{max}-P_{min})*100$).

7.2. ISRIB formulations

Cosolvents approach: ISRIB (2.5 mg) was dissolved in different volumes of PEG-400 with stirring at 65° C until the solution was clear. Distilled water and/or ethanol were then added with continuous stirring overnight at room temperature. The volumes of PEG-400 and distilled water were mixed as following:

Cosolvents A: 600 µL PEG-400, 300 µL distilled water and 100 µL Ethanol.

Cosolvents B: 700 µL PEG-400, 200 µL distilled water and 100 µL Ethanol.

Cosolvents C: 800 µL PEG-400, 200 µL distilled water.

Lipid-based formulations: ISRIB (2.5 mg) was suspended in 500 µL PEG-400 with stirring. To this mixture 500 µL of one of the lipid-based excipients (Trioctanoate, Gelucire 44/14, Tween-80, Peceol, Labrasol and Labrafac) was added. The mixture was sonicated then was stirred in water bath at 37° C for 24 hours.

7.3. General Chemistry

All chemicals, reagents and solvents were purchased from standard suppliers such as Fluorochem, Sigma Aldrich, Enamine, Alfa Aesar, Apollo scientific, abcr GMBH and Fisher Scientific.

Unless otherwise stated, reactions were carried out under inert nitrogen atmosphere at ambient temperature. All organic extracts after aqueous work-up procedures were dried over Na_2SO_4 before gravity filtering and evaporated under vacuum at $\leq$ 40°C (water bath temperature) by using rotary evaporator. Reactions were monitored by TLC on commercially available precoated aluminium and silica-backed plates (Merck Kieselgel 60 F254, Germany) and visualisation was carried out by examination under UV light (254 and 366 nm) and general staining carried out with Ninhydrin (solution in ethanol) or $KMnO_4$.

Biotage Isolera Four® was used for flash chromatography or manually, flash column chromatography cartridge was supplied by Biotage (Cardiff, Wales) and solvents were purchased from Fisher (England), Sigma-Aldrich Company Ltd (England) and Cambridge Isotope Laboratories Inc (England).

Analytical LC-MS was performed using a Shimadzu UFLCXR system coupled to an Applied Biosystems API2000 mass spectrometer. The HPLC column used was Phenomenex Gemini-NX, 3 μm-110 Å, C_{18}, 50 x 2 mm with a flow rate of 0.5 mL/min. UV detection was recorded at 220 (channel2) and 254 nm (channel1). Gradient elution: pre-equilibration for 1 min at 5% eluant B in eluant A; then 5 to 98% B over 2 min, 98% B for 2 min, 98 to 10% B over 0.5 min, then 10% B for one min. Eluant A: 0.1% formic acid in water; eluant B: 0.1% formic acid in MeCN.

Semi preparative HPLC purification performed on prep column (Phenomenex Gemini-NX 5u C18 110A, 100*21.20mm) using a linear gradient of water: acetonitrile from 85:15 to 5:95 in 13 min, (with 0.1% formic acid for both solvents).

Proton nuclear magnetic resonance (^{1}H-NMR) spectra were recorded using a Bruker-AV 400 instrument operating at 400.13 MHz and ^{13}C-NMR spectra were recorded at 101.62 MHz. Chemical shifts (δ) were recorded in parts per million (ppm) with reference to solvent chemical shift or the internal standard tetramethylsilane (TMS). Coupling constants (J) were recorded in Hz and multiplicities are given by singlet (s), doublet (d), triplet (t), quartet (q), multiplet (m), and doublet of doublets (dd). The spectra were analysed using Mastro nova software. Melting points (Mp) were recorded on a Mettler Toledo apparatus. High-resolution electrospray (TOF ES +/-) ionization time-of-flight mass spectrometry (HRMS) were recorded using a Bruker micrOTOF spectrometer.

Compounds were synthesised by the general methods described below unless otherwise stated.

General procedure A (amide coupling): To a stirred solution of amine molecule (1 eq) in dichloromethane were sequentially added DIPEA (2 eq) and 4-chlorophenoxyacetyl chloride (1 eq) dropwise at 0^{o} C (ice bath) under nitrogen. An instantaneous precipitate was formed upon addition of the acid chloride. The reaction mixture was continually stirred at 0^{o} C for a further 30 min, then at ambient temperature for between 1 and 2 hours until judged complete by TLC or LC-MS. Ethyl acetate was added to the reaction, and the mixture was then washed with saturated ammonium chloride, sodium bicarbonate, water and brine respectively. The organic layer was dried with magnesium sulfate, filtered, and

then evaporated under vacuum. The resulting product was then purified by triturated with diethyl ether, or purified by flash column chromatography.

General procedure B (amide coupling): To a stirred solution of 2-(4-chlorophenoxy)-*N*-[(1*R*,4*R*)-4-aminocyclohexyl]acetamide hydrochloride **28** (1 eq) or 2-(4-chlorophenoxy)-*N*-(piperidin-4-yl)acetamide hydrochloride **42** (1 eq) in dichloromethane, the selected acid chloride (1 eq) and DIPEA (3 eq) were added dropwise at 0^{o} C (ice bath) under nitrogen. An instantaneous precipitate was formed upon addition of the acid chloride. The reaction mixture was continually stirred at 0^{o} C for a further 30 min, then at ambient temperature for between 2 and 4 hours until judged complete by TLC or LC-MS. Ethyl acetate was added to the reaction, and the mixture was then washed with saturated ammonium chloride, sodium bicarbonate, water and brine respectively. The organic layer was dried with magnesium sulphate, filtered, and then evaporated under vacuum. The resulting product was then purified by triturated with diethyl ether, or purified by flash column chromatography.

General procedure C (amide coupling): To a stirred solution of diamine molecule (1 eq) in dichloromethane were sequentially added dropwise the selected acid chloride (2 eq) and DIPEA (4 eq) at 0^{o} C (ice bath) under nitrogen. An instantaneous precipitate was formed upon addition of the acid chloride. The reaction mixture was continually stirred at 0^{o} C for a further 30 min, then at ambient temperature for between 2 and 4 hours until judged complete by TLC or LC-MS. Ethyl acetate was added to the reaction, and the mixture was then washed with saturated ammonium chloride, sodium bicarbonate, water and brine respectively. The organic layer was dried with magnesium sulphate, filtered, and

then evaporated under vacuum. The resulting product was then purified by triturated with diethyl ether, or purified by flash column chromatography.

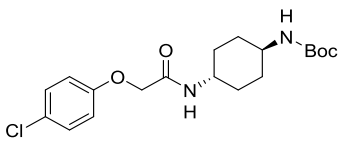
General procedure D (HBTU-Mediated amide coupling): To a stirred solution of carboxylic acid (1 eq) in dimethylformamide, triethylamine (2 eq) was added. HBTU (1.2 eq) was then added and the mixture was stirred for 10 minutes at ambient temperature. The selected amine (1 eq) was added and the reaction was stirred for 15 to overnight. The reaction mixture was then diluted with water, and then extracted twice with ethyl acetate. The combined organic layers were washed with saturated aqueous solution of hydrochloric acid, ammonium chloride and brine. The organic layer was dried over sodium sulphate and the solvent was removed under vacuum. The resulting product was purified by triturated with diethyl ether, or purified by flash column chromatography.

General procedure E (HBTU-Mediated amide coupling): To a stirred solution of carboxylic acid (2 eq) in dimethylformamide, triethylamine (3 eq) was added. HBTU (2.4 eq) was then added and the mixture was stirred for 10 minutes at ambient temperature. The selected amine (1 eq) was added and the reaction was stirred for 15 to overnight. The reaction mixture was then diluted with water, and then extracted twice with ethyl acetate. The combined organic layers were washed with saturated aqueous solution of hydrochloric acid (1M), ammonium chloride and brine. The organic layer was dried over sodium sulphate and the solvent was removed under vacuum. The resulting product was purified by triturated with diethyl ether, or purified by flash column chromatography.

General procedure F (saponification): To the solution of ester (1 eq) in water and THF (2:1), aqueous solution of lithium hydroxide (3 eq) was then

added. The resulting mixture was stirred at ambient temperature between for 2-4 hours. The reaction mixture was monitored by TLC, and then the THF was removed under vacuum. Water was added and the resulting aqueous solution was acidified with aqueous solution of hydrochloric acid (1M). The product was then extracted into ethyl acetate (3X) and the combined organic layers were dried over sodium sulphate, filtered and concentrated under vacuum to afford the desired carboxylic acid.

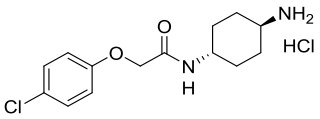
***tert*-Butyl *N*-[(1*R*,4*R*)-4-[2-(4-chlorophenoxy)acetamido]cyclohexyl]carbamate (27)** [151]



Following general procedure A, *N*-Boc-*trans*-1,4-cyclohexanediamine **25** (2.14 g, 10 mmol) and 4-chlorophenoxyacetylchloride **26** (1.56 mL, 10 mmol) in DCM (100 mL) were reacted for 1 hour. The resulting precipitate was further purified by triturated with diethyl ether (25 mL), then separated by filtration and dried in vacuo to afford the title compound as a white powder (3.17 g, yield: 83%). **^{1}H NMR (400 MHz, DMSO-*d*$_6$):** δ 7.92 (d, *J*=7.9 Hz, 1H, amide N*H*), 7.34 (dd, *J*=2.3, 2.1 Hz, 2H, Ar C-*H ortho* to chlorine), 6.97 (dd, *J*=2.3, 2.3 Hz, 2H, Ar C-*H ortho* to phenoxy), 6.71 (d, *J*=7.7 Hz, 1H, N*H*-Boc), 4.44 (s, 2H, CH_2OAr), 3.59 - 3.47 (m, 1H, ^{C}Hx C*H*), 3.18 (bs, ^{C}Hx C*H*), 1.75 (t, *J*=11.9 Hz, 4H, ^{C}Hx CH_2), 1.37 (s, 9H, Boc (CH_3)$_3$), 1.32 - 1.12 (m, 4H, ^{C}Hx CH_2). **^{13}C NMR (DMSO-*d*$_6$)**: δ 166.8 (amide *C*=O), 157.1 (Ar 4º C-phenoxy), 155.3 (*C*=O), 129.6 (Ar *C*-H *ortho* to chlorine), 125.2 (Ar 4º C-chlorine), 117.0 (Ar *C*-H *ortho* to phenoxy), 77.8 (Boc 4º C), 67.6 (*C*H$_2$), 48.9, 47.4 (^{C}Hx *C*H), 31.7, 31.3 (^{C}Hx *C*H$_2$), 28.7 (Boc *C*H$_3$). **HPLC:** $^{t}_{R}$ 2.93 min. **HRMS:** *m/z* theoretical

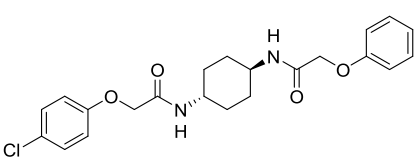
for $C_{19}H_{28}ClN_2O_4$ 383.1693 $[M+H]^+$; measured 383.1682 $[M+H]^+$. **M.p.:** 233-236 °C.

2-(4-Chlorophenoxy)-*N*-[(1*R*,4*R*)-4-aminocyclohexyl]acetamide hydrochloride (28) [151]



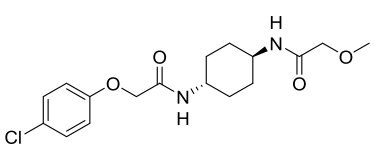
A suspension of *tert*-butyl *N*-[(1*R*,4*R*)-4-[2-(4-chlorophenoxy)acetamido]cyclohexyl]carbamate **27** (1.43 g, 3.5 mmol) was dissolved in dioxane–MeOH (2:1; 12 mL) with the aid of sonication. This was then treated with 4 M HCl in dioxane (10 mL) with vigorously stirring for 2 hours. All the solvents were removed in vacuo. The resulting hydrochloride salt of the desired compound was triturated with diethyl ether (10 mL), then separated by filtration and dried to afford the title compound as a white powder (1.07 g, yield: 96%). **^{1}H NMR (400 MHz, DMSO-*d*$_6$):** δ 8.20 (d, *J*=3.9 Hz, 2H, amine N*H*$_2$), 8.08 (d, *J*=8.2 Hz, 1H, amide N*H*), 7.33 (dd, *J*=2.3, 2.5 Hz, 2H, Ar C-*H ortho* to chlorine), 6.96 (dd, *J*=2.3, 2.4 Hz, 2H, Ar C-*H ortho* to phenoxy), 4.46 (s, 2H, C*H*$_2$OAr), 3.61 - 3.49 (m, 1H, ^{C}Hx C*H*), 2.91 (bs, 1H, ^{C}Hx C*H*), 1.98 (d, *J*=12.1 Hz, 2H, ^{C}Hx C*H*$_2$), 1.77 (d, *J*=12.9 Hz, 2H, ^{C}Hx C*H*$_2$), 1.48 - 1.24 (m, 4H, ^{C}Hx C*H*$_2$). **^{13}C NMR (DMSO-*d*$_6$)**: δ 167.0 (amide *C*=O), 157.1 (Ar 4º C-phenoxy), 129.6 (Ar *C*-H *ortho* to chlorine), 125.2 (Ar 4º C-chlorine), 116.9 (Ar *C*-H *ortho* to phenoxy), 67.6 (*C*H$_2$), 48.9, 47.0 (^{C}Hx *C*H), 30.2, 29.5 (^{C}Hx *C*H$_2$). **HPLC:** t_R 2.03 min. **LC–MS:** *m/z* = 283 $[M+H]^+$. **M.p.:** > 300 °C.

2-Phenoxy-*N*-[(1*R*,4*R*)-4-[2-(4-chlorophenoxy)acetamido]cyclohexyl]acetamide (29)



Following general procedure B, 2-(4-chlorophenoxy)-*N*-[(1*R*,4*R*)-4-aminocyclohexyl]acetamide hydrochloride **28** (0.06 g, 0.2 mmol) and phenoxyacetylchloride (0.03 mL, 0.2 mmol) in DCM (5 mL) were reacted for 1 hour. The resulting precipitate was further purified by triturated with diethyl ether (3 mL), then separated by filtration and dried in vacuo to afford the title compound as a white powder (0.08 g, yield: 96%). **^{1}H NMR (400 MHz, DMSO-*d*$_6$)**: δ 7.94 (dd, *J*=8.3, 8.0 Hz, 2H, amide N*H*), 7.34 (dd, *J*=2.3, 2.2 Hz, 2H, Ar C-*H ortho* to chlorine), 7.29 (dd, *J*=2.4, 2.1 Hz, 2H, Ar C-*H ortho* to phenoxy), 6.96 (td, *J*=2.2, 2.1, 2.3 Hz, 5H, aryl-H), 4.44 (d, *J*=6.0 Hz, 4H, C*H*$_2$OAr), 3.59 (bs, 2H, ^{C}Hx C*H*), 1.76 (d, *J*=6.0 Hz, 4H, ^{C}Hx C*H*$_2$), 1.34 (t, *J*=6.7 Hz, 4H, ^{C}Hx C*H*$_2$). **^{13}C NMR (DMSO-*d*$_6$)**: δ 167.2 (amide *C*=O), 166.9 (amide *C*=O), 158.2 (chlorophenyl 4º C-1), 157.1(aryl 4º C-1), 129.9 (aryl C-3 and C-5), 129.6 (chlorophenyl C-3 and C-5), 125.2 (chlorophenyl C-4), 121.5 (aryl C-4), 117.0 (chlorophenyl C-2 and C-6), 115.2 (aryl C-2 and C-6), 67.6, 67.4 (*C*H$_2$), 47.4 (^{C}Hx *C*H), 31.3 (^{C}Hx *C*H$_2$). **HPLC:** $^{t}_{R}$ 2.84 min. **LC–MS:** *m/z* = 417 $[M+H]^+$. **M.p.:** 227-230 °C.

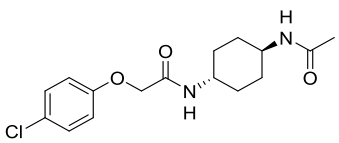
2-(4-Chlorophenoxy)-*N*-[(1*R*,4*R*)-4-(2-methoxyacetamido)cyclohexyl]acetamide (30)



Followed general procedure B, 2-(4-chlorophenoxy)-*N*-[(1*R*,4*R*)-4-aminocyclohexyl]acetamide hydrochloride **28** (0.06 g, 0.2 mmol) and methoxyacetylchloride (0.02 mL, 0.2 mmol) in DCM (5 mL) were reacted for 1 hour. The resulting precipitate was further purified by triturated with diethyl ether (3 mL), then separated by filtration and dried in

vacuo to afford the title compound as a white powder (0.06 g, yield: 92%). **^{1}H NMR (400 MHz, DMSO-*d*$_6$)**: δ 7.94 (d, *J*=8.7 Hz, 1H, amide N*H*), 7.56 (d, *J*=8.5 Hz, 1H, amide N*H*), 7.34 (dd, *J*=2.3, 2.4 Hz, 2H, Ar C-*H ortho* to chlorine), 6.96 (dd, *J*=2.3, 2.3 Hz, 2H, Ar C-*H ortho* to phenoxy), 4.45 (s, 2H, C*H*$_2$OAr), 3.76 (s, 2H, C*H*$_2$OCH$_3$), 3.57 (bs, 2H, ^{C}Hx C*H*), 3.28 (s, 3H, CH$_2$OC*H*$_3$), 1.78 - 1.69 (m, 4H, ^{C}Hx C*H*$_2$), 1.35 (dt, *J*=8.9, 8.9 Hz, 4H, ^{C}Hx C*H*$_2$). **^{13}CNMR (DMSO-*d*$_6$)**: δ 168.4 (amide *C*=O), 166.8 (amide *C*=O), 156.6 (Ar 4º C-phenoxy), 129.6 (Ar *C*-H *ortho* to chlorine), 124.2 (Ar 4º C-chlorine) , 116.5 (Ar *C*-H *ortho* to phenoxy), 71.9 (*C*H$_2$OCH$_3$), 67.6 (*C*H$_2$OAr), 58.9 (*C*H$_3$) , 46.9(^{C}Hx *C*H) , 46.5 (^{C}Hx *C*H), 30.9 (^{C}Hx *C*H$_2$), 30.8(^{C}Hx *C*H$_2$) **HPLC:** $^{t}_{R}$ 2.59 min. **HRMS:** *m/z* theoretical for $C_{17}H_{24}ClN_2O_4$ 355.1419 $[M+H]^+$; measured 355.1424 $[M+H]^+$. **M.p.:** 220-223 °C.

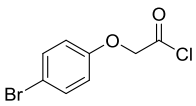
2-(4-Chlorophenoxy)-*N*-[(1*R*,4*R*)-4-acetamidocyclohexyl]acetamide (31)



Following general procedure B, 2-(4-chlorophenoxy)-*N*-[(1*R*,4*R*)-4-aminocyclohexyl]acetamide hydrochloride **28** (0.06 g, 0.2 mmol) and acetyl chloride (0.01 mL, 0.2 mmol) in DCM (5 mL) were reacted for 1 hour. The resulting precipitate was further purified by triturated with diethyl ether (3 mL), then separated by filtration and dried in vacuo to afford the title compound as a white powder (0.06 g, yield: 87%). **^{1}H NMR (400 MHz, DMSO-*d*$_6$)**: δ 7.99 (d, *J*=8.0 Hz, 1H, amide N*H*), 7.76 (d, *J*=8.5 Hz, 1H, amide N*H*), 7.33 (dd, *J*=2.4, 2.3 Hz, 2H, Ar C-*H ortho* to chlorine), 6.96 (dd, *J*=2.3, 2.2 Hz, 2H, Ar C-*H ortho* to phenoxy), 4.45 (s, 2H, C*H*$_2$OAr), 3.62 - 3.52 (m, 1H, ^{C}Hx C*H*), 3.49 - 3.38 (m, 1H, ^{C}Hx C*H*), 1.76 (t, *J*=9.9 Hz, 6H, ^{C}Hx C*H*$_2$ and C*H*$_3$), 1.38 - 1.13 (m, 5H, ^{C}Hx C*H*$_2$ and C*H*$_3$). **^{13}C**

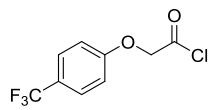
NMR (DMSO-*d*$_6$): δ 168.7 (amide *C*=O), 166.8 (amide *C*=O), 157.2 (Ar 4º C-phenoxy), 129.6 (Ar *C*-H *ortho* to chlorine), 125.2 (Ar 4º C-chlorine), 117.0 (Ar *C*-H *ortho* to phenoxy), 67.6 (*C*H$_2$OAr), 47.5(^{C}Hx *C*H), 47.4 (^{C}Hx *C*H), 31.5 (^{C}Hx *C*H$_2$), 31.3 (^{C}Hx *C*H$_2$), 23.2 (*C*H$_3$). **HPLC:** t_R 2.53 min. **HRMS:** *m/z* theoretical for $C_{16}H_{21}ClN_2O_3$ 325.1313 $[M+H]^+$, measured 325.1323 $[M+H]^+$. **M.p.:** 202-206 °C.

2-(4-Bromophenoxy)acetyl chloride (33a)



A suspension of commercially available 2-(4-bromophenoxy)acetic acid **32a** (0.23 g, 1 mmol) was dissolved in dichloromethane (5 mL) with the aid of sonication. This was then treated dropwise with oxalyl chloride (0.09 mL, 1 mmol) in dichloromethane (1 mL) at 0ºC, followed by a few drops of DMF (2-drops) with stirring for 2 hours at ambient temperature. The reaction was monitored by TLC, and once all the starting acid consumed, the solvent was removed in vacuum. The resulting product was directly used for next step without further purification (0.176 g, yield: 71%). **LC–MS:** *m/z* = 249 $[M+H]^+$.

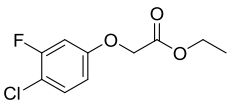
2-(4-(Trifluoromethyl)phenoxy)acetyl chloride (33ab)



A suspension of commercially available 2-[4-(trifluoromethyl)phenoxy]acetic acid **32b** (0.44 g, 2 mmol) was dissolved in dichloromethane (6 mL) with the aid of sonication. This was then treated dropwise with oxalyl chloride (0.17 mL, 2 mmol) in dichloromethane (1 mL) at 0ºC, followed by a few drops of DMF with stirring for 1 hour at ambient temperature. The reaction was monitored by TLC, and once all the starting acid consumed, the solvent was removed in vacuum. The resulting

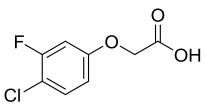
product was used for the next step without further purification (0.15 g, yield: 66%). **LC–MS:** *m/z* = 238 $[M+H]^+$.

Ethyl 2-(4-chloro-3-fluorophenoxy)acetate (35)



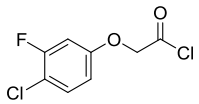
To a suspension of 4-chloro-3-flurophenol **34** (0.29 g, 2 mmol) and ethyl bromoacetate (0.24 mL, 2.2 mmol) in in anhydrous acetonitrile (5 mL) was added K_2CO_3 (0.5 g, 3.6 mmol). The resulting mixture was refluxed for 4 hours. The reaction solution was then diluted with ethyl acetate (10 mL), washed with water and brine. The organic layer was dried over sodium sulphate, filtered and concentrated under vacuum. After concentration of the organic layer, purification was achieved via column chromatography (eluent DCM/EtOAc 10:90, 20:80, then 30:70) to obtain the desired product as a colourless oil (0.36 g, yield: 80%). **^{1}H NMR (400 MHz, DMSO-*d*$_6$):** 7.26 (t, *J*= 8.6 Hz, 1H, Ar C-*H*), 6.72 (dd, *J*= 2.2, 2.2 Hz, 1H, Ar C-*H*), 6.65 (dd, J= 2.7, 2.7 1H, Ar C-*H*), 4.58 (s, 2H, CH_2OAr), 4.25 (q, *J*=6.9, 2H,CH_2CH$_3$), 1.28 (t, *J*=7.2, 3H, CH_3). **HPLC:** ^tR 2.98 min. **LC-MS:** *m/z* = 233 $[M+H]^+$.

2-(4-Chloro-3-fluorophenoxy)acetic acid (36)



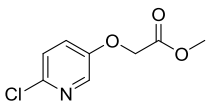
Following general procedure F, ester solution **35** (0.23 g, 1.5 mmol) was treated with aqueous solution of LiOH (0.12 g, 3 mmol) in water and THF (1:1, 10 mL) to afford the title compound as a white fluffy powder (0.17 g, yield: 85%). **^{1}H NMR (400 MHz, DMSO-*d*$_6$)**: δ 13.11 (s, 1H, O*H*), 7.47 (t, *J*=8.9 Hz, 1H, Ar C-*H*), 7.08 (dd, *J*=3.0, 2.6 Hz, 1H, Ar C-*H*), 6.83 (dd, *J*=1.9, 1.9 Hz, 1H, Ar C-*H*), 4.73 (s, 2H, CH_2OAr). **HPLC:** ^tR 2.58 min. **LC-MS:** *m/z* = 205 $[M+H]^+$.

2-(4-Chloro-3-fluorophenoxy)acetyl chloride (37)



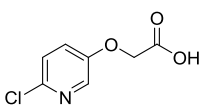
A suspension of 2-(4-chloro-3-fluorophenoxy)acetic acid **36** **(**0.15 g, 0.7 mmol) was dissolved in dichloromethane (5 mL) with the aid of sonication. This was then treated dropwise with oxalyl chloride (0.09 mL, 0.7 mmol) in dichloromethane (1 mL) at 0^{o}C, followed by a few drops of DMF with stirring for 1 hour at ambient temperature. The reaction was monitored by TLC, and once all the starting acid consumed, the solvent was removed in vacuum. The resulting product was used for the next step without further purification (0.08 g, yield: 57%). **LC–MS:** *m/z* = 223 $[M+H]^+$.

Methyl 2-[(6-chloropyridin-3-yl)oxy]acetate (39a)



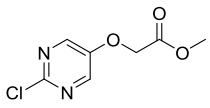
To a suspension of 6-chloro-pyridin-3-ol **38a** (0.64 g, 5 mmol) and methyl bromoactate (0.65 mL, 7 mmol) in acetonitrile (20 mL) was added Cs_2CO_3 (2.24 g, 7 mmol). The resulting mixture was stirred for overnight at ambient temperature. The reaction solution was then diluted with water and extracted with ethyl acetate. The organic phase was washed with water and brine, and then dried over sodium sulphate, filtered and concentrated under vacuum. After concentration of the organic layer, purification was achieved via column chromatography (eluent DCM/EtOAc 10:90, 20:80, then 30:70) to obtain the desired product as a white powder (0.90 g, yield: 90%). **^{1}H NMR (400 MHz, DMSO-*d*$_6$)**: δ 8.16 (d, *J* = 3.1 Hz, 1H, pyridine-H), 7.54 (dd, *J* = 3.2, 3.2 Hz, 1H, pyridine-H), 6.47 (d, *J* = 8.9 Hz, 1H, pyridine-H), 4.94 (s, 2H, C*H*$_2$O), 3.72 (s, 3H. COOC*H*$_3$). **^{13}C NMR (DMSO-*d*$_6$)**: δ 169.1 (amide *C*=O), 154.0 (pyridine C-5), 142.3 (pyridine C-2), 137.8 (pyridine C-4), 126.1 (pyridine C-1), 124.9 (pyridine C-6), 65.5 (*C*H$_2$), 52.4 (*C*H$_3$). **HPLC:** t_R 2.39 min (>95%). **LC-MS:** *m/z* = 202 $[M+H]^+$.

2-[(6-Chloropyridin-3-yl)oxy]acetic acid (40a)



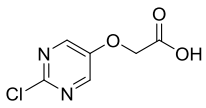
Following general procedure F, ester solution **39a** (0.7 g, 3.5 mmol) was treated with aqueous solution of LiOH (0.45 g, 10.5 mmol) in water and THF (1:1, 30 mL) to afford the title compound as a white powder (0.59 g, yield: 90%). **^{1}H NMR (400 MHz, DMSO-*d*$_6$)**: δ 13.09 (s, 1H, O*H*), 8.12 (d, *J* = 2.9 Hz, 1H, pyridine-H), 7.47 (dd, *J* = 2.8, 2.8 Hz, 1H, pyridine-H), 7.42 (d, *J* = 8.8 Hz, 1H, pyridine-H), 4.81 (s, 2H, C*H*$_2$O). **^{13}C NMR (DMSO-*d*$_6$)**: δ 170.0 (amide *C*=O), 154.2 (pyridine C-5), 142.0 (pyridine C-2), 137.7 (pyridine C-4) , 126.0 (pyridine C-1), 124.9 (pyridine C-6), 65.4 (*C*H$_2$). **HPLC:** $^{t}_{R}$ 2.09 min (>95%). **LC-MS:** *m/z* = 188 $[M+H]^+$.

Methyl 2-((2-chloropyrimidin-5-yl)oxy)acetate (39b)



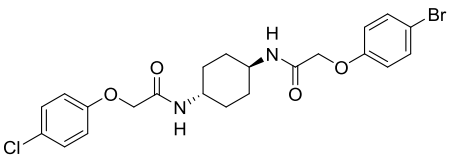
To a suspension of 2-chloro-5-hydroxypyrimidine **38b** (0.34 g, 2.6 mmol) and methyl bromoactate (0.32 ml, 3.5 mmol) in DMF (10 mL) was added K_2CO_3 (0.5 g, 3.6 mmol). The resulting mixture was stirred for overnight at ambient temperature. The reaction solution was then diluted with water and extracted with ethyl acetate. The organic phase was washed with water and brine, and then dried over sodium sulphate, filtered and concentrated under vacuum. After concentration of the organic layer, purification was achieved via column chromatography (eluent DCM/EtOAc 10:90, 20:80, then 30:70) to obtain the desired product as a yellow oil (0.42 g, yield: 81%). **^{1}H NMR (400 MHz, DMSO-*d*$_6$)**: δ 8.58 (s, 2H, pyrimidine-H), 4.88 (s, 2H, C*H*$_2$O), 3.70 (s, 3H, COOC*H*$_3$). **HPLC:** $^{t}_{R}$ 2.08 min. **LC–MS:** *m/z* = 202 $[M+H]^+$.

2-((2-Chloropyrimidin-5-yl)oxy)acetic acid (40b)



Following general procedure F, ester solution **39b** (0.2 g, 1 mmol) was treated with aqueous solution of LiOH (0.12 g, 3 mmol) in water and THF (1:1, 10 mL) to afford the title compound as a white powder (0.17 g, yield: 90%). **^{1}H NMR (400 MHz, DMSO-*d*$_6$)**: δ 12.9 (s, 1H, O*H*), 8.47 (s, 2H, pyrimidine-H), 4.66 (s, 2H, C*H*$_2$OAr). **HPLC:** ^t_R 1.11 min. **LC-MS:** *m/z* = 188 $[M+H]^+$.

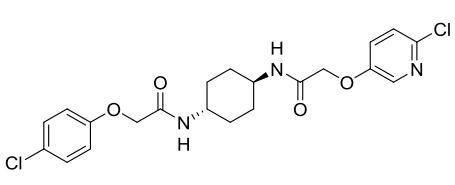
2-(4-Bromophenoxy)-*N*-[(1*R*,4*R*)-4-[2-(4-chlorophenoxy)acetamido]cyclohexyl]acetamide (41)



Following general procedure B, 2-(4-chlorophenoxy)-*N*-[(1*R*,4*R*)-4-aminocyclohexyl]acetamide hydrochloride **28** (0.06 g, 0.2 mmol) and 2-(4-bromophenoxy)acetyl chloride **33a** (0.05 g, 0.2 mmol) in DCM (5 mL) were reacted for 2 hours. The resulting precipitate was further purified by triturated with diethyl ether (3 mL), then separated by filtration and dried in vacuo to afford the title compound as a white fluffy powder (0.06 g, yield: 66%). **^{1}H NMR (400 MHz, DMSO-*d*$_6$):** δ 7.97 (d, *J*=7.7 Hz, 2H, amide N*H*), 7.45 (dd, *J*=2.3, 2.4 Hz, 2H, Ar C-*H ortho* to chlorine), 7.33 (dd, *J*=2.3, 2.3 Hz, 2H, Ar C-*H ortho* to phenoxy), 6.96 (dd, *J*=2.3, 2.2 Hz, 2H, bromophenyl 3-H and 5-H), 6.91 (dd, *J*=2.2, 2.4 Hz, 2H, bromophenyl 2-H and 6-H), 4.45 (s, 4H, C*H*$_2$OAr), 3.59 (bs, 2H, ^{C}Hx C*H*), 1.76 (d, *J*=6.7 Hz, 4H, ^{C}Hx C*H*$_2$), 1.41 - 1.25 (m, 4H, ^{C}Hx C*H*$_2$). **^{13}C NMR (DMSO-*d*$_6$):** δ 166.9 (amide *C*=O), 166.9 (amide *C*=O) , 157.6 (chlorophenyl 4º C), 157.1 (bromophenyl 4º C), 132.5 (bromophenyl C-3 and C-5), 129.6 (Ar *C*-H *ortho* to chlorine), 125.3 (chlorophenyl 4º C), 117.5 (bromophenyl C-2 and C-6), 117.0 (Ar *C*-H *ortho* to phenoxy), 113.0 (bromophenyl C-4) , 67.6 (*C*H$_2$OAr), 67.5 (*C*H$_2$OAr), 47.4

(^{C}Hx *C*H), 31.3 (^{C}Hx *C*H_2). **HPLC:** t_R 2.95 min. **HRMS:** *m/z* theoretical for $C_{22}H_{25}BrClN_2O_4$ 495.0681 $[M+H]^+$, measured 495.0673 $[M+H]^+$. **M.p.:** 267-270 °C.

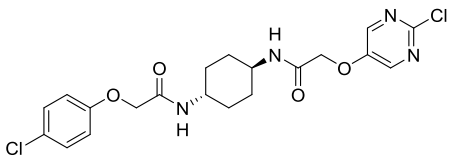
2-(4-Chlorophenoxy)-*N*-[(1*R*,4*R*)-4-{2-[(6-chloropyridin-3-yl)oxy]acetamido}cyclohexyl]acetamide (42)



Following general procedure D, 2-[(6-chloropyridin-3-yl)oxy]acetic acid **40a** (0.07 g, 0.4 mmol) was reacted with HBTU (0.17 g, 0.44 mmol), 2-(4-chlorophenoxy)-*N*-[(1*R*,4*R*)-4-aminocyclohexyl]acetamide hydrochloride **28** (0.12 g, 0.44 mmol) and triethylamine (0.10 mL, 0.88 mmol) in DMF (10 mL) for 16 hours. After concentration of the organic layer, purification was achieved via column chromatography (eluent DCM/THF 30:80) to give the desired product as a solid. The resulting solid was further purified by triturated with diethyl ether (3 mL), then separated by filtration and dried in vacuo to afford the title compound as a white powder (0.14 g, yield: 81%). **^{1}H NMR (400 MHz, DMSO-*d*$_6$)**: δ 8.12 (s, 1H, pyridine-*H*), 7.99 (dd, *J* = 9.5, 8.0 Hz, 2H, amide N*H*), 7.45 (s, 2H, pyridine-H), 7.33 (d, *J* = 8.8 Hz, 2H, Ar C-*H ortho* to chlorine), 6.96 (d, *J* = 8.9 Hz, 2H, Ar C-*H ortho* to phenoxy), 4.57 (s, 2H, C*H*$_2$OPy), 4.45 (s, 2H, C*H*$_2$OAr), 3.59 (s, 2H, ^{C}Hx C*H*), 1.77 (d, *J* = 6.6 Hz, 4H, ^{C}Hx C*H*$_2$), 1.33 (t, *J* = 9.4 Hz, 4H, ^{C}Hx C*H*$_2$). **^{13}C NMR (DMSO-d$_6$)**: δ 166.8 (amide *C*=O), 166.4 (amide *C*=O), 157.1 (pyridine 4º C-phenoxy), 154.2 (Ar 4º C-phenoxy), 142.0 (pyridine 4º C-chlorine *C*-Cl), 137.8 (Ar 4º C-chlorine), 129.6 (pyridine *C*-H), 126.2, 125.2 (2 x aryl *C*-H), 124.9 (pyridine *C*-H), 116.9 (Ar *C*-H *ortho* to phenoxy), 67.7 (*C*H$_2$OPy), 67.6 (*C*H$_2$OAr), 47.4 (^{C}Hx *C*H), 47.3 (^{C}Hx *C*H) , 31.3 (^{C}Hx *C*H$_2$). **HPLC:** t_R

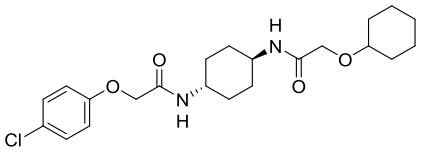
2.74 min (>95%). **HRMS:** *m/z* theoretical for $C_{21}H_{24}Cl_2N_3O_4$ 452.1138 $[M+H]^+$, measured 452.1137 $[M+H]^+$. **M.p.:** 269-273 °C.

2-(4-Chlorophenoxy)-*N*-[(1*R*,4*R*)-4-{2-[(2-chloropyrimidin-5-yl)oxy]acetamido}cyclohexyl]acetamide (43)



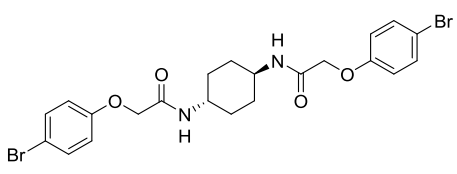
Following general procedure D, **2**-((2-Chloropyrimidin-5-yl)oxy)acetic acid **40b** (0.09 g, 0.5 mmol) was reacted with HBTU (0.21 g, 0.55 mmol), 2-(4-chlorophenoxy)-*N*-[(1*R*,4*R*)-4-aminocyclohexyl]acetamide hydrochloride **28** (0.15 g, 0.55 mmol) and triethylamine (0.12 mL, 1 mmol) in DMF (10 mL) for 19 hours. After concentration of the organic layer, purification was achieved via column chromatography (eluent DCM/THF 30:80) to give the desired product as a solid. The resulting solid was further purified by triturated with diethyl ether (3 mL), then separated by filtration and dried in vacuo to afford the title compound as a white powder (0.18 g, yield: 82%). **^{1}H NMR (400 MHz, DMSO-d$_6$)**: δ 8.53 (s, 2H, amide N*H*), 8.22 (d, *J*=7.9 Hz, 1H, pyrimidine-H), 8.06 (d, *J*=8.0 Hz, 1H, pyrimidine-H), 7.33 (d, *J*=8.9 Hz, 2H, Ar C-*H ortho* to chlorine), 6.97 (d, *J*=9.0 Hz, 2H, Ar C-*H ortho* to phenoxy), 4.71 (s, 2H, CH_2O-pyrimidine), 4.46 (s, 2H, CH_2OAr), 3.55 (s, 2H, ^{C}Hx C*H*), 1.77 (d, *J*=8.6 Hz, 4H, ^{C}Hx CH_2), 1.34 (t, *J*=9.5 Hz, 4H, ^{C}Hx CH_2). **^{13}C NMR (DMSO)**: δ 166.9 (amide *C*=O), 166.1 (amide *C*=O), 157.1 (pyrimidine 4º C-phenoxy), 152.3 (Ar 4º C-phenoxy), 151.5 (pyrimidine 4º C-chlorine), 147.7 (Ar 4º C-chlorine), 129.6, 125.2 (2 x pyrimidine *C*-H), 124.6, 116.9 (2 x aryl *C*-H), 67.8 (*C*H_2OPy), 67.6 (*C*H_2OAr), 47.5 (^{C}Hx *C*H), 47.3 (^{C}Hx *C*H), 31.3 (^{C}Hx *C*H_2). **HPLC:** ^tR 2.68 min (>95%). **LC-MS:** *m/z* = 453 $[M+H]^+$. **M.p.:** 257-260 °C.

2-(4-Chlorophenoxy)-*N*-[(1*R*,4*R*)-4-[2-(cyclohexyloxy)acetamido]cyclohexyl]acetamide (43)



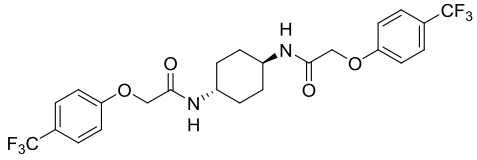
Following general procedure D, 2-(cyclohexyloxy)acetic acid (0.09 g, 0.6 mmol) was reacted with HBTU (0.25 g, 0.66 mmol) and 2-(4-chlorophenoxy)-*N*-[(1*R*,4*R*)-4-aminocyclohexyl]acetamide hydrochloride **28** (0.18 g, 0.66 mmol) and triethylamine (0.14 mL, 1.2 mmol) in DMF (10 mL) for overnight. After concentration of the organic layer, purification was achieved via column chromatography (eluent DCM/THF 30:80) to give the desired product as a solid. The resulting solid was further purified by triturated with diethyl ether (3 mL), then separated by filtration and dried in vacuo to afford the title compound as a white powder (0.21 g, yield: 86%). **^{1}H NMR (400 MHz, DMSO-*d*$_6$)**: δ 7.94 (d, *J*=8.1 Hz, 1H, amide N*H*), 7.35 (d, *J*=8.9 Hz, 2H, Ar C-*H ortho* to chlorine), 7.31 (d, *J*=8.6 Hz, 1H, amide N*H*), 6.97 (d, *J*=8.9 Hz, 2H, Ar C-*H ortho* to phenoxy), 4.46 (s, 2H, C*H*$_2$OAr), 3.83 (s, 2H, C*H*$_2$O ^{C}Hx), 3.58 (s, 2H, ^{C}Hx C*H*), 3.31 - 3.24 (m, 1H, ^{C}Hx C*H*), 1.86 (ddd, *J*=9.8, 10.8, 9.1 Hz, 8H, ^{C}Hx C*H*$_2$), 1.53 - 1.15 (m, 10H, ^{C}Hx C*H*$_2$). **^{13}C NMR (DMSO)**: δ 169.2 (amide *C*=O), 166.8 (amide *C*=O), 157.1, 129.6, 125.2, 116.9 (4 x Ar C-*H*), 77.9 (^{C}Hx *C*H), 67.7, 67.6 (2 x *C*H$_2$), 47.3 (^{C}Hx *C*H), 47.0 (^{C}Hx *C*H), 38.7, 32.0, 31.3, 31.3, 25.7, 23.9 (6 x ^{C}Hx *C*H$_2$). **HPLC:** $^{t}_{R}$ 2.90 min (>95%). **HRMS:** *m/z* theoretical for $C_{22}H_{31}Cl_1N_2O_4$ 423.2045 $[M+H]^+$, measured 423.2056 $[M+H]^+$. **M.p.:** 212-214 °C.

2-(4-Bromophenoxy)-*N*-[(1*R*,4*R*)-4-[2-(4-bromophenoxy)acetamido]cyclohexyl]acetamide (46)



Following general procedure C, *trans*-1,4-diaminocyclohexane **45** (0.05 g, 0.4 mmol) and 2-(4-bromophenoxy)acetyl chloride **33a** (0.2 g, 0.8 mmol) in DCM (5 mL) were reacted for 2 hours. The resulting precipitate was further purified by triturated with diethyl ether (3 mL), then separated by filtration and dried in vacuo to afford the title compound as a white fluffy powder (0.1 g, yield: 47%). **^{1}H NMR (400 MHz, DMSO-*d*$_6$):** δ 7.94 (d, *J* = 8.1 Hz, 2H, amide N*H*), 7.46 (d, *J* = 8.8 Hz, 4H, Ar C-*H ortho* to bromine), 6.91 (d, *J* = 8.8 Hz, 4H, Ar C-*H ortho* to phenoxy), 4.44 (s, 4H, C*H*$_2$OAr), 3.58 (bs, 2H, ^{C}Hx C*H*), 1.76 (d, *J* = 6.1 Hz, 4H, ^{C}Hx C*H*$_2$), 1.33 (t, *J* = 9.9 Hz, 4H, ^{C}Hx C*H*$_2$). **^{13}C NMR (DMSO-d6)**: δ 166.8 (amide *C*=O), 157.6 (Ar 4º C-phenoxy), 132.5 (Ar *C*-H *ortho* to bromine), 117.5 (2 x Ar *C*-H), 113.0 (Ar 4º C), 67.6 (C*H*$_2$OAr), 47.4 (^{C}Hx *C*H), 31.3 (^{C}Hx *C*H$_2$). **HPLC:** t_R 3.12 min (>95%). **HRMS:** *m/z* theoretical for $C_{22}H_{24}Br_2N_2O_4$ 539.0176 $[M+H]^+$, measured 539.0171 $[M+H]^+$. **M.p.:** 263-267 °C.

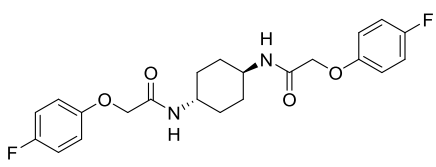
_N_-[(1_R_,4_R_)-4-{2-[4-(trifluoromethyl)phenoxy]acetamido}cyclohexyl]-2-[4-(trifluoromethyl)phenoxy]acetamide (47)[167]



Following general procedure C, *trans*-1,4-diaminocyclohexane **45** (0.05 g, 0.4 mmol) and 2-(4-(trifluoromethyl)phenoxy)acetyl chloride **33ab** (0.19 g, 0.8 mmol) in DCM (5 mL) were reacted for 2 hours. The resulting precipitate was further purified by triturated with diethyl ether (3 mL), then separated by filtration and dried in vacuo to afford the title compound as a light beige powder (0.16 g, yield: 38%). **^{1}HNMR (400 MHz, DMSO-*d*$_6$)**: δ 8.02 (d, *J* = 7.8 Hz, 2H, amide N*H*), 7.66 (d,

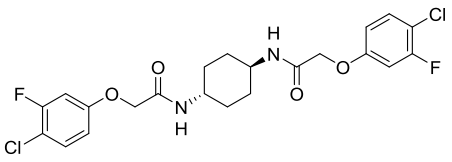
J = 8.7 Hz, 4H, Ar C-*H ortho* to trifluoromethyl), 7.12 (d, *J* = 8.6 Hz, 4H, Ar C-*H ortho* to phenoxy), 4.56 (s, 4H, C*H*$_2$OAr), 3.60 (bs, 2H, ^{C}Hx C*H*), 1.78 (d, *J* = 7.7 Hz, 4H, ^{C}Hx C*H*$_2$), 1.33 (t, *J* = 10.0 Hz, 4H, ^{C}Hx C*H*$_2$). **^{13}C NMR (DMSO)**: δ 166.6 (amide *C*=O), 161.1 (Ar 4º C), 127.3, 115.7 (Ar *C*-H), 67.4 (*C*H$_2$OAr), 47.4 (^{C}Hx *C*H), 31.3 (^{C}Hx *C*H$_2$). **HPLC:** t_R 3.02 min (>95%). **LC-MS:** *m/z* = 519 $[M+H]^+$. **M.p.:** 260-263 °C.

2-(4-Fluorophenoxy)-*N*-[(1*R*,4*R*)-4-[2-(4-fluorophenoxy)acetamido]cyclohexyl]acetamide (48) [151]



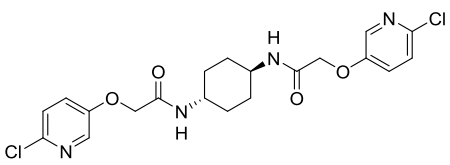
Following general procedure E, 4-fluorophenoxyacetic acid (0.17 g, 1 mmol) was reacted with HBTU (0.51 g, 1.4 mmol), *trans*-1,4-cyclohexandiamine **45** (0.06 g, 0.5 mmol) and triethylamine (0.36 mL, 3 mmol) in DMF (15 mL) for overnight. The resulting solid was further purified by triturated with diethyl ether (3 mL), then separated by filtration and dried in vacuo to afford the title compound as a beige powder (0.13 g, yield: 60%). **^{1}H NMR (400 MHz, DMSO-*d*$_6$)**: δ 7.92 (d, *J* = 8.1 Hz, 2H, amide N*H*), 7.12 (t, *J* = 8.8 Hz, 4H, Ar C-*H ortho* to fluorine), 6.96 (dd, *J* = 4.4, 4.4 Hz, 4H, Ar C-*H ortho* to phenoxy), 4.42 (s, 4H, C*H*$_2$OAr), 3.59 (bs, 2H, ^{C}Hx C*H*), 1.76 (d, *J* = 5.9 Hz, 4H, ^{C}Hx C*H*$_2$), 1.34 (t, *J* = 9.9 Hz, 4H, ^{C}Hx C*H*$_2$). **^{13}C NMR (DMSO)**: δ 167.1(amide *C*=O), 158.4 (Ar 4º C-phenoxy), 156.1(Ar *C*-H *ortho* to fluorine), 154.6 (Ar 4º C-fluorine), 116.6, 116.5, 116.3, 116.1(4 x Ar *C*-H), 68.0 (*C*H$_2$OAr), 47.4 (^{C}Hx *C*H), 31.3 (^{C}Hx *C*H$_2$). **HPLC:** t_R 2.79 min (>95%). **LC-MS:** *m/z* = 418 $[M+H]^+$. **M.p.:** 242-244°C.

2-(4-Chloro-3-fluorophenoxy)-*N*-[(1*R*,4*R*)-4-[2-(4-chloro-3-fluorophenoxy)acetamido]cyclohexyl]acetamide (49) [151]



Following general procedure C, *trans*-1,4-diaminocyclohexane **45** (0.05 g, 0.4 mmol) and 2-(4-chloro-3-fluorophenoxy)acetyl chloride **37** (0.12 g, 0.8 mmol) in DCM (5 mL) were reacted for 2 hours. The resulting precipitate was further purified by triturated with diethyl ether (3 mL), then separated by filtration and dried in vacuo to afford the title compound as a light beige powder (0.07 g, yield: 40%). **^{1}H NMR (400 MHz, DMSO-*d*$_6$)**: δ 7.97 (d, *J* = 6.7 Hz, 2H, amide N*H*), 7.49 (t, *J* = 8.3 Hz, 2H, Ar C-*H ortho* to chlorine), 7.06 (d, *J* = 10.9 Hz, 2H, Ar C-*H ortho* to phenoxy), 6.84 (d, *J* = 7.1 Hz, 2H, Ar C-*H ortho* to phenoxy), 4.49 (s, 4H, C*H*$_2$OAr), 3.58 (bs, 2H, ^{C}Hx C*H*), 1.77 (d, *J* = 7.1 Hz, 4H, ^{C}Hx C*H*$_2$), 1.33 (t, *J*=10.6 Hz, 4H, ^{C}Hx C*H*$_2$). **^{13}C NMR (DMSO):** δ 166.5 (amide *C*=O), 159.1 (Ar 4º C-fluorine), 158.3 (Ar 4º C-phenoxy), 156.7 (Ar *C*-H *ortho* to chlorine), 131.1 (Ar 4º C-chlorine), 112.8, 111.6, 111.5, 104.6, 104.4 (5 x Ar *C*-H), 67.8 (*C*H$_2$OAr), 47.4 (^{C}Hx *C*H), 31.3 (^{C}Hx *C*H$_2$). **HPLC:** t_R 2.97 min (>95%). **LC-MS:** *m/z* = 487 $[M+H]^+$. **M.p.:** 250-254 °C.

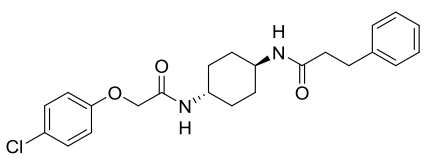
2-[(6-Chloropyridin-3-yl)oxy]-*N*-[(1*R*,4*R*)-4-{2-[(6-chloropyridin-3-yl)oxy]acetamido}cyclohexyl]acetamide (50)



Following general procedure E, 2-[(6-chloropyridin-3-yl)oxy]acetic acid **40a** (0.1 g, 0.5 mmol) was reacted with HBTU (0.22 g, 0.6 mmol), *trans*-1,4-cyclohexandiamine **45** (0.03 g, 0.25 mmol) and triethylamine (0.18 mL, 1.5 mmol) in DMF (10 mL) for overnight. After

concentration of the organic layer, purification was achieved via column chromatography (eluent DCM/THF 20:80) to give the desired product as a solid. The resulting solid was further purified by triturated with diethyl ether (3 mL), then separated by filtration and dried in vacuo to afford the title compound as a white powder (0.077 g, yield: 78%). **^{1}H NMR (400 MHz, DMSO-d_6)**: δ 8.23 (d, *J*=8.0 Hz, 2H, amide N*H*), 8.11 (d, *J*=2.7 Hz, 2H, Ar C-*H ortho* to phenoxy), 7.46 (d, *J*=3.4 Hz, 4H, Ar C-*H*), 4.58 (s, 4H, CH_2OAr), 3.56 (bs, 2H, ^{C}Hx C*H*), 1.75 (d, *J*=5.9 Hz, 4H, ^{C}Hx CH_2), 1.33 (t, *J*=9.9 Hz, 4H, ^{C}Hx CH_2). **^{13}C NMR (DMSO)**: δ 166.5 (amide *C*=O), 154.2 (Ar 4º C-phenoxy), 142.0 (Ar 4º C-chlorine), 137.8, 126.2, 124.9 (Ar *C*-H), 67.7 (*C*H_2OAr), 47.4 (^{C}Hx *C*H), 31.2 (^{C}Hx *C*H_2). **HPLC:** ^tR 2.57 min (>95%). **LC-MS:** *m/z* = 453 $[M+H]^+$. **M.p.:** 268-271 °C.

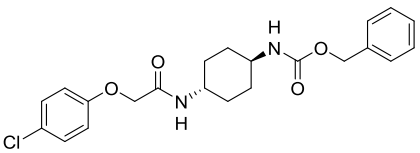
3-Phenyl-*N*-[(1*R*,4*R*)-4-[2-(4-chlorophenoxy)acetamido]cyclohexyl]propenamide (52)



Following general procedure B, 2-(4-chlorophenoxy)-*N*-[(1*R*,4*R*)-4-aminocyclohexyl]acetamide hydrochloride **28** (0.13 g, 0.4 mmol) and 3-phenylpropanoyl chloride (0.06 mL, 0.4 mmol) in DCM (5 mL) were reacted for 1 hours. The resulting precipitate was further purified by triturated with diethyl ether (3 mL), then separated by filtration and dried in vacuo to afford the title compound as a white fluffy powder (0.14 g, yield: 84%). **^{1}H NMR (400 MHz, DMSO-d_6)**: δ 7.97 (d, *J*=7.8 Hz, 1H, amide N*H*), 7.72 (d, *J*=7.6 Hz, 1H, amide N*H*), 7.33 (d, *J*=9.0 Hz, 2H, Ar C-*H ortho* to chlorine), 7.26 (t, *J*=7.3 Hz, 2H, Ar C-*H ortho* to phenoxy), 7.18 (t, *J*=6.4 Hz, 3H, aryl C-*H*), 6.96 (d, *J*=9.1 Hz, 2H, aryl C-*H*), 4.44 (s, 2H, CH_2OAr), 3.62 -

3.41 (m, 2H, ^{C}Hx C*H*), 2.78 (t, *J*=7.7 Hz, 2H, C*H*$_2$CH$_2$Ar), 2.32 (t, *J*=7.8 Hz, 2H, C*H*$_2$Ar), 1.73 (d, *J*=11.7 Hz, 4H, ^{C}Hx C*H*$_2$), 1.25 (dq, *J*=11.5, 11.5 Hz, 4H, ^{C}Hx C*H*$_2$). **^{13}C NMR (DMSO)**: δ 170.8 (amide *C*=O), 166.8 (amide *C*=O), 157.1(Ar 4º C-phenoxy), 141.8 (aryl 4º C-1), 129.6 (Ar *C*-H *ortho* to chlorine), 128.6 (aryl C-3 and C-5), 126.3 (aryl C-2 and C-6), 125.2 (aryl C-4), 117.0 (Ar *C*-H *ortho* to phenoxy), 67.6 (*C*H$_2$OAr), 47.4 (^{C}Hx *C*H), 47.3 (^{C}Hx *C*H), 37.5 (*C*H$_2$Ar), 31.6 (*C*H$_2$Ar) , 31.5 (^{C}Hx *C*H$_2$), 31.3 (^{C}Hx *C*H$_2$). **HPLC:** t_R 2.85 min. **LC-MS:** *m/z* = 415 $[M+H]^+$. **M.p.:** 253-256 °C.

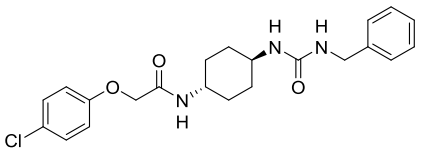
Benzyl *N*-[(1*R*,4*R*)-4-[2-(4-chlorophenoxy)acetamido]cyclohexyl]carbamate (53)



Following general procedure B, 2-(4-chlorophenoxy)-*N*-[(1*R*,4*R*)-4-aminocyclohexyl]acetamide hydrochloride **28** (0.06 g, 0.2 mmol) and benzyl chloroformate (0.03 g, 0.2 mmol) in DCM (5 mL) were reacted for 2 hours. The resulting precipitate was further purified by triturated with diethyl ether (3 mL), then separated by filtration and dried in vacuo to afford the title compound as a white fluffy powder (0.08 g, yield: 90%). **^{1}H NMR (400 MHz, DMSO-*d*$_6$):** δ 7.92 (d, *J*=7.9 Hz, 1H, amide N*H*), 7.34 (t, *J*=7.4 Hz, 7H, Ar C-*H ortho* to chlorine and aryl-*H*), 7.20 (d, *J*=7.7 Hz, 1H, amide N*H*), 6.96 (d, *J*=8.9 Hz, 2H, Ar C-*H ortho* to phenoxy), 5.00 (s, 2H, C*H*$_2$Ar), 4.44 (s, 2H, C*H*$_2$OAr), 3.62 - 3.49 (m, 1H, ^{C}Hx C*H*), 3.30 - 3.18 (m, 1H, ^{C}Hx C*H*), 1.78 (dd, *J*=11.8, 11.7 Hz, 4H, ^{C}Hx C*H*$_2$), 1.39 - 1.11 (m, 4H, ^{C}Hx C*H*$_2$). **^{13}C NMR (DMSO-*d*$_6$)**: δ 166.8 (amide *C*=O), 157.1 (Ar 4º C-phenoxy), 155.8 (amide *C*=O), 137.7 (benzyl 4º C), 129.6 (Ar *C*-H *ortho* to chlorine), 128.8, 128.2 (2 x benzyl *C*-H), 125.2 (Ar 4º C-chlorine), 117.0 (Ar *C*-H *ortho* to

phenoxy), 67.7 (*C*H_2OAr), 65.5 (*C*H_2Ar), 49.4, 47.4 (2 x ^{C}Hx *C*H), 31.7, 31.2 (2 x ^{C}Hx *C*H_2). **HPLC:** $^{t}_{R}$ 2.96 min. **LC-MS:** *m/z* = 417 $[M+H]^+$. **M.p.:** 223-226 °C.

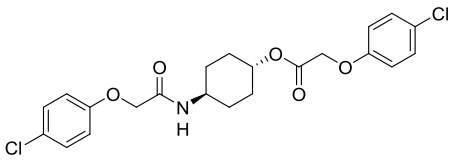
2-(4-Chlorophenoxy)-*N*-[(1*R*,4*R*)-4-[(benzylcarbamoyl)amino]cyclohexyl]acetamide (54)



To a stirred solution of 2-(4-chlorophenoxy)-*N*-[(1*R*,4*R*)-4-aminocyclohexyl]acetamide hydrochloride **28** (0.06 g, 0.2 mmol) in dichloromethane (5 mL), DIPEA (0.041 mL, 0.24 mmol) was added. Benzyl isocyanate (0.22 mmol, 0.03 mL) in DCM (0.5 mL) was then added. Instant precipitation of a white solid was noted and the reaction was allowed to stir for overnight at ambient temperature. The reaction mixture was then diluted with water, and then extracted twice with ethyl acetate. The combined organic layers were washed with saturated aqueous solution of ammonium chloride and brine. The organic layer was evaporated under vacuum. The resulting precipitate was further purified by triturated with diethyl ether (3 mL), then separated by filtration and dried in vacuo to afford the title compound as a white powder (0.07 g, yield: 80%). **^{1}H NMR (400 MHz, DMSO-d6)**: δ 7.93 (d, *J*=8.2 Hz, 1H, amide N*H*), 7.38 - 7.30 (m, 7H, Ar C-*H ortho* to chlorine and aryl-*H*), 7.19 (d, *J*=7.2 Hz, 1H, urea N*H*), 6.96 (d, *J*=11.2 Hz, 2H, Ar C-*H ortho* to phenoxy), 4.99 (s, 2H, C*H*$_2$OAr,), 4.44 (s, 2H, C*H*$_2$Ar), 3.59 - 3.50 (m, 1H, ^{C}Hx C*H*), 3.30 - 3.20 (m, 1H, ^{C}Hx C*H*), 1.82 (dd, *J*=12.3, 12.0 Hz, 4H, ^{C}Hx C*H*$_2$), 1.35 - 1.16 (m, 4H, ^{C}Hx C*H*$_2$). **^{13}C NMR (DMSO)**: δ 166.3 (amide *C*=O), 156.6 (urea *C*=O), 155.3 (Ar 4º C-phenoxy), 137.2 (Ar 4º C-aryl), 129.1, 128.3, 127.7, 124.7, 116.5 (6 x Ar), 67.1 (*C*H_2OAr), 65.0 (*C*H_2Ar), 48.9, 46.9 (2 x ^{C}Hx

*C*H), 31.2, 30.7 (2 x ^{C}Hx *C*H_2). **HPLC:** $^{t}_{R}$ 2.80 min (95%). **LC-MS:** *m/z* = 416 $[M+H]^+$. **M.p.:** 287-291 °C.

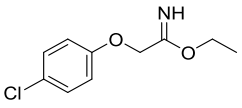
(1*R*,4*R*)-4-[2-(4-Chlorophenoxy)acetamido]cyclohexyl2-(4-chlorophenoxy)acetate (56)



4-Chlorophenoxyacetylchloride **26** (0.26 mL, 2.2 mmol) diluted in DCM (1mL) was added dropwise to a stirred solution of *trans*-4-aminocyclohexanol hydrochloride **55** (0.15 g, 1 mmol) in DCM (4 mL) and triethylamine (0.5 mL, 4 mmol) at 0°C (ice bath) under nitrogen. The reaction mixture was stirred at 0°C for a further 30 min, a suspension occurs then it was continuous stirred at at room temperature for 7 hours with monitoring by TLC. Ethyl acetate was then added to the DCM and the organic phase washed with saturated aqueous solution of NH_4Cl, $NaHCO_3$ and brine, respectively. The organic layer was then evaporated under vacuum and the resulting precipitate was further purified by triturated with diethyl ether (3 mL), then separated by filtration and dried in vacuo to afford the title compound as a white powder (0.18 g, yield: 42%). **^{1}H NMR (400 MHz, DMSO-*d*$_6$)** δ 7.94 (d, *J*=8.0 Hz, 1H, amide N*H*), 7.34 (dd, *J*=3.1, 3.1 Hz, 4H, Ar C-*H ortho* to chlorine), 6.97 (td, *J*=2.3, 3.0, 3.2 Hz, 4H, Ar C-*H ortho* to phenoxy), 4.77 (s, 2H, C*H*$_2$OAr), 4.69 (bs, 1H, ^{C}Hx C*H*), 4.46 (s, 2H, C*H*$_2$OAr), 3.67 (bs, 1H, ^{C}Hx C*H*), 1.92 (dd, *J*=9.4, 8.7 Hz, 4H, ^{C}Hx C*H*$_2$), 1.41 (q, *J*=11.5 Hz, 4H, ^{C}Hx C*H*$_2$). **^{13}C NMR (DMSO)** δ 168.5 (ester *C*=O), 167.0 (amide *C*=O), 157.1 (Ar 4º C-phenoxy), 156.9 (Ar 4º C-phenoxy), 129.6 (Ar *C*-H *ortho* to chlorine), 125.3, 125.2 (2 x Ar 4º C-chlorine), 116.8 (Ar *C*-H *ortho* to phenoxy), 73.1 (^{C}Hx *C*H), 67.6 (*C*H_2OAr), 65.4 (*C*H_2OAr), 46.7

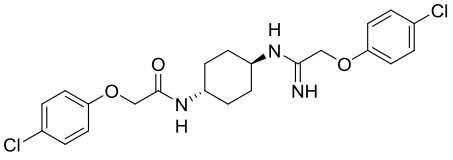
(^{C}Hx *C*H), 30.0, 29.7 (2 x ^{C}Hx *C*H_2). **HPLC:** $^{t}_{R}$ 3.07 min (96%). **LC-MS:** *m/z* = 452 $[M+H]^+$. **M.p.:** 160-163°C.

Ethyl 2-(4-chlorophenoxy)ethanecarboximidate (58) [167]



To a stirred solution of 4-chlorophenoxyacetonitrile **57** (0.42 g, 2.49 mmol) in diethyl ether (2 mL) were added 4 M HCl in dioxane (0.59 mL) and ethanol (0.145 mL, 2.49 mmol). The mixture was stirred for overnight at ambient temperature. The solvent was evaporated under vacuum and the resulting precipitate was further purified by triturated with diethyl ether (2 mL), then separated by filtration and dried to obtain the title compound as white solid, which was used for the next step without further purification (0.40 g, yield: 76%). **LC–MS:** *m/z* = 213 $[M+H]^+$.

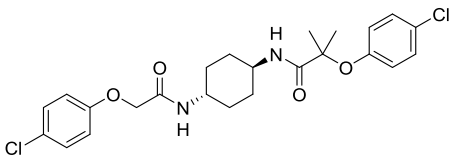
2-(4-Chlorophenoxy)-*N*-[(1*R*,4*R*)-4-[2-(4-chlorophenoxy)ethanimidamido]cyclohexyl]acetamide (59)[167]



To a stirred solution of 2-(4-chlorophenoxy)-*N*-[(1*R*,4*R*)-4-aminocyclohexyl]acetamide hydrochloride **28** (0.10 g, 0.3 mmol) in ethanol (1 mL) were added DIPEA (0.063 mL, 0.4 mmol) and ethyl 2-(4-chlorophenoxy)ethanecarboximidate **58** (0.08 g, 0.4 mmol). The mixture was stirred for overnight at ambient temperature. After concentration, purification was achieved via column chromatography (eluent NH_3 10% in methanol/DCM 5:95) to give the desired product as a white fluffy powder (0.10 g, yield: 76%). **^{1}H NMR (400 MHz, DMSO-d_6)**: δ 9.49 (d, *J*=2.4 Hz, 2H, amidine N*H*), 8.19 (d, *J*=7.9 Hz, 1H, amide N*H*), 7.40 (dd, *J*=9.0, 8.9 Hz, 4H, Ar C-*H ortho* to chlorine), 7.05 (dd, *J*=9.0, 9.0 Hz, 4H, Ar C-*H ortho* to

phenoxy), 4.97 (s, 2H, C*H*$_2$OAr), 4.47 (s, 2H, C*H*$_2$OAr), 3.73 (s, 1H, ^{C}Hx C*H*), 3.55 (s, 1H, ^{C}Hx C*H*), 1.86 (td, *J*=6.7, 7.1, 6.9 Hz, 4H, ^{C}Hx C*H*$_2$), 1.29 (dt, *J*=7.2, 8.9 Hz, 4H, ^{C}Hx C*H*$_2$). **^{13}C NMR (DMSO)**: δ 167.3 (amide *C*=O), 162.1 (amidine *C*=O), 156.65 (Ar 4º C-phenoxy), 155.3 (Ar 4º C-phenoxy), 129.2, 128.9, 126.7, 115.5 (4 x Ar), 67.1, 66.0 (2 x *C*H$_2$OAr), 55.9, 47.9 (2 x ^{C}Hx *C*H), 30.2, 29.6 (2 x ^{C}Hx *C*H$_2$) . **HPLC:** $^{t}_{R}$ 2.30 min (>95%). **LC-MS:** *m/z* = 450 $[M+H]^+$. **M.p.:** 225-228°C.

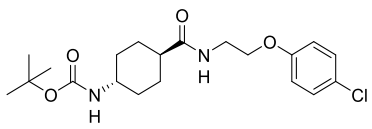
2-(4-Chlorophenoxy)-2-methyl-*N*-[(1*R*,4*R*)-4-[2-(4chlorophenoxy) acetamido] cyclohexyl] propenamide (60)



Following general procedure D, 2-(4-chlorophenoxy)-2-methylpropanoic acid (0.08 g, 0.4 mmol) was reacted with HBTU (0.17 g, 0.44 mmol), 2-(4-chlorophenoxy)-*N*-[(1*R*,4*R*)-4-aminocyclohexyl]acetamide hydrochloride **28** (0.12 g, 0.44 mmol) and triethylamine (0.10 mL, 0.88 mmol) in DMF (10 mL) for 16 hours. After concentration of the organic layer, the resulting solid was further purified by triturated with diethyl ether (3 mL), then separated by filtration and dried in vacuo to afford the title compound as a white powder (0.18 g, yield: 94%). **^{1}H NMR (400 MHz, DMSO-*d*$_6$)**: δ 7.95 (d, *J*=8.1 Hz, 1H, amide N*H*), 7.88 (d, *J*=8.4 Hz, 1H, amide N*H*), 7.34 (td, *J*=2.2, 2.2, 2.2 Hz, 4H, Ar C-*H ortho* to chlorine), 6.96 (d, *J*=9.0 Hz, 2H, Ar C-*H ortho* to phenoxy), 6.87 (d, *J*=8.9 Hz, 2H, Ar C-*H ortho* to phenoxy), 4.44 (s, 2H, C*H*$_2$OAr), 3.58 (bs, 2H, ^{C}Hx C*H*), 1.70 (dd, *J*=7.9, 8.3 Hz, 4H, ^{C}Hx C*H*$_2$), 1.40 (s, 6H, C*H*$_3$), 1.32 (t, *J*=10.3 Hz, 4H, ^{C}Hx C*H*$_2$). **^{13}C NMR (DMSO-*d*$_6$)**: δ 172.6 (amide *C*=O), 166.8 (amide *C*=O), 157.1 (Ar 4º C-phenoxy), 154.2 (Ar 4º C-phenoxy), 129.6, 129.4, 126.3,

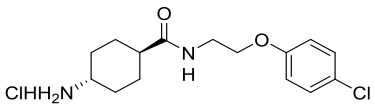
125.2, 121.8, 117.0 (6 x Ar), 80.9 (4º *C*$(CH_3)_2$OAr)), 67.68 (*C*H_2OAr), 47.6, 47.4 (2 x ^{C}Hx *C*H), 31.4, 31.0 (2 x ^{C}Hx *C*H_2), 25.3 (*C*H_3). **HPLC:** $^{t}_{R}$ 3.07 min. **LC-MS:** *m/z* = 479 $[M+H]^+$. **M.p.:** 207-210 °C.

***tert*-Butyl*N*-[(1*R*,4*R*)-4-{[2-(4-chlorophenoxy)ethyl] carbamoyl}cyclohexyl]carbamate (61a)**



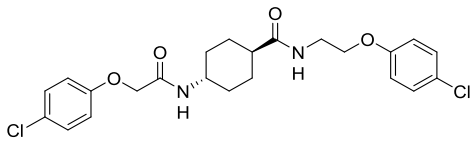
Following general procedure D, *trans*-4-(boc-amino) cyclohexanecarboxylic acid **51** (0.17 g, 0.7 mmol) was reacted with HBTU (0.27 g, 0.77 mmol), 2-(4-chlorophenoxy)ethylamine (0.16 g, 0.77 mmol) and triethylamine (0.12 mL, 1 mmol) in DMF (10 mL) for overnight. After concentration of the organic layer, purification was achieved via column chromatography (eluent DCM/EtoAC 10:90, 20:80, then 30:70) to give the desired product as a solid. The resulting solid was further purified by triturated with diethyl ether (3 mL), then separated by filtration and dried in vacuo to afford the title compound as a white powder (0.25 g, yield: 92%). **^{1}H NMR (400 MHz, DMSO-d6):** δ 7.95 (t, *J*=5.5 Hz, 1H, invers amide N*H*), 7.32 (d, *J*=8.9 Hz, 2H, Ar C-*H ortho* to chlorine), 6.96 (d, *J*=9.0 Hz, 2H, Ar C-*H ortho* to phenoxy), 6.69 (d, *J*=7.8 Hz, 1H, amide N*H*), 3.96 (t, *J*=5.7 Hz, 2H, C*H*$_2$OAr), 3.38 (q, *J*=5.6 Hz, 2H, C*H*$_2$CH_2), 3.12 (bs, 1H, ^{C}Hx C*H*), 2.03 (t, *J*=13.5 Hz, 1H, ^{C}Hx C*H*), 1.78 (dd, *J*=10.8, 12.0 Hz, 4H, ^{C}Hx C*H*$_2$), 1.37 (s, 9H, C(C*H*$_3$)$_3$), 1.34 (dd, *J*=2.5, 2.6 Hz, 2H, ^{C}Hx C*H*$_2$), 1.12 (q, *J*=11.4 Hz, 2H, ^{C}Hx C*H*$_2$). **^{13}C NMR (DMSO):** δ 175.6 (invers amide *C*=O), 157.7 (amide *C*=O), 155.2 (Ar 4º C-phenoxy), 129.7 (Ar *C*-H *ortho* to chlorine), 124.7 (Ar 4º C-chlorine), 116.7 (Ar *C*-H *ortho* to phenoxy), 77.8 (Boc 4º C), 67.1 (*C*H_2OAr), 49.1 (^{C}Hx *C*H), 43.5 (*C*H_2CH_2), 38.4 (^{C}Hx *C*H), 32.3 (Boc *C*H_3), 28.7 (^{C}Hx *C*H_2). **HPLC**: t_R 2.99 min (96%). **LC-MS**: m/z = 397 [M+H]+.

(1*R*,4*R*)-4-Amino-*N*-[2-(4-chlorophenoxy)ethyl]cyclohexane-1-carboxamide hydrochloride (61b)



A suspension of *tert*-butyl*N*-[(1*R*,4*R*)-4-{[2-(4-chlorophenoxy)ethyl] carbamoyl}cyclohexyl]carbamate **61a** (0.2 g, 0.5 mmol) was dissolved in dioxane–MeOH (2:1; 3 mL) with the aid of sonication. This was then treated with 4 M HCl in dioxane (2 mL) with vigorously stirring for 2 hours. All the solvents were removed in vacuo. The resulting hydrochloride salt of the desired compound was triturated with diethyl ether (2 mL), then separated by filtration and dried to afford the title compound as a white powder. The resulting product was used for the next step without further purification (0.15 g, yield: 90%). **LC–MS:** *m/z* = 297 $[M+H]^+$.

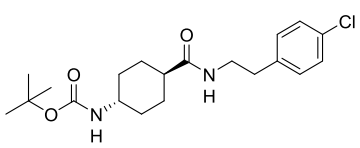
(1*R*,4*R*)-4-[2-(4-Chlorophenoxy)acetamido]-*N*-[2-(4-chlorophenoxy)ethyl]cyclohexane-1-carboxamide (61c)



Following general procedure A, (1*R*,4*R*)-4-amino-*N*-[2-(4-chlorophenoxy)ethyl]cyclohexane-1-carboxamide hydrochloride **61b** (0.15 g, 0.45 mmol) and 4-chlorophenoxyacetylchloride (0.08 mL, 0.5 mmol) in DCM (5 mL) were reacted for 1 hour. The resulting precipitate was further purified by triturated with diethyl ether (3 mL), then separated by filtration and dried in vacuo to afford the title compound as a white powder (0.18 g, yield: 87%).**^{1}H NMR (400 MHz, DMSO-*d*$_6$)**: δ 8.10 (t, *J*=7.0 Hz, 2H, amide N*H*), 7.34 (dd, *J*=6.5, 6.4 Hz, 4H, Ar C-*H ortho* to chlorine), 6.98 (dd, *J*=2.7, 2.7 Hz, 4H, Ar C-*H ortho* to phenoxy), 4.46 (s, 2H, CH_2OAr), 3.96 (t, *J*=5.6 Hz, 2H, CH_2OAr), 3.57 (bs, 1H, ^{C}Hx C*H*), 3.40

(d, *J*=5.4 Hz, 2H, C*H*$_2$CH$_2$), 2.09 (t, *J*=11.6 Hz, 1H, ^{C}Hx C*H*), 1.74 (t, *J*=13.9 Hz, 4H, ^{C}Hx C*H*$_2$), 1.39 (dq, *J*=12.1, 11.5 Hz, 4H, ^{C}Hx C*H*$_2$). **^{13}C NMR (DMSO)**: δ 175.6 (invers amide *C*=O), 166.7 (amide *C*=O), 157.7 (Ar 4º C-phenoxy), 157.1 (Ar 4º C-phenoxy), 129.7 (Ar *C*-H *ortho* to chlorine), 129.6 (Ar *C*-H *ortho* to chlorine), 125.2 (Ar 4º C-chlorine), 124.7 (Ar 4º C-chlorine), 116.9, 116.7 (2 x Ar *C*-H *ortho* to phenoxy), 67.6 (*C*H$_2$OAr), 67.1 (*C*H$_2$OAr), 47.6 (^{C}Hx *C*H), 43.4 (*C*H$_2$CH$_2$), 38.4 (^{C}Hx *C*H), 31.8, 28.6 (2 x ^{C}Hx *C*H$_2$). **HPLC:** $^{t}_{R}$ 3.01 min (96%). **HRMS:** *m/z* theoretical for $C_{23}H_{26}Cl_2N_2O_4$ 487.1162 $[M+Na]^+$, measured 487.1154 $[M+Na]^+$.**M.p.:** 234-237°C.

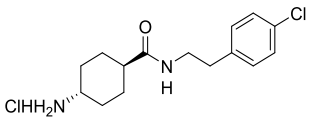
***tert*-Butyl*N*-[(1*R*,4*R*)-4-{[2-(4-chlorophenyl)ethyl] carbamoyl}cyclohexyl]carbamate (62a)**



Following general procedure D, *trans*-4-(boc-amino) cyclohexanecarboxylic acid **51** (0.17 g, 0.7 mmol) was reacted with HBTU (0.27 g, 0.77 mmol), 2-(4-chlorophenyl)ethan-1-amine (0.12 g, 0.77 mmol) and triethylamine (0.12 mL, 1 mmol) in DMF (10 mL) for 8 hours. After concentration of the organic layer, purification was achieved via column chromatography (eluent DCM/EtoAC 10:90, 20:80, then 30:70) to give the desired product as a solid. The resulting solid was further purified by triturated with diethyl ether (3 mL), then separated by filtration and dried in vacuo to afford the title compound as a white powder (0.22 g, yield: 83%). **^{1}H NMR (400 MHz, DMSO-*d*$_6$)**: δ 7.89 (t, *J*=5.5 Hz, 1H, invers amide N*H*), 7.33 (d, *J*=8.3 Hz, 2H, Ar C-*H ortho* to chlorine), 7.21 (d, *J*=8.3 Hz, 2H, Ar C-*H ortho* to phenoxy), 6.70 (d, *J*=7.9 Hz, 1H, amide N*H*), 3.22 (q, *J*=6.6 Hz, 2H, C*H*$_2$CH$_2$), 3.11 (bs, 1H, ^{C}Hx C*H*), 2.68 (t, *J*=7.1 Hz, 2H, C*H*$_2$Ar), 1.97 (t, *J*=11.9 Hz, 1H, ^{C}Hx C*H*), 1.76 (d, *J*=10.4, 11.9

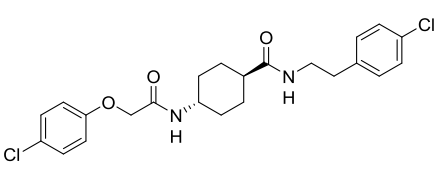
Hz, 4H, ^{C}Hx CH_2), 1.37 (s, 9H, C(CH_3)$_3$), 1.31 (dq, *J*=8.5, 11.6 Hz, 4H, ^{C}Hx CH_2). **^{13}C NMR (DMSO):** δ 175.2 (invers amide *C*=O), 155.2 (amide *C*=O), 139.0 (Ar 4º *C*-CH_2), 131.0 (Ar 4º C-chlorine), 128.5 (Ar C-*H*), 77.7 (Boc 4º C), 49.1 (^{C}Hx *C*H), 43.5 (*C*$H_2$$CH_2$), 34.8 (^{C}Hx *C*H), 32.3(*C*H_2 Ar), 28.7 (^{C}Hx *C*H_2). **HPLC:** $^{t}_{R}$ 2.86 min (96%). **LC-MS:** *m/z* = 381 $[M+H]^+$.

(1*R*,4*R*)-4-Amino-*N*-[2-(4-chlorophenyl)ethyl]cyclohexane-1-carboxamide hydrochloride (62b)



A suspension of *tert*-butyl*N*-[(1*R*,4*R*)-4-{[2-(4-chlorophenyl)ethyl] carbamoyl}cyclohexyl]carbamate **62a** (0.2 g, 0.5 mmol) was dissolved in dioxane–MeOH (2:1; 3 mL) with the aid of sonication. This was then treated with 4 M HCl in dioxane (2 mL) with vigorously stirring for 3 hours. All the solvents were removed in vacuo. The resulting hydrochloride salt of the desired compound was triturated with diethyl ether (2 mL), then separated by filtration and dried to afford the title compound as a white powder. The resulting product was used for the next step without further purification (0.14 g, yield: 93%). **LC–MS:** *m/z* = 280 $[M+H]^+$.

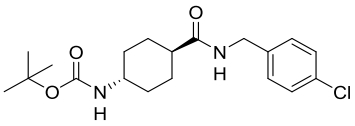
(1*R*,4*R*)-4-[2-(4-Chlorophenoxy)acetamido]-*N*-[2-(4-chlorophenyl)ethyl]cyclohexane-1-carboxamide (62c)



Following general procedure A, (1*R*,4*R*)-4-amino-*N*-[2-(4-chlorophenyl)ethyl]cyclohexane-1-carboxamide hydrochloride **62b** (0.10 g, 0.30 mmol) and 4-chlorophenoxyacetylchloride (0.04 mL, 0.35 mmol) in DCM (5 mL) were

reacted for 1 hour. The resulting precipitate was further purified by triturated with diethyl ether (3 mL), then separated by filtration and dried in vacuo to afford the title compound as a white powder (0.12 g, yield: 89%). **^{1}H NMR (400 MHz, DMSO-*d*$_6$)**: δ 7.94 (d, *J*=8.1 Hz, 1H, amide N*H*), 7.80 (t, *J*=5.5 Hz, 1H, amide N*H*), 7.35 (dd, *J*=2.7, 2.1 Hz, 4H, Ar C-*H ortho* to chlorine), 77.21 (d, *J*=8.3 Hz, 2H, Ar C-*H*), 6.97 (d, *J*=8.9 Hz, 2H, Ar C-*H ortho* to phenoxy), 4.45 (s, 2H, C*H*$_2$OAr), 3.55 (bs, 1H, ^{C}Hx C*H*), 3.24 (q, *J*=6.5 Hz, 2H, C*H*$_2$CH$_2$), 2.69 (t, *J*=7.0 Hz, 2H, C*H*$_2$Ar), 2.01 (t, *J*=11.8 Hz, 1H, ^{C}Hx C*H*), 1.78 (dd, *J*=9.8, 11.7 Hz, 4H, ^{C}Hx C*H*$_2$), 1.37 (dq, *J*=12.1, 11.6 Hz, 4H, ^{C}Hx C*H*$_2$). **^{13}C NMR (DMSO)**: δ 175.1 (invers amide *C*=O), 166.7 (amide *C*=O), 157.1 (Ar 4º C-phenoxy), 139.0 (Ar 4º *C*-CH$_2$), 131.0 (Ar 4º C-chlorine), 129.6, 128.6 (2 x Ar C-*H*), 125.2 (Ar 4º C-chlorine), 116.9 (Ar *C*-H *ortho* to phenoxy), 67.6 (*C*H$_2$OAr), 47.6 (^{C}Hx *C*H), 43.5 (*C*H$_2$CH$_2$), 34.8 (^{C}Hx *C*H), 31.8, 28.6 (2 x ^{C}Hx *C*H$_2$). **HPLC:** t_R 2.91 min (96%). **HRMS:** *m/z* theoretical for $C_{23}H_{27}Cl_2N_2O_3$ 449.1393 $[M+H]^+$, measured 449.1383 $[M+H]^+$. **M.p.:** 266-269°C.

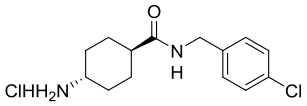
***tert*-Butyl-*N*-[(1*R*,4*R*)-4-{[(4-chlorophenyl)methyl] carbamoyl}cyclohexyl]carbamate (63a)**



Following general procedure D, *trans*-4-(boc-amino) cyclohexanecarboxylic acid **51** (0.17 g, 0.7 mmol) was reacted with HBTU (0.27 g, 0.77 mmol), 4-chlorobenzylamine (0.11 g, 0.77 mmol) and triethylamine (0.12 mL, 1 mmol) in DMF (10 mL) for 16 hours. After concentration of the organic layer, purification was achieved via column chromatography (eluent DCM/EtoAC 10:90, 20:80, then 30:70) to give the desired product as a solid. The resulting solid was further purified by triturated with diethyl ether (3 mL), then separated by filtration and dried in

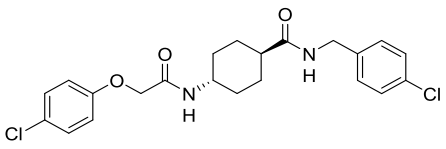
vacuo to afford the title compound as a white powder (0.22 g, yield: 86%). **^{1}H NMR (400 MHz, DMSO-d_6):** δ 8.29 (t, *J*=6.0 Hz, 1H, invers amide N*H*), 7.35 (t, *J*=7.7 Hz, 1H, amide N*H*), 7.28 (d, *J*=13.6 Hz, 2H, Ar C-*H ortho* to chlorine), 7.18 (d, *J*=7.5 Hz, 1H, Ar C-*H ortho* to phenoxy), 6.71 (d, *J*=7.9 Hz, 1H, Ar C-*H ortho* to phenoxy), 4.25 (d, *J*=5.9 Hz, 2H, CH_2Ar), 3.16 (bs, 1H, ^{C}Hx C*H*), 2.09 (t, *J*=12.0 Hz, 1H, ^{C}Hx C*H*), 1.83 (dd, *J*=8.8, 10.2 Hz, 4H, ^{C}Hx CH_2), 1.44 (d, *J*=10.5 Hz, 2H, ^{C}Hx CH_2), 1.38 (s, 9H, C(CH_3)$_3$), 1.14 (q, *J*=11.6 Hz, 2H, ^{C}Hx CH_2). **^{13}C NMR (DMSO)**: δ 175.4 (invers amide *C*=O), 155.2 (amide *C*=O), 142.9 (Ar 4º *C*), 133.4(Ar *C*-H), 130.6 (Ar 4º C-chlorine), 127.2, 126.1(Ar *C*-H *ortho* to chlorine), 77.8 (Boc 4º C), 49.1 (^{C}Hx *C*H), 43.6 (*C*H$_2$Ar), 41.7 (^{C}Hx *C*H), 32.3 (Boc *C*H$_3$), 28.7 (^{C}Hx *C*H$_2$). **HPLC:** t_R 2.69 min (96%). **LC-MS:** *m/z* = 367 $[M+H]^+$.

(1*R*,4*R*)-4-Amino-*N*-[(4-chlorophenyl)methyl]cyclohexane-1-carboxamide hydrochloride (63b)



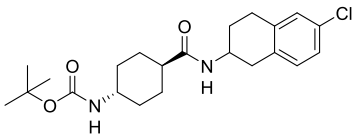
A suspension of *tert*-butyl-*N*-[(1*R*,4*R*)-4-{[(4-chlorophenyl)methyl] carbamoyl}cyclohexyl]carbamate **63a** (0.18 g, 0.5 mmol) was dissolved in dioxane–MeOH (2:1; 3 mL) with the aid of sonication. This was then treated with 4 M HCl in dioxane (2 mL) with vigorously stirring for 2 hours. All the solvents were removed in vacuo. The resulting hydrochloride salt of the desired compound was triturated with diethyl ether (2 mL), then separated by filtration and dried to afford the title compound as a white powder. The resulting product was used for the next step without further purification (0.14 g, yield: 95%). **LC–MS:** *m/z* = 268 $[M+H]^+$.

(1*R*,4*R*)-4-[2-(4-Chlorophenoxy)acetamido]-*N*-[(4-chlorophenyl)methyl]cyclohexane-1-carboxamide (63c)



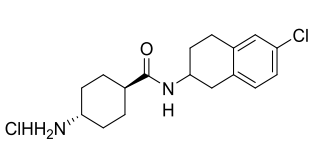
Following general procedure A, (1*R*,4*R*)-4-amino-*N*-[(4-chlorophenyl)methyl]cyclohexane-1-carboxamide hydrochloride **63b** (0.09 g, 0.30 mmol) and 4-chlorophenoxyacetylchloride (0.04 mL, 0.35 mmol) in DCM (5 mL) were reacted for 3 hour. The resulting precipitate was further purified by triturated with diethyl ether (3 mL), then separated by filtration and dried in vacuo to afford the title compound as a white powder (0.11 g, yield: 91%).**^{1}H NMR (400 MHz, DMSO-*d*$_6$)**: δ 8.33 (t, *J*=5.7 Hz, 1H, invers amide N*H*), 7.95 (d, *J*=8.0 Hz, 1H, amide N*H*), 7.37 (d, *J*=2.0 Hz, 2H, Ar C-*H ortho* to chlorine), 7.33 (s, 1H, Ar C-*H*), 7.28 (d, *J*=11.2 Hz, 2H, Ar C-*H ortho* to chlorine), 7.20 (d, *J*=7.3 Hz, 1H, Ar C-*H*), 6.98 (d, *J*=8.9 Hz, 2H, Ar C-*H ortho* to phenoxy), 4.46 (s, 2H, C*H*$_2$OAr), 4.26 (d, *J*=5.7 Hz, 2H, C*H*$_2$Ar), 3.59 (bs, 1H, ^{C}Hx C*H*), 2.14 (t, *J*=11.7 Hz, 1H, ^{C}Hx C*H*), 1.80 (d, *J*=10.0 Hz, 4H, ^{C}Hx C*H*$_2$), 1.45 (dq, *J*=11.9, 11.5 Hz, 4H, ^{C}Hx C*H*$_2$). **^{13}C NMR (DMSO)**: δ 175.3 (invers amide *C*=O), 166.7 (amide *C*=O), 157.1 (Ar 4º *C*-phenoxy), 142.9 (Ar 4º *C*), 133.4 (Ar C-*H*), 130.6 (Ar *C*-H *ortho* to chlorine), 129.6 (Ar 4º C-chlorine), 127.2, 127.0 (Ar C-*H*), 126.1 (Ar 4º C-chlorine), 125.2 (Ar C-*H*), 117.0 (Ar *C*-H *ortho* to phenoxy), 67.6 (*C*H$_2$OAr), 47.6 (^{C}Hx *C*H), 43.5 (*C*H$_2$Ar), 41.7 (^{C}Hx *C*H), 31.8 (^{C}Hx *C*H$_2$), 28.7 (^{C}Hx *C*H$_2$). **HPLC:** t_R 3.02 min (96%). **HRMS:** *m/z* theoretical for $C_{22}H_{25}Cl_2N_2O_3$ 435.1237 $[M+H]^+$, measured 435.1240 $[M+H]^+$. **M.p.:** 242-245°C.

tert-Butyl*N*-[(1*R*,4*R*)-4-[(6-chloro-1,2,3,4-tetrahydronaphthalen-2-yl)carbamoyl]cyclohexyl]carbamate (64a)



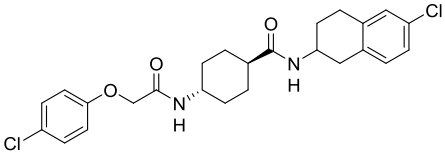
Following general procedure D, *trans*-4-(boc-amino) cyclohexanecarboxylic acid **51** (0.17 g, 0.7 mmol) was reacted with HBTU (0.27 g, 0.77 mmol), 2-amino-6-chloro-1,2,3,4-tetrahydronaphthalene (0.14 g, 0.77 mmol) and triethylamine (0.12 mL, 1 mmol) in DMF (10 mL) for 19 hours. After concentration of the organic layer, purification was achieved via column chromatography (eluent DCM/EtoAC 10:90, 20:80, then 30:70) to give the desired product as a solid. The resulting solid was further purified by triturated with diethyl ether (3 mL), then separated by filtration and dried in vacuo to afford the title compound as a white powder (0.26 g, yield: 92%). **^{1}H NMR (400 MHz, DMSO-d_6)** δ 7.78 (d, *J*=7.5 Hz, 1H, invers amide N*H*), 7.14 (dd, *J*=9.5, 8.1 Hz, 3H, Ar C-*H*), 6.70 (d, *J*=7.9 Hz, 1H, amide N*H*), 3.91 (bs, 1H, ^{C}Hx C*H*), 3.19 (bs, 1H, ^{C}Hx C*H*), 2.94 (dd, *J*=5.1, 5.1 Hz, 1H, ^{C}Hx CH_2), 2.87 - 2.75 (m, 2H, ^{C}Hx CH_2), 2.56 (d, *J*=9.2 Hz, 1H, ^{C}Hx CH_2), 2.02 (t, *J*=12.0 Hz, 1H, ^{C}Hx C*H*), 1.89 (dd, *J*=3.6, 3.5 Hz, 1H, ^{C}Hx CH_2), 1.79 (dd, *J*=10.7, 13.1 Hz, 4H, ^{C}Hx CH_2), 1.64 - 1.52 (m, 1H, ^{C}Hx CH_2), 1.43 (d, *J*=3.5 Hz, 1H, ^{C}Hx CH_2), 1.37 (s, 9H, C(CH_3)$_3$), 1.31 (d, *J*=3.7 Hz, 1H, ^{C}Hx CH_2), 1.12 (q, *J*=11.9 Hz, 2H, ^{C}Hx CH_2). **^{13}C NMR (DMSO)** δ 174.8 (invers amide *C*=O), 155.2 (amide *C*=O), 138.5, 134.3 (2 x Ar 4º C), 131.3 (Ar 4º C-chlorine), 130.5, 128.5, 125.9 (3 x Ar *C*-H), 77.7 (Boc 4º C), 49.1, 44.5, 43.5 (3 x ^{C}Hx *C*H), 34.8, 32.3, 28.7 (3 x ^{C}Hx *C*H$_2$), 28.5 (Boc *C*H$_3$), 27.5 (*C*H$_2$CH$_2$). **HPLC:** t_R 3.04 min (96%). **LC-MS:** *m/z* = 407 $[M+H]^+$.

(1*R*,4*R*)-4-Amino-*N*-(6-chloro-1,2,3,4-tetrahydronaphthalen-2-yl)cyclohexane-1-carboxamide hydrochloride (64b)



A suspension of *tert*-butyl*N*-[(1*R*,4*R*)-4-[(6-chloro-1,2,3,4-tetrahydronaphthalen-2-yl)carbamoyl]cyclohexyl]carbamate **64a** (0.20 g, 0.5 mmol) was dissolved in dioxane–MeOH (2:1; 3 mL) with the aid of sonication. This was then treated with 4 M HCl in dioxane (2 mL) with vigorously stirring for 2 hours. All the solvents were removed in vacuo. The resulting hydrochloride salt of the desired compound was triturated with diethyl ether (2 mL), then separated by filtration and dried to afford the title compound as a white powder. The resulting product was used for the next step without further purification (0.15 g, yield: 90%). **LC–MS:** *m/z* = 307 $[M+H]^+$.

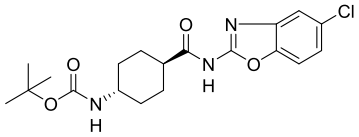
(1*R*,4*R*)-*N*-(6-Chloro-1,2,3,4-tetrahydronaphthalen-2-yl)-4-[2-(4-chlorophenoxy)acetamido]cyclohexane-1-carboxamide (64c)



Following general procedure A, (1*R*,4*R*)-4-amino-*N*-(6-chloro-1,2,3,4-tetrahydronaphthalen-2-yl)cyclohexane-1-carboxamide hydrochloride **64b** (0.15 g, 0.45 mmol) and 4-chlorophenoxyacetylchloride (0.06 mL, 0.5 mmol) in DCM (5 mL) were reacted for 3 hour. The resulting precipitate was further purified by triturated with diethyl ether (3 mL), then separated by filtration and dried in vacuo to afford the title compound as a white powder (0.16 g, yield: 79%). **^{1}H NMR (400 MHz, DMSO-*d*$_6$)** δv7.96 (d, *J*=8.1 Hz, 1H, invers amide N*H*), 7.81 (d, *J*=7.4 Hz, 1H, amide N*H*), 7.34 (d, *J*=8.9 Hz, 2H, Ar C-*H ortho* to chlorine), 7.14 (dd, *J*=9.5, 8.9 Hz, 3H, Ar C-*H*), 6.97 (d, *J*=8.9 Hz, 2H, Ar C-*H ortho* to phenoxy), 4.45 (s, 2H,

C*H*$_2$OAr), 3.91 (bs, 1H, ^{C}Hx C*H*), 3.57 (bs, 1H, ^{C}Hx C*H*), 2.95 (dd, *J*=4.8, 4.9 Hz, 1H, ^{C}Hx C*H*$_2$), 2.87 - 2.75 (m, 2H, ^{C}Hx C*H*$_2$), 2.57 (d, *J*=9.2 Hz, 1H, ^{C}Hx C*H*$_2$), 2.08 (t, *J*=11.7 Hz, 1H, ^{C}Hx C*H*), 1.89 (d, *J*=9.0 Hz, 1H, ^{C}Hx C*H*$_2$), 1.76 (t, *J*=12.4 Hz, 4H, ^{C}Hx C*H*$_2$), 1.67 - 1.54 (m, 1H, ^{C}Hx C*H*$_2$), 1.42 (dq, *J*=12.2, 11.5 Hz, 4H, ^{C}Hx C*H*$_2$). **^{13}C NMR (DMSO)** δ 174.7 (invers amide *C*=O), 166.7 (amide *C*=O), 157.1 (Ar 4º C-phenoxy), 138.5, 134.3 (2 x Ar 4º C), 131.3 (Ar 4º C-chlorine), 130.5, 129.6, 128.5, 125.9 (4 x Ar *C*-H), 125.2 (Ar 4º C-chlorine), 117.0 (Ar *C*-H *ortho* to phenoxy), 67.6 (*C*H$_2$OAr), 47.6, 44.6, 43.4 (3 x ^{C}Hx *C*H), 34.8, 31.8, 28.6, 28.5, 27.6 (5 x ^{C}Hx *C*H$_2$). **HPLC:** t_R 3.15 min (96%). **HRMS:** *m/z* theoretical for $C_{25}H_{29}Cl_2N_2O_3$ 475.1550 $[M+H]^+$, measured 475.1554 $[M+H]^+$. **M.p.:** 265-269°C.

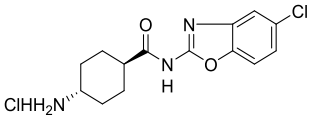
***tert*-Butyl*N*-[(1*R*,4*R*)-4-[(5-chloro-1,3-benzoxazol-2-yl)carbamoyl]cyclohexyl]carbamate (65a)**



Following general procedure D, *trans*-4-(boc-amino) cyclohexanecarboxylic acid **51** (0.17 g, 0.7 mmol) was reacted with HBTU (0.27 g, 0.77 mmol), 2-amino-5-chlorobenzoxazole (0.13 g, 0.77 mmol) and triethylamine (0.12 mL, 1 mmol) in DMF (10 mL) for overnight. After concentration of the organic layer, purification was achieved via column chromatography (eluent DCM/EtoAC 10:90, 20:80, then 30:70) to give the desired product as a solid. The resulting solid was further purified by triturated with diethyl ether (3 mL), then separated by filtration and dried in vacuo to afford the title compound as a white powder (0.2 g, yield: 72%). **^{1}H NMR (400 MHz, DMSO-*d*$_6$)** δ 11.67 (s, 1H, invers amide N*H*), 7.66 (d, *J*=2.5 Hz, 1H, Ar C-*H*), 7.63 (s, 1H, amide N*H*), 7.31 (dd, *J*=2.1, 2.1 Hz, 1H, Ar C-*H*), 6.75 (d, *J*=7.9 Hz, 1H, Ar C-*H*), 3.19

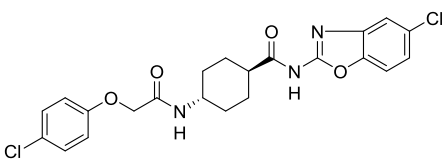
(bs,1H, ^{C}Hx C*H*), 2.43 (t, *J*=11.8 Hz, 1H, ^{C}Hx C*H*), 1.87 (t, *J*=14.6 Hz, 4H, ^{C}Hx CH_2), 1.44 (d, *J*=12.7 Hz, 2H, ^{C}Hx CH_2), 1.39 (s, 9H, C(CH_3)$_3$), 1.19 (q, *J*=12.4 Hz, 2H, ^{C}Hx CH_2). **^{13}C NMR (DMSO)** δ 173.7 (invers amide *C*=O), 156.9 (amide *C*=O), 155.2 (4º C=N), 146.8 (Ar 4º C), 129.1 (Ar 4º C-chlorine), 123.7, 118.3, 111.7 (3 x Ar *C*-H), 77.8 (Boc 4º C), 48.9, 43.8 (2 x ^{C}Hx *C*H), 32.0 (Boc *C*H_3), 28.7, 28.2 (2 x ^{C}Hx *C*H_2). **HPLC:** $^{t}_{R}$ 2.86 min (96%). **LC-MS:** *m/z* = 394 $[M+H]^+$.

(1*R*,4*R*)-4-Amino-*N*-(5-chloro-1,3-benzoxazol-2-yl)cyclohexane-1-carboxamide hydrochloride (65b)



A suspension of *tert*-butyl*N*-[(1*R*,4*R*)-4-[(5-chloro-1,3-benzoxazol-2-yl)carbamoyl]cyclohexyl]carbamate **65a** (0.2 g, 0.5 mmol) was dissolved in dioxane–MeOH (2:1; 3 mL) with the aid of sonication. This was then treated with 4 M HCl in dioxane (2 mL) with vigorously stirring for 2 hours. All the solvents were removed in vacuo. The resulting hydrochloride salt of the desired compound was triturated with diethyl ether (2 mL), then separated by filtration and dried to afford the title compound as a white powder. The resulting product was used for the next step without further purification (0.15 g, yield: 95%). **LC–MS:** *m/z* = 295 $[M+H]^+$.

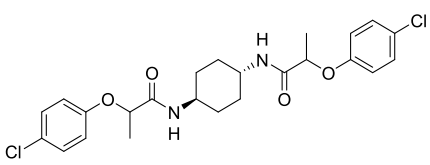
(1*R*,4*R*)-*N*-(5-Chloro-1,3-benzoxazol-2-yl)-4-[2-(4-chlorophenoxy)acetamido]cyclohexane-1-carboxamide (65c)



Following general procedure A, (1*R*,4*R*)-4-amino-*N*-(5-chloro-1,3-benzoxazol-2-yl)cyclohexane-1-carboxamide

hydrochloride **65b** (0.14 g, 0.45 mmol) and 4-chlorophenoxyacetylchloride (0.06 mL, 0.5 mmol) in DCM (5 mL) were reacted for 3 hour. The resulting precipitate was further purified by triturated with diethyl ether (3 mL), then separated by filtration and dried in vacuo to afford the title compound as a white powder (0.14 g, yield: 69%). **^{1}H NMR (400 MHz, DMSO-d_6)** δ 7.97 (dd, *J*=8.2, 8.1 Hz, 1H, amide N*H*), 7.65 (d, *J*=8.5 Hz, 1H, amide N*H*), 7.36 (dd, *J*=3.7, 3.7 Hz, 3H, Ar C-*H*), 7.31 (dd, *J*=2.1, 2.1 Hz, 1H, Ar C-*H*), 6.99 (dd, *J*=5.3, 5.4 Hz, 3H, Ar C-*H*), 4.46 (d, *J*=6.2 Hz, 2H, CH_2OAr), 3.69 - 3.52 (m, 1H, ^{C}Hx C*H*), 2.02 (t, *J*=11.0 Hz, 1H, ^{C}Hx C*H*), 1.93 (dd, *J*=9.8, 9.9 Hz, 4H, ^{C}Hx CH_2), 1.55 - 1.19 (m, 4H, ^{C}Hx CH_2). **^{13}C NMR (DMSO)** δ 166.8 (amide *C*=O), 157.1 (Ar 4º C-phenoxy), 129.6 (Ar *C*-H *ortho* to chlorine), 129.1 (Ar 4º C-chlorine), 125.2 (Ar 4º C-chlorine), 123.8, 118.3, 117.0, 111.7 (4 x Ar *C*-H), 67.6 (*C*H_2OAr), 47.6 (^{C}Hx *C*H), 47.4 (^{C}Hx *C*H), 43.8, 43.3, 31.8, 31.5, 28.6, 28.1 (6 x ^{C}Hx *C*H_2). **HPLC:** ^tR 2.90 min (96%). **HRMS:** *m/z* theoretical for $C_{25}H_{22}Cl_2N_3O_4$ 462.0982 $[M+H]^+$, measured 462.0984 $[M+H]^+$. **M.p.:** 220-224°C.

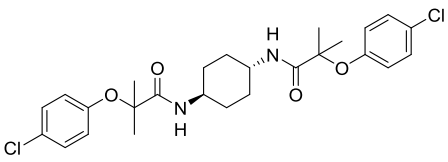
_N_-[(1_R_,4_R_)-4-{2-[4-(Chloromethyl)phenoxy]propanamido}cyclohexyl]-2-[4-(chloromethyl)phenoxy]propenamide (66)



Following general procedure E, 2-(4-chlorophenoxy)propanoic acid (0.11 g, 0.5 mmol) was reacted with HBTU (0.21 g, 0.55 mmol), *trans*-1,4-cyclohexandiamine **45** (0.025 g, 0.22 mmol) and triethylamine (0.18 mL, 1.5 mmol) in DMF (10 mL) for overnight. The resulting solid was further purified by triturated with diethyl ether (3 mL), then separated by filtration and dried in vacuo to afford the title compound as a beige powder (0.08 g, yield: 68%). **^{1}H NMR (400 MHz, DMSO-d_6)**: δ 8.04 (d, *J* = 8.0 Hz, 2H, amide

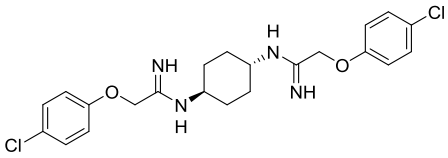
N*H*), 7.64 (d, *J* = 8.5 Hz, 4H, Ar C-*H ortho* to chlorine), 7.04 (d, *J* = 8.5 Hz, 4H, Ar C-*H ortho* to phenoxy), 4.75 (q, *J* = 6.4 Hz, 2H, C*H*OAr), 3.49 (bs, 2H, ^{C}Hx C*H*), 1.70 (dd, *J* = 6.5, 7.6 Hz, 4H, ^{C}Hx CH_2), 1.43 (d, *J* = 6.5 Hz, 6H, CH_3), 1.36 – 1.13 (m, 4H, ^{C}Hx CH_2). **^{13}C NMR (DMSO)**: δ 166.6 (amide *C*=O), 161.1 (Ar 4º C-phenoxy), 127.3 (Ar *C*-H *ortho* to chlorine), 127.3 (Ar 4º C-chlorine), 115.7 (Ar *C*-H *ortho* to phenoxy), 67.4 (CH_2OAr), 47.4 (^{C}Hx *C*H), 31.3 (^{C}Hx CH_2), 18.2 (CH_3). **HPLC:** t_R 3.08 min (>95%). **LC-MS:** *m/z* = 479 $[M+H]^+$. **M.p.:** 260-263 °C.

2-(4-Chlorophenoxy)-2-methyl-*N*-[(1*R*,4*R*)-4-[2-(4-chlorophenoxy)-2-methylpropanamido]cyclohexyl]propenamide (67)



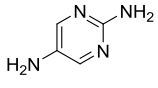
Following general procedure E, 2-(4-chlorophenoxy)-2-methylpropanoic acid (0.1 g, 0.5 mmol) was reacted with HBTU (0.21 g, 0.55 mmol), *trans*-1,4-cyclohexandiamine **45** (0.03 g, 0.22 mmol) and triethylamine (0.18 mL, 1.5 mmol) in DMF (10 mL) for overnight. The resulting solid was further purified by triturated with diethyl ether (3 mL), then separated by filtration and dried in vacuo to afford the title compound as a white powder (0.06 g, yield: 57%). **^{1}H NMR (400 MHz, DMSO-d_6):** δ 7.86 (d, *J* = 8.4 Hz, 2H, amide N*H*), 7.31 (d, *J* = 8.9 Hz, 4H, Ar C-*H ortho* to chlorine), 6.86 (d, *J* = 8.9 Hz, 4H, Ar C-*H ortho* to phenoxy), 3.53 (bs, 2H, ^{C}Hx C*H*), 1.64 (d, *J* = 5.9 Hz, 4H, ^{C}Hx CH_2), 1.39 (s, 12H, CH_3), 1.31 (t, *J* = 9.9 Hz, 4H, ^{C}Hx CH_2). **^{13}C NMR (DMSO)**: δ 172.6 (amide *C*=O), 154.2 (Ar 4º C-phenoxy), 129.4 (Ar *C*-H *ortho* to chlorine), 126.3 (Ar 4º C-chlorine), 121.8 (Ar *C*-H *ortho* to phenoxy), 80.9 (4º *C*-$(CH_3)_2$), 47.6 (^{C}Hx *C*H), 31.1 (^{C}Hx *C*H_2), 25.3 (CH_3). **HPLC:** t_R 3.12 min (>95%). **LC-MS:** *m/z* = 507 $[M+H]^+$. **M.p.:** 222-224 °C.

2-(4-Chlorophenoxy)-*N*-[(1*R*,4*R*)-4-[2-(4-chlorophenoxy)ethanimidamido]cyclohexyl]ethanimidamide (68)



To a stirred solution of *trans*-1,4-diaminocyclohexane **45** (0.05 g, 0.4 mmol) in ethanol (1 mL) were added DIPEA (0.16 mL, 1 mmol) and ethyl 2-(4-chlorophenoxy)ethanecarboximidate **58** (0.20 g, 1 mmol). The mixture was stirred for overnight at ambient temperature. After concentration, the resulting crude material was dissolved in methanol (5 mL) and resuspended with diethyl ether (10 mL), then separated by filtration and dried in vacuo to afford the title product as a light beige powder (0.11 g, yield: 63%).**^{1}H NMR (400 MHz, DMSO-d_6)**: δ 9.69 (s, 4H, amidine N*H*), 7.40 (d, *J*=8.9 Hz, 4H, Ar C-*H ortho* to chlorine), 7.06 (d, *J*=8.8 Hz, 4H, Ar C-*H ortho* to phenoxy), 5.00 (s, 4H, CH_2OAr), 3.38 (bs, 2H, ^{C}Hx C*H*), 1.89 (d, *J*=6.1 Hz, 4H, ^{C}Hx CH_2), 1.54 (t, *J*=8.8 Hz, 4H, ^{C}Hx CH_2). **^{13}C NMR (DMSO)**: δ 162.1 (amidine *C*=O), 156.65, 155.3 (Ar 4º C-phenoxy), 129.2, 128.9 (Ar *C*-H *ortho* to chlorine), 126.7 (Ar 4º C-chlorine), 115.5 (Ar *C*-H), 67.1, 66.0 (*C*H_2OAr), 55.9, 47.9 (^{C}Hx *C*H), 30.2, 29.6(^{C}Hx *C*H_2). **HPLC:** t_R 2.02 min (>95%). **LC-MS:** *m/z* = 450 $[M+H]^+$. **M.p.:** 225-228°C.

Pyrimidine-2,5-diamine (70)



In a round bottom flask, 5-Nitropyrimidin-2-amine **69** (0.28 g, 2 mmol) was dissolved in methanol (5 mL) and hydrogenated over palladium on carbon (0.2 g). The resulting mixture was stirred overnight at ambient temperature under atmospheric pressure. The suspension was filtered over celite and washed with excess MeOH. The resulting solution was concentrated under the vacuum to afforded the title compound as a light-yellow

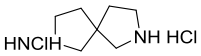
powder. The resulting product was used for the next step without further purification (0.17 g, yield: 77%).

3,9-Diazaspiro[5.5]undecane dihydrochloride (72)



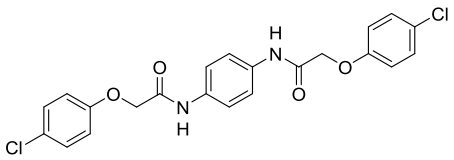
A suspension of *tert*-butyl 3,9-diazaspiro[5.5]undecane-3-carboxylate **71** (0.15 g, 0.6 mmol) was dissolved in dioxane–MeOH (2:1; 3 mL). This was then treated with 4 M HCl in dioxane (2 mL) with vigorously stirring for 1 hours. The reaction monitored by TLC, then all the solvents were removed in vacuo. The resulting hydrochloride salt of the desired compound was as dissolved in methanol (1mL) and then recrystalized with diethyl ether (2 mL), then separated by filtration and dried to afford the title compound as a white powder. The resulting product was used for the next step without further purification (0.11 g, yield: 87%).

2,7-Diaza-spiro[4.4]nonane dihydrochloride (74)



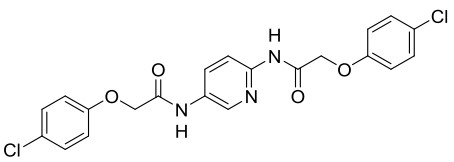
A suspension of *tert*-butyl 2,7-diazaspiro[4.4]nonane-2-carboxylate **73** (0.1 g, 0.44 mmol) was dissolved in dioxane–MeOH (2:1; 3 mL). This was then treated with 4 M HCl in dioxane (2 mL) with vigorously stirring for 1 hours. The reaction monitored by TLC, then all the solvents were removed in vacuo. The resulting hydrochloride salt of the desired compound was as dissolved in methanol (1mL) and then recrystalized with diethyl ether (2 mL), then separated by filtration and dried to afford the title compound as a white powder. The resulting product was used for the next step without further purification (0.08 g, yield: 96%).

2-(4-Chlorophenoxy)-*N*-{4-[2-(4-chlorophenoxy)acetamido]phenyl}acetamide (75)[167]



Following general procedure C, benzene-1,4-diamine (0.07 g, 0.4 mmol) and 4-chlorophenoxyacetyl chloride **26** (0.14 mL, 0.88 mmol) in DCM (5 mL) were reacted for 1 hour. The resulting precipitate was further purified by triturated with diethyl ether (3 mL), then separated by filtration and dried in vacuo to afford the title compound as a beige powder (0.14 g, yield: 76%). **^{1}H NMR (400 MHz, DMSO-*d*$_6$)** δ 10.22 (s, 2H, amide N*H*), 7.58 (s, 4H, Ar C-*H*), 7.35 (d, *J*= 9.7 Hz, 4H, Ar C-*H ortho* to chlorine), 7.03 (d, *J*= 6.8 Hz, 4H, Ar C-*H ortho* to phenoxy), 4.71 (s, 4H, C*H*$_2$OAr). **^{13}C NMR (DMSO)** δ 166.4 (amide *C*=O), 157.2 (Ar 4º C-phenoxy), 134.7 (Ar 4º C), 129.7 (Ar *C*-H *ortho* to chlorine), 125.3 (Ar 4º C-chlorine), 120.5 (Ar *C*-H), 116.9 (Ar *C*-H *ortho* to phenoxy), 67.7 (*C*H$_2$OAr). **HPLC:** $^{t}_{R}$ 3.06 min (96%) **LC-MS:** *m/z* = 445 $[M+H]^+$.. **M.p.:** 261-265°C.

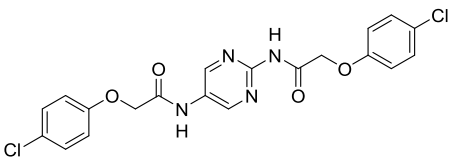
2-(4-Chlorophenoxy)-*N*-{5-[2-(4-chlorophenoxy)acetamido]pyridin-2-yl}acetamide (76)



Following general procedure C, 2,5-diaminopyridine dihydrochloride (0.14 g, 0.8 mmol) and 4-chlorophenoxyacetyl chloride **26** (0.24 mL, 1.6 mmol) in DCM (10 mL) were reacted for 2 hours. The resulting precipitate was further purified by triturated with diethyl ether (3 mL), then separated by filtration and dried in vacuo to afford the title compound as a burgundy powder (0.30 g, yield: 85%). **^{1}H NMR (400 MHz, DMSO-*d*$_6$)** δ 10.53 (s, 1H, amide N*H*), 10.26 (s, 1H, amide N*H*), 8.62 (t, *J*=1.4 Hz, 1H, pyridine C-*H*), 8.00 (d, *J* = 2.3 Hz, 2H, pyridine C-*H*), 7.36 (t, *J* = 8.6 Hz, 4H, Ar C-*H ortho* to chlorine), 7.02 (dd, *J* = 9.0, 9.0 Hz, 4H, Ar C-*H ortho* to phenoxy), 4.79 (s,

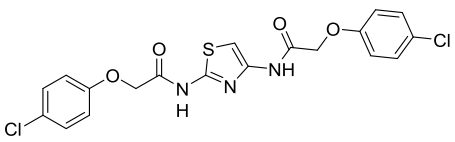
2H, C*H*$_2$OAr), 4.73 (s, 2H, C*H*$_2$OAr). **^{13}C NMR (DMSO)** δ 167.0 (amide *C*=O), 157.1 (Ar 4º C-phenoxy), 147.64, 140.1 (2 x pyridine 4º C), 131.8 (pyridine C-*H*), 129.7 (Ar *C*-H *ortho* to chlorine), 125.2 (Ar 4º C-chlorine), 116.8 (Ar *C*-H *ortho* to phenoxy), 114.0 (pyridine C-*H*), 67.7, 67.2 (2 x *C*H$_2$OAr). **HPLC:** $^{t}_{R}$ 3.01 min (>95%). **LC-MS:** *m/z* = 446 $[M+H]^+$. **M.p.:** 227-230 °C.

2-(4-Chlorophenoxy)-*N*-{5-[2-(4-chlorophenoxy)acetamido]pyrimidin-2-yl}acetamide (77)



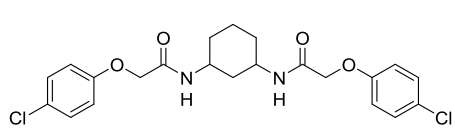
Following general procedure C, pyrimidine-2,5-diamine **70** (0.11 g, 1 mmol) and 4-chlorophenoxyacetyl chloride (0.32 mL, 2 mmol) in DCM (10 mL) were reacted for 2 hours. The resulting precipitate was further purified by triturated with diethyl ether (3 mL), then separated by filtration and dried in vacuo to afford the title compound as a white powder (0.30 g, yield: 77%). **^{1}H NMR (400 MHz, DMSO-d_6)** δ10.79 (s, 1H, amide N*H*), 10.43 (s, 1H, amide N*H*), 8.91 (s, 2H, Pyrimidine C-*H*), 7.39 (dd, *J*= 9.0, 9.0 4H, Ar C-*H ortho* to chlorine), 7.07 (dd, *J*= 9.0, 9.0, 4H, Ar C-*H ortho* to phenoxy), 4.97 (s, 2H, C*H*$_2$OAr), 4.78 (s, 2H, C*H*$_2$OAr). **^{13}C NMR (DMSO)** δ 167.5 (amide *C*=O), 157.3 (Ar 4º C-phenoxy), 157.0 (Ar 4º C-phenoxy), 153.6 (pyrimidine C-*H*), 150.1 (pyrimidine 4º C), 129.7, 129.6 (2 x Ar *C*-H *ortho* to chlorine), 125.6, 125.1 (2 x Ar 4º C-chlorine), 117.1, 116.8 (2 x Ar *C*-H *ortho* to phenoxy), 67.8, 67.6 (2 x *C*H$_2$OAr). **HPLC:** $^{t}_{R}$ 2.88 min (>95%). **LC-MS:** *m/z* = 447 $[M+H]^+$. **M.p.:** 200-204 °C.

2-(4-Chlorophenoxy)-*N*-{4-[2-(4-chlorophenoxy)acetamido]-1,3-thiazol-2-yl}acetamide (78)



Following general procedure C, 1,3-thiazole-2,4-diamine hydrochloride (0.12 g, 0.8 mmol) and 4-chlorophenoxyacetyl chloride **26** (0.24 mL, 1.6 mmol) in DCM (10 mL) were reacted for 2 hours. The resulting precipitate was further purified by triturated with diethyl ether (3 mL), then separated by filtration and dried in vacuo to afford the title compound as a beige powder (0.31 g, yield: 86%). **^{1}H NMR (400 MHz, DMSO-*d*$_6$)** δ 12.30 (s, 1H, amide N*H*), 10.74 (s, 1H, amide N*H*), 7.37 (dd, *J*=2.5, 2.5 Hz, 4H, Ar C-*H ortho* to chlorine), 7.14 (s, 1H, thiazol C-*H*), 7.01 (dd, *J*=5.6, 5.6 Hz, 4H, Ar C-*H ortho* to phenoxy), 4.90 (s, 2H, C*H*$_2$OAr), 4.77 (s, 2H, C*H*$_2$OAr). **^{13}C NMR (DMSO)** δ 167.3 (amide *C*=O), 166.2 (thiazol 4º C), 157.2, 155.7 (2 x Ar 4º C-phenoxy), 142.6 (thiazol 4º C), 129.7 (Ar *C*-H *ortho* to chlorine), 125.2 (Ar 4º C-chlorine), 116.8 (Ar *C*-H *ortho* to phenoxy), 95.9 (thiazol *C*-H), 67.1 (*C*H$_2$OAr), 66.7 (*C*H$_2$OAr). **HPLC:** $^{t}_{R}$ 2.68 min (>95%). **LC-MS:** *m/z* = 452 $[M+H]^+$. **M.p.:** 160-162 °C.

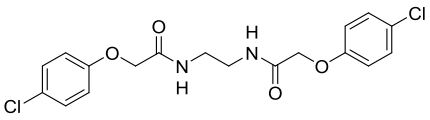
2-(4-Chlorophenoxy)-*N*-{3-[2-(4-chlorophenoxy)acetamido]cyclohexyl}acetamide (79)



Following general procedure C, 1,3-cyclohexanediamine (0.09 g, 0.8 mmol) and 4-chlorophenoxyacetyl chloride **26** (0.24 mL, 1.6 mmol) in DCM (10 mL) were reacted for 2 hours. The resulting precipitate was further purified by triturated with diethyl ether (3 mL), then separated by filtration and dried in vacuo to afford the title compound as a white powder (0.32 g, yield: 91%). **^{1}H NMR (400 MHz, DMSO-*d*$_6$)** δ 8.01 (d, *J*=8.0 Hz, 2H, amide N*H*), 7.35 (dd, *J*=2.6, 3.0 Hz, 4H, Ar C-*H ortho* to chlorine), 6.98 (dd, *J*=3.6, 3.7 Hz, 4H, Ar C-

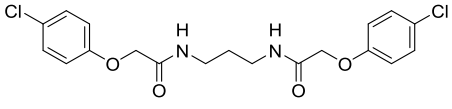
H ortho to phenoxy), 4.51 (s, 2H, C*H*$_2$OAr), 4.46 (s, 2H, C*H*$_2$OAr), 3.67 (bs, 2H, ^{C}Hx C*H*), 1.86 (dd, *J*=11.7, 8.9 Hz, 4H, ^{C}Hx C*H*$_2$), 1.41 - 1.09 (m, 4H, ^{C}Hx C*H*$_2$). **^{13}C NMR (DMSO)** δ 166.7 (amide *C*=O), 157.1 (Ar 4º C-phenoxy), 129.6 (Ar *C*-H *ortho* to chlorine), 125.2 (Ar 4º C-chlorine), 116.9 (Ar *C*-H *ortho* to phenoxy), 67.6 (*C*H$_2$OAr), 47.1 (^{C}Hx *C*H), 38.8, 31.7, 23.2 (3 x ^{C}Hx *C*H$_2$). **HPLC:** $^{t}_{R}$ 2.92 min (>95%). **LC-MS:** *m/z* = 451 $[M+H]^+$. **M.p.:** 185-188°C.

2-(4-Chlorophenoxy)-*N*-{2-[2-(4-chlorophenoxy)acetamido]ethyl}acetamide (80)



Following general procedure C, ethylenediamine (0.03 mL, 0.4 mmol) and 4-chlorophenoxyacetyl chloride **26** (0.12 mL, 0.8 mmol) in DCM (5 mL) were reacted for 2 hours. The resulting precipitate was further purified by triturated with diethyl ether (3 mL), then separated by filtration and dried in vacuo to afford the title compound as a white powder (0.13 g, yield: 83%). **^{1}H NMR (400 MHz, DMSO-*d*$_6$)** δ 8.20 (s, 2H, amide N*H*), 7.33 (d, *J* = 9.0 Hz, 4H, Ar C-*H ortho* to chlorine), 6.97 (d, *J* = 9.0 Hz, 4H, Ar C-*H ortho* to phenoxy), 4.46 (s, 4H, C*H*$_2$OAr), 3.28 (t, *J* = 2.6 Hz, 4H, C*H*$_2$C*H*$_2$). **^{13}C NMR (DMSO)** δ 168.2 (amide *C*=O), 157.0 (Ar 4º C-phenoxy), 129.7 (Ar *C*-H *ortho* to chlorine), 125.4 (Ar 4º C-chlorine), 117.0 (Ar *C*-H *ortho* to phenoxy), 67.6 (*C*H$_2$OAr), 38.6 (C*H*$_2$*C*H$_2$). **HPLC:** $^{t}_{R}$ 2.85 min (95%). **LC-MS:** *m/z* = 397 $[M+H]^+$. **M.p.:** 164-166 °C.

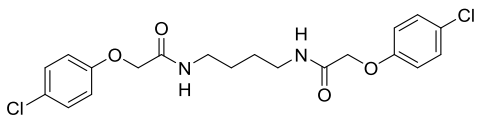
2-(4-Chlorophenoxy)-*N*-{3-[2-(4-chlorophenoxy)acetamido]propyl}acetamide (81)[151]



Following general procedure C, propane-1,3-diamine (0.03 mL, 0.4 mmol) and 4-

chlorophenoxyacetyl chloride **26** (0.12 mL, 0.8 mmol) in DCM (5 mL) were reacted for 2 hours. The resulting precipitate was further purified by triturated with diethyl ether (3 mL), then separated by filtration and dried in vacuo to afford the title compound as a white powder (0.13 g, yield: 81%). **^{1}H NMR (400 MHz, DMSO-*d*$_6$)** δ 8.25 (t, *J*=5.9 Hz, 2H, amide N*H*), 7.36 (dd, *J*=2.2, 2.3 Hz, 4H, Ar C-*H ortho* to chlorine), 7.00 (dd, *J*=2.3, 2.2 Hz, 4H, Ar C-*H ortho* to phenoxy), 4.49 (s, 4H, C*H*$_2$OAr), 3.13 (q, *J*=6.5 Hz, 4H, C*H*$_2$CH$_2$C*H*$_2$), 1.58 (t, *J*=6.8 Hz, 2H, CH$_2$C*H*$_2$CH$_2$). **^{13}C NMR (DMSO)** δ 167.8 (amide *C*=O), 157.0 (Ar 4º C-phenoxy), 129.6 (Ar *C*-H *ortho* to chlorine), 125.3 (Ar 4º C-chlorine), 117.0 (Ar *C*-H *ortho* to phenoxy), 67.6 (*C*H$_2$OAr), 36.2 (*C*H$_2$CH$_2$*C*H$_2$), 29.6 (*C*H$_2$CH$_2$). **HPLC:** ^tR 2.89 min (95%). **LC-MS:** *m/z* = 411 $[M+H]^+$. **M.p.:** 125-127 °C.

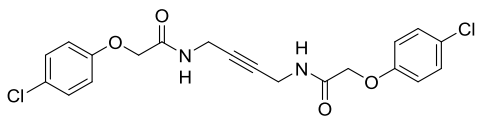
2-(4-Chlorophenoxy)-*N*-{4-[2-(4-chlorophenoxy)acetamido]butyl}acetamide (82)[151]



Following general procedure C, butane-1,4-diamine (0.04 mL, 0.4 mmol) and 4-chlorophenoxyacetyl chloride **26** (0.12 mL, 0.8 mmol) in DCM (5 mL) were reacted for 2 hours. The resulting precipitate was further purified by triturated with diethyl ether (3 mL), then separated by filtration and dried in vacuo to afford the title compound as a beige powder (0.13 g, yield: 76%). **^{1}H NMR (400 MHz, DMSO-*d*$_6$)** δ 8.21 (t, *J*=5.7 Hz, 2H, amide N*H*), 7.34 (dd, *J*=2.2, 2.2 Hz, 4H, Ar C-*H ortho* to chlorine), 6.98 (dd, *J*=2.2, 2.2 Hz, 4H, Ar C-*H ortho* to phenoxy), 4.47 (s, 4H, C*H*$_2$OAr), 3.10 (d, *J*=5.7 Hz, 4H, C*H*$_2$NH), 1.43 - 1.37 (m, 4H, C*H*$_2$C*H*$_2$). **^{13}C NMR (DMSO)** δ 167.6 (amide *C*=O), 157.1 (Ar 4º C-phenoxy), 129.6 (Ar *C*-H *ortho* to chlorine), 125.2 (Ar 4º C-chlorine), 117.0 (Ar *C*-H *ortho*

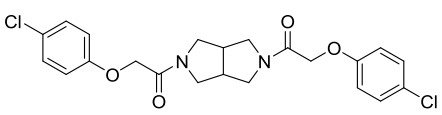
to phenoxy), 67.6 (*C*H_2OAr), 38.4 (*C*H_2NH), 26.9 (*C*$H_2$$CH_2$). **HPLC:** $^{t}_{R}$ 2.88 min (95%). **LC-MS:** *m/z* = 425 $[M+H]^+$. **M.p.:** 194-196 °C.

2-(4-Chlorophenoxy)-*N*-{4-[2-(4-chlorophenoxy)acetamido]but-2-yn-1-yl}acetamide (83)



Following general procedure C, but-2-yne-1,4-diamine dihydrochloride (0.06 g, 0.4 mmol) and 4-chlorophenoxyacetyl chloride **26** (0.12 mL, 0.8 mmol) in DCM (5 mL) were reacted for 2 hours. The resulting precipitate was further purified by triturated with diethyl ether (3 mL), then separated by filtration and dried in vacuo to afford the title compound as a white powder (0.13 g, yield: 80%). **^{1}H NMR (400 MHz, DMSO-d_6)** δ 8.65 (t, *J* = 4.7 Hz, 2H, amide N*H*), 7.35 (d, *J* = 9.0 Hz, 4H, Ar C-*H ortho* to chlorine), 6.98 (d, *J* = 9.0 Hz, 4H, Ar C-*H ortho* to phenoxy), 4.51 (s, 4H, CH_2OAr), 3.94 (d, *J* = 5.5 Hz, 4H, CH_2NH). **^{13}C NMR (DMSO)** δ 167.6 (amide *C*=O), 157.0 (Ar 4º C-phenoxy), 129.6 (Ar *C*-H *ortho* to chlorine), 125.3 (Ar 4º C-chlorine), 117.0 (Ar *C*-H *ortho* to phenoxy), 79.1 (4º C), 67.4 (*C*H_2OAr), 28.2 (*C*H_2NH). **HPLC:** $^{t}_{R}$ 2.98 min (95%). **LC-MS:** *m/z* = 421 $[M+H]^+$. **M.p.:**200-203 °C.

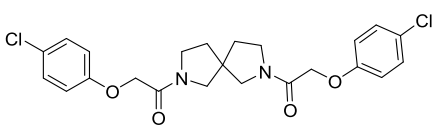
2-(4-Chlorophenoxy)-1-{5-[2-(4-chlorophenoxy)acetyl]-octahydropyrrolo[3,4-c]pyrrol-2-yl}ethan-1-one (84)



Following general procedure C, 3,7-diazabicyclo[3.3.0]octane (0.04 g, 0.4 mmol) and 4-chlorophenoxyacetyl chloride **26** (0.12 mL, 0.8 mmol) in DCM (5 mL) were reacted for 2 hour. The resulting precipitate was further purified by triturated with diethyl ether (3 mL), then separated by filtration and dried in

vacuo to afford the title compound as a white powder (0.1 g, yield: 57%). **^{1}H NMR (400 MHz, DMSO-*d*$_6$)** δ 7.32 (dd, *J*=2.0, 2.0 Hz, 4H, Ar C-*H ortho* to chlorine), 6.95 (d, *J*=2.2, 2.1 Hz, 4H, Ar C-*H ortho* to phenoxy), 4.74 (s, 4H, C*H*$_2$OAr), 3.76 - 3.65 (m, 2H, bicyclic C*H*$_2$N), 3.60 (dd, *J*=7.7, 7.4 Hz, 2H, bicyclic C*H*$_2$N), 3.42 (dd, *J*=3.8, 3.5 Hz, 2H, bicyclic C*H*$_2$N), 3.30 (ddd, *J*=4.3, 4.6, 5.0 Hz, 2H, bicyclic C*H*$_2$N), 3.09 - 2.78 (m, 2H, bicyclic C*H*). **^{13}C NMR (DMSO)** δ 166.2 (amide *C*=O), 157.4 (Ar 4º C-phenoxy), 129.5 (Ar *C*-H *ortho* to chlorine), 124.9 (Ar 4º C-chlorine), 116.8 (Ar *C*-H *ortho* to phenoxy), 66.6 (*C*H$_2$OAr), 49.9, 49.7, 48.8, 48.5 (4 x bicyclic *C*H$_2$N), 43.2, 38.5 (2 x bicyclic *C*H). **HPLC:** $^{t}_{R}$ 2.82 min (95%). **LC-MS:** *m/z* = 449 $[M+H]^+$. **M.p.:**130-133°C.

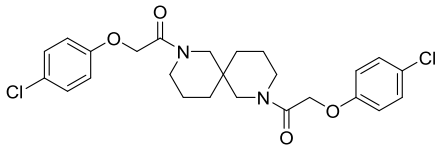
2-(4-Chlorophenoxy)-1-{7-[2-(4-chlorophenoxy)acetyl]-2,7-diazaspiro[4.4]nonan-2-yl}ethan-1-one (85)



Following general procedure C, 2,7-diaza-spiro[4.4]nonane dihydrochloride **74** (0.08 g, 0.4 mmol) and 4-chlorophenoxyacetyl chloride **26** (0.12 mL, 0.8 mmol) in DCM (5 mL) were reacted for 2 hour. After concentration of the solvent, purification was achieved via column chromatography (eluent DCM/THF 20:80) to give the desired product as a solid. The resulting solid was further purified by triturated with diethyl ether (3 mL), then separated by filtration and dried in vacuo to afford the title compound as a white crystal (0.1 g, yield: 22%). **^{1}H NMR (400 MHz, DMSO-*d*$_6$)** δ 7.31 (d, *J*=8.7 Hz, 4H, Ar C-*H ortho* to chlorine), 6.96 (dd, *J*=2.4, 2.5 Hz, 4H, Ar C-*H ortho* to phenoxy), 4.76 (s, 2H, C*H*$_2$OAr), 4.72 (d, *J*=4.5 Hz, 2H, C*H*$_2$OAr), 3.60 (d, *J*=6.5 Hz, 2H, spiro C*H*$_2$N), 3.51 - 3.36 (m, 4H, spiro C*H*$_2$N), 3.27 (t, *J*=12.3 Hz, 1H, spiro C*H*$_2$N), 3.17 (d, *J*=5.2 Hz, 1H, spiro C*H*$_2$N), 1.87 - 1.77 (m, 4H, spiro C*H*$_2$CH$_2$). **^{13}C NMR (DMSO)** δ

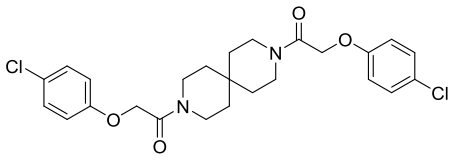
166.1 (amide *C*=O), 157.4 (Ar 4º C-phenoxy), 129.5 (Ar *C*-H *ortho* to chlorine), 124.9 (Ar 4º C-chlorine), 116.8 (Ar *C*-H *ortho* to phenoxy), 66.7 (*C*H_2OAr), 65.4 (*C*H_2OAr), 53.6, 49.0, 47.7, 45.2 (4 x spiro *C*H_2N), 40.4 (spiro 4º C), 34.8, 32.9 (spiro *C*H_2CH_2). **HPLC:** $^{t}_{R}$ 2.86 min (95%). **LC-MS:** *m/z* = 463 $[M+H]^+$. **M.p.:**166-170°C.

2-(4-Chlorophenoxy)-1-{8-[2-(4-chlorophenoxy)acetyl]-2,8-diazaspiro[5.5]undecan-2-yl}ethan-1-one (86)



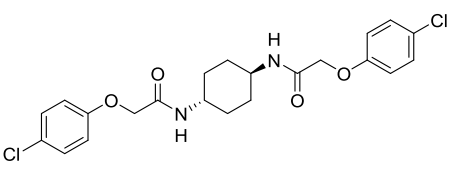
Following general procedure C, 2,8-diazaspiro[5.5]undecane (0.06 g, 0.4 mmol) and 4-chlorophenoxyacetyl chloride **26** (0.12 mL, 0.8 mmol) in DCM (5 mL) were reacted for 2 hour. The resulting precipitate was further purified by triturated with diethyl ether (3 mL), then separated by filtration and dried in vacuo to afford the title compound as a white powder (0.09 g, yield: 46%). **^{1}H NMR (400 MHz, DMSO-*d*$_6$)** δ 7.29 (dd, *J*=9.0, 7.8 Hz, 4H, Ar C-*H ortho* to chlorine), , 6.93 (dd, *J*=8.1, 8.9 Hz, 4H, Ar C-*H ortho* to phenoxy), 4.84 (s, 4H, C*H*$_2$OAr), 3.45 - 3.26 (m, 6H, spiro C*H*$_2$N), 3.10 (dd, *J*=13.0, 13.7 Hz, 2H, spiro C*H*$_2$N), 1.59 - 1.21 (m, 8H, spiro C*H*$_2$CH_2). **^{13}C NMR (DMSO)** δ 166.1 (amide *C*=O), 157.4 (Ar 4º C-phenoxy), 129.5 (Ar *C*-H *ortho* to chlorine), 124.9 (Ar 4º C-chlorine), 116.8 (Ar *C*-H *ortho* to phenoxy), 66.5 (*C*H_2OAr), 51.3, 48.8, 47.2, 45.5 (4 x spiro *C*H_2N), 34.8 (spiro *C*H_2CH_2), 32.0 (spiro 4º C), 21.8., 21.5, 20.0 (3 x spiro *C*H_2CH_2). **HPLC:** $^{t}_{R}$ 3.02 min (96%). **LC-MS:** *m/z* = 491 $[M+H]^+$. **M.p.:**134-137°C.

2-(4-Chlorophenoxy)-1-{9-[2-(4-chlorophenoxy)acetyl]-3,9-diazaspiro[5.5]undecan-3-yl}ethan-1-one (87)



Following general procedure C, 3,9-diazaspiro[5.5]undecane dihydrochloride **72** (0.101 g, 0.4 mmol) and 4-chlorophenoxyacetyl chloride **26** (0.12 mL, 0.8 mmol) in DCM (5 mL) were reacted for 2 hour. After concentration of the solvent, purification was achieved via column chromatography (eluent DCM/THF 20:80) to give the desired product as a solid. The resulting solid was further purified by triturated with diethyl ether (3 mL), then separated by filtration and dried in vacuo to afford the title compound as a light-yellow powder (0.17 g, yield: 86%). **^{1}H NMR (400 MHz, DMSO-*d*$_6$)** δ 7.32 (dd, *J*=2.1, 2.1 Hz, 4H, Ar C-*H ortho* to chlorine), 6.94 (dd, *J*=2.1, 2.0 Hz, 4H, Ar C-*H ortho* to phenoxy), 4.82 (s, 4H, C*H*$_2$OAr), 3.45 (dt, *J*=5.2, 5.9 Hz, 8H, spiro C*H*$_2$N), 1.49 (dt, *J*=5.7, 5.7 Hz, 8H, spiro C*H*$_2$CH$_2$). **^{13}C NMR (DMSO)** δ 165.8 (amide *C*=O), 157.5 (Ar 4º C-phenoxy), 129.5 (Ar *C*-H *ortho* to chlorine), 124.9 (Ar 4º C-chlorine), 116.8 (Ar *C*-H *ortho* to phenoxy), 66.6 (*C*H$_2$OAr), 37.5, 35.6 (2 x spiro *C*H$_2$N), 34.8 (spiro *C*H$_2$CH$_2$), 30.7 (spiro 4º C). **HPLC:** $^{t}_{R}$ 2.99 min (>95%) **LC-MS:** *m/z* = 491 $[M+H]^+$. **M.p.:**110-113°C.

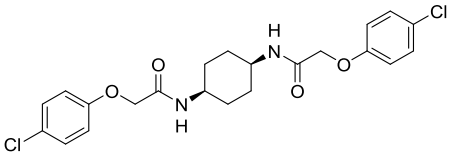
2-(4-Chlorophenoxy)-*N*-[(1*R*,4*R*)-4-[2-(4-chlorophenoxy)acetamido]cyclohexyl]acetamide (*trans*-ISRIB, 1) [149]



Following general procedure C, *trans*-1,4-diaminocyclohexane **45** (0.05 g, 0.4 mmol) and 4-chlorophenoxyacetyl chloride **26** (0.14 mL, 0.88 mmol) in DCM (5 mL) were reacted for 1 hour. The resulting precipitate was further purified by triturated with diethyl ether (3 mL), then separated by filtration and dried in vacuo to afford the title compound as a

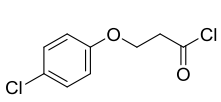
white powder (0.16 g, yield: 88%). **^{1}H NMR (400 MHz, DMSO-*d*$_6$)**: δ 7.97 (d, *J*=8.2 Hz, 2H, amide N*H*), 7.33 (dd, *J*=2.1, 6.8 Hz, 4H, Ar C-*H ortho* to chlorine), 6.96 (dd, *J*=2.4, 6.6 Hz, 4H, Ar C-*H ortho* to phenoxy), 4.45 (s, 4H, C*H*$_2$OAr), 3.58 (bs, 2H, ^{C}Hx C*H*), 1.76 (d, *J*=5.9 Hz, 4H, ^{C}Hx C*H*$_2$), 1.33 (quin, *J* = 10.2 Hz, 4H, ^{C}Hx C*H*$_2$). **^{13}C NMR (DMSO-*d*$_6$)**: δ 166.8 (amide *C*=O), 157.1 (Ar 4º C-phenoxy), 129.6 (Ar *C*-H *ortho* to chlorine), 125.2 (Ar 4º C-chlorine), 117 (Ar *C*-H *ortho* to phenoxy), 67.6 (*C*H$_2$OAr), 47.4 (^{C}Hx *C*H), 31.3(^{C}Hx *C*H$_2$). **HPLC:** $^{t}_{R}$ 2.92 min. **LC–MS:** *m/z* = 451 $[M+H]^+$. **M.p.:** 271-274 °C.

2-(4-Chlorophenoxy)-*N*-[(1*S*,4*S*)-4-[2-(4-chlorophenoxy)acetamido]cyclohexyl]acetamide (*cis*-ISRIB, 8) [149]



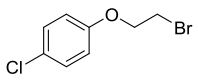
Following general procedure C, *cis*-1,4-diaminocyclohexane (0.05 g, 0.4 mmol) and 4-chlorophenoxyacetyl chloride **26** (0.14 mL, 0.88 mmol) in DCM (5 mL) were reacted for 2 hours. After concentration of the organic layer, purification was achieved via column chromatography (eluent DCM/THF 20:80) to give the desired product as a white fluffy powder (0.13 g, yield: 70%). **^{1}H NMR (400 MHz, DMSO-*d*$_6$)**: δ 7.79 (d, *J*=7.7 Hz, 2H, amide N*H*), 7.34 (dd, *J*=2.8, 2.5 Hz, 4H, Ar C-*H ortho* to chlorine), 6.96 (dd, *J*=2.8, 2.9 Hz, 4H, Ar C-*H ortho* to phenoxy), 4.50 (s, 4H, C*H*$_2$OAr), 3.73 (bs, 2H, ^{C}Hx C*H*), 1.67 - 1.50 (m, 8H, ^{C}Hx C*H*$_2$). **^{13}C NMR (DMSO-*d*$_6$)**: δ 167.0 (amide *C*=O), 157.2 (Ar 4º C-phenoxy), 129.6 (Ar *C*-H *ortho* to chlorine), 125.2 (Ar 4º C-chlorine), 116.9 (Ar *C*-H *ortho* to phenoxy), 67.5 (*C*H$_2$OAr), 45.7(^{C}Hx *C*H) , 27.9 (^{C}Hx *C*H$_2$). **HPLC:** $^{t}_{R}$ 2.96 min. **LC–MS:** *m/z* = 451 $[M+H]^+$. **M.p.:** 162-164 °C.

3-(4-Chlorophenoxy)propanoyl chloride (94)



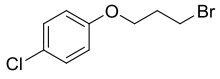
A suspension of commercially available 3-(4-chlorophenoxy)propanoic acid **93** (0.20 g, 1mmol) was dissolved in dichloromethane (5 mL) with the aid of sonication. This was then treated dropwise with oxalylchloride (0.09 mL, 1 mmol) in dichloromethane (1 mL) at 0^{o}C, followed by a few drops of DMF (2-drops) with stirring for 1 hour at ambient temperature. The reaction was monitored by TLC, and once all the starting acid consumed, the solvent removed in vacuum. The resulting product was directly used for next step without further purification (0.18 g, yield: 81%). **LC–MS:** *m/z* = 219 $[M+H]^+$.

1-(2-Bromoethoxy)-4-chlorobenzene (96a)



To a stirred solution of *p*-chlorophenol **95** (0.32 g, 2.5 mmol) and K_2CO_3 (0.30 g, 4 mmol,) in DMF (3 mL) was added a solution of 1,2-dibromethane (0.93 mL, 5 mmol) in DMF (10 mL) at room temperature. The resulting mixture was stirred at the same temperature for 24 hours. The reaction solution was then diluted with ether (25 mL), washed with water (25 mL x3). The organic layer was dried over sodium sulphate, filtered and concentrated under vacuum. After concentration of the organic layer, purification was achieved via column chromatography (eluent DCM/Pet.ether 10:90, 20:80, then 30:70) to obtain the desired product as a colourless oil (0.34 g, yield: 58%). The resulting product was directly used for next step **LC–MS:** *m/z* = 236 $[M+H]^+$.

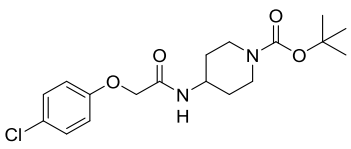
1-(3-Bromopropoxy)-4-chlorobenzene (96b)



To a stirred solution of *p*-chlorophenol **95** (0.32 g, 2.5 mmol) and K_2CO_3 (0.30 g, 4 mmol,) in DMF (3 mL) was added a

solution of 1,3-dibrompropane (1.0 g, 5 mmol) in DMF (10 mL) at room temperature. The resulting mixture was stirred at the same temperature for 24 hours. The reaction solution was then diluted with ether (25 mL), washed with water (25 ml x3). The organic layer was dried over sodium sulphate, filtered and concentrated under vacuum. After concentration of the organic layer, purification was achieved via column chromatography (eluent DCM/Pet.ether 10:90, 20:80, then 30:70) to obtain the desired product as a colourless oil (0.32 g, yield: 51%). **^{1}H NMR (400 MHz, DMSO-*d*$_6$)** δ 7.31 (d, *J*=9.0 Hz, 2H, Ar C-*H ortho* to chlorine), 6.95 (d, *J*=9.0 Hz, 2H, Ar C-*H ortho* to phenoxy), 4.05 (t, *J*=6.0 Hz, 2H, C*H*$_2$OAr), 3.64 (t, *J*=6.6 Hz, 2H, C*H*$_2$Br), 2.24 (quin, *J*=6.3 Hz, 2H, C*H*$_2$CH$_2$Br). **^{13}C NMR (DMSO)** δ 157.6 (Ar 4º C-phenoxy), 129.6 (Ar *C*-H *ortho* to chlorine), 124.9 (Ar 4º C-chlorine), 116.6 (Ar *C*-H *ortho* to phenoxy), 66.1 (*C*H$_2$OAr), 32.2 (*C*H$_2$Br), 31.4 (*C*H$_2$CH$_2$Br). **LC–MS:** *m/z* = 250 $[M+H]^+$.

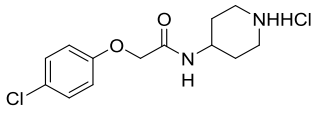
***tert*-Butyl 4-[2-(4-chlorophenoxy)acetamido]piperidine-1-carboxylate (98)**



Following general procedure A, 4-amino-1-Boc-piperidine **97** (0.2 g, 1 mmol) and 4-chlorophenoxyacetylchloride **26** (0.15 mL, 1 mmol) in DCM (10 mL) were reacted for 2 hour. After concentration of the solvent, purification was achieved via column chromatography (eluent DCM/EtOAc 20:80) to give the desired product as a white waxy solid. The resulting solid was further purified by triturated with diethyl ether (3 mL), then separated by filtration and dried in vacuo to afford the title compound as a white powder (0.34 g, yield: 93%). **^{1}H NMR (400 MHz, DMSO-*d*$_6$)** δ 8.02 (d, *J*=8.0 Hz, 1H, amide N*H*), 7.35 (dd, *J*=2.2, 2.2 Hz, 2H, Ar C-*H ortho* to chlorine), 6.99 (dd, *J*=2.2, 2.2 Hz, 2H, Ar C-*H ortho* to phenoxy), 4.48 (s, 2H, C*H*$_2$OAr), 3.95 -

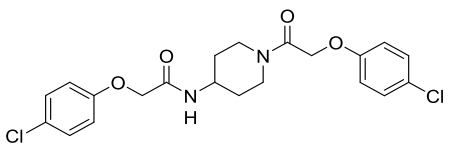
3.79 (m, 3H, piperidine C*H*$_2$), 2.82 (s, 2H, piperidine C*H*$_2$), 1.71 (dd, *J*=3.0, 2.9 Hz, 2H, piperidine C*H*$_2$), 1.41 (s, 9H, C(C*H*$_3$)$_3$), 1.37 (td, *J*=3.9, 3.6, 4.2 Hz, 2H, piperidine C*H*$_2$). **^{13}C NMR (DMSO)** δ 170.7 (amide *C*=O), 166.9 (amide *C*=O), 157.1 (Ar 4º C-phenoxy), 154.3, 129.6 (Ar *C*-H *ortho* to chlorine), 125.3 (Ar 4º C-chlorine), 116.9 (Ar *C*-H *ortho* to phenoxy), 79.0 (Boc 4º C), 67.6 (*C*H$_2$OAr), 60.2 (piperidine *C*H), 46.1, 31.6, 28.5 (3 x piperidine *C*H$_2$), 21.1 (Boc *C*H$_3$). **HPLC:** $^{t}_{R}$ 2.95 min (96%). **LC-MS:** *m/z* = 369 $[M+H]^+$.

2-(4-Chlorophenoxy)-*N*-(piperidin-4-yl)acetamide hydrochloride (99)



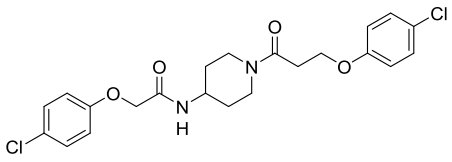
A suspension of *tert*-butyl 4-[2-(4-chlorophenoxy)acetamido]piperidine-1-carboxylate **98** (0.3 g, 0.8 mmol) was dissolved in dioxane–MeOH (2:1; 3 mL). This was then treated with 4 M HCl in dioxane (3 mL) with vigorously stirring for 2 hours. The reaction monitored by TLC, then all the solvents were removed in vacuo. The resulting hydrochloride salt of the desired compound was as dissolved in methanol (1mL) and then recrystalized with diethyl ether (2 mL), then separated by filtration and dried to afford the title compound as a light yellow powder (0.23 g, yield: 95%). **^{1}H NMR (400 MHz, DMSO-*d*$_6$)** δ 8.41 (d, *J*=7.6 Hz, 1H, amide N*H*), 7.33 (dd, *J*=2.1, 2.2 Hz, 2H, Ar C-*H ortho* to chlorine), 6.96 (dd, *J*=2.2, 2.2 Hz, 2H, Ar C-*H ortho* to phenoxy), 4.50 (s, 2H, C*H*$_2$OAr), 3.95 - 3.82 (m, 1H, piperidine C*H*), 3.24 (d, *J*=12.9 Hz, 2H, piperidine C*H*$_2$), 2.99 - 2.86 (m, 2H, piperidine C*H*$_2$), 1.88 (dd, *J*=3.3, 3.2 Hz, 2H, piperidine C*H*$_2$), 1.77 (td, *J*=3.8, 2.9, 3.9 Hz, 2H, piperidine C*H*$_2$). **^{13}C NMR (DMSO)** δ 167.3 (amide *C*=O), 157.2 (Ar 4º C-phenoxy), 129.6 (Ar *C*-H *ortho* to chlorine), 125.2 (Ar 4º C-chlorine), 116.9 (Ar *C*-H *ortho* to phenoxy), 67.4 (*C*H$_2$OAr), 66.8 (piperidine *C*H), 44.0, 42.2, 28.3 (3 x piperidine *C*H$_2$). **HPLC:** $^{t}_{R}$ 2.77 min (96%).

2-(4-Chlorophenoxy)-*N*-{1-[2-(4-chlorophenoxy)acetyl]piperidin-4-yl}acetamide (100)



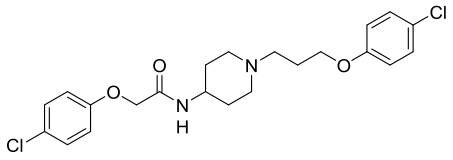
Following general procedure B, 2-(4-chlorophenoxy)-*N*-(piperidin-4-yl)acetamide hydrochloride **99** (0.09 g, 0.3 mmol) and 4-chlorophenoxyacetylchloride (0.04 mL, 0.3 mmol) in DCM (5 mL) were reacted for 2 hours. The resulting precipitate was further purified by triturated with diethyl ether (3 mL), then separated by filtration and dried in vacuo to afford the title compound as a white powder (0.09 g, yield: 72%). **^{1}H NMR (400 MHz, DMSO-*d*$_6$)** δ 8.08 (d, *J*=7.9 Hz, 1H, amide N*H*), 7.33 (t, *J*=9.3 Hz, 4H, Ar C-*H ortho* to chlorine), 6.97 (dd, *J*=9.0, 9.0 Hz, 4H, Ar C-*H ortho* to phenoxy), 4.83 (q, *J*=14.5 Hz, 2H, C*H*$_2$OAr), 4.48 (s, 2H, C*H*$_2$OAr), 4.21 (d, *J*=13.0 Hz, 1H, piperidine C*H*$_2$), 3.95 - 3.86 (m, 1H, piperidine C*H*), 3.79 (d, *J*=13.4 Hz, 1H, piperidine C*H*$_2$), 3.12 (t, *J*=11.9 Hz, 1H, piperidine C*H*$_2$), 2.76 (t, *J*=11.7 Hz, 1H, piperidine C*H*$_2$), 1.75 (t, *J*=13.4 Hz, 2H, piperidine C*H*$_2$), 1.46 (dq, *J*=10.4, 10.4 Hz, 2H, piperidine C*H*$_2$). **^{13}C NMR (101 MHz, DMSO)** δ 167.0 (amide *C*=O), 165.8 (amide *C*=O), 157.4 (Ar 4º C-phenoxy), 157.1 (Ar 4º C-phenoxy), 129.6, 129.5 (2 x Ar *C*-H *ortho* to chlorine), 125.3, 124.9 (2 x Ar 4º C-chlorine), 116.9, 116.8 (2 x Ar *C*-H *ortho* to phenoxy), 67.6, 66.6 (2 x *C*H$_2$OAr), 46.1 (piperidine *C*H), 43.5, 32.2, 31.4 (3 x piperidine *C*H$_2$). **HPLC:** $^{t}_{R}$ 2.89 min (96%). **HRMS:** *m/z* theoretical for $C_{21}H_{23}Cl_2N_2O_4$ 437.1029 $[M+H]^+$, measured 437.1031 $[M+H]^+$. **M.p.:** 150-154°C.

2-(4-Chlorophenoxy)-*N*-{1-[3-(4-chlorophenoxy)propanoyl]piperidin-4-yl}acetamide (101)



Following general procedure B, 2-(4-chlorophenoxy)-*N*-(piperidin-4-yl)acetamide hydrochloride **99** (0.09 g, 0.3 mmol) and 3-(4-chlorophenoxy)propanoyl chloride **94** (0.07 mL, 0.3 mmol) in DCM (5 mL) were reacted for 2 hours. The resulting precipitate was further purified by triturated with diethyl ether (3 mL), then separated by filtration and dried in vacuo to afford the title compound as a white powder (0.12 g, yield: 92%). **^{1}H NMR (400 MHz, DMSO-d_6)** δ 8.05 (d, *J*=7.9 Hz, 1H, amide N*H*), 7.34 (dd, *J*=9.0, 9.0 Hz, 4H, Ar C-*H ortho* to chlorine), 6.96 (t, *J*=9.5 Hz, 4H, Ar C-*H ortho* to phenoxy), 4.48 (s, 2H, C*H*$_2$OAr), 4.29 (d, *J*=13.2 Hz, 1H, piperidine C*H*), 4.18 (t, *J*=6.2 Hz, 2H, C*H*$_2$OAr), 3.88 (d, *J*=11.5 Hz, 2H, piperidine C*H*$_2$), 3.12 (t, *J*=11.6 Hz, 1H, piperidine C*H*$_2$), 2.80 (t, *J*=6.0 Hz, 2H, piperidine C*H*$_2$), 2.71 (t, *J*=11.3 Hz, 1H, piperidine C*H*$_2$), 1.74 (t, *J*=13.2 Hz, 2H, piperidine C*H*$_2$), 1.49 - 1.25 (m, 2H, piperidine C*H*$_2$). **^{13}C NMR (DMSO)** δ 168.4 (amide *C*=O), 167.0 (amide *C*=O), 157.8, 157.1 (2 x Ar 4º C-phenoxy), 129.7, 129.6 (2 x Ar *C*-H *ortho* to chlorine), 125.3, 124.6 (2 x Ar 4º C-chlorine), 116.9, 116.6 (2 x Ar *C*-H *ortho* to phenoxy), 67.6, 64.9 (2 x *C*H$_2$OAr), 46.2 (piperidine *C*H), 44.2, 32.4 (2 x piperidine *C*H$_2$), 32.3 (*C*H$_2$CH$_2$OAr), 31.4 (piperidine *C*H$_2$). **HPLC:** $^{t}_{R}$ 2.95 min (95%). **HRMS:** *m/z* theoretical for $C_{22}H_{25}Cl_2N_2O_4$ 451.1186 $[M+H]^+$, measured 451.1185 $[M+H]^+$. **M.p.:** 155-157 °C.

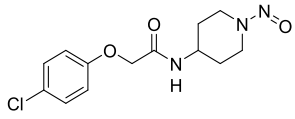
2-(4-Chlorophenoxy)-*N*-{1-[3-(4-chlorophenoxy)propyl]piperidin-4-yl}acetamide (102)



To a suspension of 2-(4-chlorophenoxy)-*N*-(piperidin-4-yl)acetamide hydrochloride **99** (0.15 g, 0.5 mmol) and K_2CO_3 (0.27 g, 2 mmol) in MeOH (10 mL) was added a solution of 1-(3-bromopropoxy)-4-chlorobenzene **96b** (0.25 g, 1 mmol) in MeOH (5 mL). The resulting mixture was refluxed at 60 C^o for 12 hours. The reaction solution was then diluted with ethyl acetate (10 mL), washed with water and brine. The organic layer was dried over sodium sulphate, filtered and concentrated under vacuum. After concentration of the organic layer, purification was achieved via column chromatography (eluent DCM/EtOAc 20:80) to obtain the desired product as a white solid. The resulting solid was further purified by triturated with diethyl ether (3 mL), then separated by filtration and dried in vacuo to afford the title compound as a white powder (0.11 g, yield: 53%). **^{1}H NMR (400 MHz, DMSO-*d*$_6$)** δ 7.94 (d, *J*=7.9 Hz, 1H, amide N*H*), 7.33 (dd, *J*=9.0, 9.0 Hz, 4H, Ar C-*H ortho* to chlorine), 6.97 (dd, *J*=9.1, 9.0 Hz, 4H, Ar C-*H ortho* to phenoxy), 4.45 (s, 2H, C*H*$_2$OAr), 3.97 (t, *J*=6.4 Hz, 2H, C*H*$_2$OAr), 3.67 - 3.54 (m, 1H, piperidine C*H*), 2.80 (d, *J*=11.6 Hz, 2H, piperidine C*H*$_2$), 2.38 (t, *J*=7.1 Hz, 2H, C*H*$_2$CH$_2$CH$_2$OAr), 1.94 (t, *J*=10.7 Hz, 2H, piperidine C*H*$_2$), 1.88 (quin, *J*=1.8 Hz, 2H, C*H*$_2$CH$_2$OAr), 1.68 (d, *J*=9.9 Hz, 2H, piperidine C*H*$_2$), 1.52 (qd, *J*=3.6, 2.9, 2.9, 3.6 Hz, 2H, piperidine C*H*$_2$). **^{13}C NMR (DMSO)** δ 166.9 (amide *C*=O), 158.0, 157.1 (2 x Ar 4^o C-phenoxy), 129.6, 129.5 (2 x Ar *C*-H *ortho* to chlorine), 125.2, 124.5 (2 x Ar 4^o C-chlorine), 117.0, 116.6 (Ar *C*-H *ortho* to phenoxy), 67.6, 66.7 (2 x *C*H$_2$OAr), 54.7 (*C*H$_2$CH$_2$CH$_2$OAr), 52.6 (piperidine *C*H$_2$), 46.5 (piperidine *C*H), 31.9 (piperidine *C*H$_2$), 26.8 (*C*H$_2$CH$_2$OAr). **HPLC:** ^tR 2.33 min

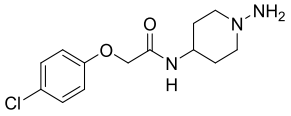
(95%). **HRMS:** *m/z* theoretical for $C_{22}H_{27}Cl_2N_2O_3$ 437.1393 $[M+H]^+$, measured 437.1412 $[M+H]^+$. **M.p.:** 140-142°C.

2-(4-Chlorophenoxy)-*N*-(1-nitrosopiperidin-4-yl)acetamide (99a)



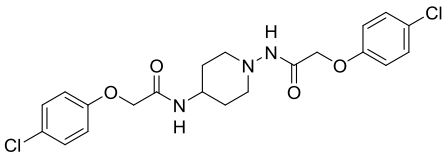
To a stirred suspension of 2-(4-chlorophenoxy)-*N*-(piperidin-4-yl)acetamide hydrochloride **99** (0.3 g, 1 mmol) in acetic acid and water (2:2, 5 mL) was dropwise added a solution of $NaNO_2$ (0.12 g, 2 mmol) in water (1 mL) at room temperature. The resulting mixture was stirred at room temperature for 10 hours. The reaction solution was monitored by TLC then diluted with ethyl acetate (10 mL), washed with water. The organic layer was dried over sodium sulphate, filtered and concentrated under vacuum. After concentration of the organic layer, purification was achieved via column chromatography (eluent DCM/EtOAc 20:80) to obtain the desired product as a light-yellow powder (0.22 g, yield: 73%). **^{1}H NMR (400 MHz, DMSO-d_6)** δ 8.15 (d, *J*=7.9 Hz, 1H, amide N*H*), 7.35 (dd, *J*=2.2, 2.2 Hz, 2H, Ar C-*H ortho* to chlorine), 6.98 (dd, *J*=2.2, 2.3 Hz, 2H, Ar C-*H ortho* to phenoxy), 4.66 (tt, *J*=4.1, 5.1, 4.3 Hz, 2H, piperidine CH_2), 4.49 (s, 2H, CH_2OAr), 4.14 - 4.02 (m, 1H, piperidine CH_2), 3.92 (td, *J*=3.5, 2.0, 3.5 Hz, 1H, piperidine CH_2), 2.94 (td, *J*=3.9, 3.9, 3.9 Hz, 1H, piperidine CH_2), 2.01 - 1.94 (m, 1H, piperidine CH_2), 1.80 - 1.73 (m, 1H, piperidine CH_2), 1.67 (qd, *J*=4.7, 4.6, 4.6, 4.8 Hz, 1H, piperidine CH_2), 1.32 (td, *J*=3.9, 3.6, 3.9 Hz, 1H, piperidine CH_2). **^{13}C NMR (DMSO)** δ 167.2 (amide *C*=O), 157.1 (Ar 4º C-phenoxy), 129.6 (Ar *C*-H *ortho* to chlorine), 125.3 (Ar 4º C-chlorine), 116.9 (Ar *C*-H *ortho* to phenoxy), 67.6 (*C*H_2OAr), 48.3 (piperidine *C*H), 45.5, 37.5, 32.0, 30.3 (4 x piperidine *C*H_2). **HPLC:** ^tR 2.61 min. **LC-MS:** *m/z* = 298 $[M+H]^+$.

_N_-(1-Aminopiperidin-4-yl)-2-(4-chlorophenoxy)acetamide (99b)



2-(4-Chlorophenoxy)-*N*-(1-nitrosopiperidin-4-yl)acetamide **99a** (0.12 g, 0.4 mmol) was dissolved in acetic acid (5 mL), then the solution was dropwise added to a suspension of Zn (0.13 g, 2 mmol) in acetic acid and water (1:1, 2 mL). The resulting mixture was stirred at ambient temperature for 10 hours. The reaction monitored by LC/MS, and then filtered through celite-pad, washed with aqueous HCl solution (1N) and DCM. The aqueous layer was then extracted with DCM (3x 10 mL). The combined organic layer was washed with brine solution, dried over anhydrous Na_2SO_4, filtered and concentrated under vacuum to afford the desired product as a white powder. The resulting product was directly used for next step without further purification (0.08 g, yield: 66%). **LC–MS:** *m/z* = 284 $[M+H]^+$.

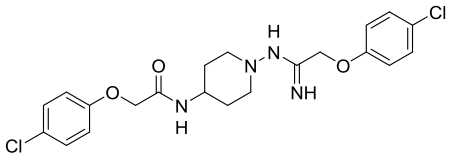
2-(4-Chlorophenoxy)-*N*-{1-[2-(4-chlorophenoxy)acetamido]piperidin-4-yl}acetamide (103)



Following general procedure B, *N*-(1-aminopiperidin-4-yl)-2-(4-chlorophenoxy)acetamide **99b** (0.19 g, 0.6 mmol) and 4-chlorophenoxyacetylchloride **26** (0.09 mL, 0.6 mmol) in DCM (10 mL) were reacted for 2 hours. After concentration of the organic layer, purification was achieved via column chromatography (eluent DCM/EtoAC 10:90, 20:80, then 30:70) to give the desired product as a solid. The resulting solid was further purified by triturated with diethyl ether (3 mL), then separated by filtration and dried in vacuo to afford the title compound as a white powder (0.14 g, yield: 51%). **^{1}H NMR (400 MHz, DMSO-d_6)** δ 9.25 (s, 0.5H (split), NH hydrazide), 8.78 (s, 0.5H (split), NH hydrazide), 8.11 (d, *J*=7.8 Hz, 1H, amide

N*H*), 7.34 (dd, *J*=9.0, 9.0 Hz, 4H, Ar C-*H ortho* to chlorine), 6.97 (dd, *J*=8.7, 9.0 Hz, 4H, Ar C-*H ortho* to phenoxy), 4.84 (s, 1H, C*H*$_2$OAr), 4.47 (s, 2H, C*H*$_2$OAr), 4.44 (s, 1H, C*H*$_2$OAr), 3.64 - 3.56 (m, 1H, piperidine C*H*), 3.16 (d, *J*=5.1 Hz, 1H, piperidine C*H*$_2$), 3.04 (bs, 1H, piperidine C*H*$_2$), 2.88 (d, *J*=11.0 Hz, 1H, piperidine C*H*$_2$), 2.68 (td, *J*=2.7, 2.1, 2.7 Hz, 1H, piperidine C*H*$_2$), 1.73 (dt, *J*=12.0, 11.7 Hz, 4H, piperidine C*H*$_2$). **^{13}C NMR (DMSO)** δ 167.1 (amide *C*=O), 164.9 (amide *C*=O), 157.7, 157.1 (2 x Ar 4º C-phenoxy), 129.6, 129.5 (2 x Ar *C*-H *ortho* to chlorine), 125.3, 124.6 (2 x Ar 4º C-chlorine), 117.0, 116.9, 116.9, 116.7 (4 x Ar *C*-H *ortho* to phenoxy), 67.6, 65.4 (2 x *C*H$_2$OAr), 55.3 (piperidine *C*H), 53.9, 45.6, 31.4, 15.6 (4 x piperidine *C*H$_2$). **HPLC:** $^{t}_{R}$ 2.82 min (95%). **HRMS:** *m/z* theoretical for $C_{21}H_{23}Cl_2N_3O_4$ 452.1138 $[M+H]^+$, measured 452.1138 $[M+H]^+$. **M.p.:** 257-260 °C.

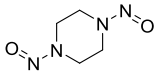
2-(4-Chlorophenoxy)-*N*-{1-[2-(4-chlorophenoxy)ethanimidamido]piperidin-4-yl}acetamide (104)



To a stirred solution of *N*-(1-aminopiperidin-4-yl)-2-(4-chlorophenoxy)acetamide **99b** (0.10 g, 0.3 mmol) in ethanol (1 mL) were added DIPEA (0.063 mL, 0.4 mmol) and ethyl 2-(4-chlorophenoxy)ethanecarboximidate **58** (0.08 g, 0.4 mmol). The mixture was stirred for overnight at ambient temperature. After concentration, purification was achieved via column chromatography (eluent NH_3 10% in methanol/DCM 5:95) to afford the desired product as a white powder (0.06 g, yield: 45%). **^{1}H NMR (400 MHz, DMSO-*d*$_6$)** δ 9.40 (s, 1H, amidine N*H*), 8.88 (s, 1H, amide N*H*), 7.40 (d, *J*=8.7 Hz, 2H, Ar C-*H ortho* to chlorine), 7.34 (dd, *J*=8.8, 8.9 Hz, 2H, Ar C-*H ortho* to chlorine), 7.05 (d, *J*=8.5 Hz, 2H, Ar C-*H ortho* to phenoxy),

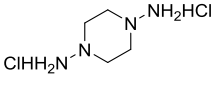
6.96 (dd, *J*=8.7, 8.7 Hz, 2H, Ar C-*H ortho* to phenoxy), 4.97 (d, *J*=5.0 Hz, 2H, C*H*$_2$OAr), 4.86 (s, 1H, C*H*$_2$OAr), 4.45 (s, 1H, C*H*$_2$OAr), 3.77 (s, 1H, piperidine C*H*), 3.03 (s, 1H, piperidine C*H*$_2$), 2.90 (tt, *J*=11.6, 11.0 Hz, 2H, piperidine C*H*$_2$), 2.60 (s, 1H, piperidine C*H*$_2$), 1.86 (tt, *J*=11.3, 11.0 Hz, 4H, piperidine C*H*$_2$). **^{13}C NMR (DMSO)** δ 165.1 (amide *C*=O), 161.9 (amidine *C*=O), 157.7, 156.1 (2 x Ar 4º C-phenoxy), 129.9, 129.6, 129.4 (3 x Ar *C*-H *ortho* to chlorine), 126.3, 125.2 (2 x Ar 4º C-chlorine), 117.2, 117.2, 116.9, 116.7 (4 x Ar C-*H ortho* to phenoxy), 66.9, 65.0 (*C*H$_2$OAr), 53.1 (piperidine *C*H$_2$), 49.1, 30.3 (2 x piperidine *C*H$_2$). **HPLC:** $^{t}_{R}$ 2.80 min (95%). **HRMS:** *m/z* theoretical for $C_{21}H_{24}Cl_2N_4O_3$ 452.1196 $[M+H]^+$, measured 452.1147 $[M+H]^+$. **M.p.:** 255-258°C.

1,4-Dinitrosopiperazine (106a)



To a stirred solution of piperazine **105a** (0.20 g, 2.5 mmol) in acetic acid and water (1:2, 6 mL) was dropwise added a solution of $NaNO_2$ (0.45 g, 7 mmol) in water (3 mL) at room temperature. The resulting mixture was stirred at room temperature for 24 hours. The reaction solution was monitored by TLC then diluted with ethyl acetate (20 mL), washed with water. The organic layer was dried over sodium sulphate, filtered and concentrated under vacuum to afford the desired product as a yellow powder. The resulting product was directly used for next step without further purification (0.32 g, yield: 89%).

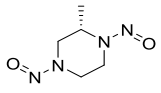
Piperazine-1,4-diamine dihydrochloride (107a)



1,4-Dinitrosopiperazine **106a** (0.25 g, 1.7 mmol) was dissolved in acetic acid (5 mL), then the solution was dropwise added to a suspension of Zn (0.26 g, 4 mmol) in acetic acid and water

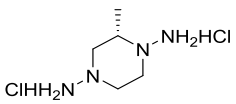
(1:1, 2 mL). The resulting mixture was stirred at ambient temperature for 10 hours. The reaction monitored by TLC, and then filtered through celite-pad, washed with aqueous HCl solution (1N) and DCM. The aqueous layer was then extracted with DCM (3x 10 mL). The combined organic layer was washed with brine solution, dried over anhydrous Na_2SO_4, filtered and concentrated under vacuum to afford the desired product as a yellow powder. The resulting product was directly used for next step without further purification (0.24 g, yield: 76%).

(2*S*)-2-Methyl-1,4-dinitrosopiperazine (106b)



To a stirred solution of (*S*)-2-methylpiprazine **105b** (0.25 g, 2.5 mmol) in acetic acid and water (1:2, 6 mL) was dropwise added a solution of $NaNO_2$ (0.45 g, 7 mmol) in water (3 mL) at room temperature. The resulting mixture was stirred at room temperature for 24 hours. The reaction solution was monitored by TLC then diluted with ethyl acetate (20 mL), washed with water. The organic layer was dried over sodium sulphate, filtered and concentrated under vacuum to afford the desired product as a yellow powder. The resulting product was directly used for next step without further purification (0.29 g, yield: 74%)

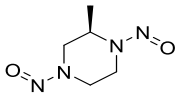
(2*S*)-2-Methylpiperazine-1,4-diamine dihydrochloride (107b)



(2*S*)-2-Methyl-1,4-dinitrosopiperazine **106b** (0.26 g, 1.7 mmol) was dissolved in acetic acid (5 mL), then the solution was dropwise added to a suspension of Zn (0.26 g, 4 mmol) in acetic acid and water (1:1, 2 mL). The resulting mixture was stirred at ambient temperature for 10 hours. The reaction monitored by TLC, and then filtered through celite-pad, washed with aqueous HCl solution (1N) and DCM. The aqueous layer was then

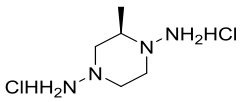
extracted with DCM (3x 10 mL). The combined organic layer was washed with brine solution, dried over anhydrous Na_2SO_4, filtered and concentrated under vacuum to afford the desired product as a yellow powder. The resulting product was directly used for next step without further purification (0.23 g, yield: 69%).

(2*R*)-2-Methyl-1,4-dinitrosopiperazine (106c)



To a stirred solution of (*R*)-2-methylpiprazine **105c** (0.25 g, 2.5 mmol) in acetic acid and water (1:2, 6 mL) was dropwise added a solution of $NaNO_2$ (0.45 g, 7 mmol) in water (3 mL) at room temperature. The resulting mixture was stirred at room temperature for 24 hours. The reaction solution was monitored by TLC then diluted with ethyl acetate (20 mL), washed with water. The organic layer was dried over sodium sulphate, filtered and concentrated under vacuum to afford the desired product as a yellow powder. The resulting product was directly used for next step without further purification (0.26 g, yield: 68%)

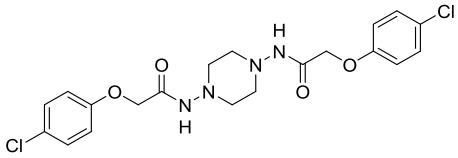
(2*R*)-2-Methylpiperazine-1,4-diamine dihydrochloride (107c)



(2*R*)-2-Methyl-1,4-dinitrosopiperazine **106c** (0.26 g, 1.7 mmol) was dissolved in acetic acid (5 mL), then the solution was dropwise added to a suspension of Zn (0.26 g, 4 mmol) in acetic acid and water (1:1, 2 mL). The resulting mixture was stirred at ambient temperature for 10 hours. The reaction monitored by TLC, and then filtered through celite-pad, washed with aqueous HCl solution (1N) and DCM. The aqueous layer was then extracted with DCM (3x 10 mL). The combined organic layer was washed with brine solution, dried over anhydrous Na_2SO_4, filtered and concentrated under vacuum to afford the desired product as a yellow powder.

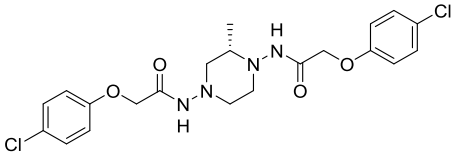
The resulting product was directly used for next step without further purification (0.21 g, yield: 62%).

2-(4-Chlorophenoxy)-*N*-{4-[2-(4-chlorophenoxy)acetamido]piperazin-1-yl}acetamide (108a)



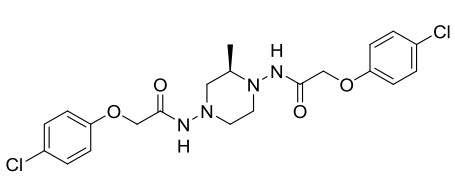
Following general procedure C, piperazine-1,4-diamine dihydrochloride **107a** (0.23 g, 2 mmol) and 4-chlorophenoxyacetyl chloride **26** (0.62 mL, 4 mmol) in DCM (10 mL) were reacted for 2 hours. After concentration of the solvent, purification was achieved via column chromatography (eluent DCM/ EtOAc 20:80) to give the desired product as a solid. The resulting solid was further purified by triturated with diethyl ether (5 mL), then separated by filtration and dried in vacuo to afford the title compound as a white powder (0.32 g, yield: 36%). **^{1}H NMR (400 MHz, DMSO-d_6)** δ 9.20 (d, *J* = 5.1 Hz, 1H, amide N*H*), 8.82 (d, *J* = 6.8 Hz, 1H, amide N*H*), 7.34 (dd, *J* = 8.8, 8.8 Hz, 4H, Ar C-*H ortho* to chlorine), 6.96 (dd, *J* = 8.8, 7.4 Hz, 4H, Ar C-*H ortho* to phenoxy), 4.85 (s, 2H, CH_2OAr), 4.44 (s, 2H, CH_2OAr), 2.84 (t, *J* = 12.8, 8H, piperazine CH_2). **^{13}C NMR (DMSO)** δ 169.6 (amide *C*=O), 165.1 (amide *C*=O), 157.7, 157.1 (2 x Ar 4º C-phenoxy), 129.6, 129.5 (2 x Ar *C*-H *ortho* to chlorine), 125.3, 124.6 (2 x Ar 4º C-chlorine), 116.9, 116.7, 116.7 (3 x Ar *C*-H *ortho* to phenoxy), 67.1, 65.4 (2 x *C*H_2OAr), 55.4, 55.2, 54.0, 53.9 (4 x piperazine *C*H_2). **HPLC:** ^{t}R 2.73 min (95%). **HRMS:** *m/z* theoretical for $C_{20}H_{23}Cl_2N_4O_4$ 454.1996 $[M+H]^+$, measured 454.1947 $[M+H]^+$. **M.p.:** 271-275 °C.

2-(4-Chlorophenoxy)-*N*-[(3*S*)-4-[2-(4-chlorophenoxy)acetamido]-3-methylpiperazin-1-yl]acetamide (108b)



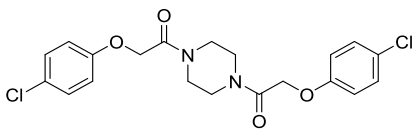
Following general procedure C, (2*S*)-2-methylpiperazine-1,4-diamine dihydrochloride **107b** (0.13 g, 1 mmol) and 4-chlorophenoxyacetyl chloride **26** (0.25 mL, 2 mmol) in DCM (5 mL) were reacted for 2 hours. After concentration of the solvent, purification was achieved via column chromatography (eluent DCM/ EtOAc 20:80) to give the desired product as a solid. The resulting solid was further purified by triturated with diethyl ether (5 mL), then separated by filtration and dried in vacuo to afford the title compound as a white powder (0.30 g, yield: 66%). **^{1}H NMR (400 MHz, DMSO-*d*$_6$)** δ 9.22 (d, *J*=6.0 Hz, 1H, amide N*H*), 8.99 (d, *J*=5.6 Hz, 1H, amide N*H*), 7.32 (dd, *J*=2.4, 2.2 Hz, 4H, Ar C-*H ortho* to chlorine), 6.98 (dd, *J*=2.2, 2.2 Hz, 4H, Ar C-*H ortho* to phenoxy), 4.82 (s, 2H, C*H*$_2$OAr), 4.44 (s, 2H, C*H*$_2$OAr), 3.09 - 2.68 (m, 7H, piperazine C*H*,C*H*$_2$), 1.02 (t, *J*=5.8 Hz, 3H, C*H*$_3$). **^{13}C NMR (DMSO)** δ 170.1 (amide *C*=O), 157.6, 157.1 (2 x Ar 4º C-phenoxy), 129.6, 129.5, 129.4 (3 x Ar *C*-H *ortho* to chlorine), 125.3, 124.6 (2 x Ar 4º C-chlorine), 116.9, 116.7 (Ar *C*-H *ortho* to phenoxy), 67.1 (*C*H$_2$OAr), 65.4 (piperazine *C*H), 54.1 (piperazine *C*H$_2$) 16.8 (*C*H$_3$). **HPLC:** $^{t}_{R}$ 2.74 min (95%). **HRMS:** *m/z* theoretical for $C_{21}H_{25}Cl_2N_4O_4$ 467.1247 $[M+H]^+$, measured 467.1239 $[M+H]^+$. **M.p.:** 259-261°C.

2-(4-Chlorophenoxy)-*N*-[(3*R*)-4-[2-(4-chlorophenoxy)acetamido]-3-methylpiperazin-1-yl]acetamide (108c)



Following general procedure C, (2*R*)-2-methylpiperazine-1,4-diamine dihydrochloride **107c** (0.13 g, 1 mmol) and 4-chlorophenoxyacetyl chloride **26** (0.25 mL, 2 mmol) in DCM (5 mL) were reacted for 2 hours. After concentration of the solvent, purification was achieved via column chromatography (eluent DCM/ EtOAc 20:80) to give the desired product as a solid. The resulting solid was further purified by triturated with diethyl ether (5 mL), then separated by filtration and dried in vacuo to afford the title compound as a white powder (0.31 g, yield: 70%). **^{1}H NMR (400 MHz, DMSO-*d*$_6$)** δ 9.21 (d, *J*=6.0 Hz, 1H, amide N*H*), 8.99 (d, *J*=6.0 Hz, 1H, amide N*H*), 7.32 (dd, *J*=2.4, 2.4 Hz, 4H, Ar C-*H ortho* to chlorine), 6.98 (dd, *J*=2.3, 2.2 Hz, 4H, Ar C-*H ortho* to phenoxy), 4.82 (s, 2H, C*H*$_2$OAr), 4.44 (s, 2H, C*H*$_2$OAr), 3.11 - 2.68 (m, 7H, piperazine C*H*,C*H*$_2$), 1.01 (t, *J*=5.8 Hz, 3H, C*H*$_3$). **^{13}C NMR (DMSO)** δ 170.4 (amide *C*=O), 157.7, 157.1 (2 x Ar 4º C-phenoxy), 129.5, 129.4 (2 x Ar *C*-H *ortho* to chlorine), 125.3 (Ar 4º C-chlorine), 116.9, 116.7 (Ar *C*-H *ortho* to phenoxy), 67.1 (*C*H$_2$OAr), 65.4 (piperazine *C*H), 54.1 (piperazine *C*H$_2$) 16.8 (*C*H$_3$). **HPLC:** $^{t}_{R}$ 2.74 min (95%). **LC-MS:** *m/z* = 467 $[M+H]^+$. **M.p.:** 260-262°C.

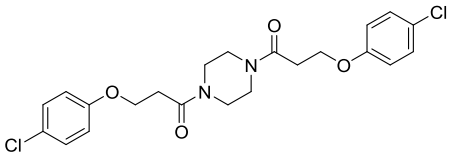
2-(4-Chlorophenoxy)-1-{4-[2-(4-chlorophenoxy)acetyl]piperazin-1-yl}ethan-1-one (109a)



Following general procedure C, piperazine **105a** (0.09 g, 1 mmol) and 4-chlorophenoxyacetyl chloride **26** (0.32 mL, 2 mmol) in DCM (10 mL) were reacted for 2 hours. The resulting precipitate was further purified by triturated with diethyl ether (3 mL), then separated by

filtration and dried in vacuo to afford the title compound as a white powder (0.40 g, yield: 95%). **^{1}H NMR (400 MHz, DMSO-*d*$_6$)** δ 7.31 (d, *J* = 8.8 Hz, 4H, Ar C-*H ortho* to chlorine), 6.95 (d, *J* = 8.9 Hz, 4H, Ar C-*H ortho* to phenoxy), 4.88 (s, 4H, C*H*$_2$OAr), 3.48 (d, *J* = 25.0 Hz, 8H, piperazine C*H*$_2$). **^{13}C NMR (DMSO)** δ 166.3 (amide *C*=O), 157.4 (Ar 4º C-phenoxy), 129.5 (Ar *C*-H *ortho* to chlorine), 125.0 (Ar 4º C-chlorine), 116.9 (Ar *C*-H *ortho* to phenoxy), 66.5 (*C*H$_2$OAr), 44.5, 44.2, 41.7, 41.4 (4 x piperazine *C*H$_2$). **HPLC:** ^tR 2.87 min (95%). **HRMS:** *m/z* theoretical for $C_{20}H_{20}Cl_2N_2O_4$ 423.0873 $[M+H]^+$, measured 423.0862 $[M+H]^+$. **M.p.:** 225-228 °C.

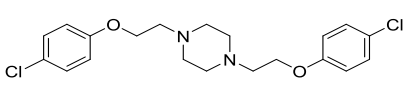
3-(4-Chlorophenoxy)-1-{4-[3-(4-chlorophenoxy)propanoyl]piperazin-1-yl}propan-1-one (109b)



Following general procedure C, piperazine **105a** (0.04 g, 0.5 mmol) and 3-(4-chlorophenoxy)propanoyl chloride **94** (0.15 mL, 1 mmol) in DCM (5 mL) were reacted for 2 hours. The resulting precipitate was further purified by triturated with diethyl ether (3 mL), then separated by filtration and dried in vacuo to afford the title compound as a white powder (0.17 g, yield: 75%). **^{1}H NMR (400 MHz, DMSO-*d*$_6$)** δ 7.32 (d, *J*=8.8 Hz, 4H, Ar C-*H ortho* to chlorine), 6.96 (d, *J*=8.5 Hz, 4H, Ar C-*H ortho* to phenoxy), 4.20 (t, *J*=6.1 Hz, 4H, C*H*$_2$OAr), 3.53 (dd, *J*=11.0, 13.0 Hz, 8H, piperazine C*H*$_2$), 2.84 (d, *J*=5.9 Hz, 4H, C*H*$_2$C=O). **^{13}C NMR (DMSO)** δ 166.7 (amide *C*=O), 157.9 (Ar 4º C-phenoxy), 129.6 (Ar *C*-H *ortho* to chlorine), 125.5 (Ar 4º C-chlorine), 116.6 (Ar *C*-H *ortho* to phenoxy), 65.4 (*C*H$_2$OAr), 44.7 (piperazine *C*H$_2$), 33.3 (*C*H$_2$). **HPLC:** ^tR 2.97 min (96%). **HRMS:** *m/z*

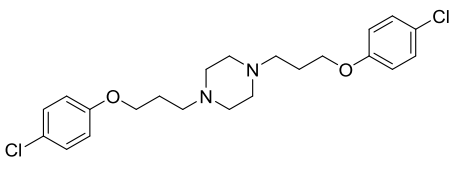
theoretical for $C_{22}H_{24}Cl_2N_2O_4$ 451.1186 $[M+H]^+$, measured 451.1187 $[M+H]^+$. **M.p.:** 227-230 °C.

1,4-Bis[2-(4-chlorophenoxy)ethyl]piperazine (109c)



To a suspension of piperazine **105a** (0.05 g, 0.5 mmol) and K_2CO_3 (0.27 g, 2 mmol) in MeOH (10 mL) was added a solution of 1-(2-bromoethoxy)-4-chlorobenzene **96a** (0.19 g, 1 mmol) in MeOH (5 mL). The resulting mixture was refluxed at 60 C^o for 10 hours. The reaction solution was then diluted with ethyl acetate (10 mL), washed with water and brine. The organic layer was dried over sodium sulphate, filtered and concentrated under vacuum. After concentration of the organic layer, purification was achieved via column chromatography (eluent Pet.ether/EtOAc) to obtain the desired product as a white solid. The resulting solid was further purified by triturated with diethyl ether (3 mL), then separated by filtration and dried in vacuo to afford the title compound as a white powder (0.08 g, yield: 43%). **^{1}H NMR (400 MHz, DMSO-*d*$_6$)** δ 7.30 (d, *J*=8.9 Hz, 4H, Ar C-*H ortho* to chlorine), 6.95 (d, *J*=8.9 Hz, 4H, Ar C-*H ortho* to phenoxy), 4.05 (t, *J*=5.8 Hz, 4H, C*H*$_2$OAr), 2.66 (t, *J*=5.8 Hz, 4H, C*H*$_2$CH$_2$), 2.50 (t, *J*=1.6 Hz, 8H, piperazine C*H*$_2$). **^{13}C NMR (DMSO-d$_6$):** 157.8 (Ar 4^o C-phenoxy), 129.6 (Ar *C*-H *ortho* to chlorine), 124.6 (Ar 4^o C-chlorine), 116.7 (Ar *C*-H *ortho* to phenoxy), 66.3 (*C*H$_2$OAr), 56.9 (piperazine *C*H$_2$), 53.5 (*C*H$_2$CH$_2$). **HPLC:** ^tR 2.36 min (95%). **LC-MS:** *m/z* = 395 $[M+H]^+$. **M.p.:** 128-130°C.

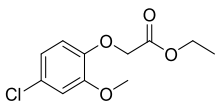
1,4-Bis[3-(4-chlorophenoxy)propyl]piperazine (109d)



To a suspension of piperazine **105a** (0.045 g, 0.5 mmol) and K_2CO_3 (0.27 g, 2 mmol)

in MeOH (10 mL) was added a solution of 1-(3-bromopropoxy)-4-chlorobenzene **96b** (0.25 g, 1 mmol) in MeOH (5 mL). The resulting mixture was refluxed at 60 C^{o} for 10 hours. The reaction solution was then diluted with ethyl acetate (10 mL), washed with water and brine. The organic layer was dried over sodium sulphate, filtered and concentrated under vacuum. After concentration of the organic layer, purification was achieved via column chromatography (eluent Pet.ether/EtOAc) to obtain the desired product as a white solid. The resulting solid was further purified by triturated with diethyl ether (3 mL), then separated by filtration and dried in vacuo to afford the title compound as a white powder (0.088 g, yield: 42%). **^{1}H NMR (400 MHz, DMSO-d_6)** δ 7.30 (d, *J*=8.9 Hz, 4H, Ar C-*H ortho* to chlorine), 6.93 (d, *J*=8.9 Hz, 4H, Ar C-*H ortho* to phenoxy), 3.97 (t, *J*=6.3 Hz, 4H, C*H*$_2$OAr), 3.45 (t, *J*=6.3 Hz, 4H, C*H*$_2$N), 2.37 (t, *J*=7.1 Hz, 8H, piperazine C*H*$_2$), 1.82 (p, 4H, C*H*$_2$CH$_2$). **^{13}C NMR (DMSO)** δ 158.5 (Ar 4^{o} C-phenoxy), 129.7 (Ar *C*-H *ortho* to chlorine), 116.6 (Ar *C*-H *ortho* to phenoxy), 68.8 (*C*H$_2$OAr), 66.7, 65.4 (*C*H$_2$N), 58.4, 54.8, 53.3 (piperazine *C*H$_2$), 29.3 (*C*H$_2$CH$_2$). **HPLC:** $^{t}_{R}$ 2.36 min (95%). **LC-MS:** *m/z* = 423[M+H]$^{+}$. **M.p.:** 125-128°C.

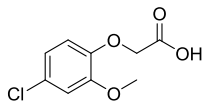
Ethyl 2-(4-chloro-2-methoxyphenoxy)acetate (116)



To a suspension of 4-chloro-2-methoxyphenol **115** (0.31 g, 2 mmol) and ethyl bromoacetate (0.24 mL, 2.2 mmol) in DMF (10 mL) was added K_2CO_3 (0.55 g, 4 mmol). The resulting mixture refluxed for 8h. The reaction solution was then diluted with water and extracted with ethyl acetate. The organic phase was washed with water and brine, and then dried over sodium sulphate, filtered and concentrated under vacuum. After concentration of the organic layer, purification was achieved via column chromatography (eluent

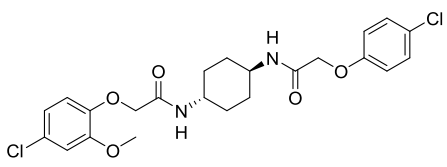
Pet.ether/EtOAc 10:90, 20:80, then 30:70) to obtain the desired product as colourless oil (0.39 g, yield: 80%). **LC-MS:** *m/z* = 245 $[M+H]^+$.

2-(4-Chloro-2-methoxyphenoxy)acetic acid (117)



Following general procedure F, ester solution **116** (0.36 g, 1.5 mmol) was treated with aqueous solution of LiOH (0.12 g, 3mmol) in water and THF (1:1, 10 mL) to afford the title compound as a white shiny crystal (0.26 g, yield: 81%). **^{1}H NMR (400 MHz, DMSO-*d*$_6$)**: δ 7.05 (d, *J*=2.3 Hz, 1H, Ar C-*H ortho* to methoxy), 6.92 (dd, *J*=2.3, 2.3 Hz, 1H, Ar C-*H ortho* to chlorine), 6.87 (d, *J*=8.6 Hz, 1H, Ar C-*H ortho* to phenoxy), 4.67 (s, 2H, C*H*$_2$OAr), 3.80 (s, 3H, C*H*$_3$). **^{13}C NMR (DMSO-d$_6$)**: δ 170.4 (amide *C*=O), 150.1 (Ar 4º C-methoxy), 146.7 (Ar 4º C-phenoxy), 125.4 (Ar 4º C-chlorine), 120.3(Ar *C*-H *ortho* to chlorine), 114.7 (Ar C-H *ortho* to phenoxy), 113.0 (Ar *C*-H *ortho* to methoxy), 65.6 (*C*H$_2$OAr), 56.3 (*C*H$_3$). **HPLC:** t_R 2.50 min (95%). **LC-MS:** *m/z* = 217 $[M+H]^+$.

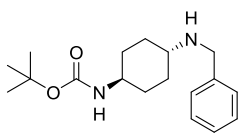
2-(4-Chloro-2-methoxyphenoxy)-*N*-[(1*R*,4*R*)-4-[2-(4-chlorophenoxy)acetamido]cyclohexyl]acetamide (118)



Following general procedure D, 2-(4-hloro-2-methoxyphenoxy)acetic acid **117** (0.09 g, 0.4 mmol) was reacted with HBTU (0.16 g, 0.44 mmol), 2-(4-chlorophenoxy)-*N*-[(1*R*,4*R*)-4-aminocyclohexyl]acetamide hydrochloride **28** (0.12 g, 0.44 mmol) and triethylamine (0.12 mL, 1 mmol) in DMF (10 mL) for 19 hours. After concentration of the organic layer, purification was achieved via column chromatography (eluent DCM/EtoAC 10:90, 20:80, then 30:70) to give the

desired product as a solid. The resulting solid was further purified by triturated with diethyl ether (3 mL), then separated by filtration and dried in vacuo to afford the title compound as a white powder (0.15 g, yield: 76%). **^{1}H NMR (400 MHz, DMSO-*d*$_6$)** 7.94 (d, *J*= 8.2 Hz, 1H, amide N*H*), 7.79 (d, *J*= 8.2 Hz, 1H, amide N*H*), 7.32 (d, *J*= 8.2, 2H, Ar C-*H ortho* to chlorine), 7.05 (s, 1H, Ar C-*H ortho* to methoxy), 6.95 (d, *J*= 8.8, 2H, Ar C-*H ortho* to phenoxy), 6.91 (s, 2H, Ar C-*H meta/para* to methoxy), 4.44 (d, *J*=6.0, 4H, C*H*$_2$OAr), 3.80 (s, 3H, methoxy C*H*$_3$), 3.56 (br. s, 2H, ^{C}Hx C*H*), 1.77 (d, *J* = 9.3 Hz, 4H, ^{C}Hx C*H*$_2$), 1.45 - 1.28 (m, 4H, ^{C}Hx C*H*$_2$). **^{13}C NMR (DMSO)** δ 167.5, 167.1 (2 x amide *C*=O), 157.5 (Ar 4º C-phenoxy), 150.9 (Ar 4º C-methoxy), 147.6 (Ar 4º C-phenoxy), 130.2 (Ar *C*-H *ortho* to chlorine), 126.3 (Ar 4º C-chlorine), 125.5 (Ar *C*-H *para* to methoxy), 117.3, 116.4 (2 x Ar *C*-H *ortho* to phenoxy), 113.1 (Ar *C*-H *ortho* to methoxy), 69.8 68.7 (2 x *C*H$_2$OAr), 56.9 (methoxy *C*H$_3$), 47.9 (^{C}Hx *C*H), 31.8 (^{C}Hx *C*H$_2$). **HPLC:** ^t_R 2.93 min (95%). **LC-MS:** *m/z* = 481 $[M+H]^+$. **M.p.:** 198-200 °C.

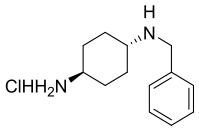
tert-Butyl _N_-[(1_R_,4_R_)-4-(benzylamino)cyclohexyl]carbamate (119)



Benzaldehyde (0.2 mL, 2 mmol) and Boc-*trans*-1,4-cyclohexanediamine **25** (0.45 g, 2.1 mmol) were mixed in ethanol (8 mL) at room temperature under nitrogen. The mixture was stirred for 3 h, to formed imine intermediate and then monitored by TLC which indicated that the reaction was completed. After that, the mixture was treated with solid $NaBH_4$ (0.12 g, 3.2 mmol) a clear solution was formed and the reaction was continued stirred for 1 hour, then 2 M NaOH was added. The product was then extracted with ether and the organic layer washed with brine solution, dried over sodium sulphate, filter and concentrated under the

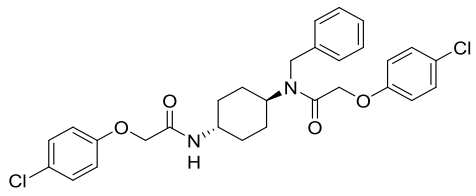
vacuum to afford crude product as a white powder. The resulting product was directly used for next step without further purification (0.30 g, yield: 51%). **LC–MS:** *m/z* = 305 $[M+H]^+$.

(1*R*,4*R*)-N1-Benzylcyclohexane-1,4-diamine hydrochloride (120)



A suspension of *tert*-butyl *N*-[(1*R*,4*R*)-4-(benzylamino)cyclohexyl]carbamate **119** (0.3 g, 1 mmol) was dissolved in dioxane (2 mL). This was then treated with 4 M HCl in dioxane (3 mL) with vigorously stirring for 2 hours. The reaction monitored by TLC, then all the solvents were removed in vacuo. The resulting hydrochloride salt of the desired compound was dried to afford the title compound as a light yellow powder. The resulting product was directly used for next step without further purification (0.23 g, yield: 96%). **LC–MS:** *m/z* = 204 $[M+H]^+$.

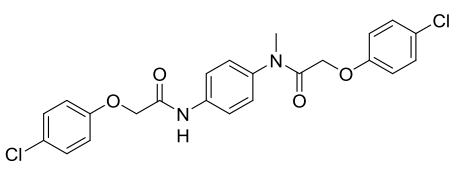
***N*-Benzyl-2-(4-chlorophenoxy)-*N*-[(1*R*,4*R*)-4-[2-(4-chlorophenoxy)acetamido]cyclohexyl]acetamide (121)**



Following general procedure C, (1*R*,4*R*)-N1-benzylcyclohexane-1,4-diamine hydrochloride **120** (0.1 g, 0.5 mmol) and 4-chlorophenoxyacetyl chloride **26** (0.15 mL, 1 mmol) in DCM (5 mL) were reacted for 3 hours. After concentration of the solvent, purification was achieved via column chromatography (eluent DCM/ EtOAc) to give the desired product as a solid. The resulting solid was further purified by triturated with diethyl ether (5 mL), then separated by filtration and dried in vacuo to afford the title compound as a light yellow powder (0.10 g, yield: 37%). **^{1}H NMR (400 MHz, $CDCl_3$- d_6)** δ 7.35 (d, *J*=7.4 Hz, 1H, amide N*H*), 7.26 (t, *J*=4.4 Hz, 3H, Ar C-*H*),

7.22 (dd, *J*=7.3, 9.0 Hz, 4H, Ar C-*H ortho* to chlorine), 7.12 (d, *J*=6.8 Hz, 1H, Ar C-*H*), 6.91 (td, *J*=8.5, 8.8, 8.8 Hz, 4H, Ar C-*H ortho* to phenoxy), 6.30 (d, *J*=8.3 Hz, 1H, Ar C-*H*), 4.79 (s, 1H, ^{C}Hx C*H*), 4.57 (s, 4H, CH_2OAr), 4.41 (s, 2H, CH_2Ar), 3.76 (bs, 1H, ^{C}Hx C*H*), 1.81 - 1.31 (m, 8H, ^{C}Hx CH_2). **^{13}C NMR (101 MHz, $CDCl_3$)** δ 171.1, 167.0 (2 x amide *C*=O), 156.7, 155.6 (2 x Ar 4º C-phenoxy), 137.5 (Ar 4º C-CH_2), 129.7, 129.6 (2 x Ar *C*-H *ortho* to chlorine), 129.3, 128.9, 128.4, 127.7, 127.2 (5 x Ar *C*-H), 126.9, 125.9 (2 x Ar 4º C-chlorine), 116.0, 115.9 (2 x Ar *C*-H *ortho* to phenoxy), 67.7, 67.5 (2 x *C*H_2OAr), 60.4 (^{C}Hx *C*H), 53.5 (^{C}Hx *C*H), 47.2 (*C*H_2Ar), 31.9, 30.4, 28.6, 21.0 (4 x ^{C}Hx *C*H_2). **HPLC:** $^{t}_{R}$ 2.91 min (95%). **LC-MS:** *m/z* = 541 $[M+H]^+$. **M.p.:** 125-128 °C.

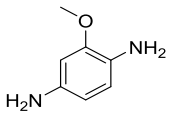
2-(4-Chlorophenoxy)-*N*-{4-[2-(4-chlorophenoxy)acetamido]phenyl}-*N*-methylacetamide (125)



Following general procedure C, *N*-methylbenzene-1,4-diamine **124** (0.09 g, 0.5 mmol) and 4-chlorophenoxyacetyl chloride (0.15 mL, 1 mmol) in DCM (5 mL) were reacted for 2 hours. The resulting precipitate was further purified by triturated with diethyl ether (3 mL), then separated by filtration and dried in vacuo to afford the title compound as a white crystals (0.16 g, yield: 71%). **^{1}H NMR (400 MHz, DMSO-d_6)** δ 10.26 (s, 1H, amide N*H*), 7.71 (d, *J*=8.3, Hz, 2H, Ar C-*H ortho* to NHCO), 7.43 (dd, *J*=6.2, 8.6 Hz, 4H, Ar C-*H ortho* to chlorine), 7.27 (dd, *J*=7.7, 8.6 Hz, 4H, Ar C-*H ortho* to phenoxy), 6.79 (d, *J*=6.4 Hz, 2H, Ar C-*H ortho* to NCH_3CO), 4.73 (s, 2H, CH_2OAr), 4.44 (s, 2H, CH_2OAr), 3.16 (s, 3H, CH_3). **^{13}C NMR (DMSO)** δ 166.9 (amide *C*=O), 157.2, 157.1 (2 x Ar 4º C-phenoxy), 138.5 (Ar 4º C-NH),

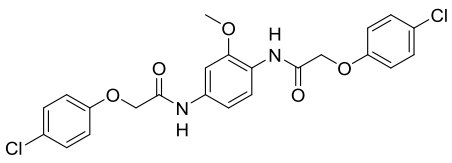
137.7 (Ar 4º C-NCH_3), 129.7, 129.5, 128.0 (3 x Ar *C*-H *ortho* to chlorine, and *ortho* to NCH_3), 125.4, 124.9 (2 x Ar 4º C-chlorine), 121.1 (Ar *C*-H *ortho* to NHCO), 116.9, 116.6 (2 x Ar *C*-H *ortho* to phenoxy), 67.8, 65.4 (*C*H_2OAr), 37.4 (*C*H_3). **HPLC:** $^{t}_{R}$ 3.02 min (95%). **HRMS:** *m/z* theoretical for $C_{23}H_{20}Cl_2N_2O_4$ 459.0872 $[M+H]^+$, measured 459.0864 $[M+H]^+$. **M.p.:** 232-235°C.

2-Methoxybenzene-1,4-diamine (127)



In a round bottom flask, 3-methoxy-4-nitroaniline **126** (0.5 g, 3.25 mmol) was dissolved in methanol (10 mL) and hydrogenated over palladium on carbon (0.3 g). The resulting mixture was stirred overnight at ambient temperature under atmospheric pressure. The suspension was filtered over celite and washed with excess MeOH. The resulting solution was concentrated under the vacuum to afforded the title compound as a light-red powder (0.42 g, yield: 95%). **^{1}H NMR (400 MHz, DMSO-*d*$_6$)** δ 6.38 (d, *J*=8.1 Hz, 1H, Ar C-*H meta* to metoxy), 6.19 (d, *J*=2.1 Hz, 1H, Ar C-*H ortho* to methoxy), 6.00 (dd, *J*=2.0, 2.0 Hz, 1H, Ar C-*H para* to chlorine), 4.06 (s, 4H, N*H*$_2$), 3.67 (s, 3H, CH_3). **^{13}C NMR (DMSO)** δ 147.9 (Ar 4º C-methoxy), 140.4 (Ar 4º C-NH), 127.8 (Ar 4º C-NH), 115.8 (Ar *C*-H *meta* to methoxy), 106.9 (Ar *C*-H *para* to methoxy), 99.7 (Ar *C*-H *ortho* to methoxy), 55.4 (*C*H_3).

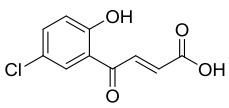
2-(4-Chlorophenoxy)-*N*-{4-[2-(4-chlorophenoxy)acetamido]-3-methoxyphenyl}acetamide (128)



Following general procedure C, 2-methoxybenzene-1,4-diamine **127** (0.07 g, 0.5 mmol) and 4-chlorophenoxyacetyl chloride (0.15 mL, 1 mmol) in DCM (5 mL) were reacted for 2 hours. The resulting precipitate was further purified by triturated with diethyl ether (3 mL),

then separated by filtration and dried in vacuo to afford the title compound as a pink powder (0.19 g, yield: 82%). **^{1}H NMR (400 MHz, DMSO-*d*$_6$)** δ 10.44 (s, 1H, amide N*H*), 9.21 (s, 1H, amide N*H*), 7.88 (d, *J*=8.7 Hz, 1H, Ar C-*H ortho* to methoxy), 7.53 (d, *J*=1.9 Hz, 1H, Ar C-*H para* to methoxy), 7.37 (dd, *J*=6.5, 6.5 Hz, 4H, Ar C-*H ortho* to chlorine), 7.23 (dd, *J*=1.8, 1.9 Hz, 1H, Ar C-*H meta* to metoxy), 7.04 (t, *J*=8.1 Hz, 4H, Ar C-*H ortho* to phenoxy), 4.74 (s, 4H, C*H*$_2$OAr), 3.81 (s, 3H, C*H*$_3$). **^{13}C NMR (DMSO)** δ 166.6, 166.3 (2 x amide *C*=O), 157.2, 156.9 (2 x Ar 4º C-phenoxy), 150.0 (Ar 4º C-methoxy), 136.1 (Ar 4º C-*meta* to methoxy), 129.8, 129.7 (2 x Ar *C*-H *ortho* to chlorine), 125.5, 125.3 (2 x Ar 4º C-chlorine), 122.5 (Ar 4º C-*ortho* to methoxy), 122.0 (Ar C-H *meta* to methoxy), 117.0, 116.9 (2 x Ar *C*-H *ortho* to phenoxy), 111.6 (Ar C-H *para* to methoxy), 103.6 (Ar C-H *ortho* to methoxy), 67.7 67.6 (2 x *C*H$_2$OAr), 56.2 (*C*H$_3$). **HPLC:** $^{t}_{R}$ 3.09 min (>95%). **LC-MS:** *m/z* = 475 $[M+H]^+$. **M.p.:** 247-250°C.

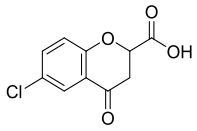
4-(5-Chloro-2-hydroxy-phenyl)-4-oxo-but-2-enoicacid (131)



Maleic anhydride **130** (0.51 g, 6 mmol) and anhydrous aluminum chloride (1.6 g, 12.5 mmol) were dissolved in 1,2-dichloroethane (5 mL) by heating at 50 ^{0}C for 15 minutes and then 4-chloroanisole **129** (0.7 mL, 5.5 mmol) was added dropwise. The mixture was refluxed for 1 hour and poured into concentrated hydrochloric acid (5 mL) with cracked ice. The resulting solids were filtered, washed with water, DCM and dried under vacuum to afford the titled compound as a yellow powder (0.96 g, yield: 71%). **^{1}H NMR (400 MHz, DMSO-*d*$_6$)** δ 13.11 (bs, 1H, O*H*), 11.31 (s, 1H, O*H*), 7.86 (d, *J*=13.5 Hz, 1H, C*H*=CH), 7.67 (d, *J*=2.7 Hz, 1H, Ar C-*H ortho* to chlorine), 7.52 (dd, *J*=2.7, 2.7 Hz, 1H, Ar C-*H ortho* to chlorine), 7.04 (d,

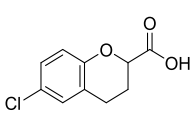
J=8.8 Hz, 1H, Ar C-*H ortho* to OH), 6.61 (d, *J*=14.5 Hz, 1H, CH=C*H*). **^{13}C NMR (DMSO)** δ 190.8 (ketone *C*=O), 166.8 (carboxylic *C*=O), 158.3 (Ar 4º C-hydroxy), 139.0 (*C*H=CH), 135.4, 132.2 (2 x Ar *C*-H *ortho* to chlorine), 129.9 (CH=*C*H), 124.9 (Ar 4º C-chlorine), 123.6 (Ar 4º C-ketone), 120.0 (Ar *C*-H *ortho* to hydroxy). **HPLC:** $^{t}_{R}$ 2.65 min (95%). **LC-MS:** *m/z* = 226 $[M+H]^{+}$.

6-Chloro-4-oxo-chroman-2-carboxylicacid (132)



To a stirred suspension of 4-(5-chloro-2-hydroxy-phenyl)-4-oxo-but-2-enoicacid **131** (0.86 g, 3.6 mmol) in water (25 mL) was added dropwise 1N sodium hydroxide aqueous solution (4 mL, 4 mmol). The mixture was refluxed for 3 hours at 100 ^{0}C, then was cooled down to room temperature and acidified with concentrated HCl until pH about 1. The resulting residues were filtered, washed with water and dried in vacuum to afford the titeld product as a beige powder (0.69 g, yield: 85%). **^{1}H NMR (400 MHz, DMSO-*d*$_6$)** δ 7.66 (dd, *J*=4.2, 2.5 Hz, 2H, Ar C-*H ortho* to chlorine), 7.19 (d, *J*=8.7 Hz, 1H, Ar C-*H ortho* to phenoxy), 5.37 (t, *J*=6.2 Hz, 1H, C*H*OAr), 3.18 (dd, *J*=5.2, 5.3 Hz, 1H, CH_2C=O), 3.03 (dd, *J*=7.2, 7.3 Hz, 1H, CH_2C=O). **^{13}C NMR (101 MHz, DMSO)** δ 189.4 (ketone *C*=O), 170.6 (carboxylic *C*=O), 159.2 (Ar 4º C-phenoxy), 136.4, 126.2 (2 x Ar *C*-H *ortho* to chlorine), 125.5 (Ar 4º C-chlorine), 122.1(Ar 4º C-ketone), 120.8 (Ar *C*-H *ortho* to phenoxy), 75.2 (*C*HOAr), 65.4 (*C*H_2C=O). **HPLC:** $^{t}_{R}$ 2.51 min (95%). **LC-MS:** *m/z* = 226 $[M+H]^{+}$.

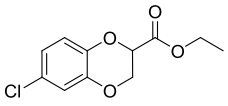
6-Chloro-chroman-2-carboxylicacid (133)



To a stirred suspension of 6-chloro-4-oxo-chroman-2-carboxylicacid **132** (0.6 g, 2.5 mmol) in trifluoroacetic acid (2.5 mL) was added dropwise triethylsilane (1.2 mL, 6.25 mmol). The mixture

was stirred at 50 ^{0}C for three days. After cooled down to room temperature, the excess triethylsilane and solvent were removed under reduced pressure and the residue was dissolved in 1N NaOH. The aqueous solution was washed with diethyl ether, acidified with 6N HCl acid until pH about 1, and then extracted with ethyl acetate. The combined extracts organic layers were washed with water, brine, dried over anhydrous sodium sulfate, filtered, concentrated under reduced pressure, and dried in vacuo to afford the titled compound as a beige powder (0.49 g, yield: 93%). **^{1}H NMR (400 MHz, DMSO-*d*$_6$)** δ 13.09 (bs, 1H, O*H*), 7.13 (s, 1H, Ar C-*H ortho* to chlorine), 7.11 (d, *J*=2.7 Hz, 1H, Ar C-*H ortho* to chlorine), 6.83 (d, *J*=8.6 Hz, 1H, Ar C-*H ortho* to phenoxy), 4.82 (dd, *J*=4.0, 4.0 Hz, 1H, C*H*OAr), 2.85 - 2.73 (m, 1H, chromane CH_2), 2.69 - 2.58 (m, 1H, chromane CH_2), 2.18 - 1.99 (m, 2H, chromane CH_2). **^{13}C NMR (DMSO)** δ 172.2 (carboxylic *C*=O), 152.7 (Ar 4º C-phenoxy), 129.3, 127.5 (2 x Ar *C*-H *ortho* to chlorine), 124.2 (Ar 4º C-chlorine), 118.4 (Ar *C*-H *ortho* to phenoxy), 73.3 (*C*HOAr), 23.8, 22.6 (*C*H$_2$ chromane). **HPLC:** ^tR 2.64 min (95%). **LC-MS:** *m/z* = 213 $[M+H]^+$.

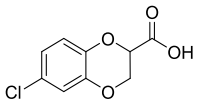
Ethyl 6-chloro-2,3-dihydro-1,4-benzodioxine-2-carboxylate (135a)



To a solution of 4-chlorocatechol **134a** (0.40 g, 2.8 mmol) in acetone (10 mL) was added K_2CO_3 (0.96 g, 7 mmol), then dropwise added ethyl-2,3-dibromopropionate (0.44 mL, 3 mmol). The mixture was refluxed for 20 hour and monitored by TLC. The solvent was removed and the residue was mixed with equal portion of water and EtOAc (10 mL). The layer was separated and the aqueous phase was washed with ethyl acetate (2X, 10 mL). The organic layer was combined, dried with sodium sulphate and concentrated then the crude product was purified by column chromatography using gradients

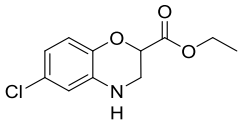
of (pet.ether/EtOAc). The combined fractions were concentrated to afford a regioisomeric mixture of its benzodioxane derivatives as colourless oil (0.5 g, yield: 74%). **^{1}H NMR (400 MHz, DMSO-*d*$_6$)** δ 6.97 (d, *J*=2.7 Hz, 1H, Ar C-*H ortho* to chlorine), 6.93 (dd, *J*=2.5, 2.5 Hz, 1H, Ar C-*H ortho* to chlorine), 6.89 (d, *J*=1.0 Hz, 1H, Ar C-*H ortho* to phenoxy), 5.23 (dt, *J*=2.9, 3.0 Hz, 1H, C*H*OAr), 4.49 (dq, *J*=1.6, 1.6 Hz, 1H, benzodioxane CH_2), 4.32 (dtd, *J*=2.8, 3.1, 2.8 Hz, 1H, benzodioxane CH_2), 4.19 (qd, *J*=0.6, 0.7, 0.7, 0.7 Hz, 2H, COOCH_2CH$_3$), 1.18 (t, *J*=7.1 Hz, 3H, CH$_3$). **^{13}C NMR (DMSO)** δ 168.1 (carboxylate *C*=O), 144.0, 142.5 (2 x Ar 4º C-phenoxy), 125.5 (Ar 4º C-chlorine), 122.1(Ar *C*-H *ortho* to chlorine), 118.7 (Ar *C*-H *ortho* to phenoxy), 117.2 (Ar *C*-H *ortho* to chlorine and phenoxy), 71.7 (*C*HOAr), 65.2 (benzodioxane *C*H_2), 61.8 (COO*C*H_2CH$_3$), 14.3 (CH$_3$). **HPLC:** $^{t}_{R}$ 2.92 min (95%). **LC-MS:** *m/z* = 242 $[M+H]^+$.

6-Chloro-2,3-dihydro-1,4-benzodioxine-2-carboxylic acid (136a)



Following general procedure F, ester solution **135a** (0.36 g, 1.5 mmol) was treated with aqueous solution of LiOH (0.12 g, 3 mmol) in water and THF (1:1, 10 mL) to afford the title compound as a light yellow powder 93%. The resulting product was directly used for next step without further purification (0.29 g, yield: 93%). **LC–MS:** *m/z* = 215 $[M+H]^+$.

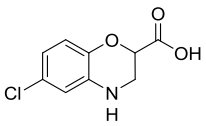
Ethyl 6-chloro-3,4-dihydro-2H-1,4-benzoxazine-2-carboxylate (135b)



To a solution of 2-amino-4-chlorophenol **134b** (0.40 g, 2.8 mmol) in acetone (10 mL) was added K_2CO_3 (0.96 g, 7 mmol), then dropwise added ethyl-2,3-dibromopropionate (0.44 mL, 3 mmol). The mixture was refluxed for 20 hour and monitored by TLC. The solvent was removed and the residue was mixed with equal portion of

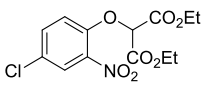
water and EtOAc (10 mL). The layer was separated and the aqueous phase was washed with ethyl acetate (2X, 10 mL). The organic layer was combined, dried with sodium sulphate and concentrated then the crude product was purified by column chromatography using gradients of (Pet.ether/EtOAc). The combined fractions were concentrated to afford a regioisomeric mixture of product as a light beige crystals (0.37 g, yield: 55%). **^{1}H NMR (400 MHz, DMSO-*d*$_6$)** δ 6.74 (d, *J*=8.5 Hz, 1H, Ar C-*H ortho* to chlorine), 6.59 (d, *J*=2.5 Hz, 1H, Ar C-*H ortho* to phenoxy), 6.52 (dd, *J*=2.5, 2.5 Hz, 1H, Ar C-*H ortho* to chlorine), 6.14 (s, 1H, N*H*), 4.94 (t, *J*=3.6 Hz, 1H, C*H*OAr), 4.13 (q, *J*=7.1 Hz, 2H, C*H*$_2$CH$_3$), 3.45 (dtd, *J*=3.9, 3.3, 3.4 Hz, 2H, benzoxazine C*H*$_2$N), 1.17 (t, *J*=7.1 Hz, 3H, C*H*$_3$). **^{13}C NMR (DMSO)** δ 169.4 (carboxylate *C*=O), 141.3 (Ar 4º C-NH), 135.9 (Ar 4º C-phenoxy), 125.1 (Ar 4º C-chlorine), 117.6 (Ar *C*-H *ortho* to phenoxy), 116.9, 114.2 (2 x Ar *C*-H *ortho* to chlorine), 72.2 (*C*HOAr), 61.3 (*C*H$_2$CH$_3$), 55.3 (*C*H$_2$NH), 14.4 (*C*H$_3$). **HPLC:** ^{t}$_R$ 2.78min (95%). **LC-MS:** *m/z* = 242 $[M+H]^+$.

6-Chloro-3,4-dihydro-2H-1,4-benzoxazine-2-carboxylic acid (136b)



Following general procedure F, ester solution **135b** (0.24 g, 1mmol) was treated with aqueous solution of LiOH (0.12 g, 3 mmol) in water and THF (1:1, 10 mL) to afford the title compound as a brown powder 88%. The resulting product was directly used for next step without further purification (0.18 g, yield: 88%). **LC–MS:** *m/z* = 214 $[M+H]^+$.

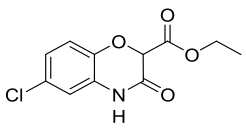
2-(4-Chloro-2-nitrophenoxy)-malonic acid diethyl ester (138)



4-Chloro-2-nitrophenol **137** (0.53 g, 3 mmol) was dissolved in (2 mL) of DMF, and then K_2CO_3 (0.83 g, 6 mmol) and diethyl-2-bromomalonate (0.52 mL, 3.1 mmol) were added to the solution. The

resulting mixture was stirred at ambient temperature for overnight, then diluted with ice water and extracted with EtOAc. The organic layer washed with water and brine solution, dried over sodium sulphate, and concentrated under vacuum. After concentration of the organic layer, the resulting product was purified by column chromatography using gradients of (Pet.ether/EtOAc). The combined fractions were concentrated to afford the title compound as orang oily product (0.44 g, yield: 45%). **^{1}H NMR (400 MHz, DMSO-*d*$_6$)** δ 8.08 (d, *J*=2.6 Hz, 1H, Ar C-*H ortho* to chlorine), 7.74 (dd, *J*=2.7, 2.7 Hz, 1H, Ar C-*H ortho* to chlorine), 7.38 (d, *J*=9.2 Hz, 1H, Ar C-*H ortho* to phenoxy), 6.00 (s, 1H, C*H*OAr), 4.29 - 4.19 (m, 4H, C*H*$_2$CH$_3$), 1.20 (t, *J*=7.1 Hz, 6H, C*H*$_3$). **^{13}C NMR (DMSO)** δ 164.7 (carboxylate *C*=O), 148.2 (Ar 4º C-phenoxy), 141.2 (Ar 4º C-nitro), 134.1 (Ar *C*-H *ortho* to chlorine), 126.5 (Ar 4º C-chlorine), 125.1 (Ar *C*-H *ortho* to chlorine), 118.7 (Ar *C*-H *ortho* to phenoxy), 77.3 (*C*HOAr), 62.7 (*C*H$_2$CH$_3$), 14.2 (*C*H$_3$). **HPLC:** ^{t}R 2.94min (95%). **LC-MS:** *m/z* = 331[M+H]$^+$.

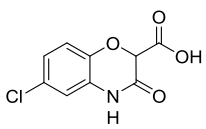
Ethyl 6-chloro-3-oxo-3,4-dihydro-2H-1,4-benzoxazine-2-carboxylate (139)



2-(4-Chloro-2-nitrophenoxy)-malonic acid diethyl ester **138** (0.33 g, 1 mmol) was dissolved in (9 mL) EtOH:H$_2$O (4:5) and then Na$_2$S$_2$O$_4$ (1.1 g, 6 mmol) was added. The reaction mixture was stirred at 60 °C for 5 hours. The reaction mixture was concentrated under reduce pressure and diluted with water then extracted with ethyl acetate. The organic layer washed with water and brine solution, dried over sodium sulphate and concentrated under vacuum to afford the title product as a white powder (0.21 g, yield: 85%). **^{1}H NMR (400 MHz, DMSO-*d*$_6$)** δ 11.13 (s, 1H, N*H*), 7.08 (d, *J*=8.6 Hz, 1H, Ar C-*H ortho* to chlorine), 7.02 (dd, *J*=2.4, 2.4 Hz, 1H, Ar C-*H ortho* to chlorine), 6.92 (d, *J*=2.4 Hz, 1H, Ar C-*H ortho* to

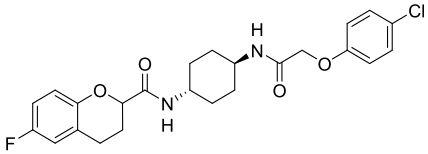
phenoxy), 5.50 (s, 1H, C*H*OAr), 4.20 - 4.11 (m, 2H, CH_2CH$_3$), 1.17 (d, *J*=2.1 Hz, 3H, CH_3). **^{13}C NMR (DMSO)** δ 166.9 (carboxylate *C*=O), 166.1 (amide *C*=O), 160.7 (Ar 4º C-phenoxy), 128.1(Ar 4º C-phenoxy), 126.7(Ar 4º C-NH), 123.4 (Ar *C*-H *ortho* to phenoxy), 118.5, 115.8 (2 x Ar *C*-H *ortho* to chlorine), 75.9 (*C*HOAr), 62.1 (*C*H_2CH$_3$), 14.2 (*C*H_3),. **HPLC:** $^{t}_{R}$ 2.64min (95%). **LC-MS:** *m/z* = 255 $[M+H]^+$.

6-Chloro-3-oxo-3,4-dihydro-2H-1,4-benzoxazine-2-carboxylic acid (140)



Following general procedure F, ester solution **139** (0.13 g, 0.5 mmol) was treated with aqueous solution of LiOH (0.06 g, 1.5 mmol) in water and THF (1:1, 5 mL) to afford the title compound as a light brown powder 85%. The resulting product was directly used for next step without further purification (0.09 g, yield: 85%). **LC–MS:** *m/z* = 228 $[M+H]^+$.

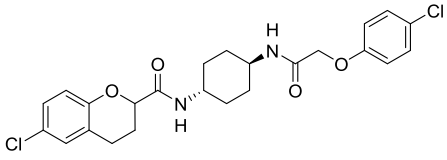
6-Fluoro-*N*-[(1*R*,4*R*)-4-[2-(4-chlorophenoxy)acetamido]cyclohexyl]-3,4-dihydro-2H-1-benzopyran-2-carboxamide (141)



Following general procedure D, commercially available 6-fluorochroman-2-carboxylic acid (0.1 g, 0.5 mmol) was reacted with HBTU (0.21 g, 0.55 mmol), 2-(4-chlorophenoxy)-*N*-[(1*R*,4*R*)-4-aminocyclohexyl]acetamide hydrochloride **28** (0.15 g, 0.55 mmol) and triethylamine (0.17 mL, 1.35 mmol) in DMF (10 mL) for 15 hours. After concentration of the organic layer, purification was achieved via column chromatography (eluent DCM/THF) to give the desired product as a solid. The resulting solid was further purified by triturated with diethyl ether (3 mL), then separated by filtration and dried in vacuo to afford the title compound as a white powder (0.2 g, yield: 86%). **^{1}H NMR (400 MHz,**

DMSO-*d*$_6$) δ 7.94 (d, *J*=8.1 Hz, 1H, amide N*H*), 7.79 (d, *J*=8.1 Hz, 1H, amide N*H*), 7.33 (d, *J*=8.9 Hz, 2H, Ar C-*H ortho* to chlorine), 6.96 (dd, *J*=9.0, 8.6 Hz, 4H, Ar C-*H ortho* to fluorine and *ortho* to phenoxy) 6.88 (d, *J*=5.2 Hz, 1H, Ar C-*H meta* to fluorine), 4.47 (d, *J*=2.9 Hz, 1H, C*H*OAr), 4.44 (s, 2H, C*H*$_2$OAr), 3.55 (bs, 2H, ^{C}Hx C*H*), 2.86 - 2.63 (m, 2H, benzyl C*H*$_2$ of chromane), 2.16 - 2.09 (m, 1H, C*H*$_2$ of chromane), 1.90 - 1.81 (m, 1H, C*H*$_2$ of chromane), 1.78 (d, *J*=7.4 Hz, 4H, ^{C}Hx C*H*$_2$), 1.34 (q, *J*=9.8 Hz, 4H, ^{C}Hx C*H*$_2$). **^{13}C NMR (DMSO)** δ 169.3 (amide *C*=O), 166.9 (amide *C*=O), 157.1 (Ar 4º C-phenoxy), 155.4 (Ar 4º C-fluorine), 150.0 (Ar 4º C-phenoxy), 129.6 (Ar *C*-H *ortho* to chlorine), 125.3 (Ar 4º C-chlorine), 124.0 (Ar 4º C-chromane), 118.2 (Ar *C*-H *meta* to fluorine), 117.0, 115.8 (2 x Ar *C*-H *ortho* to phenoxy), 114.3, 114.1 (2 x Ar *C*-H *ortho* to fluorine), 75.2 (*C*HOAr), 67.6 (*C*H$_2$OAr), 47.4 (^{C}Hx *C*H), 31.3, 31.2 (2 x ^{C}Hx *C*H$_2$), 24.7, 23.9 (2 x chromane *C*H$_2$). **HPLC:** $^{t}_{R}$ 2.94 min (95%). **HRMS:** *m/z* theoretical for $C_{24}H_{27}ClFN_2O_4$ 461.1638 $[M+H]^+$, measured 461.1625 $[M+H]^+$. **M.p.:** 252-254°C.

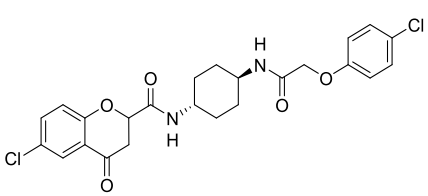
6-Chloro-*N*-[(1*R*,4*R*)-4-[2-(4-chlorophenoxy)acetamido]cyclohexyl]-3,4-dihydro-2H-1-benzopyran-2-carboxamide (142)



Following general procedure D, 6-chloro-chroman-2-carboxylicacid **133** (0.1 g, 0.5 mmol) was reacted with HBTU (0.21 g, 0.55 mmol), 2-(4-chlorophenoxy)-*N*-[(1*R*,4*R*)-4-aminocyclohexyl]acetamide hydrochloride **28** (0.15 g, 0.55 mmol) and triethylamine (0.17 mL, 1.35 mmol) in DMF (10 mL) for 19 hours. After concentration of the organic layer, purification was achieved via column chromatography (eluent DCM/THF) to give the desired product as a solid. The resulting solid was further purified by

triturated with diethyl ether (3 mL), then separated by filtration and dried in vacuo to afford the title compound as a beige powder (0.15 g, yield: 65%). **^{1}H NMR (400 MHz, DMSO-*d*$_6$)** δ 7.96 (d, *J*=8.1 Hz, 1H, amide N*H*), 7.84 (d, *J*=8.1 Hz, 1H, amide N*H*), 7.36 (dd, *J*=2.1, 2.1 Hz, 2H, Ar C-*H ortho* to chlorine), 7.15 (s, 1H, Ar C-*H ortho* to chlorine), 7.13 (d, *J*=2.6 Hz, 1H, Ar C-*H ortho* to chlorine), 6.99 (dd, *J*=2.2, 2.2 Hz, 2H, Ar C-*H ortho* to phenoxy), 6.91 (dd, *J*=1.2, 1.3 Hz, 1H, Ar C-*H ortho* to phenoxy), 4.52 (dd, *J*=3.0, 3.0 Hz, 1H, C*H*OAr), 4.46 (s, 2H, C*H*$_2$OAr), 3.59 (bs, 2H, ^{C}Hx C*H*), 2.86 - 2.64 (m, 2H, chromane C*H*$_2$), 2.17 - 2.08 (m, 1H, chromane C*H*$_2$), 1.93 - 1.82 (m, 1H, chromane C*H*$_2$), 1.77 (t, *J*=7.7 Hz, 4H, ^{C}Hx C*H*$_2$), 1.36 (q, *J*=10.2 Hz, 4H, ^{C}Hx C*H*$_2$). **^{13}C NMR (DMSO)** δ 169.1, 166.8 (2 x amide *C*=O), 157.1, 152.7 (2 x Ar 4º C-phenoxy), 129.6, 129.3, 127.3 (3 x Ar *C*-H *ortho* to chlorine), 125.2, 124.6 (2 x Ar 4º C-chlorine), 124.3 (Ar 4º C-*ortho* to phenoxy), 118.7, 116.9 (2 x Ar *C*-H *ortho* to phenoxy), 75.2 (*C*HOAr), 67.6 (*C*H$_2$OAr), 47.4, 47.4 (^{C}Hx *C*H), 31.3, 31.3, 31,2 (3 x ^{C}Hx *C*H$_2$), 24.6 (chromane *C*H$_2$), 23.5 (chromane *C*H$_2$). **HPLC:** ^{t}$_R$ 3.01min (95%). **HRMS:** *m/z* theoretical for $C_{24}H_{27}Cl_2N_2O_4$ 477.1342 $[M+H]^+$, measured 477.1350 $[M+H]^+$. **M.p.:** 248-250°C.

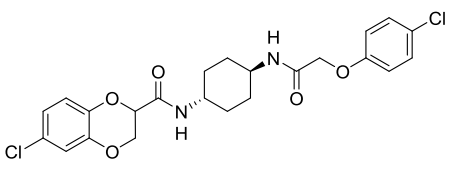
6-Chloro-4-oxo-*N*-[(1*R*,4*R*)-4-[2-(4-chlorophenoxy)acetamido]cyclohexyl]-3,4-dihydro-2H-1-benzopyran-2-carboxamide (143)



Following general procedure D, 6-chloro-4-oxo-chroman-2-carboxylicacid **132** (0.11 g, 0.5 mmol) was reacted with HBTU (0.21 g, 0.55 mmol), 2-(4-chlorophenoxy)-*N*-[(1*R*,4*R*)-4-aminocyclohexyl]acetamide hydrochloride **28** (0.15 g, 0.55 mmol) and triethylamine (0.17 mL, 1.35 mmol) in DMF (10 mL) for 19 hours. After concentration of the organic layer,

purification was achieved via column chromatography (eluent DCM/THF) to give the desired product as a solid. The resulting solid was further purified by triturated with diethyl ether (3 mL), then separated by filtration and dried in vacuo to afford the title compound as off-white powder (0.16 g, yield: 68%). **^{1}H NMR (400 MHz, DMSO-*d*$_6$)** δ 8.21 (d, *J*=8.0 Hz, 1H, amide N*H*), 7.97 (d, *J*=8.1 Hz, 1H, amide N*H*), 7.66 (dd, *J*=2.3, 2.7 Hz, 2H, Ar C-*H ortho* to chlorine), 7.36 (dd, *J*=2.0, 2.3 Hz, 2H, Ar C-*H ortho* to chlorine), 7.18 (d, *J*=8.6 Hz, 1H, Ar C-*H ortho* to phenoxy), 6.98 (dd, *J*=2.1, 1.9 Hz, 2H, Ar C-*H ortho* to phenoxy), 5.14 (dd, *J*=5.5, 5.5 Hz, 1H, C*H*OAr), 4.46 (s, 2H, C*H*$_2$OAr), 3.56 (bs, Hz, 2H, ^{C}Hx C*H*), 3.08 (q, *J*=7.1 Hz, 1H, oxo-chromane C*H*$_2$), 2.99 (dd, *J*=2.0, 4.8 Hz, 1H, oxo-chromane C*H*$_2$), 1.75 (t, *J*=12.3 Hz, 4H, ^{C}Hx C*H*$_2$), 1.32 (q, *J*=9.7 Hz, 4H, ^{C}Hx C*H*$_2$). **^{13}C NMR (DMSO)** δ 189.8 (ketone *C*=O), 167.2, 166.8 (2 x amide *C*=O), 158.9, 157.1 (2 x Ar 4º C-phenoxy), 136.1, 129.6, 126.1 (3 x Ar *C*-H *ortho* to chlorine), 125.4, 125.2 (2 x Ar 4º C-chlorine), 122.3 (Ar 4º C-*ortho* to phenoxy), 120.8, 116.9 (Ar *C*-H *ortho* to phenoxy), 76.6 (*C*HOAr), 67.6 (*C*H$_2$OAr), 47.7, 47.3(2 x ^{C}Hx *C*H), 45.9 (oxo-chromane *C*H$_2$), 31.2, 31.1 (^{C}Hx *C*H$_2$). **HPLC:** ^{t}$_R$ 2.92 min (95%). **HRMS:** *m/z* theoretical for $C_{24}H_{25}Cl_2N_2O_5$ 491.1135 $[M+H]^+$, measured 491.1127 $[M+H]^+$. **Mp:** 255-257°C.

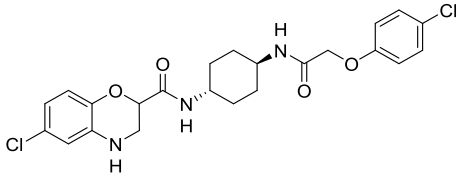
6-Chloro-*N*-[(1*R*,4*R*)-4-[2-(4-chlorophenoxy)acetamido]cyclohexyl]-2,3-dihydro-1,4-benzodioxine-2-carboxamide (144)



Following general procedure D, 6-chloro-2,3-dihydro-1,4-benzodioxine-2-carboxylic acid **136a** (0.1 g, 0.5 mmol) was reacted with HBTU (0.21 g, 0.55 mmol), 2-(4-chlorophenoxy)-*N*-[(1*R*,4*R*)-4-aminocyclohexyl]acetamide hydrochloride **28** (0.15 g, 0.55 mmol) and

triethylamine (0.17 mL, 1.35 mmol) in DMF (10 mL) for overnight. After concentration of the organic layer, purification was achieved via column chromatography (eluent DCM/THF) to give the desired product as a solid. The resulting solid was further purified by triturated with diethyl ether (3 mL), then separated by filtration and dried in vacuo to afford the title compound as off white powder (0.17 g, yield: 73%). **^{1}H NMR (400 MHz, DMSO-*d*$_6$)** δ 8.04 (dd, *J*=3.4, 2.9 Hz, 1H, amide N*H*), 7.94 (d, *J*=8.0 Hz, 1H, amide N*H*), 7.34 (d, *J*=8.8 Hz, 2H, Ar C-*H ortho* to chlorine), 7.05 (s, 1H, Ar C-*H ortho* to chlorine), 7.01 (d, *J*=9.0 Hz, 1H, Ar C-*H ortho* to chlorine), 6.97 (s, 1H, Ar C-*H ortho* to phenoxy), 6.95 (dd, *J*=9.8, 7.1 Hz, 2H, Ar C-*H ortho* to phenoxy), 4.81 - 4.72 (m, 1H, C*H*OAr), 4.45 (s, 2H, C*H*$_2$OAr), 4.38 (td, *J*=2.2, 2.1, 2.2 Hz, 1H, benzodioxane C*H*$_2$), 4.24 - 4.15 (m, 1H, benzodioxane C*H*$_2$), 3.54 (bs, 2H, ^{C}Hx C*H*), 1.74 (t, *J*=12.1 Hz, 4H, ^{C}Hx C*H*$_2$), 1.33 (q, *J*=10.2 Hz, 4H, ^{C}Hx C*H*$_2$). **^{13}C NMR (DMSO)** δ 166.9, 166.0 (2 x amide *C*=O), 157.1, 144.1, 143.5 (3 x Ar 4º C-phenoxy), 129.6 (Ar *C*-H *ortho* to chlorine), 125.2, 125.1 (2 x Ar 4º C-chlorine), 121.8 (Ar *C*-H *ortho* to chlorine), 119.0, 118.7, 117.5 (2 x Ar *C*-H *ortho* to phenoxy), 117.0 (Ar *C*-H *ortho* to chlorine), 72.7 (*C*HOAr), 67.6 (*C*H$_2$OAr), 65.5 (benzodioxane *C*H$_2$), 47.7, 47.3 (2 x ^{C}Hx *C*H), 31.2, 31.1 (^{C}Hx *C*H$_2$). **HPLC:** ^{t}$_R$ 2.96min (95%). **HRMS:** *m/z* theoretical for $C_{23}H_{25}Cl_2N_2O_5$ 479.1135 $[M+H]^+$, measured 479.1130 $[M+H]^+$. **M.p.:** 244-247°C.

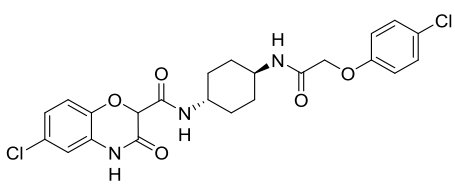
6-Chloro-*N*-[(1*R*,4*R*)-4-[2-(4-chlorophenoxy)acetamido]cyclohexyl]-3,4-dihydro-2H-1,4-benzoxazine-2-carboxamide (145)



Following general procedure D, 6-chloro-3,4-dihydro-2H-1,4-benzoxazine-2-carboxylic acid **136b** (0.1 g, 0.5 mmol)

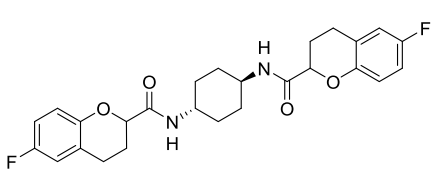
was reacted with HBTU (0.21 g, 0.55 mmol), 2-(4-chlorophenoxy)-*N*-[(1*R*,4*R*)-4-aminocyclohexyl]acetamide hydrochloride **28** (0.15 g, 0.55 mmol) and triethylamine (0.17 mL, 1.35 mmol) in DMF (10 mL) for overnight. After concentration of the organic layer, purification was achieved via column chromatography (eluent DCM/THF) to give the desired product as a solid. The resulting solid was further purified by triturated with diethyl ether (3 mL), then separated by filtration and dried in vacuo to afford the title compound as off white powder (0.16 g, yield: 65%). **^{1}H NMR (400 MHz, DMSO-*d*$_6$)** δ 8.08 (d, *J*=8.1 Hz, 1H, amide N*H*), 7.92 (d, *J*=8.1 Hz, 1H, amide N*H*), 7.35 (dd, *J*=2.1, 2.2 Hz, 2H, Ar C-*H ortho* to chlorine), 6.99 (dd, *J*=2.1, 2.2 Hz, 2H, Ar C-*H ortho* to chlorine), 6.78 (d, *J*=8.5 Hz, 1H, Ar C-*H ortho* to phenoxy), 6.63 (d, *J*=2.5 Hz, 1H, Ar C-*H ortho* to phenoxy), 6.51 (dd, *J*=2.5, 2.5 Hz, 1H, Ar C-*H ortho* to phenoxy), 6.32 (s, 1H, benzoxazine N*H*), 4.47 (s, 2H, C*H*$_2$OAr), 4.45 (dd, *J*=2.8, 2.8 Hz, 1H, C*H*OAr), 3.59 (bs, 2H, ^{C}Hx C*H*), 3.46 (dt, *J*=3.1, 3.1 Hz, 1H, benzoxazine C*H*$_2$), 3.20 (td, *J*=1.6, 2.7, 1.5 Hz, 1H, benzoxazine C*H*$_2$), 1.75 (t, *J*=14.2 Hz, 4H, ^{C}Hx C*H*$_2$), 1.42 - 1.30 (m, 4H, ^{C}Hx C*H*$_2$). **^{13}C NMR (DMSO)** δ 167.6, 166.9 (2 x amide *C*=O), 157.1, 141.2 (2 x Ar 4º C-phenoxy), 136.1 (Ar 4º C-NH), 129.6 (Ar *C*-H *ortho* to chlorine), 125.3, (Ar 4º C-chlorine), 125.2, 117.9, 116.9 (3 x Ar *C*-H *ortho* to phenoxy), 116.2, 113.9 (Ar *C*-H *ortho* to chlorine), 73.3 (*C*HOAr), 67.6 (*C*H$_2$OAr), 47.5 (benzoxazine *C*H$_2$), 47.3 (^{C}Hx *C*H), 31.3, 31.2, 31.1 (^{C}Hx *C*H$_2$). HPLC: ^{t}$_R$ 2.90min (95%). **HRMS:** *m/z* theoretical for $C_{23}H_{26}Cl_2N_3O_4$ 478.1295 $[M+H]^+$, measured 478.1286 $[M+H]^+$. **M.p.:** 255-259 °C.

6-Chloro-3-oxo-*N*-[(1*R*,4*R*)-4-[2-(4-chlorophenoxy)acetamido]cyclohexyl]-3,4-dihydro-2H-1,4-benzoxazine-2-carboxamide (146)



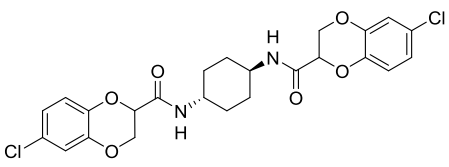
Following general procedure D, 6-chloro-3-oxo-3,4-dihydro-2H-1,4-benzoxazine-2-carboxylic acid **140** (0.11 g, 0.5 mmol) was reacted with HBTU (0.21 g, 0.55 mmol), 2-(4-chlorophenoxy)-*N*-[(1*R*,4*R*)-4-aminocyclohexyl]acetamide hydrochloride **28** (0.15 g, 0.55 mmol) and triethylamine (0.17 mL, 1.35 mmol) in DMF (10 mL) for overnight. After concentration of the organic layer, purification was achieved via column chromatography (eluent DCM/THF) to give the desired product as a solid. The resulting solid was further purified by triturated with diethyl ether (3 mL), then separated by filtration and dried in vacuo to afford the title compound as a beige powder (0.15 g, yield: 61%). **^{1}H NMR (400 MHz, DMSO-d_6)** δ 10.96 (s, 1H, oxo-benzoxazine N*H*), 8.39 (d, *J*=7.8 Hz, 1H, amide N*H*), 7.93 (d, *J*=8.1 Hz, 1H, amide N*H*), 7.35 (dd, *J*=2.5, 2.5 Hz, 2H, Ar C-*H ortho* to chlorine), 6.97 (dd, *J*=2.5, 2.3 Hz, 4H, Ar C-*H ortho* to chlorine and phenoxy), 6.86 (d, *J*=2.3 Hz, 1H, Ar C-*H ortho* to phenoxy), 5.07 (s, 1H, C*H*OAr), 4.44 (s, 2H, CH_2OAr), 3.59 (bs, 2H, ^{C}Hx C*H*), 1.74 (q, *J*=5.4 Hz, 4H, ^{C}Hx CH_2), 1.30 (q, *J*=9.8 Hz, 4H, ^{C}Hx CH_2). **^{13}C NMR (DMSO)** δ 167.0, 164.7, 162.6 (3 x amide *C*=O), 160.9, 157.1 (2 x Ar 4º C-phenoxy), 129.6, 128.4 (2 x Ar *C*-H *ortho* to chlorine), 126.0, 125.2 (2 x Ar 4º C-chlorine), 122.9 (Ar 4º C-NH), 118.0, 116.9 (Ar *C*-H *ortho* to phenoxy), 115.4 (Ar *C*-H *ortho* to chlorine), 76.6 (*C*HOAr), 67.6 (*C*H_2OAr), 47.9, 47.2 (2 x ^{C}Hx *C*H), 32.1, 31.1, 31.0 (^{C}Hx *C*H_2). **HPLC:** t_R 2.8min (95%). **HRMS:** *m/z* theoretical for $C_{23}H_{24}Cl_2N_3O_5$ 492.1088 $[M+H]^+$, measured 492.1082 $[M+H]^+$. **M.p.:** 260-263°C.

6-Fluoro-*N*-[(1*R*,4*R*)-4-(6-fluoro-3,4-dihydro-2H-1-benzopyran-2-amido)cyclohexyl]-3,4-dihydro-2H-1-benzopyran-2-carboxamide (147)



Following general procedure E, commercially available 6-fluorochroman-2-carboxylic acid (0.1 g, 0.5 mmol) was reacted with HBTU (0.21 g, 0.55 mmol), *trans*-1,4-cyclohexandiamine **45** (0.03 g, 0.22 mmol) and triethylamine (0.18 mL, 1.5 mmol) in DMF (10 mL) for 15 hours. After concentration of the organic layer, the resulting solid was further purified by triturated with diethyl ether (3 mL), then separated by filtration and dried in vacuo to afford the title compound as a white powder (0.09 g, yield: 91%). **^{1}H NMR (400 MHz, DMSO-*d*$_6$)** δ 7.86 (d, *J*=7.9 Hz, 2H, amide N*H*), 6.92 (d, *J*=8.5 Hz, 4H, Ar C-*H ortho* and *meta* to fluorine), 6.86 (d, *J*=4.9 Hz, 2H, Ar C-*H ortho* to fluorine), 4.46 (d, *J*=7.1 Hz, 2H, C*H*OAr), 3.53 (bs, 2H, ^{C}Hx C*H*), 2.82 - 2.62 (m, 4H, chromane C*H*$_2$), 2.11 (t, *J*=5.4 Hz, 2H, chromane C*H*$_2$), 1.91 - 1.81 (m, 2H, chromane C*H*$_2$), 1.73 (d, *J*=14.9 Hz, 4H, ^{C}Hx C*H*$_2$), 1.35 (q, *J*=9.7 Hz, 4H, ^{C}Hx C*H*$_2$). **^{13}C NMR (DMSO)** δ 169.3 (amide *C*=O), 155.6 (Ar 4º C-fluorine), 150.1(2 x Ar 4º C-phenoxy), 124.0 (Ar 4º C- *ortho* to phenoxy), 118.1(Ar *C*-H *ortho* to phenoxy), 115.8, 115.5, 114.3, 114.1 (4 x Ar *C*-H *ortho* to fluorine), 75.1 (*C*HOAr), 47.4 (^{C}Hx *C*H), 31.2 (chromane *C*H$_2$), 24.7 (*C*H$_2$CH$_2$), 23.8 (chromane *C*H$_2$). **HPLC:** ^{t}$_R$ 3.04min (95%). **LC-MS:** *m/z* = 471[M+H]$^+$. **M.p.:** 266-268°C.

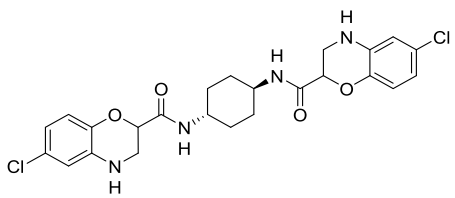
6-Chloro-*N*-[(1*R*,4*R*)-4-(6-chloro-2,3-dihydro-1,4-benzodioxine-2-amido)cyclohexyl]-2,3-dihydro-1,4-benzodioxine-2-carboxamide (148)



Following general procedure E, 6-chloro-2,3-dihydro-1,4-benzodioxine-2-carboxylic acid **136a** (0.1 g, 0.5 mmol) was reacted with HBTU (0.21 g, 0.55 mmol), *trans*-1,4-cyclohexandiamine (0.03 g, 0.22

mmol) and triethylamine (0.18 mL, 1.5 mmol) in DMF (10 mL) for overnight. After concentration of the organic layer, the resulting solid was further purified by triturated with diethyl ether (3 mL), then separated by filtration and dried in vacuo to afford the title compound as a light beige powder (0.05 g, yield: 50%). **^{1}H NMR (400 MHz, DMSO-*d*$_6$)** δ 8.03 (dd, *J*=3.2, 3.3 Hz, 2H, amide N*H*), 7.04 (s, 1H, Ar C-*H ortho* to chlorine), 7.00 (s, 1H, Ar C-*H ortho* to chlorine), 6.97 (t, *J*=2.6 Hz, 1H, Ar C-*H ortho* to chlorine), 6.92 (dd, *J*=2.4, 2.5 Hz, 1H, Ar C-*H ortho* to chlorine), 6.88 (s, 2H, Ar C-*H ortho* to phenoxy), 4.79 - 4.72 (m, 2H, C*H*OAr), 4.37 (td, *J*=2.5, 2.5, 2.5 Hz, 2H, benzodioxane CH_2), 4.23 - 4.15 (m, 2H, benzodioxane CH_2), 3.57 (bs, 2H, ^{C}Hx C*H*), 1.78 (dt, *J*=8.9, 8.2 Hz, 4H, ^{C}Hx CH_2), 1.38 - 1.25 (m, 4H, ^{C}Hx CH_2). **^{13}C NMR (DMSO)** δ 166.0, 165.9 (2 x amide *C*=O), 144.1, 143.5, 142.6, 141.9 (4 x Ar 4º C-phenoxy), 125.1, 125.1 (Ar 4º C-chlorine), 121.8, 121.6 (2 x Ar *C*-H *ortho* to chlorine), 119.0, 118.7 (2 x Ar *C*-H *ortho* to phenoxy), 117.5, 117.2 (2 x Ar *C*-H *ortho* to chlorine), 72.8, 72.7 (2 x *C*HOAr), 65.6, 65.4 (benzodioxane *C*H$_2$), 47.6 (^{C}Hx *C*H), 31.1(^{C}Hx *C*H$_2$). **HPLC:** ^{t}R 3.01min (95%). **LC-MS:** *m/z* = 507 $[M+H]^+$. **M.p.:** 250-253°C.

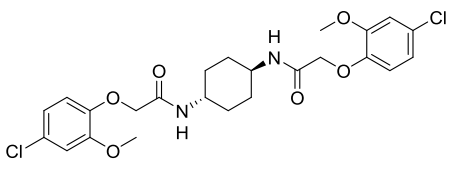
6-Chloro-*N*-[(1*R*,4*R*)-4-(6-chloro-3,4-dihydro-2H-1,4-benzoxazine-2-amido)cyclohexyl]-3,4-dihydro-2H-1,4-benzoxazine-2-carboxamide (149)



Following general procedure E, 6-chloro-3,4-dihydro-2H-1,4-benzoxazine-2-carboxylic acid **136b** (0.1 g, 0.5 mmol) was reacted with HBTU (0.21 g, 0.55 mmol), *trans*-1,4-cyclohexandiamine (0.03 g, 0.22 mmol) and triethylamine (0.18 mL, 1.5 mmol) in DMF (10 mL) for overnight. After concentration of the organic layer, the resulting solid was further purified by dissolved in methanol filtered and then re-precipitated with

diethyl ether (3 mL), then separated by filtration and dried in vacuo to afford the title compound as a beige powder (0.07 g, yield: 65%). **^{1}H NMR (400 MHz, DMSO-*d*$_6$)** δ 7.81 (d, *J*=8.1 Hz, 2H, amide N*H*), 6.78 (d, *J*=8.5 Hz, 2H, benzoxazine N*H*), 6.60 (d, *J*=2.2 Hz, 2H, Ar C-*H ortho* to chlorine), 6.51 (dd, *J*=2.2, 2.2 Hz, 2H, Ar C-*H ortho* to chlorine), 6.17 (s, 2H, Ar C-*H ortho* to phenoxy), 4.44 (dd, *J*=2.5, 2.4 Hz, 2H, C*H*OAr), 3.56 (bs, 2H, ^{C}Hx C*H*), 3.46 (dt, *J*=3.1, 3.4 Hz, 2H, benzoxazine C*H*$_2$), 3.20 (dd, *J*=7.8, 7.9 Hz, 2H, benzoxazine C*H*$_2$), 1.79 (dt, *J*=8.7, 7.7 Hz, 4H, ^{C}Hx C*H*$_2$), 1.38 (s, 4H, ^{C}Hx C*H*$_2$). **^{13}C NMR (DMSO)** δ 167.6 (amide *C*=O), 141.2 (Ar 4º C-phenoxy), 136.0 (Ar 4º C-NH), 125.4 (Ar 4º C-chlorine), 117.9 (Ar *C*-H *ortho* to phenoxy), 116.3, 114.0 (2 x Ar *C*-H *ortho* to chlorine), 73.4 (*C*HOAr), 47.5 (benzoxazine *C*H$_2$), 42.1 (^{C}Hx *C*H), 31.2, 31.2 (2 x ^{C}Hx *C*H$_2$). **HPLC:** ^{t}$_R$ 2.89min (95%). **HRMS:** *m/z* theoretical for $C_{24}H_{27}Cl_2N_4O_4$ 505.1404 $[M+H]^+$, measured 505.1396 $[M+H]^+$. **Mp:** 281-284°C.

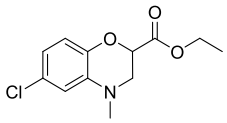
2-(4-Chloro-2-methoxyphenoxy)-*N*-[(1*R*,4*R*)-4-[2-(4-chloro-2-methoxyphenoxy)acetamido]cyclohexyl]acetamide (150)



Following general procedure E, compound 2-(4-chloro-2-methoxyphenoxy)acetic acid **117** (0.10 g, 0.5 mmol) was reacted with HBTU (0.21 g, 0.55 mmol), *trans*-1,4-cyclohexandiamine (0.025 g, 0.22 mmol) and triethylamine (0.18 mL, 1.5 mmol) in DMF (10 mL) for 19 hour. After concentration of the organic layer, the resulting solid was further purified by triturated with diethyl ether (3 mL), then separated by filtration and dried in vacuo to afford the title compound as a white powder (0.09 g, yield: 79%). **^{1}H NMR (400 MHz, DMSO-*d*$_6$)** δ 7.80 (d, *J* = 8.8 Hz, 2H, amide N*H*), 7.07 (s, 2H,

Ar C-*H ortho* to methoxy), 6.91 (s, 4H, Ar C-*H meta/para* to methoxy), 4.43 (s, 4H, CH_2OAr), 3.81 (s, 6H, methoxy CH_3), 3.56 (bs, 2H, ^{C}Hx C*H*), 1.77 (d, *J* = 8.8 Hz, 4H, ^{C}Hx CH_2), 1.31 ppm (t, J= 9.9 Hz, 4H, ^{C}Hx CH_2). **^{13}C NMR (DMSO)** δ 167.1 (amide *C*=O), 150.5 (Ar 4º C-methoxy), 146.9 (Ar 4º C-phenoxy), 126.1 (Ar 4º C-chlorine), 120.5 (Ar *C*-H *para* to methoxy), 116.3 (Ar *C*-H *ortho* to phenoxy), 113.1 (Ar *C*-H *ortho* to methoxy), 69.1 (*C*H_2OAr), 56.4 (methoxy *C*H_3), 47.3 (^{C}Hx *C*H), 31.2 (^{C}Hx *C*H_2). **HPLC:** $^{t}_{R}$ 2.91 min (95%). **HRMS:** *m/z* theoretical for $C_{24}H_{28}Cl_2N_2O_6$ 511.1397 $[M+H]^+$, measured 511.1388 $[M+H]^+$. **M.p.:** 230-233°C.

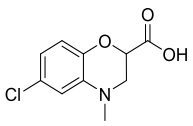
Ethyl 6-chloro-4-methyl-3,4-dihydro-2H-1,4-benzoxazine-2-carboxylate (151)



To a solution of ethyl 6-chloro-3,4-dihydro-2H-1,4-benzoxazine-2-carboxylate **135b** (0.26 g, 1.1 mmol) in DMF (5 mL) was added K_2CO_3 (0.47g, 3.3mmol) and methyl iodide (0.2 mL, 3.3 mmol) at 0° C. The reaction mixture was stirred at 40° C for 3 hours and then diluted with water. The organic layer was then extracted with ethyl acetate (10 mL) and washed with water then dried over sodium sulfate. The resulting suspension was purified by column chromatography using gradients of (Pet.ether/EtOAc). The combined fractions were concentrated to afford the title product as a light orange oily product (0.16 g, yield: 57%). **^{1}H NMR (400 MHz, DMSO-*d*$_6$)** δ 6.78 (d, *J*=8.4 Hz, 1H, Ar C-*H ortho* to chlorine), (d, *J*=2.4 Hz, 1H, Ar C-*H ortho* to phenoxy), 6.65 (dd, *J*=2.4, 2.4 Hz, 1H, Ar C-*H ortho* to chlorine), 5.07 (t, *J*=3.6 Hz, 1H, C*H*OAr), 4.19 - 4.11 (m, 2H, CH_2CH$_3$), 3.46 (qd, *J*=4.0, 4.0, 3.3, 3.3 Hz, 2H, benzoxazine CH_2N), 2.83 (s, 3H, NCH_3), 1.19 (t, *J*=7.1 Hz, 3H, CH_3). **^{13}C NMR (DMSO)** δ 169.2 (amide *C*=O), 142.1 (Ar 4º

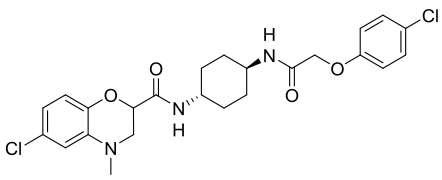
C-NCH_3), 137.7 (Ar 4º C-phenoxy), 125.6 (Ar 4º C-chlorine), 117.7 (Ar *C*-H *ortho* to phenoxy), 116.9, 112.3 (2 x Ar *C*-H *ortho* to chlorine), 72.3 (*C*HOAr), 61.4 (CH_2CH_3), 49.6 (CH_2NH), 38.5 ($NHCH_3$), 14.4 (CH_2CH_3). **HPLC:** $^{t}_{R}$ 2.95min (95%). **LC-MS:** *m/z* = 256 $[M+H]^+$.

6-Chloro-4-methyl-3,4-dihydro-2H-1,4-benzoxazine-2-carboxylic acid (152)



Following general procedure F, ester solution **151** (0.13 g, 0.5 mmol) was treated with aqueous solution of LiOH (0.06 g, 1.5 mmol) in water and THF (1:1, 5 mL) to afford the title compound as a light orange powder (0.10 g, yield: 95%). **^{1}H NMR (400 MHz, DMSO-*d*$_6$)** δ 6.76 (d, *J*=8.4 Hz, 1H, Ar C-*H ortho* to chlorine), 6.70 (d, *J*=2.4 Hz, 1H, Ar C-*H ortho* to phenoxy), 6.64 (dd, *J*=2.4, 2.4 Hz, 1H, Ar C-*H ortho* to chlorine), 6.61 4.95 (t, *J*=3.7 Hz, 1H, C*H*OAr), 3.44 (qd, *J*=4.0, 4.0, 3.4, 3.4 Hz, 2H, benzoxazine CH_2N), 2.83 (s, 3H, NCH_3). **^{13}C NMR (DMSO)** δ 170.9 (amide *C*=O), 142.3 (Ar 4º C-NCH_3), 137.8 (Ar 4º C-phenoxy), 125.4 (Ar 4º C-chlorine), 117.6 (Ar *C*-H *ortho* to phenoxy), 116.9, 112.3 (2 x Ar *C*-H *ortho* to chlorine), 72.1 (*C*HOAr), 49.6 (CH_2NH), 38.5 ($NHCH_3$). **HPLC:** $^{t}_{R}$ 2.64min (95%). **LC-MS:** *m/z* = 227 $[M+H]^+$.

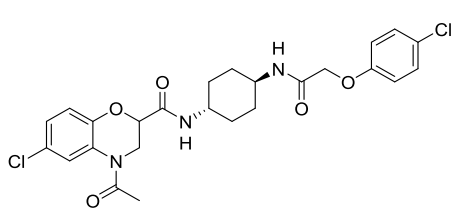
6-Chloro-4-methyl-*N*-[(1*R*,4*R*)-4-[2-(4-chlorophenoxy)acetamido]cyclohexyl]-3,4-dihydro-2H-1,4-benzoxazine-2-carboxamide (153)



Following general procedure D, 6-chloro-4-methyl-3,4-dihydro-2H-1,4-benzoxazine-2-carboxylic acid **152** (0.11 g, 0.5 mmol) was reacted with HBTU (0.21 g, 0.55 mmol), 2-(4-chlorophenoxy)-

N-[(1*R*,4*R*)-4-aminocyclohexyl]acetamide hydrochloride **28** (0.15 g, 0.55 mmol) and triethylamine (0.17 mL, 1.35 mmol) in DMF (10 mL) for overnight. After concentration of the organic layer, purification was achieved via column chromatography (eluent DCM/THF) to give the desired product as a solid. The resulting solid was further purified by triturated with diethyl ether (3 mL), then separated by filtration and dried in vacuo to afford the title compound as a white powder (0.20 g, yield: 84%). **^{1}H NMR (400 MHz, DMSO-*d*$_6$)** δ 7.96 (d, *J*=8.1 Hz, 1H, amide N*H*), 7.86 (d, *J*=8.2 Hz, 1H, amide N*H*), 7.36 (dd, *J*=2.2, 2.1 Hz, 2H, Ar C-*H ortho* to chlorine), 6.99 (dd, *J*=2.1, 2.1 Hz, 2H, Ar C-*H ortho* to chlorine), 6.83 (d, *J*=8.4 Hz, 1H, Ar C-*H ortho* to phenoxy), 6.71 (d, *J*=2.4 Hz, 1H, Ar C-*H ortho* to phenoxy), 6.63 (dd, *J*=2.4, 2.4 Hz, 1H, Ar C-*H ortho* to phenoxy), 4.65 (dd, *J*=2.9, 2.9 Hz, 1H, C*H*OAr), 4.46 (s, 2H, C*H*$_2$OAr), 3.59 (bs, 2H, ^{C}Hx C*H*), 3.43 (dd, *J*=2.9, 2.8 Hz, 1H, benzoxazine C*H*$_2$N), 3.21 (dd, *J*=7.4, 7.4 Hz, 1H, benzoxazine C*H*$_2$N), 2.84 (s, 3H, NC*H*$_3$), 1.77 (q, *J*=11.6 Hz, 4H, ^{C}Hx C*H*$_2$), 1.42 - 1.30 (m, 4H, ^{C}Hx C*H*$_2$). **^{13}C NMR (DMSO)** δ 167.3, 166.8 (amide *C*=O), 157.1 (Ar 4º C-phenoxy), 142.1 (Ar 4º C-NCH$_3$), 137.7 (Ar 4º C-phenoxy), 129.6 (Ar *C*-H *ortho* to chlorine), 125.8 (Ar 4º C-chlorine), 125.2 (Ar *C*-H *ortho* to phenoxy), 117.2, 117.1 (2 x Ar *C*-H *ortho* to phenoxy), 116.9, 112.1 (Ar *C*-H *ortho* to chlorine), 73.4 (*C*HOAr), 67.6 (*C*H$_2$OAr), 50.1 (*C*H$_2$N), 47.5, 47.3 (2 x ^{C}Hx *C*H), 38.5 (NH*C*H$_3$), 31.3, 31.2, 31.1 (3 x ^{C}Hx *C*H$_2$). **HPLC:** t_R 3.02 min (95%). **HRMS:** *m/z* theoretical for $C_{24}H_{28}Cl_2N_3O_4$ 492.1451 $[M+H]^+$, measured 492.1448 $[M+H]^+$. **M.p.:** 251-254°C.

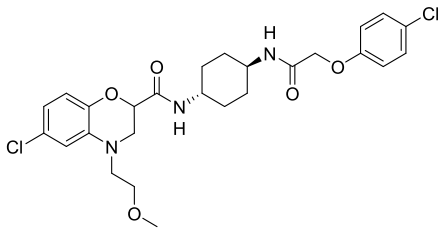
4-Acetyl-6-chloro-*N*-[(1*R*,4*R*)-4-[2-(4-chlorophenoxy)acetamido]cyclohexyl]-3,4-dihydro-2H-1,4-benzoxazine-2-carboxamide (154)



A stirred solution of 6-chloro-*N*-[(1*R*,4*R*)-4-[2-(4-chlorophenoxy)acetamido]cyclohexyl]-3,4-dihydro-2H-1,4-benzoxazine-2-carboxamide **145** (0.19 g, 0.4 mmol) in DCM (5 mL) and DIPEA (0.16 mL, 1 mmol) was cooled to 0° C (ice bath) under nitrogen. To this mixture was added dropwise Acetyl chloride (0.03 mL, 0.44 mmol) diluted in DCM (0.5 mL). The mixture was stirred at 0° C for a further 30 min then for 3 hours at room temperature until detected the desired product by LC-MS. The mixture then diluted with water, and the organic layer extracted with ethyl acetate (10 mL) and washed with saturated aqueous solution of NH4Cl and brine, respectively. The organic phase was dried over sodium sulphate then filtered and concentrated under vacuum. The resulting product was purified by column chromatography using gradients of (DCM/EtOAc) to afford the title as a beige powder (0.09 g, yield: 45%). **^{1}H NMR (400 MHz, DMSO-*d*$_6$)** δ 8.00 (d, *J*=8.0 Hz, 1H, amide N*H*), 7.94 (d, *J*=8.1 Hz, 1H, amide N*H*), 7.35 (dd, *J*=2.2, 2.2 Hz, 2H, Ar C-*H ortho* to chlorine), 7.13 (d, *J*=8.8 Hz, 1H, Ar C-*H ortho* to chlorine), 7.03 (d, *J*=8.8 Hz, 1H, Ar C-*H ortho* to phenoxy), 6.98 (dd, *J*=2.2, 2.2 Hz, 2H, Ar C-*H ortho* to phenoxy), 4.87 (bs, 1H, C*H*OAr), 4.45 (s, 2H, C*H*$_2$OAr), 4.15 (dd, *J*=4.8, 4.8 Hz, 1H, benzoxazine C*H*$_2$N), 3.80 (dd, *J*=3.3, 3.3 Hz, 1H, benzoxazine C*H*$_2$N), 3.54 (s, 2H, ^{C}Hx C*H*), 2.23 (s, 3H, acetyl C*H*$_3$), 1.73 (t, *J*=14.1 Hz, 4H, ^{C}Hx C*H*$_2$), 1.37 - 1.25 (m, 4H, ^{C}Hx C*H*$_2$). **^{13}C NMR (DMSO)** δ 167.6, 166.9 (2 x amide *C*=O), 157.1, 141.2 (2 x Ar 4º C-phenoxy), 136.0 (Ar 4º C-NCH$_3$), 129.6 (Ar *C*-H *ortho* to chlorine), 125.2 (Ar 4º C-chlorine), 117.9, 116.9 (2 x Ar *C*-H *ortho* to phenoxy), 116.3, 114.0 (Ar *C*-H *ortho* to chlorine), 73.4 (*C*HOAr), 67.6 (*C*H$_2$OAr), 47.5 (*C*H$_2$N), 47.3, 42.5 (2 x

^{C}Hx *C*H), 31.3 (^{C}Hx *C*H_2), 323.2 (*C*H_3). **HPLC:** $^{t}_{R}$ 2.86 min (95%). **HRMS:** *m/z* theoretical for $C_{25}H_{28}Cl_2N_3O_5$ 520.1401 $[M+H]^+$, measured 520.1429 $[M+H]^+$. **Mp:** 214-216°C.

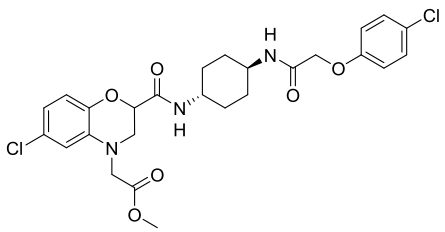
6-Chloro-4-(2-methoxyethyl)-*N*-[(1*R*,4*R*)-4-[2-(4-chlorophenoxy)acetamido]cyclohexyl]-3,4-dihydro-2H-1,4-benzoxazine-2-carboxamide (155)



To a mixture of 6-chloro-*N*-[(1*R*,4*R*)-4-[2-(4-chlorophenoxy)acetamido]cyclohexyl]-3,4-dihydro-2H-1,4-benzoxazine-2-carboxamide **145** (0.19 g, 0.4 mmol) in DMF (5 mL) was added K_2CO_3 (0.15 g, 1 mmol) NaI (0.09 g, 0.6 mmol) and 2-bromoethyl methyl ether (0.05 mL, 0.48 mmol). The reaction mixture was stirred at 125°C for overnight and then diluted with water (5 mL), the aqueous mixture was extracted twice with ethyl acetate (10 mL). The combined organic layers were washed with water and brine, dried over sodium sulphate then filtered and concentrated under vacuum. The resulting product was then purified by column chromatography using gradients of (DCM/THF) to afford the title product as a white powder (0.08 g, yield: 35%). **^{1}H NMR (400 MHz, DMSO-*d*$_6$)** δ 7.94 (d, *J*=8.1 Hz, 1H, amide N*H*), 7.87 (d, *J*=8.1 Hz, 1H, amide N*H*), 7.35 (d, *J*=2.2, 2.2 Hz, 2H, Ar C-*H ortho* to chlorine), 6.97 (d, *J*=2.2, 2.2 Hz, 2H, Ar C-*H ortho* to chlorine), (d, *J*=8.4 Hz, 1H, Ar C-*H ortho* to phenoxy), 6.75 (d, *J*=2.4 Hz, 1H, Ar C-*H ortho* to phenoxy), 6.56 (dd, *J*=2.4, 2.4 Hz, 1H, Ar C-*H ortho* to phenoxy), 4.47 (t, *J*=3.9 Hz, 1H, C*H*OAr), 4.45 (s, 2H, C*H*$_2$OAr), 3.59 (bs, 2H, ^{C}Hx C*H*), 3.55 - 3.46 (m, 4H, C*H*$_2$C*H*$_2$OCH$_3$), 3.45 - 3.37 (m, 2H, benzoxazine C*H*$_2$N), 3.25 (s, 3H, OC*H*$_3$), 1.76 (t, *J*=14.7 Hz, 4H, ^{C}Hx C*H*$_2$), 1.41 - 1.29 (m,

4H, ^{C}Hx CH_2). **^{13}C NMR (DMSO)** δ 167.2, 166.8 (2 x amide *C*=O), 157.1, 141.6 (2 x Ar 4º C-phenoxy), 136.0 (Ar 4º C-NCH_2), 129.6 (Ar *C*-H *ortho* to chlorine), 126.0, 125.2 (2 x Ar 4º C-chlorine), 117.7, 116.9 (2 x Ar *C*-H *ortho* to phenoxy), 116.3, 111.7 (2 x Ar *C*-H *ortho* to chlorine), 72.9 (*C*HOAr), 69.7 (*C*H_2OCH_3), 67.6 (*C*H_2OAr), 58.7 (O*C*H_3), 50.1 (*C*$H_2CH_2OCH_3$), 49.2 (*C*H_2N), 47.3 (^{C}Hx *C*H), 31.3, 31.2 (2 x ^{C}Hx *C*H_2) . **HPLC:** $^{t}_{R}$ 3.02min (95%). **HRMS:** *m/z* theoretical for $C_{26}H_{32}Cl_2N_3O_5$ 536.1714 $[M+H]^+$, measured 536.1709 $[M+H]^+$. **M.p.:** 225-228°C.

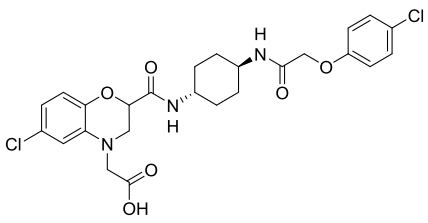
Methyl2-(6-chloro-2-{[(1*R*,4*R*)-4-[2-(4-chlorophenoxy) acetamido]cyclohexyl]carbamoyl}-3,4-dihydro-2H-1,4-benzoxazin-4-yl)acetate (156a)



To a mixture of 6-chloro-*N*-[(1*R*,4*R*)-4-[2-(4-chlorophenoxy)acetamido]cyclohexyl]-3,4-dihydro-2H-1,4-benzoxazine-2-carboxamide **145** (0.19 g, 0.4 mmol) in DMF (5 mL) was added K_2CO_3 (0.15 g, 1 mmol) NaI (0.09 g, 0.6 mmol) and methyl bromoacetate (0.04 mL, 0.44 mmol). The reaction mixture was stirred at 125°C for overnight and then diluted with water (5 mL), the aqueous mixture was extracted twice with ethyl acetate (10 mL). The combined organic layers were washed with water and brine, dried over sodium sulphate then filtered and concentrated under vacuum. The resulting product was then purified by column chromatography using gradients of DCM/THF, to afford the title product as a beige powder (0.14 g, yield: 67%). **^{1}H NMR (400 MHz, DMSO-d_6)** δ 7.95 (t, *J*=7.5 Hz, 2H, amide N*H*), 7.36 (dd, *J*=2.0, 2.4 Hz, 2H, Ar C-*H ortho* to chlorine), 6.99 (dd, *J*=2.2, 2.2 Hz, 2H, Ar C-*H ortho* to chlorine), 6.89 (dd, *J*=4.8,

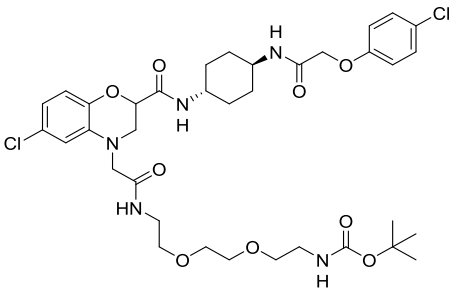
5.8 Hz, 1H, Ar C-*H ortho* to phenoxy), 6.71 (dd, *J*=2.3, 2.2 Hz, 1H, Ar C-*H ortho* to phenoxy), 6.64 (dd, *J*=2.2, 2.2 Hz, 1H, Ar C-*H ortho* to phenoxy), 4.65 (qd, *J*=2.8, 2.8, 2.6, 2.8 Hz, 1H, C*H*OAr), 4.46 (s, 2H, CH_2OAr), 4.28 (q, *J*=12.4 Hz, 2H, CH_2COO), 3.66 (s, 3H, COOCH_3), 3.63 - 3.52 (m, 4H, benzoxazine CH_2N and ^{C}Hx C*H*), 1.73 (q, *J*=7.4 Hz, 4H, ^{C}Hx CH_2), 1.35 (t, *J*=11.5 Hz, 4H, ^{C}Hx CH_2). **^{13}C NMR (DMSO)** δ 170.6 (carboxylic *C*=O), 167.1, 166.9 (2 x amide *C*=O), 157.1, 141.8 (2 x Ar 4º C-phenoxy), 135.8 (Ar 4º C-NCH_2), 129.6 (Ar *C*-H *ortho* to chlorine), 125.9, 125.2 (2 x Ar 4º C-chlorine), 117.9, 117.4 (2 x Ar *C*-H *ortho* to phenoxy), 116.9, 111.8 (2 x Ar *C*-H *ortho* to chlorine), 73.1 (*C*HOAr), 67.6 (*C*H_2OAr), 55.3 (*C*H_2COOCH_3), 52.3(*C*H_3), 51.1 (*C*H_2N), 47.5, 47.3 (2 x ^{C}Hx *C*H), 31.3, 31.2, 31.1 (3 x *C*$H_2$$CH_2$). **HPLC:** $^{t}_{R}$ 2.97min (95%). **HRMS:** *m/z* theoretical for $C_{26}H_{30}Cl_2N_3O_6$ 550.1506 $[M+H]^+$, measured 550.1474 $[M+H]^+$. **M.p.:** 247-249°C.

2-(6-Chloro-2-{[(1*R*,4*R*)-4-[2-(4-chlorophenoxy)acetamido]cyclohexyl]carbamoyl}-3,4-dihydro-2H-1,4-benzoxazin-4-yl)acetic acid (156b)



Following general procedure F, methyl2-(6-chloro-2-{[(1*R*,4*R*)-4-[2-(4-chlorophenoxy) acetamido]cyclohexyl]carbamoyl}-3,4-dihydro-2H-1,4-benzoxazin-4-yl)acetate **156a** (0.27 g, 0.5 mmol) was treated with aqueous solution of LiOH (0.06 g, 1.5 mmol) in water and THF (1:1, 5 mL) to afford the title compound as a white powder 84%. The resulting product was directly used for next step without further purification (0.22 g, yield: 84%). **LC–MS:** *m/z* = 537 $[M+H]^+$.

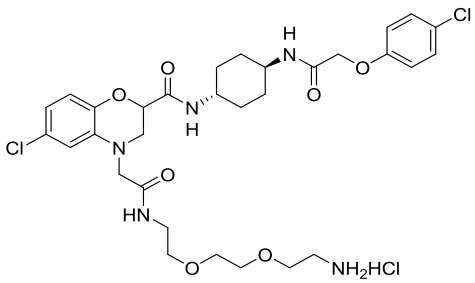
tert-Butyl _N_-{2-[2-(2-{2-[6-chloro-2-({4-[2-(4-chlorophenoxy) acetamido]cyclohexyl}carbamoyl)-3,4-dihydro-2H-1,4-benzoxazin-4-yl]acetamido}ethoxy)ethoxy]ethyl}carbamate (156c)



Following general procedure D, carboxylic acid compound **156b** (0.18 g, 0.4 mmol) was reacted with HBTU (0.16 g, 0.44 mmol), *tert*-butyl *N*-{2-[2-(2-aminoethoxy)ethoxy]ethyl}carbamate (0.10 g, 0.44 mmol) and triethylamine (0.12 mL, 1 mmol) in DMF (10 mL) for 9 hours. After concentration of the organic layer, purification was achieved via column chromatography (eluent DCM/ CH_3OH) to give the desired product as a solid. The resulting solid was further purified by triturated with diethyl ether (3 mL), then separated by filtration and dried in vacuo to afford the title compound as a white powder (0.24 g, yield: 80%). **^{1}H NMR (400 MHz, DMSO-d_6)** δ 8.09 (t, *J*=5.6 Hz, 1H, amide N*H*), 7.96 (dd, *J*=3.6, 3.5 Hz, 2H, amide N*H*), 7.34 (dd, *J*=2.2, 2.2 Hz, 2H, Ar C-*H ortho* to chlorine), 6.97 (dd, *J*=2.2, 2.2 Hz, 2H, Ar C-*H ortho* to phenoxy), 6.83 (d, *J*=8.5 Hz, 1H, Ar C-*H ortho* to chlorine), 6.74 (t, *J*=5.2 Hz, 1H, amide N*H*), 6.60 (dd, *J*=2.4, 2.3 Hz, 1H, Ar C-*H ortho* to chlorine), 6.50 (d, *J*=2.3 Hz, 1H, Ar C-*H ortho* to phenoxy), 4.63 (dd, *J*=2.8, 2.9 Hz, 1H, C*H*OAr), 4.45 (s, 2H, CH_2OAr), 3.60 (bs, 1H, benzoxazine CH_2), 3.59 (dd, *J*=2.8, 2.7 Hz, 2H, CH_2CONH), 3.48 (s, 4H, CH_2O, OCH_2), 3.44 (d, *J*=7.6 Hz, 1H, benzoxazine CH_2), 3.41 (dt, *J*=5.8, 5.7 Hz, 5H, OCH_2CH_2O, ^{C}Hx C*H*), 3.23 (q, *J*=5.7 Hz, 2H, CH_2CH$_2$O), 3.05 (q, *J*=6.0 Hz, 2H, CH_2NBoc), 2.90 (bs, 1H, ^{C}Hx C*H*), 1.74 (q, *J*=12.9 Hz, 4H, ^{C}Hx CH_2), 1.37 (s, 9H, Boc CH_3), 1.30 (t, *J*=7.2 Hz, 4H, ^{C}Hx CH_2). **^{13}C NMR (DMSO)** δ 169.3, 167.4, 166.9, 157.1 (4 x

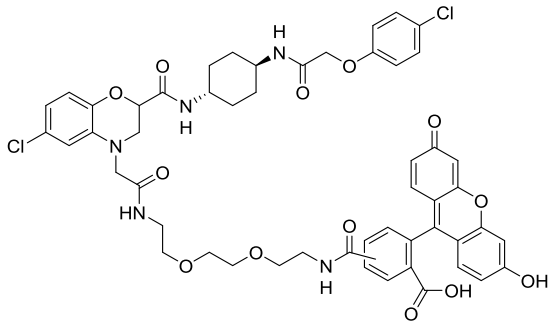
amide *C*=O), 156.0 (Ar 4º C-phenoxy), 141.7 (Ar 4º C- NCH_2), 136.2 (Ar 4º C-phenoxy), 129.6 (Ar *C*-H *ortho* to chlorine), 125.8, 125.2 (2 x Ar 4º C-chlorine), 117.7, 117.0 (2 x Ar *C*-H *ortho* to phenoxy), 116.9, 111.6 (2 x Ar *C*-H *ortho* to chlorine), 78.0 (*C*HOAr), 73.0 (Boc 4º C), 70.0, 69.9, 69.6, 69.5 (4 x CH_2O), 67.6 (CH_2OAr), 65.3 (NCH_2), 53.7 (CH_2N), 47.5, 47.3 (3 x ^{C}Hx *C*H), 38.9 (CH_2NHCO), 31.3, 31.2, 31.1, (3 x CH_2CH_2), 28.7 (Boc CH_3). **HPLC:** $^{t}_{R}$ 2.96min (95%). **HRMS:** *m/z* theoretical for $C_{36}H_{50}Cl_2N_5O_9$ 766.2980 $[M+H]^+$, measured 766.2963 $[M+H]^+$.

4-[({2-[2-(2-Aminoethoxy)ethoxy]ethyl}carbamoyl)methyl]-6-chloro-*N*-{4-[2-(4-chlorophenoxy)acetamido]cyclohexyl}-3,4-dihydro-2H-1,4-benzoxazine-2-carboxamide hydrochloride (156d)



A solution of *tert*-butyl *N*-{2-[2-(2-{2-[6-chloro-2-({4-[2-(4-chlorophenoxy) acetamido]cyclohexyl}carbamoyl)-3,4-dihydro-2H-1,4-benzoxazin-4-yl]acetamido}ethoxy)ethoxy]ethyl}carbamate **156c** (0.12 g, 0.15 mmol) in dioxane (0.5 mL) was treated with 4 M HCl in dioxane (1 mL, 4 mmol). After stirring for 2 hours the solution was evaporated. The residue was dissolved in MeOH (0.5 mL) and the product was precipitated by addition of excess diethyl ether. The resulting precipitate was collected and dried to afford the HCl salt of the titled product as a white fluffy powder. The resulting product was directly used for next step without further purification (0.10 g, yield: 98%). **HPLC:** $^{t}_{R}$ 2.36 min (95%). **LC–MS:** *m/z* = 667 $[M+H]^+$.

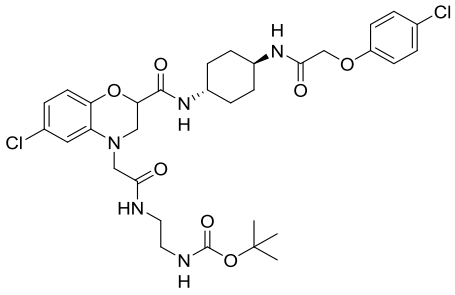
2-(6-Hydroxy-3-oxo-3H-xanthen-9-yl)benzoic acid; 6-chloro-*N*-{4-[2-(4-chlorophenoxy) acetamido]cyclohexyl}-4-[({2-[2-(2-acetamidoethoxy)ethoxy]ethyl}carbamoyl)methyl]-3,4-dihydro-2H-1,4-benzoxazine-2-carboxamide (156e)



4-[({2-[2-(2-Aminoethoxy)ethoxy]ethyl}carbamoyl)methyl]-6-chloro-*N*-{4-[2-(4-chlorophenoxy)acetamido]cyclohexyl}-3,4-dihydro-2H-1,4-benzoxazine-2-carboxamide hydrochloride **156d** (28 mg, 0.04 mmol) and 5/6-carboxyfluorescein succinimidyl ester (18.8 mg, 0.04 mmol), were dissolved in DMF (2 mL) with triethylamine (8μL). The mixture was stirred overnight at 31 ^{o}C and the solvent was evaporated under vacuum. The residue was fractionated by semi-preparative HPLC (Phenomenex Gemini 5 μm-110 Å, C18, 150 x 10 mm column; 5 mL/min flow rate) with linear gradient elution of H2O–MeCN (containing 0.1% HCOOH) from 85:15 to 5:95 over 13 min to afford the title fluorescent compound as an orange powder (0.03 g, yield: 75%). **^{1}H NMR (400 MHz, DMSO-d_6)** δ 8.88 (tt, *J*=5.4, 5.4 Hz, 1H, amide N*H*), 8.46 (s, 1H, benzoic acid C-*H*), 8.31 (s, 1H, benzoic acid C-*H*), 8.22 (dd, *J*=8.0, 8.0 Hz, 1H, amide N*H*), 8.11 (dd, *J*=5.4, 8.1 Hz, 1H, benzoic acid C-*H*), 7.95 (d, *J*=8.0 Hz, 2H, amide N*H*), 7.68 (s, 1H, phenol C-*H*), 7.33 (d, *J*=8.9 Hz, 2H, Ar C-*H ortho* to chlorine), 6.96 (d, *J*=8.8 Hz, 2H, Ar C-*H ortho* to phenoxy), 6.82 (d, *J*=8.3 Hz, 1H, Ar C-*H ortho* to chlorine), 6.67 (s, 2H, cyclohexanone C-*H*), 6.58 (d, *J*=8.3

Hz, 2H, Ar C-*H ortho* to chlorine, Ar C-*H ortho* to phenoxy), 6.54 (dd, *J*=4.3, 2.2 Hz, 2H, phenol C-*H*), 6.50 (dd, *J*=1.7, 2.4 Hz, 1H, cyclohexanone C-*H*), 4.62 (t, *J*=8.0 Hz, 1H, C*H*OAr), 4.44 (s, 2H, CH_2OAr), 3.96 (qd, *J*=6.9, 6.2, 6.3, 6.6 Hz, 2H, benzoxazine CH_2), 3.56 – 3.50 (m, Hz, 6H, alkyl chain CH_2, ^{C}Hx C*H*), 3.47 (t, *J*=8.2 Hz, 6H, alkyl chain CH_2), 3.22 (dd, *J*=5.6, 5.5 Hz, 4H, alkyl chain CH_2), 1.74 (q, *J*=12.5 Hz, 4H, ^{C}Hx CH_2), 1.34 (q, *J*=11.0 Hz, 4H, ^{C}Hx CH_2). **HPLC:** $^{t}_{R}$ 2.81 min (95%); **HRMS:** *m/z* theoretical for $C_{52}H_{52}Cl_2N_5O_{13}$ 1024.2933 $[M+H]^+$, measured 1024.2920 $[M+H]^+$.

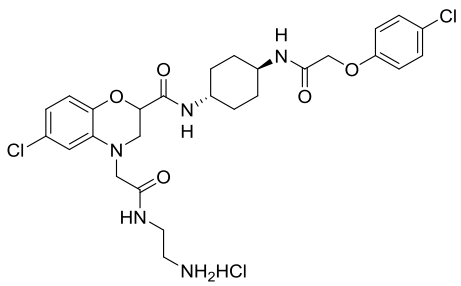
***tert*-Butyl *N*-(2-{2-[6-chloro-2-({4-[2-(4-chlorophenoxy) acetamido]cyclohexyl}carbamoyl)-3,4-dihydro-2H-1,4-benzoxazin-4-yl]acetamido}ethyl)carbamate (156f)**



Following general procedure D, carboxylic acid compound **156b** (0.18 g, 0.4 mmol) was reacted with HBTU (0.16 g, 0.44 mmol), *tert*-butyl *N*-(2-aminoethyl)carbamate (0.26 mL, 0.44 mmol) and triethylamine (0.12 mL, 1 mmol) in DMF (10 mL) for 6 hours. After concentration of the organic layer, purification was achieved via column chromatography (eluent DCM/ CH_3OH) to give the desired product as a solid. The resulting solid was further purified by triturated with diethyl ether (3 mL), then separated by filtration and dried in vacuo to afford the title compound as a white powder (0.17 g, yield: 63%). **^{1}H NMR (400 MHz, DMSO-d_6)** δ 8.04 (t, *J*=5.2 Hz, 1H, amide N*H*), 7.97 (dd, *J*=8.2, 6.4 Hz, 2H, amide N*H*), 7.33 (d, *J*=8.9 Hz, 2H, Ar C-*H ortho* to chlorine), 6.96 (d, *J*=8.8 Hz, 2H, Ar C-*H ortho* to phenoxy), 6.85 (dd, *J*=5.6, 5.8 Hz, 1H, Ar C-*H ortho* to chlorine), 6.78 (t,

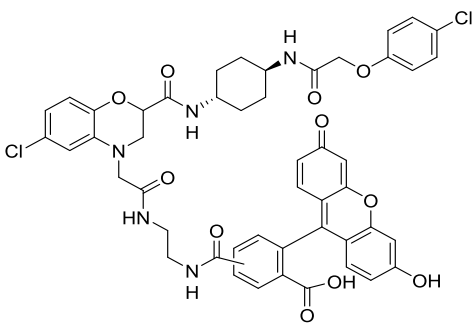
J=5.9 Hz, 1H, amide N*H*), 6.61 (dd, *J*=2.2, 2.1 Hz, 1H, Ar C-*H ortho* to chlorine), 6.51 (d, *J*=2.0 Hz, 1H, Ar C-*H ortho* to phenoxy), 4.64 (qd, *J*=2.6, 2.9, 2.8, 2.4 Hz, 1H, C*H*OAr), 4.45 (s, 2H, CH_2OAr), 3.87 (q, *J*=14.0 Hz, 2H, CH_2CONH), 3.59 (dd, *J*=2.8, 2.3 Hz, 3H, benzoxazine CH_2, ^{C}Hx C*H*), 3.45 (q, *J*=6.0 Hz, 1H, benzoxazine CH_2), 3.09 (dq, *J*=6.1, 6.2 Hz, 4H, NHCH_2CH_2NH), 1.77 (dd, *J*=7.4, 6.4 Hz, 4H, ^{C}Hx CH_2), 1.37 (s, 9H, Boc CH_3), 1.30 (t, *J*=10.2 Hz, 4H, ^{C}Hx CH_2). **HPLC:** $^{t}_{R}$ 2.95min (95%). **HRMS:** *m/z* theoretical for $C_{32}H_{42}Cl_2N_5O_7$ 678.2456 $[M+H]^+$, measured 678.2445 $[M+H]^+$.

4-{[(2-Aminoethyl)carbamoyl]methyl}-6-chloro-*N*-{4-[2-(4-chlorophenoxy) acetamido]cyclohexyl}-3,4-dihydro-2H-1,4-benzoxazine-2-carboxamide hydrochloride (156g)



A solution of *tert*-butyl *N*-(2-{2-[6-chloro-2-({4-[2-(4-chlorophenoxy) acetamido]cyclohexyl}carbamoyl)-3,4-dihydro-2H-1,4-benzoxazin-4-yl]acetamido}ethyl)carbamate **156f** (0.10 g, 0.15 mmol) in dioxane (0.5 mL) was treated with 4 M HCl in dioxane (1 mL, 4 mmol). After stirring for 2 hours the solution was evaporated. The residue was dissolved in MeOH (0.5 mL) and the product was precipitated by addition of excess diethyl ether. The resulting precipitate was collected and dried to afford the HCl salt of the titled product as a white fluffy powder. The resulting product was directly used for next step without further purification (0.09 g, yield: 95%). **HPLC:** $^{t}_{R}$ 2.33 min (95%). **LC–MS:** *m/z* = 579 $[M+H]^+$.

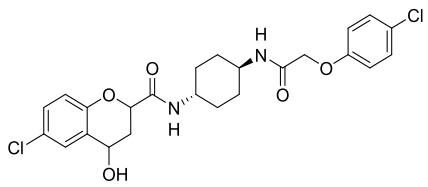
4-[(2-{2-[6-Chloro-2-({4-[2-(4 chlorophenoxy)acetamido]cyclohexyl}carbamoyl)-3,4-dihydro-2H-1,4-benzoxazin-4-yl]acetamido}ethyl)carbamoyl]-2-(6-hydroxy-3-oxo-3H-xanthen-9-yl)benzoic acid (156h)



4-{[(2-Aminoethyl)carbamoyl]methyl}-6-chloro-*N*-{4-[2-(4-chlorophenoxy) acetamido]cyclohexyl}-3,4-dihydro-2H-1,4-benzoxazine-2-carboxamide hydrochloride **156g** (25 mg, 0.04 mmol) and 5/6-carboxyfluorescein succinimidyl ester (18.8 mg, 0.04 mmol), were dissolved in DMF (2 mL) with Et3N (8μL). The mixture was stirred overnight at 31 ºC and the solvent was evaporated under vacuum. The residue was fractionated by semi-preparative HPLC (Phenomenex Gemini 5 μm-110 Å, C18, 150 x 10 mm column; 5 mL/min flow rate) with linear gradient elution of H2O–MeCN (containing 0.1% HCOOH) from 85:15 to 5:95 over 13 min to afford the title fluorescent compound as an orange powder (0.03 g, yield: 80%). **^{1}H NMR (400 MHz, DMSO-d_6)** δ 8.84 (dt, *J*=5.3, 5.4 Hz, 1H, amide N*H*), 8.44 (s, 1H, benzoic acid C-*H*), 8.36 (s, 1H, benzoic acid C-*H*), 8.20 (t, *J*=7.9 Hz, 1H, amide N*H*), 8.12 (td, *J*=5.8, 7.9, 8.1 Hz, 1H, benzoic acid C-*H*), 7.98 - 7.92 (q, *J*=3.8 Hz, 2H, amide N*H*), 7.65 (s, 1H, phenol C-*H*), 7.35 (dd, *J*=1.1, 1.2 Hz, 2H, Ar C-*H ortho* to chlorine), 6.97 (d, *J*=8.9 Hz, 2H, Ar C-*H ortho* to phenoxy)), 6.83 (d, *J*=2.8, 2.9 Hz, 1H, Ar C-*H ortho* to chlorine), 6.68 (s, 2H, cyclohexanone C-*H*), 6.60 (d, *J*=3.0 Hz, 1H, Ar C-*H ortho* to chlorine), 6.58 (d, *J*=3.1, 1.9 Hz, 2H, phenol C-*H*), 6.53 (d, *J*=2.8 Hz, 1H, Ar C-*H ortho* to phenoxy), 6.49 (d, *J*=2.2 Hz, 1H, cyclohexanone C-*H*), 4.66 (qd, *J*=2.6, 2.9, 2.7, 2.9 Hz, 1H, C*H*OAr),

4.45 (s, 2H, C*H*$_2$OAr), 3.99 (tdt, *J*=12.4, 2.8, 13.6 Hz, 2H, benzoxazine C*H*$_2$), 3.59 (qd, *J*=3.7, 2.5, 3.3, 3.0 Hz, 2H, alkyl chain C*H*$_2$), 3.47 (dd, *J*=7.6, 7.1 Hz,, 2H, ^{C}Hx C*H*), 3.21 (t, *J*=5.4 Hz, 1H, alkyl chain C*H*$_2$), 3.17 (s, 1H, alkyl chain C*H*$_2$), 2.68 (t, *J*=1.8 Hz, 1H, alkyl chain C*H*$_2$), 2.34 (t, *J*=1.7 Hz, 1H, alkyl chain C*H*$_2$), 1.74 (q, *J*=11.9 Hz, 4H, ^{C}Hx C*H*$_2$), 1.39 - 1.27 (m, 4H, ^{C}Hx C*H*$_2$). **HPLC:** ^{t}$_R$ 2.76 min (95%); **HRMS:** *m/z* theoretical for $C_{48}H_{44}Cl_2N_5O_{11}$ 936.2409 $[M+H]^+$, measured 936.2378 $[M+H]^+$.

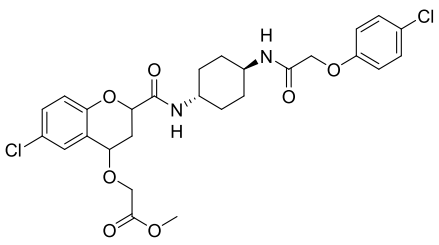
6-Chloro-4-hydroxy-*N*-[(1*R*,4*R*)-4-[2-(4-chlorophenoxy)acetamido]cyclohexyl]-3,4-dihydro-2H-1-benzopyran-2-carboxamide (157a)



6-Chloro-4-oxo-*N*-[(1*R*,4*R*)-4-[2-(4-chlorophenoxy)acetamido]cyclohexyl]-3,4-dihydro-2H-1-benzopyran-2-carboxamide **143** (0.25 g, 0.5 mmol) and sodium borohydride (0.05 g, 1.5 mmol) were added to DCE (10 mL), and the reaction mixture was stirred at ambient temperature for 2 hours. The reaction was monitored by TLC and then diluted with water (20 mL). The organic layer was then extracted with ethyl acetate (10 mL) and dried over sodium sulphate then filtered and concentrated under vacuum, resulting in precipitation of a white powder, which were collected to afford the title compound (0.23 g, yield: 95%). **^{1}H NMR (400 MHz, DMSO-*d*$_6$)** δ 8.30 (d, *J*=7.8 Hz, 1H, amide N*H*), 8.04 (d, *J*=7.8 Hz, 1H, amide N*H*), 7.64 (s, 1H, O*H*), 7.62 (d, *J*=2.6 Hz, 1H, Ar C-*H ortho* to chlorine), 7.32 (d, *J*=2.0 Hz, 3H, Ar C-*H ortho* to chlorine), 7.18 (d, *J*=8.3 Hz, 1H, Ar C-*H ortho* to phenoxy), 6.99 (d, *J*=3.0 Hz, 2H, Ar C-*H ortho* to phenoxy), 5.16 (dd, *J*=5.5, 5.4 Hz, 1H, C*H*OH), 4.82 (dd, *J*=5.4, 6.1 Hz, 1H, C*H*OAr), 4.45 (s, 2H, C*H*$_2$OAr), 3.58 (bs, 2H, ^{C}Hx C*H*

), 2.97 (t, *J*=2.5 Hz, 2H, C*H*$_2$CHOH), 1.38 - 1.24 (m, 4H, ^{C}Hx C*H*$_2$), 1.38 - 1.24 (m, 4H, ^{C}Hx C*H*$_2$). **^{13}C NMR (DMSO)** δ 170.7, 168.3 (2 x amide *C*=O), 157.4, 153.4 (2 x Ar 4º C-phenoxy), 130.6, 129.3, 128.3 (3 x Ar *C*-H *ortho* to chlorine), 125.7, 125.1 (2 x Ar 4º C-chlorine), 124.7 (Ar 4º C-*ortho* to phenoxy), 117.8, 116.9 (2 x Ar *C*-H *ortho* to phenoxy), 73.4 (*C*HOAr), 66.6 (*C*H$_2$OAr), 64.9 (*C*HOH), 47.7, 47.3 (2 x ^{C}Hx *C*H), 34.3 (*C*H$_2$CHOH), 30.9, 30.1 (2 x ^{C}Hx *C*H$_2$). **HPLC:** ^{t}$_R$ 2.92min (95%). **LC-MS:** *m/z* = 493 $[M+H]^+$. **M.p.:** 230-233°C.

Methyl 2-[(6-chloro-2-{[(1*R*,4*R*)-4-[2-(4-chlorophenoxy) acetamido]cyclohexyl]carbamoyl}-3,4-dihydro-2H-1-benzopyran-4-yl)oxy]acetate (157b)



6-Chloro-4-hydroxy-*N*-[(1*R*,4*R*)-4-[2-(4-chlorophenoxy)acetamido]cyclohexyl]-3,4-dihydro-2H-1-benzopyran-2-carboxamide **157a** (0.1 g, 0.2 mmol) was added to DMF (5 mL) and the reaction mixture cooled in an ice bath. Sodium hydride 60% dispersion in mineral oil (0.04 g, 1mmol) was added and the reaction mixture was stirred under nitrogen for 20 min. Methyl bromoacetate (0.09 mL, 1mmol) was then added dropwise, and continued stirred for 3 hours, during which time the reaction was allow to warm to room temperature. Water (10 mL) was then added to the reaction mixture, and the aqueous mixture was extracted twice with ethyl acetate (10 mL). The combined organic layers were washed water and brine, dried over sodium sulphate then filtered and concentrated under vacuum. The resulting precipitate was purified by column chromatography using gradients of DCM/THF. The combined fractions were concentrated to afford a white solid. The resulting solid was further purified by

triturated with diethyl ether (3 mL), then separated by filtration and dried in vacuo to afford the title compound as off-white powder (0.097 g, yield: 86%). **^{1}H NMR (400 MHz, DMSO-*d*$_6$)** δ 7.95 (d, *J*=8.0 Hz, 1H, amide N*H*), 7.84 (d, *J*=8.1 Hz, 1H, amide N*H*), 7.56 (d, *J*=2.1 Hz, 1H, Ar C-*H ortho* to chlorine), 7.34 (d, *J*=8.8 Hz, 2H, Ar C-*H ortho* to chlorine), 7.27 (dd, *J*=2.3, 2.4 Hz, 1H, Ar C-*H ortho* to chlorine), 6.97 (d, *J*=8.9 Hz, 2H, Ar C-*H ortho* to phenoxy), 6.92 (d, *J*=8.8 Hz, 1H, Ar C-*H ortho* to phenoxy), 4.78 (dt, *J*=3.4, 4.7 Hz, 1H, C*H*OAr), 4.62 (dd, *J*=2.1, 2.2 Hz, 1H, C*H*OCH2COO), 4.44 (s, 2H, C*H*$_2$OAr), 4.33 (d, *J*=2.5 Hz, 2H, C*H*$_2$COOCH$_3$), 3.69 (s, 3H, COOC*H*$_3$), 3.58 (bs,2H, ^{C}Hx C*H*), 2.60 (dd, *J*=3.1, 2.4 Hz, 1H, chromane C*H*$_2$), 2.56 (dd, *J*=2.5, 2.5 Hz, 1H, chromane C*H*$_2$), 1.77 (t, *J*=11.6 Hz, 4H, ^{C}Hx C*H*$_2$), 1.42 - 1.27 (m, 4H, ^{C}Hx C*H*$_2$). **^{13}C NMR (DMSO)** δ 171.5 (carboxylic *C*=O), 168.4, 166.9 (2 x amide *C*=O), 157.1, 152.4 (2 x Ar 4º C-phenoxy), 129.6, 129.2, 128.0 (3 x Ar *C*-H *ortho* to chlorine), 125.8, 125.2 (2 x Ar 4º C-chlorine), 124.7 (Ar 4º *C-ortho* to phenoxy), 118.8, 116.9 (2 x Ar *C*-H *ortho* to phenoxy), 74.4 (*C*HOAr), 71.5 (*C*HOCH$_2$COO), 67.6 (*C*H$_2$OAr), 65.9 (*C*H$_2$COOCH$_3$), 52.0 (*C*H$_3$), 47.5, 47.4 (2 x ^{C}Hx *C*H), 31.3, 31.1, 30.0 (3 x *C*H$_2$CH$_2$). **HPLC:** ^{t}$_R$ 2.97min (95%). **HRMS:** *m/z* theoretical for $C_{27}H_{31}Cl_2N_2O_7$ 565.1503 $[M+H]^+$, measured 565.1505 $[M+H]^+$. **M.p.:** 245-248°C.

References:

1. Meyers, R. A.; Meyers, R. A. *Encyclopedia of molecular cell biology and molecular medicine*. Wiley-Vch Weinheim: 2004.
2. Proud, C. G. Regulation of mRNA translation. *Essays in biochemistry* **2001,** 37, 97-108.
3. GM., C. The Cell: *A Molecular Approach*. 2nd edition ed.; Sunderland (MA): Sinauer Associates: 2000.
4. Spilka, R.; Ernst, C.; Mehta, A. K.; Haybaeck, J. Eukaryotic translation initiation factors in cancer development and progression. *Cancer Lett* **2013,** 340, 9-21.
5. Kapp, L. D.; Lorsch, J. R. The molecular mechanics of eukaryotic translation. *Annual review of biochemistry* **2004,** 73, 657-704.
6. Laursen, B. S.; Sorensen, H. P.; Mortensen, K. K.; Sperling-Petersen, H. U. Initiation of protein synthesis in bacteria. *Microbiology and Molecular Biology Reviews* **2005,** 69, 101-23.
7. Kimball, S. R. Eukaryotic initiation factor eIF2. *The international journal of biochemistry & cell biology* **1999,** 31, 25-29.
8. Pavitt, G. eIF2B, a mediator of general and gene-specific translational control. *Biochemical Society transactions* **2005,** 33, 1487-1492.
9. Lourenco, M. V.; Ferreira, S. T.; De Felice, F. G. Neuronal stress signaling and eIF2alpha phosphorylation as molecular links between Alzheimer's disease and diabetes. *Progress in Neurobiology* **2015,** 129, 37-57.
10. Rowlands, A.; Panniers, R.; Henshaw, E. The catalytic mechanism of guanine nucleotide exchange factor action and competitive inhibition by phosphorylated eukaryotic initiation factor 2. *Journal of Biological Chemistry* **1988,** 263, 5526-5533.
11. Kolitz, S. E.; Lorsch, J. R. Eukaryotic initiator tRNA: finely tuned and ready for action. *FEBS letters* **2010,** 584, 396-404.
12. Gingras, A.-C.; Raught, B.; Sonenberg, N. eIF4 initiation factors: effectors of mRNA recruitment to ribosomes and regulators of translation. *Annual review of biochemistry* **1999,** 68, 913-963.
13. Schmidt, C.; Beilsten-Edmands, V.; Robinson, C. V. Insights into Eukaryotic Translation Initiation from Mass Spectrometry of Macromolecular Protein Assemblies. *Journal of molecular biology* **2016,** 428, 344-356.
14. Jackson, R. J.; Hellen, C. U.; Pestova, T. V. The mechanism of eukaryotic translation initiation and principles of its regulation. *Nature reviews. Molecular cell biology* **2010,** 11, 113-27.

15. Fletcher, C. M.; Pestova, T. V.; Hellen, C. U.; Wagner, G. Structure and interactions of the translation initiation factor eIF1. *The EMBO journal* **1999,** 18, 2631-2637.

16. Dever, T. E.; Green, R. The elongation, termination, and recycling phases of translation in eukaryotes. *Cold Spring Harbor perspectives in biology* **2012,** 4, a013706.

17. Hellen, C. U. Translation termination and ribosome recycling in eukaryotes. *Cold Spring Harbor perspectives in biology* **2018,** 10, a032656.

18. Kapur, M.; Monaghan, C. E.; Ackerman, S. L. Regulation of mRNA translation in neurons—a matter of life and death. *Neuron* **2017,** 96, 616-637.

19. Turner, P.; McLennan, A.; Bates, A.; White, M. *BIOS Instant Notes in Molecular Biology*. Garland Science: 2007.

20. Zhan, K.; Vattem, K. M.; Bauer, B. N.; Dever, T. E.; Chen, J. J.; Wek, R. C. Phosphorylation of eukaryotic initiation factor 2 by heme-regulated inhibitor kinase-related protein kinases in Schizosaccharomyces pombe is important for fesistance to environmental stresses. *Molecular cell biology* **2002,** 22, 7134-46.

21. Donnelly, N.; Gorman, A. M.; Gupta, S.; Samali, A. The eIF2α kinases: their structures and functions. *Cellular and molecular life sciences* **2013,** 70, 3493-3511.

22. Francesconi, A.; Duvoisin, R. M. Opposing effects of protein kinase C and protein kinase A on metabotropic glutamate receptor signaling: Selective desensitization of the inositol trisphosphate/Ca21 pathway by phosphorylation of the receptor-G protein-coupling domain. *Proceedings of the National Academy of Sciences* **2000,** 97, 6185–6190.

23. Holcik, M.; Sonenberg, N. Translational control in stress and apoptosis. *Nature reviews. Molecular cell biology* **2005,** 6, 318-27.

24. Kimball, S. R.; Heinzinger, N. K.; Horetsky, R. L.; Jefferson, L. S. Identification of interprotein interactions between the subunits of eukaryotic initiation factors eIF2 and eIF2B. *Journal of Biological Chemistry* **1998,** 273, 3039-3044.

25. Dey, S.; Baird, T. D.; Zhou, D.; Palam, L. R.; Spandau, D. F.; Wek, R. C. Both transcriptional regulation and translational control of ATF4 are central to the integrated stress response. *Journal of Biological Chemistry* **2010,** 285, 33165-74.

26. Young, S. K.; Wek, R. C. Upstream Open Reading Frames Differentially Regulate Gene-specific Translation in the Integrated Stress Response. *Journal of Biological Chemistry* **2016,** 291, 16927-35.

27. Leppek, K.; Das, R.; Barna, M. Functional 5' UTR mRNA structures in eukaryotic translation regulation and how to find them. *Nature reviews. Molecular cell biology* **2018,** 19, 158-174.

28. Proud, C. G. Regulation of eukaryotic initiation factor eIF2B. In *Signaling Pathways for Translation*, Springer: 2001; pp 95-114.

29. Woods, Y. L.; Cohen, P.; Becker, W.; Jakes, R.; Goedert, M.; Wang, X.; Proud, C. G. The kinase DYRK phosphorylates protein-synthesis initiation factor eIF2Bε at Ser539 and the microtubule-associated protein tau at Thr212: potential role for DYRK as a glycogen synthase kinase 3-priming kinase. *Biochemical Journal* **2001,** 355, 609-615.

30. Welsh, G. I.; Miller, C. M.; Loughlin, A. J.; Price, N. T.; Proud, C. G. Regulation of eukaryotic initiation factor eIF2B: glycogen synthase kinase-3 phosphorylates a conserved serine which undergoes dephosphorylation in response to insulin. *FEBS letters* **1998,** 421, 125-130.

31. Wang, X.; Proud, C. G. A novel mechanism for the control of translation initiation by amino acids, mediated by phosphorylation of eukaryotic initiation factor 2B. *Molecular and cellular biology* **2008,** 28, 1429-1442.

32. Woods, Y. L.; Cohen, P.; Becker, W.; Jakes, R.; Goedert, M.; Wang, X.; Proud, C. G. The kinase DYRK phosphorylates protein-synthesis initiation factor eIF2Bepsilon at Ser539 and the microtubule-associated protein tau at Thr212: potential role for DYRK as a glycogen synthase kinase 3-priming kinase. *The Biochemical journal* **2001**, *355*, 609–615.

33. Williams, D. D.; Price, N. T.; Loughlin, A. J.; Proud, C. G. Characterization of the mammalian initiation factor eIF2B complex as a GDP dissociation stimulator protein. *Journal of Biological Chemistry* **2001,** 276, 24697-24703.

34. Wortham, N. C.; Martinez, M.; Gordiyenko, Y.; Robinson, C. V.; Proud, C. G. Analysis of the subunit organization of the eIF2B complex reveals new insights into its structure and regulation. *The Federation of American Societies for Experimental Biology* **2014,** 28, 2225-2237.

35. Wortham, N. C.; Proud, C. G. eIF2B: recent structural and functional insights into a key regulator of translation. *Biochemical Society Transactions* **2015,** 43, 1234-1240.

36. Gordiyenko, Y.; Schmidt, C.; Jennings, M. D.; Matak-Vinkovic, D.; Pavitt, G. D.; Robinson, C. V. eIF2B is a decameric guanine nucleotide exchange factor with a γ 2 ε 2 tetrameric core. *Nature communications* **2014,** 5, 1-12.

37. Gordiyenko, Y.; Schmidt, C.; Jennings, M. D.; Matak-Vinkovic, D.; Pavitt, G. D.; Robinson, C. V. eIF2B is a decameric guanine nucleotide exchange factor with a gamma2epsilon2 tetrameric core. *Nature communications* **2014,** 5, 3902.

38. Yang, W.; Hinnebusch, A. G. Identification of a regulatory subcomplex in the guanine nucleotide exchange factor eIF2B that mediates inhibition by phosphorylated eIF2. M*olecular and cellular biology* **199**6, 16, 6603–6616.

39. Graham D. Pavitt, K. V. A. R., Scot R. Kimball, and Alan G. Hinnebusch. eIF2 independently binds two distincteIF2B subcomplexes that catalyze and regulate guanine–nucleotide exchange. *Genes & development* **1997,** 12, 514–526.

40. Kashiwagi, K.; Takahashi, M.; Nishimoto, M.; Hiyama, T. B.; Higo, T.; Umehara, T.; Sakamoto, K.; Ito, T.; Yokoyama, S. Crystal structure of eukaryotic translation initiation factor 2B. *Nature* **2016,** 531, 122-5.

41. Kashiwagi, K.; Ito, T.; Yokoyama, S. Crystal structure of eIF2B and insights into eIF2–eIF2B interactions. *The FEBS journal* **2017,** 284, 868-874.

42. Bogorad, A. M.; Lin, K. Y.; Marintchev, A. eIF2B Mechanisms of Action and Regulation: A Thermodynamic View. *Biochemistry* **2018,** 57, 1426-1435.

43. Sharma, S.; Sourirajan, A.; Dev, K. Role of Saccharomyces cerevisiae TAN1 (tRNA acetyltransferase) in eukaryotic initiation factor 2B (eIF2B)-mediated translation control and stress response. *3 Biotech* **2017,** 7, 223.

44. Zyryanova, A. F.; Weis, F.; Faille, A.; Alard, A. A.; Crespillo-Casado, A.; Sekine, Y.; Harding, H. P.; Allen, F.; Parts, L.; Fromont, C.; Fischer, P. M.; Warren, A. J.; Ron, D. Binding of ISRIB reveals a regulatory site in the nucleotide exchange factor eIF2B. *Science* **2018,** 359, 1533-1536.

45. Tsai, J. C.; Miller-Vedam, L. E.; Anand, A. A.; Jaishankar, P.; Nguyen, H. C.; Renslo, A. R.; Frost, A.; Walter, P. Structure of the nucleotide exchange factor eIF2B reveals mechanism of memory-enhancing molecule. *Science* **2018,** 359.

46. Kenner, L. R.; Anand, A. A.; Nguyen, H. C.; Myasnikov, A. G.; Klose, C. J.; McGeever, L. A.; Tsai, J. C.; Miller-Vedam, L. E.; Walter, P.; Frost, A. eIF2B-catalyzed nucleotide exchange and phosphoregulation by the integrated stress response. *Science* **2019,** 364, 491-495.

47. Kashiwagi, K.; Yokoyama, T.; Nishimoto, M.; Takahashi, M.; Sakamoto, A.; Yonemochi, M.; Shirouzu, M.; Ito, T. Structural basis for eIF2B inhibition in integrated stress response. *Science* **2019,** 364, 495-499.

48. Mei, Y.; Thompson, M. D.; Cohen, R. A.; Tong, X. Endoplasmic reticulum stress and related pathological processes. *Journal of pharmacological & biomedical analysis* **2013,** 1, 1000107.

49. Chaudhari, N.; Talwar, P.; Parimisetty, A.; Lefebvre d'Hellencourt, C.; Ravanan, P. A molecular web: endoplasmic reticulum stress, inflammation, and oxidative stress. *Frontiers in cellular neuroscience* **2014,** 8, 213.

50. Ron, D.; Walter, P. Signal integration in the endoplasmic reticulum unfolded protein response. *Nature reviews Molecular cell biology* **2007,** 8, 519-529.

51. Haeri, M.; Knox, B. E. Endoplasmic reticulum stress and unfolded protein response pathways: potential for treating age-related retinal degeneration. *Journal of ophthalmic & vision research* **2012,** 7, 45.

52. Asada, R.; Kanemoto, S.; Kondo, S.; Saito, A.; Imaizumi, K. The signalling from endoplasmic reticulum-resident bZIP transcription factors involved in diverse cellular physiology. *The Journal of Biochemistry* **2011,** 149, 507-518.

53. Lin, J. H.; Li, H.; Zhang, Y.; Ron, D.; Walter, P. Divergent effects of PERK and IRE1 signaling on cell viability. *PloS one* **2009,** 4, e4170.

54. Lin, J. H.; Li, H.; Yasumura, D.; Cohen, H. R.; Zhang, C.; Panning, B.; Shokat, K. M.; LaVail, M. M.; Walter, P. IRE1 signaling affects cell fate during the unfolded protein response. *science* **2007,** 318, 944-949.

55. Korennykh, A.; Walter, P. Structural basis of the unfolded protein response. *Annual review of cell and developmental biology* **2012,** 28, 251-277.

56. Walter, P.; Ron, D. The unfolded protein response: from stress pathway to homeostatic regulation. *Science* **2011,** 334, 1081-1086.

57. Hiramatsu, N.; Chiang, W.-C.; Kurt, T. D.; Sigurdson, C. J.; Lin, J. H. Multiple mechanisms of unfolded protein response–induced cell death. *The American journal of pathology* **2015,** 185, 1800-1808.

58. Lai, E.; Teodoro, T.; Volchuk, A. Endoplasmic reticulum stress: signaling the unfolded protein response. *Physiology* **2007,** 22, 193-201.

59. Wang, X. Z.; Harding, H. P.; Zhang, Y.; Jolicoeur, E. M.; Kuroda, M.; Ron, D. Cloning of mammalian Ire1 reveals diversity in the ER stress responses. *The EMBO journal* **1998,** 17, 5708-5717.

60. Hetz, C.; Glimcher, L. H. Fine-tuning of the unfolded protein response: assembling the IRE1α interactome. *Molecular cell* **2009,** 35, 551-561.

61. Tirasophon, W.; Lee, K.; Callaghan, B.; Welihinda, A.; Kaufman, R. J. The endoribonuclease activity of mammalian IRE1 autoregulates its mRNA and is required for the unfolded protein response. *Genes & development* **2000,** 14, 2725-2736.

62. Arensdorf, A. M.; Diedrichs, D.; Rutkowski, D. T. Regulation of the transcriptome by ER stress: non-canonical mechanisms and physiological consequences. *Front Genet* **2013,** 4, 256.

63. Harding, H. P.; Zhang, Y.; Ron, D. Protein translation and folding are coupled by an endoplasmic-reticulum-resident kinase. *Nature* **1999,** 397, 271-274.

64. Rajesh, K.; Krishnamoorthy, J.; Kazimierczak, U.; Tenkerian, C.; Papadakis, A.; Wang, S.; Huang, S.; Koromilas, A. Phosphorylation of the translation initiation factor eIF2 α at serine 51 determines the cell fate decisions of Akt in response to oxidative stress. *Cell death & disease* **2015,** 6, e1591-e1591.

65. Wang, S.; Kaufman, R. J. The impact of the unfolded protein response on human disease. *Journal of Cell Biology* **2012,** 197, 857-67.

66. Blais, J. D.; Filipenko, V.; Bi, M.; Harding, H. P.; Ron, D.; Koumenis, C.; Wouters, B. G.; Bell, J. C. Activating transcription factor 4 is translationally regulated by hypoxic stress. *Molecular cell biology* **2004,** 24, 7469-82.

67. Han, J.; Back, S. H.; Hur, J.; Lin, Y. H.; Gildersleeve, R.; Shan, J.; Yuan, C. L.; Krokowski, D.; Wang, S.; Hatzoglou, M.; Kilberg, M. S.; Sartor, M. A.; Kaufman, R. J. ER-stress-induced transcriptional regulation increases protein synthesis leading to cell death. *Nature cell biology* **2013,** 15, 481-90.

68. Ma, Y. F.; Wu, Z. H.; Gao, M.; Loor, J. J. Nuclear factor erythroid 2-related factor 2 antioxidant response element pathways protect bovine mammary epithelial cells against H2O2-induced oxidative damage in vitro. *Journal of dairy science* **2018,** 101, 5329-5344.

69. Rozpedek, W.; Pytel, D.; Mucha, B.; Leszczynska, H.; Diehl, J. A.; Majsterek, I. The role of the PERK/eIF2α/ATF4/CHOP signaling pathway in tumor progression during endoplasmic reticulum stress. *Current molecular medicine* **2016,** 16, 533-544.

70. Sano, R.; Reed, J. C. ER stress-induced cell death mechanisms. *Biochimica et Biophysica Acta (BBA)-Molecular Cell Research* **2013,** 1833, 3460-3470.

71. Rutkowski, D. T.; Arnold, S. M.; Miller, C. N.; Wu, J.; Li, J.; Gunnison, K. M.; Mori, K.; Akha, A. A. S.; Raden, D.; Kaufman, R. J. Adaptation to ER stress is mediated by differential stabilities of pro-survival and pro-apoptotic mRNAs and proteins. *PLoS biology* **2006,** 4, e374.

72. Oslowski, C. M.; Urano, F. Measuring ER stress and the unfolded protein response using mammalian tissue culture system. *Methods Enzymol* **2011,** 490, 71-92.

73. Lee, A. H.; Iwakoshi, N. N.; Glimcher, L. H. XBP-1 regulates a subset of endoplasmic reticulum resident chaperone genes in the unfolded protein response. *Molecular cell biology* **2003,** 23, 7448-59.

74. Yarapureddy, S.; Abril, J.; Foote, J.; Kumar, S.; Asad, O.; Sharath, V.; Faraj, J.; Daniel, D.; Dickman, P.; White-Collins, A.; Hingorani, P.; Sertil, A. R. ATF6alpha Activation Enhances Survival against Chemotherapy and Serves as a Prognostic Indicator in Osteosarcoma. *Neoplasia* **2019,** 21, 516-532.

75. Halliday, M.; Mallucci, G. R. Modulating the unfolded protein response to prevent neurodegeneration and enhance memory. *Neuropathology and applied neurobiology* **2015,** 41, 414-427.

76. Taniuchi, S.; Miyake, M.; Tsugawa, K.; Oyadomari, M.; Oyadomari, S. Integrated stress response of vertebrates is regulated by four eIF2alpha kinases. *Scientific reports* **2016,** 6, 32886.

77. Wek, R.; Jiang, H.-Y.; Anthony, T. Coping with stress: eIF2 kinases and translational control. In Portland Press Ltd.: 2006.

78. Pakos-Zebrucka, K.; Koryga, I.; Mnich, K.; Ljujic, M.; Samali, A.; Gorman, A. M. The integrated stress response. *EMBO reports* **2016,** 17, 1374-1395.

79. Hamanaka, R. B.; Bennett, B. S.; Cullinan, S. B.; Diehl, J. A. PERK and GCN2 contribute to eIF2α phosphorylation and cell cycle arrest after activation of the unfolded protein response pathway. *Molecular biology of the cell* **2005,** 16, 5493-5501.

80. Yuan, W.; Guo, S.; Gao, J.; Zhong, M.; Yan, G.; Wu, W.; Chao, Y.; Jiang, Y. General Control Nonderepressible 2 (GCN2) Kinase Inhibits Target of Rapamycin Complex 1 in Response to Amino Acid Starvation in Saccharomyces cerevisiae. *Journal of Biological Chemistry* **2017,** 292, 2660-2669.

81. Berlanga, J. J.; Ventoso, I.; Harding, H. P.; Deng, J.; Ron, D.; Sonenberg, N.; Carrasco, L.; de Haro, C. Antiviral effect of the mammalian translation initiation factor 2α kinase GCN2 against RNA viruses. *The EMBO journal* **2006,** 25, 1730-1740.

82. Anda, S.; Zach, R.; Grallert, B. Activation of Gcn2 in response to different stresses. *PLoS One* **2017,** 12, e0182143.

83. Dang Do, A. N.; Kimball, S. R.; Cavener, D. R.; Jefferson, L. S. eIF2alpha kinases GCN2 and PERK modulate transcription and translation of distinct sets of mRNAs in mouse liver. *Physiol Genomics* **2009,** 38, 328-41.

84. Garcia, M. A.; Gil, J.; Ventoso, I.; Guerra, S.; Domingo, E.; Rivas, C.; Esteban, M. Impact of protein kinase PKR in cell biology: from antiviral to antiproliferative action. *Microbiology and molecular biology reviews* **2006,** 70, 1032-60.

85. Sunita, S.; Schwartz, S. L.; Conn, G. L. The Regulatory and Kinase Domains but Not the Interdomain Linker Determine Human Double-stranded RNA-activated Kinase (PKR) Sensitivity to Inhibition by Viral Non-coding RNAs. *Journal of Biological Chemistry* **2015,** 290, 28156-28165.

86. Williams, B. R. PKR; a sentinel kinase for cellular stress. *Oncogene* **1999,** 18, 6112-6120.

87. Losada, A.; Munoz-Alonso, M. J.; Martinez-Diez, M.; Gago, F.; Dominguez, J. M.; Martinez-Leal, J. F.; Galmarini, C. M. Binding of eEF1A2 to the RNA-dependent protein kinase PKR modulates its activity and promotes tumour cell survival. *British journal of cancer* **2018,** 119, 1410-1420.

88. Suragani, R. N.; Zachariah, R. S.; Velazquez, J. G.; Liu, S.; Sun, C.-W.; Townes, T. M.; Chen, J.-J. Heme-regulated eIF2α kinase activated Atf4 signaling pathway in oxidative stress and erythropoiesis. *Blood, The Journal of the American Society of Hematology* **2012,** 119, 5276-5284.

89. Burwick, N.; Aktas, B. H. The eIF2-alpha kinase HRI: a potential target beyond the red blood cell. *Expert opinion on therapeutic targets* **2017,** 21, 1171-1177.

90. Chen, J.-J. Translational control by heme-regulated eIF2α kinase during erythropoiesis. *Current opinion in hematology* **2014,** 21, 172.

91. Rafie-Kolpin, M.; Chefalo, P. J.; Hussain, Z.; Hahn, J.; Uma, S.; Matts, R. L.; Chen, J.-J. Two Heme-binding Domains of Heme-regulated Eukaryotic Initiation Factor-2α Kinase N TERMINUS AND KINASE INSERTION. *Journal of Biological Chemistry* **2000,** 275, 5171-5178.

92. Dugger, B. N.; Dickson, D. W. Pathology of Neurodegenerative Diseases. *Cold Spring Harbor perspectives in biology* **2017,** 9, a028035.

93. Kovacs, G. G. Molecular Pathological Classification of Neurodegenerative Diseases: Turning towards Precision Medicine. *International journal of molecular sciences* **2016,** 17, 189.

94. https://www.who.int/news-room/fact-sheets/detail/dementia

95. Scheper, W.; Hoozemans, J. J. The unfolded protein response in neurodegenerative diseases: a neuropathological perspective. *Acta neuropathologica* **2015,** 130, 315-331.

96. Henstridge, C. M.; Tzioras, M.; Paolicelli, R. C. Glial Contribution to Excitatory and Inhibitory Synapse Loss in Neurodegeneration. *Frontiers in cellular neuroscience*, **2019,** 13, 63.

97. Armstrong, R. A. A Possible Explanation For Neurodegenerative Disease. *EMJ Neurol.* **2019,** 7, 80-89.

98. Alexander, G. E. Biology of Parkinson's disease: pathogenesis and pathophysiology of a multisystem neurodegenerative disorder. *Dialogues in clinical neuroscience* **2004,** 6, 259.

99. Hetz, C.; Mollereau, B. Disturbance of endoplasmic reticulum proteostasis in neurodegenerative diseases. *Nature Reviews Neuroscience* **2014,** 15, 233-249.

100. Hetz, C.; Saxena, S. ER stress and the unfolded protein response in neurodegeneration. *Nature Reviews Neurology* **2017,** 13, 477.

101. Stutzbach, L. D.; Xie, S. X.; Naj, A. C.; Albin, R.; Gilman, S.; Lee, V. M.; Trojanowski, J. Q.; Devlin, B.; Schellenberg, G. D.; Group, P. G. S. The unfolded protein response is activated in disease-affected brain regions in progressive supranuclear palsy and Alzheimer's disease. *Acta neuropathologica communications* **2013,** 1, 31.

102. Hoozemans, J. J.; van Haastert, E. S.; Nijholt, D. A.; Rozemuller, A. J.; Eikelenboom, P.; Scheper, W. The unfolded protein response is activated in pretangle neurons in Alzheimer's disease hippocampus. *The American journal of pathology* **2009,** 174, 1241-1251.

103. Hetz, C.; Russelakis-Carneiro, M.; Maundrell, K.; Castilla, J.; Soto, C. Caspase-12 and endoplasmic reticulum stress mediate neurotoxicity of pathological prion protein. *The EMBO journal* **2003,** 22, 5435-5445.

104. Nardo, G.; Pozzi, S.; Pignataro, M.; Lauranzano, E.; Spano, G.; Garbelli, S.; Mantovani, S.; Marinou, K.; Papetti, L.; Monteforte, M. Amyotrophic lateral sclerosis multiprotein biomarkers in peripheral blood mononuclear cells. *PloS one* **2011,** 6.

105. Höglinger, G. U.; Melhem, N. M.; Dickson, D. W.; Sleiman, P. M.; Wang, L.-S.; Klei, L.; Rademakers, R.; De Silva, R.; Litvan, I.; Riley, D. E. Identification of common variants influencing risk of the tauopathy progressive supranuclear palsy. *Nature genetics* **2011,** 43, 699.

106. Saxena, S.; Cabuy, E.; Caroni, P. A role for motoneuron subtype–selective ER stress in disease manifestations of FALS mice. *Nature neuroscience* **2009,** 12, 627.

107. Abisambra, J. F.; Jinwal, U. K.; Blair, L. J.; O'Leary, J. C.; Li, Q.; Brady, S.; Wang, L.; Guidi, C. E.; Zhang, B.; Nordhues, B. A. Tau accumulation activates the unfolded protein response by impairing endoplasmic reticulum-associated degradation. *Journal of Neuroscience* **2013,** 33, 9498-9507.

108. Devi, L.; Ohno, M. PERK mediates eIF2α phosphorylation responsible for BACE1 elevation, CREB dysfunction and neurodegeneration in a mouse model of Alzheimer's disease. *Neurobiology of aging* **2014,** 35, 2272-2281.

109. Leegwater, P. A.; Vermeulen, G.; Könst, A. A.; Naidu, S.; Mulders, J.; Visser, A.; Kersbergen, P.; Mobach, D.; Fonds, D.; Van Berkel, C. G. Subunits of the translation initiation factor eIF2B are mutant in leukoencephalopathy with vanishing white matter. *Nature genetics* **2001,** 29, 383-388.

110. Paschen, W.; Mengesdorf, T. Endoplasmic reticulum stress response and neurodegeneration. *Cell calcium* **2005,** 38, 409-415.

111. Ma, T.; Trinh, M. A.; Wexler, A. J.; Bourbon, C.; Gatti, E.; Pierre, P.; Cavener, D. R.; Klann, E. Suppression of eIF2α kinases alleviates AD-related synaptic plasticity and spatial memory deficits. *Nature neuroscience* **2013,** 16, 1299.

112. Serrano-Pozo, A.; Frosch, M. P.; Masliah, E.; Hyman, B. T. Neuropathological alterations in Alzheimer disease. *Cold Spring Harbor perspectives in biology* **2011,** 1, a006189.

113. Murphy, M. P.; LeVine, H., 3rd. Alzheimer's disease and the amyloid-beta peptide. *Journal of Alzheimer's disease* **2010,** 19, 311-23.

114. DeTure, M. A.; Dickson, D. W. The neuropathological diagnosis of Alzheimer's disease. *Molecular neurodegeneration* **2019,** 14, 32.

115. Boluda, S.; Toledo, J. B.; Irwin, D. J.; Raible, K. M.; Byrne, M. D.; Lee, E. B.; Lee, V. M.; Trojanowski, J. Q. A comparison of Abeta amyloid

pathology staging systems and correlation with clinical diagnosis. *Acta neuropathologica* **2014,** 128, 543-50.

116. Kovacs, G. G.; Budka, H. Molecular pathology of human prion diseases. *International journal of molecular sciences* **2009,** 10, 976-99.

117. Jellinger, K. A. Interaction between pathogenic proteins in neurodegenerative disorders. *J Journal of cellular and molecular medicine* **2012,** 16, 1166-83.

118. Moreno, J. A.; Radford, H.; Peretti, D.; Steinert, J. R.; Verity, N.; Martin, M. G.; Halliday, M.; Morgan, J.; Dinsdale, D.; Ortori, C. A. Sustained translational repression by eIF2α-P mediates prion neurodegeneration. *Nature* **2012,** 485, 507-511.

119. Mhyre, T. R.; Boyd, J. T.; Hamill, R. W.; Maguire-Zeiss, K. A. Parkinson's disease. *Sub-cellular biochemistry* **2012,** 65, 389-455.

120. Moore, D. J.; West, A. B.; Dawson, V. L.; Dawson, T. M. Molecular pathophysiology of Parkinson's disease. *Annual review of neuroscience.* **2005,** 28, 57-87.

121. Martinez, A.; Lopez, N.; Gonzalez, C.; Hetz, C. Targeting of the unfolded protein response (UPR) as therapy for Parkinson's disease. *Biology of the Cell* **2019,** 111, 161-168.

122. Qiu, C.; Kivipelto, M.; von Strauss, E. Epidemiology of Alzheimer's disease: occurrence, determinants, and strategies toward intervention. *Dialogues in clinical neuroscience* **2009,** 11, 111.

123. Rakesh, G.; Szabo, S. T.; Alexopoulos, G. S.; Zannas, A. S. Strategies for dementia prevention: latest evidence and implications. *Therapeutic advances in chronic disease* **2017,** 8, 121-136.

124. de la Monte, S. M. Insulin Resistance and Neurodegeneration: Progress Towards the Development of New Therapeutics for Alzheimer's Disease. *Drugs* **2017,** 77, 47-65.

125. van Dyck, C. H. Anti-Amyloid-beta Monoclonal Antibodies for Alzheimer's Disease: Pitfalls and Promise. *Biological psychiatry* **2018,** 83, 311-319.

126. Yan, R.; Vassar, R. Targeting the β secretase BACE1 for Alzheimer's disease therapy. *The Lancet Neurology* **2014,** 13, 319-329.

127. Cao, J.; Hou, J.; Ping, J.; Cai, D. Advances in developing novel therapeutic strategies for Alzheimer's disease. *Molecular neurodegeneration* **2018,** 13, 64.

128. Ricciarelli, R.; Fedele, E. The Amyloid Cascade Hypothesis in Alzheimer's Disease: It's Time to Change Our Mind. *Current neuropharmacology* **2017,** 15, 926-935.

129. Coimbra, J. R. M.; Marques, D. F. F.; Baptista, S. J.; Pereira, C. M. F.; Moreira, P. I.; Dinis, T. C. P.; Santos, A. E.; Salvador, J. A. R. Highlights

in BACE1 Inhibitors for Alzheimer's Disease Treatment. *Frontiers in chemistry* **2018,** 6, 178.

130. Smith, H. L.; Mallucci, G. R. The unfolded protein response: mechanisms and therapy of neurodegeneration. *Brain* **2016,** 139, 2113-2121.

131. Mitra, S. P. Drug− receptor interaction: pharmacology, binding and thermodynamics− A Review. *Journal of Surface Science and Technology* **2009,** 25, 103-152.

132. Lambert, D. Drugs and receptors. *Continuing education in anaesthesia critical care & pain* **2004,** 4, 181-184.

133. Berg, K. A.; Clarke, W. P. Making sense of pharmacology: inverse agonism and functional selectivity. *International Journal of Neuropsychopharmacology* **2018,** 21, 962-977.

134. Maïofiss, L.; Thomas-Haimez, C.; Maccario, P. J. Competitive antagonism in pharmacology: A proposed single step evaluation. *Drug information journal* **1997,** 31, 563-572.

135. Foster, D. J.; Conn, P. J. Allosteric modulation of GPCRs: new insights and potential utility for treatment of schizophrenia and other CNS disorders. *Neuron* **2017,** 94, 431-446.

136. Axten, J. M.; Medina, J. s. R.; Feng, Y.; Shu, A.; Romeril, S. P.; Grant, S. W.; Li, W. H. H.; Heerding, D. A.; Minthorn, E.; Mencken, T. Discovery of 7-methyl-5-(1-{[3-(trifluoromethyl) phenyl] acetyl}-2, 3-dihydro-1 H-indol-5-yl)-7 H-pyrrolo [2, 3-d] pyrimidin-4-amine (GSK2606414), a potent and selective first-in-class inhibitor of protein kinase R (PKR)-like endoplasmic reticulum kinase (PERK). *Journal of medicinal chemistry* **2012,** 55, 7193-7207.

137. Atkins, C.; Liu, Q.; Minthorn, E.; Zhang, S.-Y.; Figueroa, D. J.; Moss, K.; Stanley, T. B.; Sanders, B.; Goetz, A.; Gaul, N. Characterization of a novel PERK kinase inhibitor with antitumor and antiangiogenic activity. *Cancer research* **2013,** 73, 1993-2002.

138. Mercado, G.; Castillo, V.; Soto, P.; López, N.; Axten, J. M.; Sardi, S. P.; Hoozemans, J. J.; Hetz, C. Targeting PERK signaling with the small molecule GSK2606414 prevents neurodegeneration in a model of Parkinson's disease. *Neurobiology of disease* **2018,** 112, 136-148.

139. Rojas-Rivera, D.; Delvaeye, T.; Roelandt, R.; Nerinckx, W.; Augustyns, K.; Vandenabeele, P.; Bertrand, M. J. M. When PERK inhibitors turn out to be new potent RIPK1 inhibitors: critical issues on the specificity and use of GSK2606414 and GSK2656157. *Cell death and differentiation* **2017,** 24, 1100-1110.

140. Moreno, J. A.; Halliday, M.; Molloy, C.; Radford, H.; Verity, N.; Axten, J. M.; Ortori, C. A.; Willis, A. E.; Fischer, P. M.; Barrett, D. A.; Mallucci, G. R. Oral treatment targeting the unfolded protein response prevents neurodegeneration and clinical disease in prion-infected mice. *Science translational medicine* **2013,** 5, 206ra138.

141. Mahameed, M.; Wilhelm, T.; Darawshi, O.; Obiedat, A.; Tommy, W. S.; Chintha, C.; Schubert, T.; Samali, A.; Chevet, E.; Eriksson, L. A.; Huber, M.; Tirosh, B. The unfolded protein response modulators GSK2606414 and KIRA6 are potent KIT inhibitors. *Cell death & disease* **2019,** 10, 300.

142. Yu, Q.; Zhao, B.; Gui, J.; Katlinski, K. V.; Brice, A.; Gao, Y.; Li, C.; Kushner, J. A.; Koumenis, C.; Diehl, J. A. Type I interferons mediate pancreatic toxicities of PERK inhibition. *Proceedings of the National Academy of Sciences* **2015,** 112, 15420-15425.

143. Uma, S.; Yun, B.-G.; Matts, R. L. The heme-regulated eukaryotic initiation factor 2alpha kinase. A potential regulatory target for control of protein synthesis by diffusible gases. *Journal of Biological Chemistry* **2001,** 276, 14875-14883.

144. Kanelakis, K. C.; Pyati, J.; Wagaman, P. C.; Chuang, J. C.; Yang, Y.; Shankley, N. P. Functional Characterization of the Canine Heme-Regulated eIF2 Kinase: Regulation of Protein Synthesis. *Advances in hematology* **2009,** 2009.

145. Rosen, M. D.; Woods, C. R.; Goldberg, S. D.; Hack, M. D.; Bounds, A. D.; Yang, Y.; Wagaman, P. C.; Phuong, V. K.; Ameriks, A. P.; Barrett, T. D. Discovery of the first known small-molecule inhibitors of heme-regulated eukaryotic initiation factor 2α (HRI) kinase. *Bioorganic & medicinal chemistry letters* **2009,** 19, 6548-6551.

146. Huang, J.; Schneider, R. J. Adenovirus inhibition of cellular protein synthesis is prevented by the drug 2-aminopurine. *Proceedings of the National Academy of Sciences* **1990,** 87, 7115-7119.

147. Jammi, N. V.; Whitby, L. R.; Beal, P. A. Small molecule inhibitors of the RNA-dependent protein kinase. *Biochemical and biophysical research communications* **2003,** 308, 50-57.

148. Meggio, F.; Deana, A. D.; Ruzzene, M.; Brunati, A. M.; Cesaro, L.; Guerra, B.; Meyer, T.; Mett, H.; Fabbro, D.; Furet, P. Different susceptibility of protein kinases to staurosporine inhibition: kinetic studies and molecular bases for the resistance of protein kinase CK2. *European journal of biochemistry* **1995,** 234, 317-322.

149. Sidrauski, C.; Acosta-Alvear, D.; Khoutorsky, A.; Vedantham, P.; Hearn, B. R.; Li, H.; Gamache, K.; Gallagher, C. M.; Ang, K. K.; Wilson, C.; Okreglak, V.; Ashkenazi, A.; Hann, B.; Nader, K.; Arkin, M. R.; Renslo, A. R.; Sonenberg, N.; Walter, P. Pharmacological brake-release of mRNA translation enhances cognitive memory. *Elife* **2013,** 2, e00498.

150. Walter, P.; Sidrauski, C.; Alvear, D. A.; Arkin, M. R.; Wilson, C. G.; Ang, K. H.; Hearn, B. R.; Vedantham, P.; Renslo, A. R.; Maze, M. Screening methods for identifying modulators of the EIF2α pathway and uses thereof for treating various diseases and improving long term memory. PCT Int. Pat. Appl. Publ. WO2014144952, 2014, USA, 2014.

151. Sidrauski, C.; Tsai, J. C.; Kampmann, M.; Hearn, B. R.; Vedantham, P.; Jaishankar, P.; Sokabe, M.; Mendez, A. S.; Newton, B. W.; Tang, E. L.; Verschueren, E.; Johnson, J. R.; Krogan, N. J.; Fraser, C. S.; Weissman, J. S.; Renslo, A. R.; Walter, P. Pharmacological dimerization and activation of the exchange factor eIF2B antagonizes the integrated stress response. *Elife* **2015,** 4, e07314.

152. Halliday, M.; Radford, H.; Sekine, Y.; Moreno, J.; Verity, N.; le Quesne, J.; Ortori, C. A.; Barrett, D. A.; Fromont, C.; Fischer, P. M.; Harding, H. P.; Ron, D.; Mallucci, G. R. Partial restoration of protein synthesis rates by the small molecule ISRIB prevents neurodegeneration without pancreatic toxicity. *Cell death & disease* **2015,** 6, e1672.

153. Chou, A.; Krukowski, K.; Jopson, T.; Zhu, P. J.; Costa-Mattioli, M.; Walter, P.; Rosi, S. Inhibition of the integrated stress response reverses cognitive deficits after traumatic brain injury. *Proceedings of the National Academy of Sciences* **2017,** 114, e6420-e6426.

154. Hinnebusch, A. G. Mechanism and regulation of initiator methionyl-tRNA binding to ribosomes. *Cold Spring Harbor monograph series* **2000,** 39, 185-244.

155. Sekine, Y.; Zyryanova, A.; Crespillo-Casado, A.; Fischer, P. M.; Harding, H. P.; Ron, D. Stress responses. Mutations in a translation initiation factor identify the target of a memory-enhancing compound. *Science* **2015,** 348, 1027-30.

156. Zyryanova, A. F.; Kashiwagi, K.; Rato, C.; Harding, H. P.; Crespillo-Casado, A.; Perera, L. A.; Sakamoto, A.; Nishimoto, M.; Yonemochi, M.; Shirouzu, M. ISRIB blunts the integrated stress response by allosterically antagonising the inhibitory effect of phosphorylated eIF2 on eIF2B. *Molecular Cell* **2020,** 81, 88-103.

157. Rabouw, H. H.; Langereis, M. A.; Anand, A. A.; Visser, L. J.; de Groot, R. J.; Walter, P.; van Kuppeveld, F. J. M. Small molecule ISRIB suppresses the integrated stress response within a defined window of activation. *Proceedings of the National Academy of Sciences of the United States of America* **2019,** 116, 2097-2102.

158. Saxena, S.; Cabuy, E.; Caroni, P. A role for motoneuron subtype-selective ER stress in disease manifestations of FALS mice. *Nature neuroscience* **2009,** 12, 627-36.

159. Pun, S.; Santos, A. F.; Saxena, S.; Xu, L.; Caroni, P. Selective vulnerability and pruning of phasic motoneuron axons in motoneuron disease alleviated by CNTF. *Nature neuroscience* **2006,** 9, 408-19.

160. D'Antonio, M.; Musner, N.; Scapin, C.; Ungaro, D.; Del Carro, U.; Ron, D.; Feltri, M. L.; Wrabetz, L. Resetting translational homeostasis restores myelination in Charcot-Marie-Tooth disease type 1B mice. *The Journal of Experimental Medicine* **2013,** 210, 821-838.

161. Das, I.; Krzyzosiak, A.; Schneider, K.; Wrabetz, L.; D'Antonio, M.; Barry, N.; Sigurdardottir, A.; Bertolotti, A. Preventing proteostasis

diseases by selective inhibition of a phosphatase regulatory subunit. *Science* **2015,** 348, 239-42.

162. Ron, D. eIF2α phosphorylation in cellular stress responses and disease. *Translational Control in Biology and Medicine* **2007,** 13, 349-372.

163. Uma, S.; Yun, B. G.; Matts, R. L. The heme-regulated eukaryotic initiation factor 2alpha kinase. A potential regulatory target for control of protein synthesis by diffusible gases. *Journal of Biological Chemistry* **2001,** 276, 14875-83.

164. Wong, Y. L.; LeBon, L.; Edalji, R.; Lim, H. B.; Sun, C.; Sidrauski, C. The small molecule ISRIB rescues the stability and activity of Vanishing White Matter Disease eIF2B mutant complexes. *Elife* **2018,** 7, e32733.

165. Harding, H. P.; Zeng, H.; Zhang, Y.; Jungries, R.; Chung, P.; Plesken, H.; Sabatini, D. D.; Ron, D. Diabetes mellitus and exocrine pancreatic dysfunction in perk−/− mice reveals a role for translational control in secretory cell survival. *Molecular cell* **2001,** 7, 1153-1163.

166. Wong, Y. L.; LeBon, L.; Basso, A. M.; Kohlhaas, K. L.; Nikkel, A. L.; Robb, H. M.; Donnelly-Roberts, D. L.; Prakash, J.; Swensen, A. M.; Rubinstein, N. D. eIF2B activator prevents neurological defects caused by a chronic integrated stress response. *Elife* **2019,** 8, e42940.

167. Hearn, B. R.; Jaishankar, P.; Sidrauski, C.; Tsai, J. C.; Vedantham, P.; Fontaine, S. D.; Walter, P.; Renslo, A. R. Structure–Activity Studies of Bis-O-Arylglycolamides: Inhibitors of the Integrated Stress Response. *ChemMedChem* **2016,** 11, 870-880.

168. Sekine, Y.; Zyryanova, A.; Crespillo-Casado, A.; Fischer, P. M.; Harding, H. P.; Ron, D. Mutations in a translation initiation factor identify the target of a memory-enhancing compound. *Science* **2015,** 348, 1027-1030.

169. Mandal, S.; Moudgil, M.; Mandal, S. K. Rational drug design. *European journal of pharmacology* **2009,** 625, 90-100.

170. Acharya, C.; Coop, A.; E Polli, J.; D MacKerell, A. Recent advances in ligand-based drug design: relevance and utility of the conformationally sampled pharmacophore approach. *Current computer-aided drug design* **2011,** 7, 10-22.

171. Merz Jr, K. M.; Ringe, D.; Reynolds, C. H. *Drug design: structure-and ligand-based approaches*. Cambridge University Press: 2010.

172. Fischer, P. M. Computational chemistry approaches to drug discovery in signal transduction. *Biotechnology journal* **2008,** 3, 452-70.

173. Wilson, G. L.; Lill, M. A. Integrating structure-based and ligand-based approaches for computational drug design. *Future medicinal chemistry* **2011,** 3, 735-750.

174. Huuskonen, J.; Livingstone, D. J.; Manallack, D. T. Prediction of drug solubility from molecular structure using a drug-like training set. *SAR and QSAR in Environmental Research* **2008,** 19, 191-212.

175. Hann, M. M. Molecular obesity, potency and other addictions in drug discovery. *Medicinal Chemistry Communications* **2011,** 2, 349-355.

176. Walker, M. A. Improvement in aqueous solubility achieved via small molecular changes. *Bioorganic & medicinal chemistry letters* **2017,** 27, 5100-5108.

177. Cao, X.; Sun, Z.; Cao, Y.; Wang, R.; Cai, T.; Chu, W.; Hu, W.; Yang, Y. Design, synthesis, and structure–activity relationship studies of novel fused heterocycles-linked triazoles with good activity and water solubility. *Journal of medicinal chemistry* **2014,** 57, 3687-3706.

178. Ritchie, T. J.; Macdonald, S. J.; Peace, S.; Pickett, S. D.; Luscombe, C. N. The developability of heteroaromatic and heteroaliphatic rings–do some have a better pedigree as potential drug molecules than others? *Medicinal Chemistry Communications* **2012,** 3, 1062-1069.

179. Bruckner, R. *Advanced organic chemistry: reaction mechanisms*. Elsevier: 2001.

180. Montalbetti, C. A. G. N.; Falque, V. Amide bond formation and peptide coupling. *Tetrahedron* **2005,** 61, 10827-10852.

181. Rawn, J. D.; Ouellette, R. J. *Organic Chemistry: Structure, Mechanism, Synthesis*. Academic Press: 2018.

182. Kumari, S.; Carmona, A.; Tiwari, A. K.; Trippier, P. C. Amide Bond Bioisosteres: Strategies, Synthesis and Successes. *Journal of Medicinal Chemistry* **2020,** 63, 12290–12358.

183. Patani, G. A.; LaVoie, E. J. Bioisosterism: a rational approach in drug design. *Chemical reviews* **1996,** 96, 3147-3176.

184. Waldvogel, S. R. *Comprehensive Organic Name Reactions and Reagents*. In 2010.

185. Zheng, Y.; Tice, C. M.; Singh, S. B. The use of spirocyclic scaffolds in drug discovery. *Bioorganic & medicinal chemistry letters* **2014,** 24, 3673-3682.

186. Marson, C. M. New and unusual scaffolds in medicinal chemistry. *Chemical Society Reviews* **2011,** 40, 5514-5533.

187. Veber, D. F.; Johnson, S. R.; Cheng, H.-Y.; Smith, B. R.; Ward, K. W.; Kopple, K. D. Molecular properties that influence the oral bioavailability of drug candidates. *Journal of medicinal chemistry* **2002,** 45, 2615-2623.

188. Zheng, Y.-J.; Tice, C. M. *The utilization of spirocyclic scaffolds in novel drug discovery*. In Taylor & Francis: 2016.

189. Leo, A. J.; Hansch, C. Role of hydrophobic effects in mechanistic QSAR. *Perspectives in Drug Discovery and Design* **1999,** 17, 1-25.

190. Novoa, I.; Zeng, H.; Harding, H. P.; Ron, D. Feedback inhibition of the unfolded protein response by GADD34-mediated dephosphorylation of eIF2α. *The Journal of cell biology* **2001,** 153, 1011-1022.

191. Batsanov, S. Van der Waals radii of elements. *Inorganic materials* **2001,** 37, 871-885.

192. Wilcken, R.; Zimmermann, M. O.; Lange, A.; Joerger, A. C.; Boeckler, F. M. Principles and applications of halogen bonding in medicinal chemistry and chemical biology. *Journal of medicinal chemistry* **2013,** 56, 1363-1388.

193. Choudhary, A.; Raines, R. T. An evaluation of peptide-bond isosteres. *ChemBioChem* **2011,** 12, 1801-1807.

194. Ahmad, N. M. Solubility-driven lead optimisation: Recent examples and personal perspectives. *Bioorganic & medicinal chemistry letters* **2016,** 26, 2975-2979.

195. Walker, M. A. Novel tactics for designing water-soluble molecules in drug discovery. *Expert opinion on drug discovery* **2014,** 9, 1421-1433.

196. Wright, M.; Sieber, S. Chemical proteomics approaches for identifying the cellular targets of natural products. *Natural product reports* **2016,** 33, 681-708.

197. Witiak, D. T.; Stratford, E. S.; Nazareth, R.; Wagner, G.; Feller, D. R. 6-Chlorochroman-2-carboxylic acids. Synthesis and biological evaluation as antagonists for cholesterol biosynthesis and lipolysis in vitro. *Journal of medicinal chemistry* **1971,** 14, 758-766.

198. Mayr, H.; Dogan, B. Selectivities in ionic reductions of alcohols and ketones with triethylsilane/trifluoroacetic acid. *Tetrahedron letters* **1997,** 38, 1013-1016.

199. Koo, J.; Avakian, S.; Martin, G. J. Derivatives of 1, 4-benzodioxan. I. 1, 4-Benzodioxan-2-carboxamides. *Journal of the American Chemical Society* **1955,** 77, 5373-5375.

200. Hall, M. D.; Yasgar, A.; Peryea, T.; Braisted, J. C.; Jadhav, A.; Simeonov, A.; Coussens, N. P. Fluorescence polarization assays in high-throughput screening and drug discovery: a review. *Methods and applications in fluorescence* **2016,** 4, 022001.

201. Nosjean, O.; Souchaud, S.; Deniau, C.; Geneste, O.; Cauquil, N.; Boutin, J. A. A simple theoretical model for fluorescence polarization binding assay development. *Journal of biomolecular screening* **2006,** 11, 949-958.

202. Rossi, A. M.; Taylor, C. W. Analysis of protein-ligand interactions by fluorescence polarization. *Nature protocols* **2011,** 6, 365.

203. Caldwell, J.; Gardner, I.; Swales, N. An introduction to drug disposition: the basic principles of absorption, distribution, metabolism, and excretion. *Toxicologic pathology* **1995,** 23, 102-14.

204. Augustijns, P.; Wuyts, B.; Hens, B.; Annaert, P.; Butler, J.; Brouwers, J. A review of drug solubility in human intestinal fluids: implications for the prediction of oral absorption. *European Journal of Pharmaceutical Sciences* **2014,** 57, 322-332.

205. Amidon, G. L.; Lennernäs, H.; Shah, V. P.; Crison, J. R. A theoretical basis for a biopharmaceutic drug classification: the correlation of in vitro drug product dissolution and in vivo bioavailability. *Pharmaceutical research* **1995,** 12, 413-420.

206. Cai, Z.-W.; Wei, D.; Schroeder, G. M.; Cornelius, L. A.; Kim, K.; Chen, X.-T.; Schmidt, R. J.; Williams, D. K.; Tokarski, J. S.; An, Y. Discovery of orally active pyrrolopyridine-and aminopyridine-based Met kinase inhibitors. *Bioorganic & medicinal chemistry letters* **2008,** 18, 3224-3229.

207. Choi, H.; Lee, J.; Kim, Y. H.; Hwang, I.-C.; Kim, S. J.; Moon, S. K.; Lee, H. W.; Lee, S. S.; Ahn, S. K.; Kim, S. W. Discovery of potent, selective, and orally bioavailable PDE5 inhibitor: Methyl-4-(3-chloro-4-methoxybenzylamino)-8-(2-hydroxyethyl)-7-methoxyquinazolin-6-ylmethylcarbamate (CKD 533). *Bioorganic & medicinal chemistry letters* **2010,** 20, 383-386.

208. Larregieu, C. A.; Benet, L. Z. Distinguishing between the permeability relationships with absorption and metabolism to improve BCS and BDDCS predictions in early drug discovery. *Molecular pharmaceutics* **2014,** 11, 1335-1344.

209. Cheng, A.; Merz, K. M. Prediction of aqueous solubility of a diverse set of compounds using quantitative structure− property relationships. *Journal of medicinal chemistry* **2003,** 46, 3572-3580.

210. Di, L.; Kerns, E. H. Profiling drug-like properties in discovery research. *Current opinion in chemical biology* **2003,** 7, 402-408.

211. FDA, U.S.D.o.H.a.H. *Guidance for Industry, Bioanalyical Method Validation.* 2001.

212. Kim, M. G.; Kim, T. H.; Shin, B. S.; Lee, Y.-B.; Lee, J. B.; Choi, H. G.; Lee, Y.; Yoo, S. D. Sensitive liquid chromatography-tandem mass spectrometry method for the simultaneous determination of benzyl butyl phthalate and its metabolites, monobenzyl phthalate and monobutyl phthalate, in rat plasma, urine, and various tissues collected from a toxicokinetic study. *Analytical and bioanalytical chemistry* **2015,** 407, 7391-7400.

213. Echizen, H.; Eichelbaum, M. Clinical pharmacokinetics of verapamil, nifedipine and diltiazem. *Clinical pharmacokinetics* **1986,** 11, 425-449.

214. Artursson, P.; Palm, K.; Luthman, K. Caco-2 monolayers in experimental and theoretical predictions of drug transport. *Advanced drug delivery reviews* **2001,** 46, 27-43.

215. Obach, R. S. Prediction of human clearance of twenty-nine drugs from hepatic microsomal intrinsic clearance data: an examination of in vitro half-life approach and nonspecific binding to microsomes. *Drug Metabolism and Disposition* **1999,** 27, 1350-1359.

216. Kwon, Y. *Handbook of essential pharmacokinetics, pharmacodynamics and drug metabolism for industrial scientists*. Springer Science & Business Media: 2001.

217. Houston, J. B. Utility of in vitro drug metabolism data in predicting in vivo metabolic clearance. *Biochemical pharmacology* **1994,** 47, 1469-1479.

218. Li, A. P. In vitro approaches to evaluate ADMET drug properties. *Current topics in medicinal chemistry* **2004,** 4, 701-706.

219. Turksen, K. *Permeability barrier: methods and protocols*. Springer: 2011.

220. Hubatsch, I.; Ragnarsson, E. G.; Artursson, P. Determination of drug permeability and prediction of drug absorption in Caco-2 monolayers. *Nature protocols* **2007,** 2, 2111.

221. Pauli-Magnus, C.; von Richter, O.; Burk, O.; Ziegler, A.; Mettang, T.; Eichelbaum, M.; Fromm, M. F. Characterization of the major metabolites of verapamil as substrates and inhibitors of P-glycoprotein. *Journal of Pharmacology and Experimental Therapeutics* **2000,** 293, 376-382.

222. Polli, J. W.; Wring, S. A.; Humphreys, J. E.; Huang, L.; Morgan, J. B.; Webster, L. O.; Serabjit-Singh, C. S. Rational use of in vitro P-glycoprotein assays in drug discovery. *Journal of Pharmacology and Experimental Therapeutics* **2001,** 299, 620-628.

223. Mensch, J.; Jaroskova, L.; Sanderson, W.; Melis, A.; Mackie, C.; Verreck, G.; Brewster, M. E.; Augustijns, P. Application of PAMPA-models to predict BBB permeability including efflux ratio, plasma protein binding and physicochemical parameters. *International journal of pharmaceutics* **2010,** 395, 182-197.

224. Davis, T. P.; Sanchez-Covarubias, L.; Tome, M. E. P-glycoprotein trafficking as a therapeutic target to optimize CNS drug delivery. In *Advances in Pharmacology*, **2014,** 71, 25-44.

225. Amin, M. L. P-glycoprotein inhibition for optimal drug delivery. *Drug target insights* **2013,** 7, 27-34.

226. Shah, S. M.; Jain, A. S.; Kaushik, R.; Nagarsenker, M. S.; Nerurkar, M. J. Preclinical formulations: insight, strategies, and practical considerations. *American Association of Pharmaceutical Scientists PharmSciTech* **2014,** 15, 1307-1323.

227. Halliday, M.; Radford, H.; Sekine, Y.; Moreno, J.; Verity, N.; Le Quesne, J.; Ortori, C.; Barrett, D.; Fromont, C.; Fischer, P. Partial restoration of protein synthesis rates by the small molecule ISRIB prevents neurodegeneration without pancreatic toxicity. *Cell death & disease* **2015,** 6, 1672-1672.

228. Ishikawa, M.; Hashimoto, Y. Improvement in aqueous solubility in small molecule drug discovery programs by disruption of molecular

planarity and symmetry. *Journal of medicinal chemistry* **2011,** 54, 1539-1554.

229. Stepan, A. F.; Subramanyam, C.; Efremov, I. V.; Dutra, J. K.; O'Sullivan, T. J.; DiRico, K. J.; McDonald, W. S.; Won, A.; Dorff, P. H.; Nolan, C. E. Application of the bicyclo [1.1. 1] pentane motif as a nonclassical phenyl ring bioisostere in the design of a potent and orally active γ-secretase inhibitor. *Journal of medicinal chemistry* **2012,** 55, 3414-3424.

230. Mykhailiuk, P. K. Saturated bioisosteres of benzene: where to go next? *Organic & biomolecular chemistry* **2019,** 17, 2839-2849.

231. Houston, S. D.; Fahrenhorst-Jones, T.; Xing, H.; Chalmers, B. A.; Sykes, M. L.; Stok, J. E.; Soto, C. F.; Burns, J. M.; Bernhardt, P. V.; De Voss, J. J. The cubane paradigm in bioactive molecule discovery: further scope, limitations and the cyclooctatetraene complement. *Organic & biomolecular chemistry* **2019,** 17, 6790-6798.

232. Auberson, Y. P.; Brocklehurst, C.; Furegati, M.; Fessard, T. C.; Koch, G.; Decker, A.; La Vecchia, L.; Briard, E. Improving Nonspecific Binding and Solubility: Bicycloalkyl Groups and Cubanes as para-Phenyl Bioisosteres. *ChemMedChem* **2017,** 12, 590-598.

233. Hosea, N. A.; Jones, H. M. Predicting pharmacokinetic profiles using in silico derived parameters. *Molecular pharmaceutics* **2013,** 10, 1207-1215.

234. Taha, D. A.; De Moor, C. H.; Barrett, D. A.; Lee, J. B.; Gandhi, R. D.; Hoo, C. W.; Gershkovich, P. The role of acid-base imbalance in statin-induced myotoxicity. *Translational Research* **2016,** 174, 140-160. e14.

Appendix

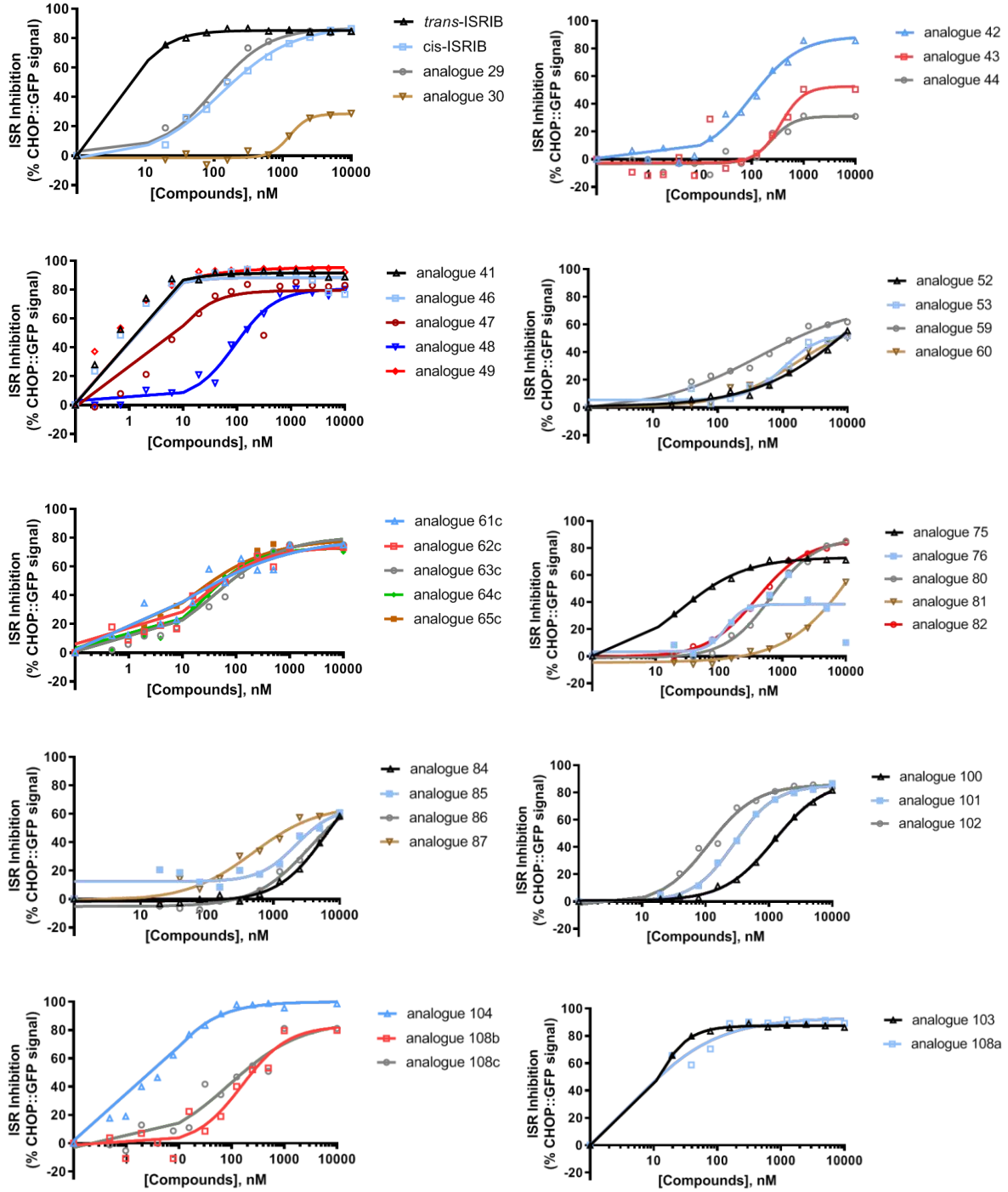


Figure A1: ISRIB and its analogues (**29**-**108a**) inhibit the ISR in CHO-K1 cells. Plot of the inhibition of ISR activated CHOP::GFP signal, stimulated upon treating the cells with histidinol (HIS) (0.5 mM), in the presence of escalating concentrations of ISRIB and its analogues. Shown is a representative from three independent experiments conducted for *trans*-ISRIB and of a single 12-point titration experiment conducted for ISRIB analogues. Concentration of ISRIB and its analogues is represented on a log10 scale. Curve fitting and EC_{50} was generated using agonist vs. response function on GraphPad Prism.

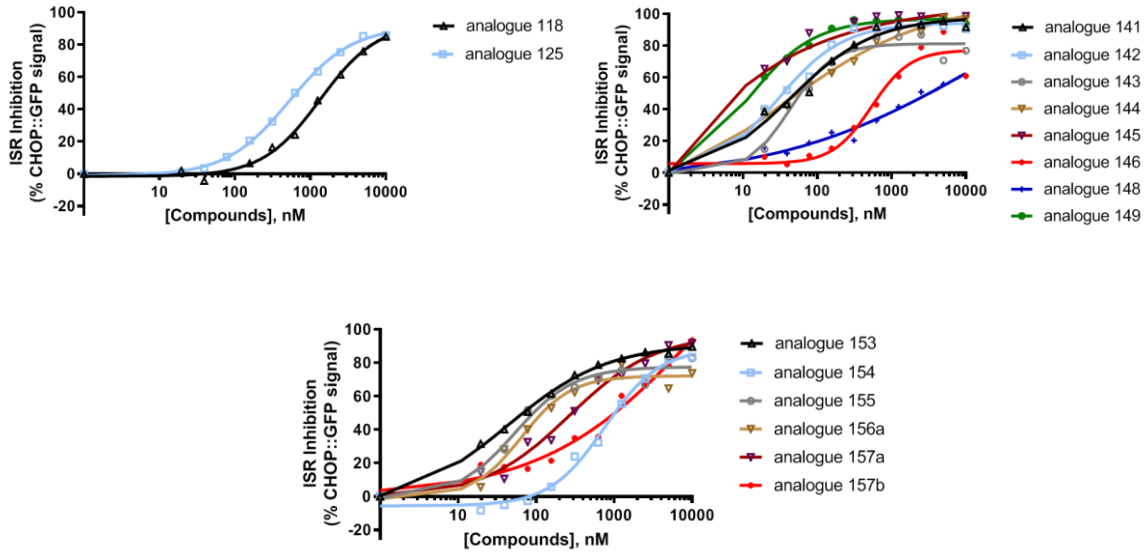


Figure A2: ISRIB and its analogues (**118**-**157b**) inhibit the ISR in CHO-K1 cells. Plot of the inhibition of ISR activated CHOP::GFP signal, stimulated upon treating the cells with histidinol (HIS) (0.5 mM), in the presence of escalating concentrations of ISRIB and its analogues. Shown is a representative from three independent experiments conducted for *trans*-ISRIB and of a single 12-point titration experiment conducted for ISRIB analogues. Concentration of ISRIB and its analogues is represented on a log10 scale. Curve fitting and EC_{50} was generated using agonist vs. response function on GraphPad Prism.